Genetic regulation of photoreceptor specification in the tetrachromat zebrafish retina

by

Adam Phillip Oel

A thesis submitted in partial fulfillment of the requirements for the degree of

Doctor of Philosophy

in

Physiology, Cell, and Developmental Biology

Department of Biological Sciences
University of Alberta

Abstract

Vertebrate vision is mediated through the absorption of light by the rod and the cone photoreceptors. Early jawed vertebrates initially had four cone subtypes, which sampled different regions of the visual spectrum to allow colour vision, and a single rod type which enabled vision in dim light. Many lineages of vertebrates retain this original complement of photoreceptors, but genetic mechanisms of photoreceptor specification have been chiefly explored in mammals, which have lost two cone subtypes. Our understanding of the genetic regulation of photoreceptor diversity in the archetypical vertebrate eye, and how this regulation has evolved in different lineages, is therefore incomplete. I used the zebrafish, a diurnal vertebrate that produces the four original cone subtypes and one rod subtype, to investigate the genetic specification of photoreceptor diversity in tetrachromats, and to identify possible genetic mechanisms exploited by various vertebrate lineages to recalibrate their photoreceptor diversity in response to novel evolutionary pressures.

The zebrafish UV cone is homologous to the mouse S cone, while the zebrafish blue cone has no mouse homolog. It was previously demonstrated that the T-box transcription factor gene tbx2b modulates UV cone and rod abundances in larval zebrafish, but regulators of tbx2b were unknown. Furthermore, regulation of the blue cone type was wholly unknown. On the basis of genetic interaction in early retinogenesis, my colleagues and I examined the genetic interaction of the BMP ligand gene gdf6a and tbx2b on larval photoreceptor diversity. We found that gdf6a modulates the actions of tbx2b in governing UV cone and rod abundance, and on its own modulates blue cone abundance. Together, this represents the beginning of the first genetic pathway regulating tetrachromat cone diversity, including of the ancient blue cones not found in mammalian retinas.

Molecular evidence suggests that rod genes evolved out of pre-existing cone genes, and the current consensus is that rods probably evolved from cones. Previous work profiling the gene expression of developing mouse rods had suggested a transient cone signature. This led to the hypothesis that vertebrate rods routinely develop from cone-fated precursors. My colleagues and I tested this hypothesis by comparing mouse and

zebrafish photoreceptor development. We found that a majority of mouse rods transiently but robustly expressed signature cone genes, but some small proportion of mouse rods did not. I found that zebrafish larvae did not have rods with cone gene expression history. In light of additional evidence that early mammals increased the abundance of rod photoreceptors for a nocturnal lifestyle, we proposed that mammals diverted normally highly abundant cone-destined cells to the rod phenotype. We further proposed that early mammals may have exploited regulatory or activity changes in the transcription factor Nrl as a mechanism.

The body of mouse photoreceptor specification literature features Nrl as a central node in that transcription factor network, and it was not known whether nrl had conserved activity in zebrafish or any species beyond mouse or mammals. I therefore examined the role of nrl in zebrafish photoreceptor specification. I found nrl to be necessary and sufficient for the rod phenotype in larvae, indicating conservation of nrl function between fish and mammals. Unlike in mammals, I further found that nrl was not required for adult rod production. This is the first evidence for an nrl-independent rod developmental pathway. Finally, I tested the rod-inductive ability of a panel of nrl homologs from several vertebrate taxa, and found that even basally-branching vertebrates have an nrl homolog which can promote the rod phenotype. This suggests that a role for nrl in rod specification may be ancestral in vertebrates.

Cumulatively, the work in this thesis identified the first genetic regulator of the tetrachromat blue cone, established a novel regulatory pathway governing UV cone and rod abundance, and identified a deep conservation in rod developmental genetics between mammals and zebrafish larvae. It also identified a possible novel rod developmental pathway, which may be a genetic mechanism by which other vertebrate lineages modulate photoreceptor diversity. Finally, it positioned zebrafish to serve as the basis for future direct comparisons of photoreceptor specification genetics between tetrachromats and mammals.

Preface

Two chapters in this PhD thesis have been previously published:

Chapter 2 was published as:

Michèle G. DuVal, **A. Phillip Oel**, and W. Ted Allison. 2014. "gdf6a *Is Required for Cone Photoreceptor Subtype Differentiation and for the Actions of* tbx2b *in Determining Rod Versus Cone Photoreceptor Fate*". PloS One 9, e92991.

All authors conceived, designed, and performed the experiments, and analyzed the data, and edited the manuscript. MGD and WTA wrote the manuscript. I was an equal contributor to 6 of the 9 major experiments, and to 6 of 12 total figure elements.

Chapter 3 was published as:

Jung-Woong Kim[1], Hyun-Jin Yang[1], **A. Phillip Oel[1]**, Matthew John Brooks, Li Jia, David Charles Plachetzki, Wei Li, W. Ted Allison[2], and Anand Swaroop[2]. 2016. "*Recruitment of Rod Photoreceptors from Short-Wavelength-Sensitive Cones during the Evolution of Nocturnal Vision in Mammals*". Developmental Cell 37, 520-532.

[1]Co-first authors; [2]co-corresponding authors. JK: mouse experiments, data analysis, evolutionary analysis, next-gen sequencing analysis, original draft. HY: mouse experiments, data analysis, next-gen sequencing analysis, original draft. **APO:** data analysis, and zebrafish experiment conceptualization, performance, and analysis. MJB: next-gen sequencing experiments, data curation, and analysis, and evolutionary analysis. LJ: mouse resource generation. DCP: next-gen sequencing analysis, and phylogenetic analysis. WL: mouse resource generation. **WTA**: zebrafish experiment conceptualization, data analysis, supervision. AS: data analysis, supervision, project administrator. JK, HY, APO, MJB, DCP, WL, WTA, and AS reviewed and edited the manuscript.

Acknowledgements

This journey was only possible because of the enormous amount of support I received while undertaking it. I received this support from many sources over the years, but chiefly among them:

I would like to gratefully honour my supervisor, Ted Allison, for taking a chance on me six years ago as I wandered out of my undergrad ago toward what I hoped was the right way to do science. Throughout this time, he has made room for me to learn, grow, disagree, and more frequently to initially disagree and then learn more and agree later. I have truly felt like a peer in the design and execution of the research I performed under his supervision. I thank him for his long-term confidence in me, for helping me to become a scientist, and for encouraging me to dream big.

I thank the many and varied members of the Allison lab, with whom it has been a pleasure to work, and who have been another enormous source of support for me over the years. I especially wish to thank Michèle Duval, who has continually inspired me in every way, from work ethic, to service, wisdom and perspective.

I thank my family and friends for their constant support and for providing a moment away from it all whenever I needed it. This includes my mother and sister Shelley and Sara Traves, and my second family Bonnie and Lester Shantz and Michelle Sims.

Finally, I thank my partner Kailen Shantz for everything over the years. We have done our graduate programs in separate countries, but his love, support, and wisdom have always been immediate and invaluable. I could not have done this without him.

Table of Contents

List of Tables

List of Figures

List of Abbreviations

BAC	Bacterial artificial chromosome
CMZ	Ciliary marginal zone
DPF	Days post fertilization
FACS	Fluorescence-activated cell sorting
INL	Inner nuclear layer
IPL	Inner plexiform layer
IS	Inner segment
MTD	Minimal transactivation domain
MWU	Mann-Whitney U test
MYA	Million years ago
ONH	Optic nerve head
ONL	Outer nuclear layer
OPL	Outer plexiform layer
OS	Outer segment
RGL	Retinal ganglion cell layer
PDE	Phosphodiesterase
Rh*	Light-stimulated (activated) rhodopsin; Meta-rhodopsin II
RPE	Retinal pigmented epithelium
RRBS	Reduced representation bisulfide sequencing
SNP	Single nucleotide polymorphism
SVD	Synaptic vesicle density
UTR	Untranslated region
5’ RACE	5’ Rapid amplification of cDNA ends

Gene and protein notation conventions per model organism

Species	**Gene convention**	**Protein convention**
Human (*homo sapiens*)	*NRL* (italics, capitals)	NRL (capitals)
Mouse (*Mus musculus*) and most other vertebrates (frog, salamander, etc.)	*Nrl* (italics, initial capital)	Nrl (initial capital)
Chicken (*Gallus gallus*)	*MAFA* (italics, capitals)	MAFA (capitals)
Zebrafish (*Danio rerio*)	*nrl* (italics)	Nrl (initial capital)
Lamprey *spp.*	*MAFBA* (italics, capitals)	MAFBA (capitals)
Fruit fly (*Drosophila melanogaster*)	*trafficjam* (italics)	Trafficjam (initial capital)

CHAPTER 1:

GENERAL INTRODUCTION

1.1 Anatomy and development of the retina

The goal of Section 1.1 is to provide a conceptual framework for the reader regarding what a vertebrate retina is and does. This short section aims to grant familiarity with the major retinal cell types and their principal functions. Model organism-specific information is invoked primarily to demonstrate: (1) the multitude of cell subtypes which we are just now beginning to identify in specific model organisms; (2) the deep conservation of retinal structure and function in vertebrates, or (3) the flexibility in the structure/function/physiology that has allowed some lineages to originate novel adaptations. It is not intended to be a definitive review of all retinal developmental biology, as this thesis chiefly pertains to the genetic regulation of vertebrate photoreceptor diversity (reviewed in Section 1.2) and the evolution of this regulation (reviewed in Section 1.3).

1.1.1 Structure and elements of the retina

The mature vertebrate retina is composed of 5 major neural cell types and a single endogenous glial cell type, arranged in three nuclear layers and two synaptic layers (Fig. 1.1). The photoreceptors, which are the rods and cones, collect photons of light and convert the information into chemical signals, and pass the information on to the bipolar cells. The bipolar cells relay the information on to the retinal ganglion cells, whose axons project from the retina, through the optic nerve, and into the visual centers of the brain. The signaling between photoreceptors and bipolar cells is modulated by the horizontal cells, and transmission between the bipolar cells and retinal ganglion cells is modulated by the amacrine cells. The Müller glia extend radially throughout the whole neural retina, contacting all cell types and mediating numerous homeostatic and trophic support functions for the neural cells (Dowling, 2012).

The outer nuclear layer (ONL) houses the nuclei of the rod and cone photoreceptors, while the bipolar, horizontal, and amacrine cell nuclei occupy the inner nuclear layer (INL). The ONL and INL are separated by the outer plexiform layer (OPL), a thin neuropil composed of the synapses of the photoreceptors, bipolar cells, and horizontal cells. The retinal ganglion cell layer (RGL) and inner plexiform layer (IPL) are vitread of the INL; the RGL is mainly comprised of retinal ganglion cell nuclei, but the

nuclei of a subset of amacrine cells, the displaced amacrine cells, are also located in the RGL. The IPL is a much thicker neuropil than the OPL, consisting of the numerous synapses between bipolar cells, amacrine cells, and ganglion cells. The IPL is arranged into sublaminae, arranged to separate the differing physiological roles of the various bipolar and amacrine cell subtypes (Dowling, 2012; Wong, 2006).

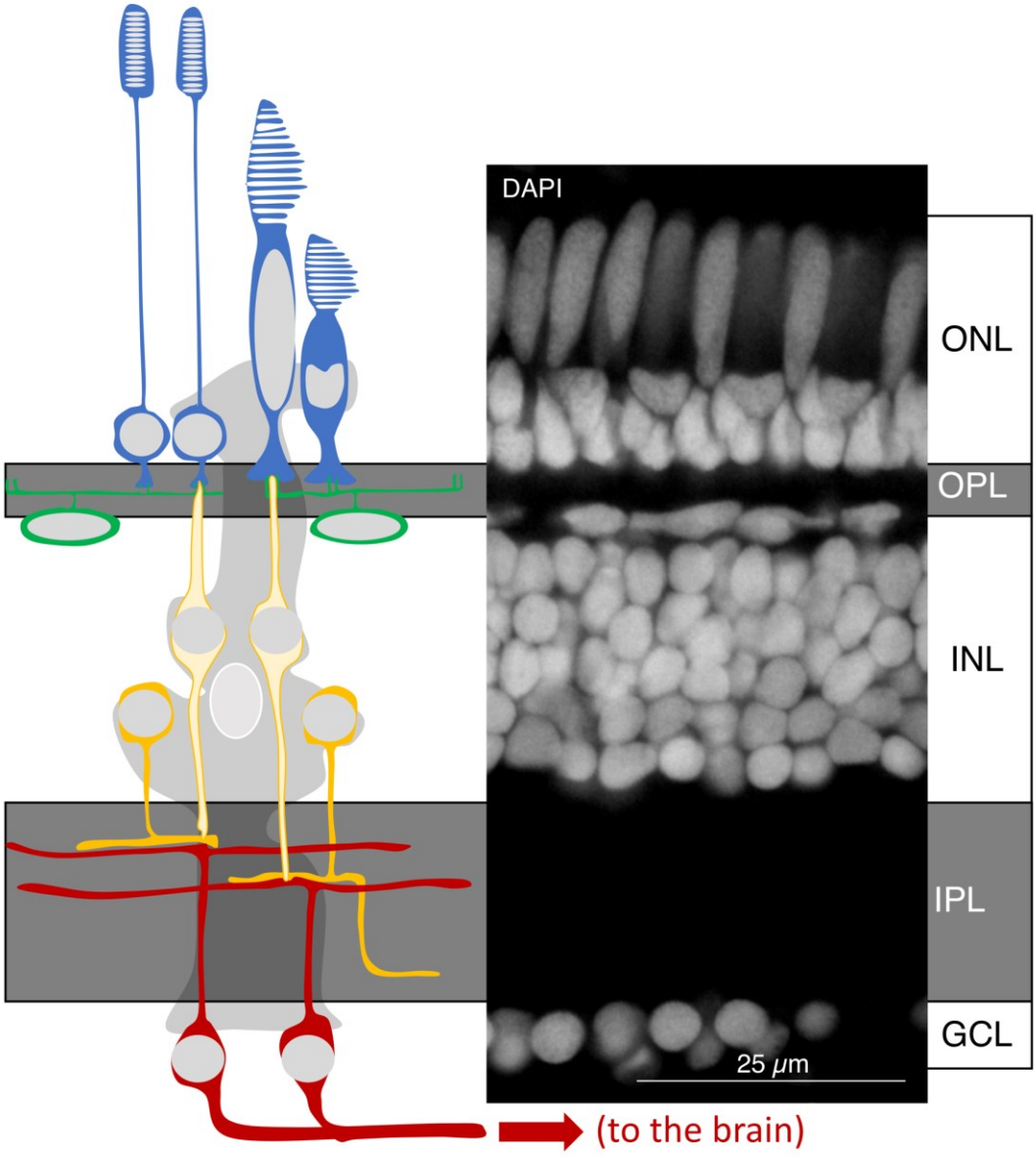

Figure 1.1: Basic structure and components of the adult vertebrate retina. Depicted: a confocal micrograph of a radial-cut frozen section of an adult zebrafish retina with DAPI nuclear stain, showing the outer nuclear layer (ONL), outer plexiform layer (OPL), inner nuclear layer (INL), inner plexiform layer (IPL), and ganglion cell layer (GCL). Beside it, a schematic of the 5 major classes of retinal neurons, and the sole endogenous glial type, the Müller glia. Photoreceptors in blue, horizontal cells in green, bipolar cells in bright yellow, amacrine cells in orange, and ganglion cells in red. Shown in dark gray with a fainter nucleus is a representative Müller glia, which spans the retinal layers to contact all cell types. Scale bar is 25 microns.

1.1.2 Function of the retinal components

The functions of the rod and cone photoreceptors will be discussed in more detail in Section 1.1.3. In brief, light strikes the opsin G-protein coupled receptor proteins, triggering a cascade that lowers intracellular cGMP concentration and briefly hyperpolarizes the cell. The hyperpolarized photoreceptor reduces its otherwise constitutive glutamate release from its synapse, and this reduction is the signal detected by the bipolar cells. Neighboring photoreceptor termini are connected by telodendria (Noel and Allison, 2018), which are fine processes emanating from one synapse to neighbouring telodendria and electrically coupled by connexin-mediated gap junctions (Asteriti et al., 2014). The physiological consequence of the telodendria is not currently understood.

The photoreceptor synaptic termini are invaginated, and the spaces are filled by processes of bipolar and horizontal cells (Tarboush et al., 2012). Two major classes of horizontal cells exist, based on presence/absence of a short axon. There appears to be relaxed constraint in horizontal cell subtype variability (Boije et al., 2016); in humans, there are 3 types of the axon-bearing horizontal cell, and no axon-less horizontal cell; in rat and mouse, there are only axon-bearing horizontal cells, and apparently only a single type, based on morphological, electrophysiological, and immunological characterization. In the fishes, a third major class of horizontal cells exist, and in zebrafish there are two subtypes of these. It appears that a rule-of-thumb for the dendrites of all horizontal cell types is to wire with cone synapses, while the processes of the axon-bearing horizontal cells wire with rods. Horizontal cells participate in the synapses of numerous neighbouring photoreceptors, and inhibit the signaling from a given photoreceptor as a function of local signal intensity; the outcome of this is known as surround inhibition and center-surround organization with reciprocal inhibition. In surround inhibition, when a patch of photoreceptors responds to light, the centre of the patch is allowed to signal downstream to the bipolar cells, while transmission from the surrounding photoreceptors to the downstream bipolar cells is inhibited by the horizontal cells; this is the first site of contrast enhancement in the retina, and contributes to spatial acuity and colour vision. Horizontal cells hyperpolarize when glutamate levels decrease (i.e., when light stimulates photoreceptors), and the method by which they inhibit the

signal transduction between photoreceptors and bipolar cells is not fully understood, but likely involves modulating cone polarization (reducing apparent signal amplitude received by bipolar cells) as well as modulating bipolar cell dendrites (decreasing the effect of incoming glutamate from the photoreceptor).

While all bipolar cell types receive glutamate from photoreceptors, the receptor they express dictates how they respond to the graded changes in glutamate they receive. Bipolar cells are physiologically grouped as ON or OFF bipolar cells, in reference to their response to input from photoreceptors. ON bipolar cells hyperpolarize in darkness (high glutamate from photoreceptors), and depolarize when glutamate decreases, thereby relaying information about a local *increase* in light. OFF bipolar cells depolarize in response to photoreceptor glutamate, and hyperpolarize after that photoreceptor returns to an unstimulated state (returns to high glutamate release in the dark), thereby communicating a local *decrease* in illumination. Typically, rod bipolar cells are of the ON type; cone bipolar cells are either ON or OFF. Similar to photoreceptors, bipolar cell downstream signalling is through graded potential, not through action potential. The ON/OFF bipolar cell paradigm is another layer of visual information processing that occurs in the retina. Although these are the two major physiological groups of bipolar cells, there are subtypes which wire to various proportions of cones and downstream cells differently. A recent study which combined single cell RNAseq with morphological and histological categories has put the number of mouse bipolar cell subtypes at 15 (Shekhar et al., 2016).

Amacrine cells mediate the signals transmitted from the bipolar cells to the retinal ganglion cells, which then fire an action potential upon receipt of stimulus. Amacrine cells exist in a variety of subtypes with various physiological roles. There are at least 33 morphologically-defined amacrine subtypes in the mouse retina (Helmstaedter et al., 2013), but most appear to be predominantly inhibitory of the transmission of signal from bipolar cell to ganglion cell. Mechanisms for this include direct feedback inhibition of the bipolar cell, or feed-forward inhibition of the retinal ganglion cell. The former is achieved by synapsing onto a bipolar terminus and hyperpolarizing it, and the latter by interfering with signal transduction within a retinal ganglion cell dendrite, thereby stopping a signal from reaching the soma and triggering an action potential. Some amacrine cells

arborize in multiple sublaminae of the IPL, allowing simultaneous regulation of ON and OFF bipolar cell signaling. The outcome of amacrine cell-mediated modulation of visual signals includes enhanced center-surround signals (first refined by the horizontal cells), as well as refining the spatial and temporal information integrated by retinal ganglion cells, a single one of which might receive input from tens to hundreds of bipolar cells.

In the mouse, there are more than 32 functionally distinct subtypes of retinal ganglion cells, with each type each tiling the retina separately with approximately 30% overlap between them (Baden et al., 2016). Retinal ganglion cells transduce their signal to the brain along their axons in an action potential, but the frequency and probability of action potentials is modulated in poorly understood ways. There are ON and OFF RGCs, similar to the ON and OFF bipolar cells, but also ON-OFF RGCs, which only signal when illumination decreases within a short timeframe; many are direction selective, firing only when a stimulus crosses the field of view in a specific direction. Others are orientation sensitive, and integrate information on object edges in order to convey information about elongated objects, but only when the objects are perceived at a preferred angle for that cell. A small population are intrinsically photosensitive, and express an invertebrate opsin-like nonvisual opsin (melanopsin), with roles for entraining the circadian rhythm to ambient photoperiods. The RGCs are the final step of retinal processing of visual information before it is sent to the brain, and at or by this stage colour vision, loom/shadow expansion, edge detection, motion detection, and motion orientation have been selectively processed in parallel and sent out of the eye.

1.1.3 Function of the photoreceptors

Rods and cones have essentially the same physiology, and differences in the phototransduction machinery largely explains their differing sensitivities and responses to light. The photoreceptor is a sensory neuron that relies on an elaborate primary cilium, termed the outer segment (Fig. 1.2), which deploys various strategies to generate extra membrane surface area. This extra surface area maximizes the density of the transmembrane opsin G-protein coupled receptors critical for detecting photons. In rods, the extra surface area comes from a series of internal membrane discs, free-

floating within the outer segment. The density of rhodopsin achieved in the rod photoreceptor discs of mouse has been assessed by atomic force microscopy (Liang et al., 2003), and is between 30,000 and 55,000 single rhodopsin monomers within a single square micron. The membrane-bound G-proteins, known as transducins for visual photoreceptors, are typically localized to the discs, as is their downstream effector enzyme phosphodiesterase (Wensel, 2008). In cones, the extra membrane surface area is provided by extensive invagination of the plasma membrane (Fig. 1.2).

The specific opsin used in a photoreceptor varies by photoreceptor type; rods express rhodopsin, whereas cones express any of a small variety of cone opsins, each of which have differing peak sensitivities to colour of light. For example, zebrafish UV light-sensitive cones express Short wavelength-sensitive1 (Sws1) opsin, which has a peak spectral sensitivity in the ultraviolet wavelength range (Raymond et al., 1996; Robinson et al., 1993). For rod and cone opsins, the critical light-receptive component is a covalently bound 11-*cis*-retinal molecule, which maintains the opsin in an inactive conformation (Palczewski et al., 2000). In some amphibians, reptiles, and fishes including zebrafish, alternative moieties of 11-*cis*-retinal are used in certain circumstances instead, which shift the absorption spectra for an opsin slightly (Allison et al., 2004; Enright et al., 2015b; Morshedian et al., 2017). While all wavelengths of light are capable of eliciting a response from the chromophore, the specific opsin subtype bound to it conveys selectivity, such that a narrow range of wavelengths are most likely to stimulate a response. For a given opsin, a photon of the appropriate wavelength that strikes the 11-*cis*-retinal induces an isomerization to all-*trans*-retinal, which induces conformational changes in the associated opsin, activating it. In rods, activated rhodopsin is termed MetarhodopsinII, or Rh*. Rh* binds the transducin complex and releases the alpha subunit from the inhibitory beta and gamma subunits; a single mouse Rh* activates about 20-50 units of transducin alpha (Kawamura and Tachibanaki, 2008; Krispel et al., 2006) before it is silenced; activated cone opsins are silenced more rapidly, and only activate about 2 units (Kawamura and Tachibanaki, 2008). Rh* activity is attenuated first by phosphorylation by a G-protein receptor kinase, and then fully silenced by arrestin. Silenced Rh* eventually decays from phospho-metarhodopsinII to phospho-metarhodopsinIII (Yau and Hardie, 2009), and after the arrestin dissociates,

phospho-metarhodopsinIII is dephosphorylated, perhaps by PP2A (Palczewski et al., 1989), regenerating the opsin. A silenced opsin cannot participate in photoreception again until it has exchanged all-*trans*-retinal for a fresh 11-*cis*-retinal molecule.

After activation by Rh* and release from inhibitory transducin beta and gamma subunits, the GTP-bearing transducin alpha catalyzes the separation of phosphodiesterase (PDE) inhibitory subunit gamma from the rest of the PDE complex, activating it. Activated PDE hydrolyzes cytosolic cGMP, lowering the intracellular concentration at the rate of more than 1000 units of cGMP per PDE per second (Kawamura and Tachibanaki, 2008). The outer segment is host to a high density of cGMP-gated ion channels, which non-selectively allow cations to flow into the cell, as well as constitutively active sodium exporters. When the cGMP-gated channels are open, the overall voltage is low and the cell is at most slightly polarized. With low cGMP concentration, the cGMP-gated channels close, and the influx of cations ceases. This results in hyperpolarization of the cell, because the cell constitutively exports sodium.

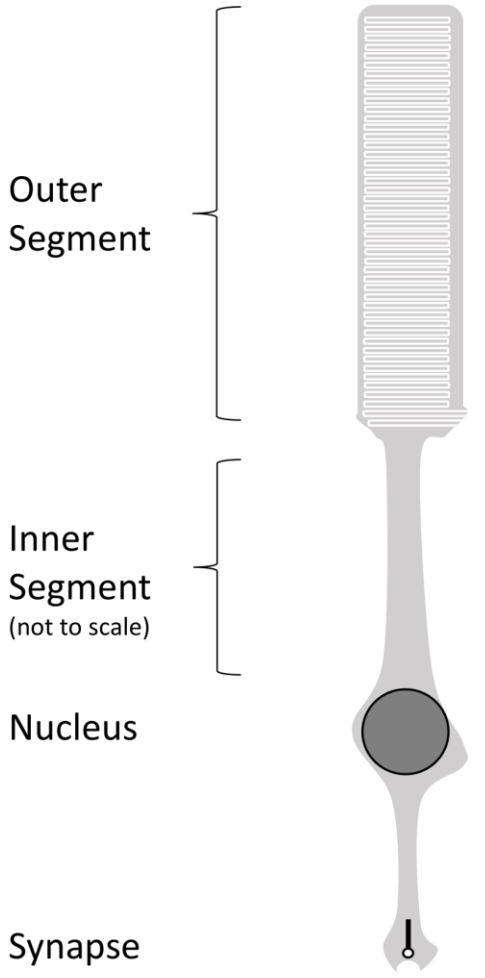

Character	Rods	Cones
Outer Segment	Long and slender; internalized membrane discs	Short and tapered; membrane invaginations
Nucleus	Electron-dense; hetero- and euchromatin relatively unmixed or segregated	Electrolucent; mottled with intermixed hetero- and euchromatin
Synapse	*Spherule*; smaller, often single and longer synaptic ribbon	*Pedicle*; larger, multiple shorter synaptic ribbons

Figure 1.2: Schematic representation of the chief morphological and structural distinctions of the rod and cone photoreceptors.

In adult mouse and zebrafish, the rod inner segment is often many times longer than depicted here; otherwise, the cartoons are roughly to scale for a zebrafish rod and short cone.

1.1.4 Rod/Cone differences in phototransduction

Functionally, rods saturate in bright light, and cannot mediate vision in strong illumination, but are capable of detecting single photons of light, which after signal amplification can close 3-5% of cGMP-gated ion channels (D-G Luo et al., 2008). A single Rh* represents a single photon capture event, and in the carp, rods reach their half-maximum response to a flash of light that produces 23 Rh* (Kawamura and Tachibanaki, 2008). Cones do not saturate even in very brightly lit physiological conditions (Burkhardt, 1994), but are less sensitive and require much more light than rods in order to communicate a signal; carp cones reach half-maximum response at light intensities that produce 8,400 Rh*. The difference in responses is at least partially due to inefficient signal amplification in cones; upon stimulation, a carp cone opsin is phosphorylated about 50 times faster than a carp rod opsin. In its brief period of activity, cone Rh* catalyzes only a thirtieth as much transducin activation as rods do, and active cone transducin stimulates PDE activation about a tenth as quickly as in rods (Kawamura and Tachibanaki, 2008).

While the physiology of phototransduction is qualitatively the same in rods and cones (outlined above), the quantitative differences in signal propagation may lie mainly in the efficiencies of differing paralogs of the phototransduction machinery expressed in cones and rods. However, there are structural differences that might explain the differences in cone/rod responses to light. The rod outer segment is typically longer and more densely packed with its opsin than the cones (Fain et al., 2010), and rods have longitudinal plasma membrane invaginations along their outer segments called incisures, thought to aid in propagating signals from local photon responses to the rest of the cell (Caruso et al., 2006).

1.1.5 Retinal histogenesis

The first step in retinal development is the production of the eye field from the embryonic forebrain (Wong, 2006). First, bilateral optic vesicles evaginate from the forebrain, and extend to touch the ectoderm. Ectoderm contacted by the optic vesicle is

instructed to a lens placode fate, and together with the contacting region of the optic vesicle, begins to fold into the vesicle as it becomes the optic cup. As the vesicle collapses into a cup linked by a thin stalk to the forebrain, the lens placode becomes the lens vesicle, eventually budding off from the rest of the ectoderm and eventually becoming the lens. The optic cup collapses further, eliminating much of the lumen between the outer and inner layer, which differentiate into the retinal pigment epithelium and the neural retina, respectively. The neural retinal cells proliferate, becoming the retinal progenitor cells that ultimately give rise to all the major cell types of the mature retina.

Retinal progenitor cells exit the proliferative cycle and differentiate into their final cell types in an order that is stereotyped across tetrapods, and similar in fishes, examined by determining cells born during a BrdU or tritiated thymidine pulse/chase birthdating experiment. In tetrapods, the order of cell birth occurs in two phases; the first phase is quick in all species examined, and produces the retinal ganglion cells, then the horizontal cells, and then the cones (Rapaport, 2006) (Table 1.1). After a period of time of proliferative growth, a second, slower phase begins, producing the Müller glia, bipolar cells, and the majority of rods. In the monkey, amacrine cells are generated during the second phase (la Vail et al., 1991); in the rat, during the otherwise proliferative interphase period (Rapaport et al., 2004); in the mouse and quokka (Harman and Beazley, 1989), displaced amacrine cells are generated in the first phase and orthotopic amacrine cells in the second phase; and in the chicken and frog, during the first phase (Prada et al., 1991; Wong and Rapaport, 2009). The significance in the variability in amacrine cell generation among vertebrates is not understood. Interestingly, the marsupial quokka generates its horizontal cells in Phase2 (Harman and Beazley, 1989), at odds with all other species in this section; the significance of this is not understood. A significant limitation to these studies is the contemporary lack of cell type-specific markers to enable identification of cells studied; in most cases, cells were determined to be photoreceptors due to the nuclei being localized in the photoreceptor-only outer nuclear layer, but a distinction between rods and cones was not possible. Indeed, more careful analysis revealed that at least in rat, a small number of rods are born early, perhaps in Phase1, and apparently wait as post-mitotic, undifferentiated cells until the

majority of rods are born during Phase2 (Morrow et al., 1998), at which time they being to express detectable rod markers.

In the fishes, ganglion cells are the first cells to exit the cell cycle in developing retinas (Table 1.1) (Hollyfield, 1972; Nawrocki, 1985; Sharma and Ungar, 1980), as in tetrapods. They are followed by amacrine cells, bipolar cells, Müller glia, horizontal cells, and the majority of photoreceptors; the contemporary lack of markers precludes discriminating between rods and cones. However, in these fish, the larval retinas are cone-dominated, so most photoreceptors described in these works would have been cones. Broadly then, it seems that the bipolar cells and Müller glia are produced early, in Phase1 of fish, but later, in Phase2 of tetrapods. Or, if one excludes retinal ganglion cells from being produced in a “phase”, then the Phases are [cones + horizontal cells] and {bipolar cells, Müller glia, and rods}; the order of these phases are then switched in tetrapods versus the fishes, and amacrine cells remain difficult to assign.

Species	Phase1			Inter.	Phase2			
Mouse[1,4]	RGC	Cones, HC, AC			Rods, BPC, Müller glia			
Rat[2]	RGC	HC	Cones	AC	Rods	BPC/MG		
Rhesus monkey[3]	RGC, HC	Cones		AC	Müller glia, BPC, rods			
Quokka[4]	RGC, cones, some AC				Rods, HC, BPC, MG, some AC			
Chicken[5]	RGC	AC	HC/PR		MG	BPC		
Xenopus[6]	RGC	HC	Cones		Rods	AC	BPC	MG
Killifish[7]	In order: RGC, AC, [BPC/ MG?], {HC/PR}							
Goldfish[8]	In order: [RGC, AC, BPC?], {MG?, PR/HC}							
Zebrafish[9]	In order: RGC, AC, BPC/MG, HC/Cone							

Table 1.1: Summary of birthdating information for various vertebrate retinal neurons.

All studies by radioautographic birthdating, except Xenopus (BrdU). Mouse[1]: (Young, 1984). Rat[2]: (Rapaport et al., 2004). Rhesus monkey[3]: (la Vail et al., 1991). Quokka[4]: (Harman and Beazley, 1989). Chicken[5]: (Prada et al., 1991). Xenopus[6]: (Wong and Rapaport, 2009). Killifish[7]: (Hollyfield, 1972). Goldfish[8]: (Sharma and Ungar, 1980). Zebrafish[9]: (Nawrocki, 1985). *?* denotes difficult interpretation without cell identity markers; author was unsure, or the data were difficult to interpret with certainty, and this assignment to birth order is with low confidence. In the teleosts shown here, retinogenesis progresses faster than in most of the tetrapods above, and these works were unable to distinguish exact order of production. Teleost details: **Killifish**: by 112hpf (stage 27), most RGC are born and perhaps a few AC. [Stage 28, 128hpf, RGC, AC, many INL and some ONL cells are post-mitotic]. {Stage 29, 144hpf, a few HC and PR cells still mitotic}. **Goldfish**: [between 30-36hpf, stages 19-21] and {60hpf, stage 23}. **Zebrafish**: 50% of cell type is postmitotic by time: RGC, 33hpf; AC, 38hpf; BPC+MG, 43hpf; HC+Cones, 48hpf. While the radioautography would have been able to label rods in the preparation of Nawrocki, he reported all ONL nuclei as cones, which I have preserved in my table. *Inter.* is *interphase*. RGC, AC, BPC, HC, PR, MG are

retinal ganglion cell, amacrine cell, bipolar cell, horizontal cell, photoreceptor, and Müller glia.

1.2 Genetic control of the production of photoreceptors

This section is split into three subsections, which deal sequentially: with genes implicated in the pro-photoreceptor specification of multi- or bipotent progenitor cells (Section 1.2.1); with genes governing the specification of rods (Section 1.2.2); and finally, with genes governing or implicated in cone specification (Section 1.2.3).

Section 1.2.1 chiefly aims to demonstrate the shared genetics that regulate the ultimate production of cones and rods. Much of the work in the field has been done in the mouse, where 97% of photoreceptors are rods (Young, 1984); thus, it is occasionally unclear when certain findings are actually shared between rods and cones, or whether the literature over-generalizes to cones when only rod markers have been assessed. I highlight this wherever relevant. The reader is advised to consult Fig. 1.3 in this section.

Section 1.2.2 aims to provide the state of our understanding of rod photoreceptor specification, and includes work published well after the start of my PhD research (2012). As for Section 1.2.1, much of this work was established in the mouse model, and where possible I review information from other model organisms. The reader is advised to consult Fig. 1.4 in this section.

Section 1.2.3 aims to provide a current understanding of cone specification, including of the cone subtypes. Much of the research with clear genetic links to Section 1.2.1 and 1.2.2 has been done in the mouse. However, there is information available for non-murine models, which I detail where possible. The reader is advised to consult Fig. 1.5 and Fig 1.6 for this section.

At the start of my program and up until now, very little work has been published to bridge the findings of mouse photoreceptor specification and non-mammalian photoreceptor specification. That is a major motivator for undertaking the research in Chapter 4, where I examine the role of a gene from Section 1.2.2 in the generation of zebrafish photoreceptors.

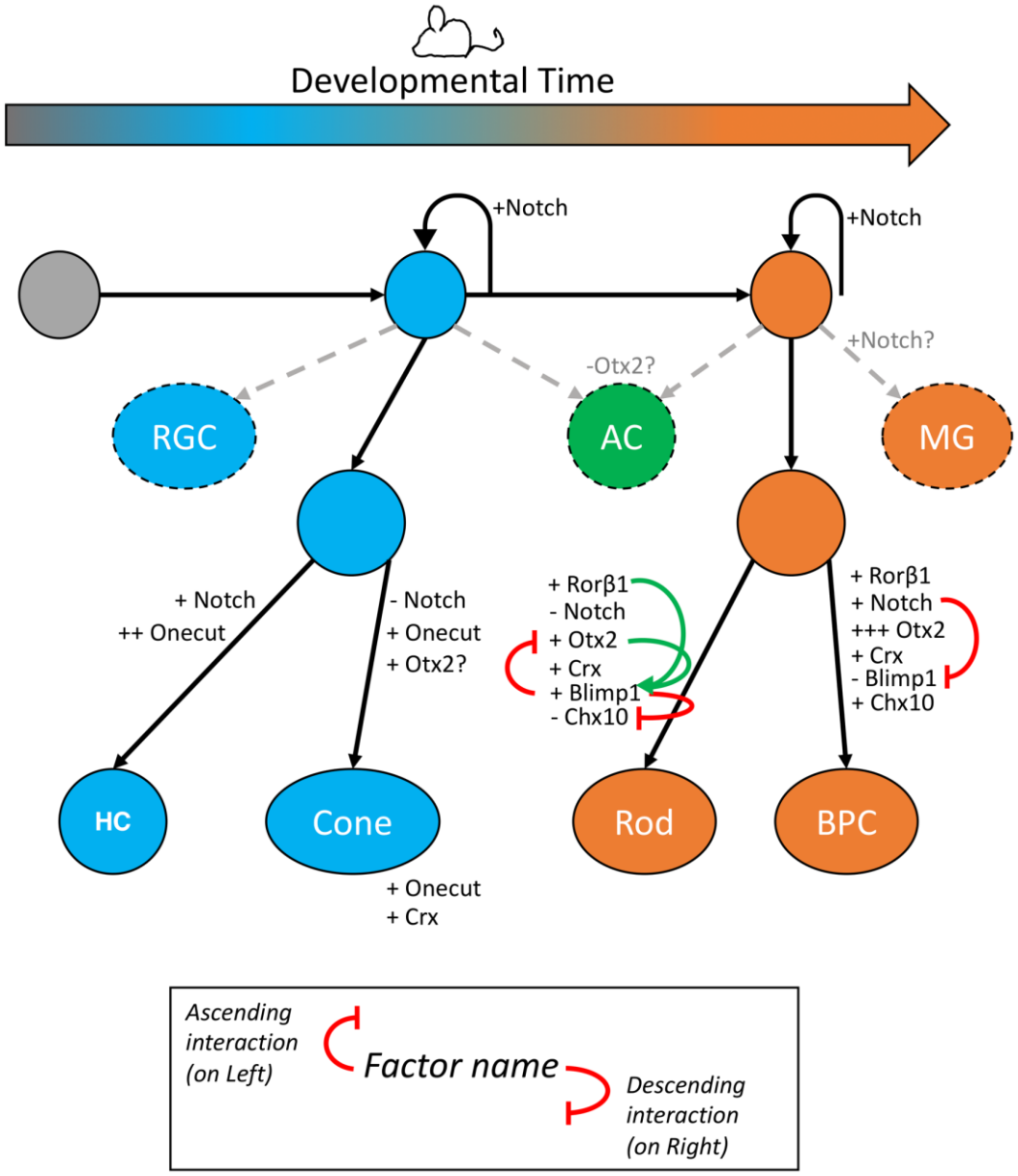

Figure 1.3: Schematic summary of the genetic network governing specification of the rod and cone precursor cells from the proliferating retinal progenitor cell population.

This information is based on literature derived from the mouse model. Colour scheme is as in Table 1.1, to improve ease of comparison. To disambiguate clustered genetic interactions: for a given factor, interaction schematics emanating from the right side of a factor regulate a lower factor, while those emanating from the left regulate a factor positioned above. RGC, AC, BPC, and HC are retinal ganglion cell, amacrine cell, bipolar cell, and horizontal cell.

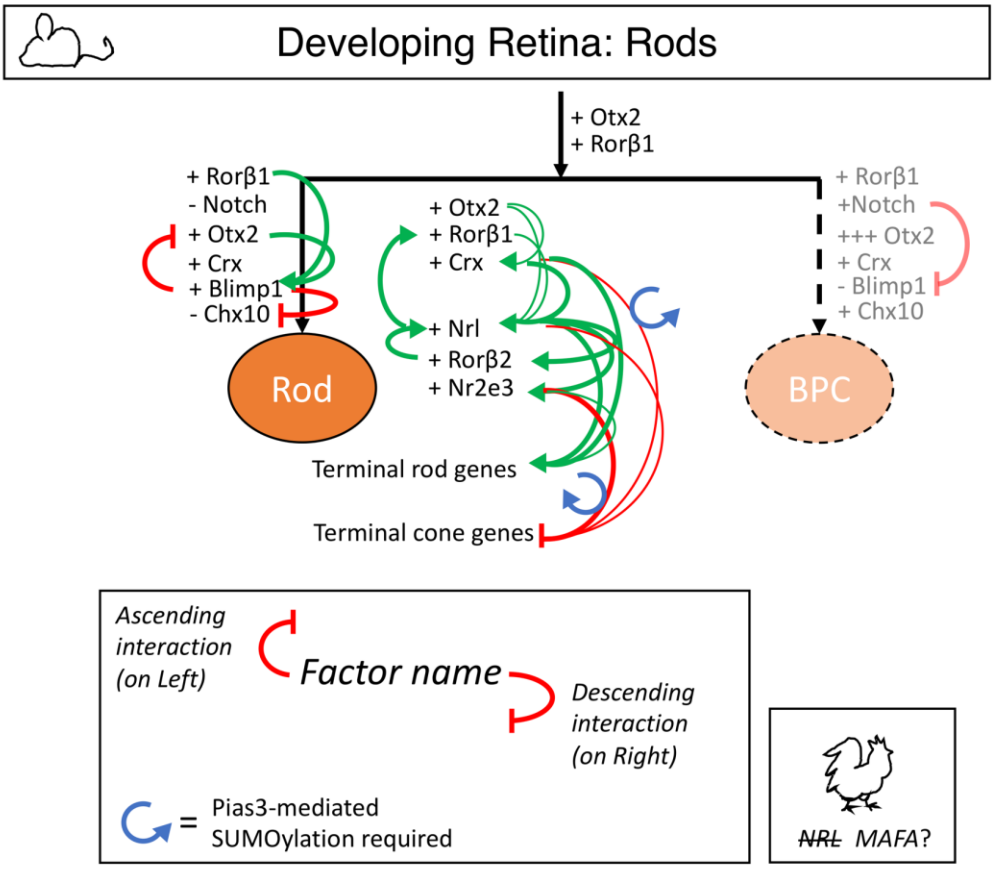

Figure 1.4: Schematic summary of the genetic network governing specification of the rod cells from a bipotent progenitor.

This information is based on literature derived from the mouse model, with a note about the proposed role for *MAFA* in chicken where indicated. Colour scheme is as in Table 1.1, to improve ease of comparison. To disambiguate clustered genetic interactions: for a given factor, interaction schematics emanating from the right side of a factor regulate a lower factor, while those emanating from the left regulate a factor positioned above. BPC is bipolar cell.

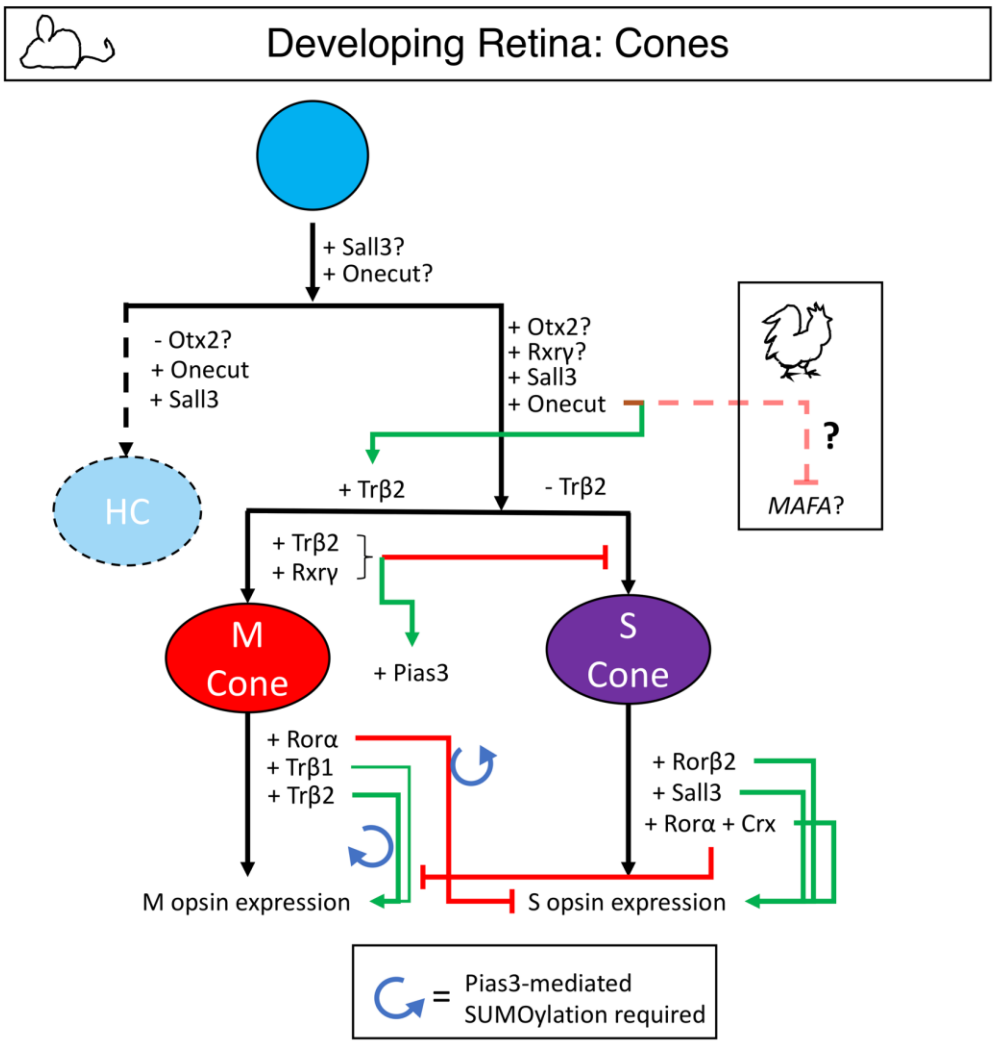

Figure 1.5: Schematic summary of the genetic network governing specification of the cone cells from a bipotent progenitor.

This information is based on literature derived from the mouse model, with a note about the proposed role for *MAFA* in chicken where indicated. Colour scheme has been modified from Fig. 1.3-1.4, to improve ease of comparison between the mouse and tetrachromat (Fig. 1.6) cone specification schematics. Typically, S cones are coloured with blue and M cones with green to reflect general views about their function in the mouse retina, but here I have coloured them to match the homologous cone type in the tetrachromat retina (Fig. 1.6). HC is horizontal cell.

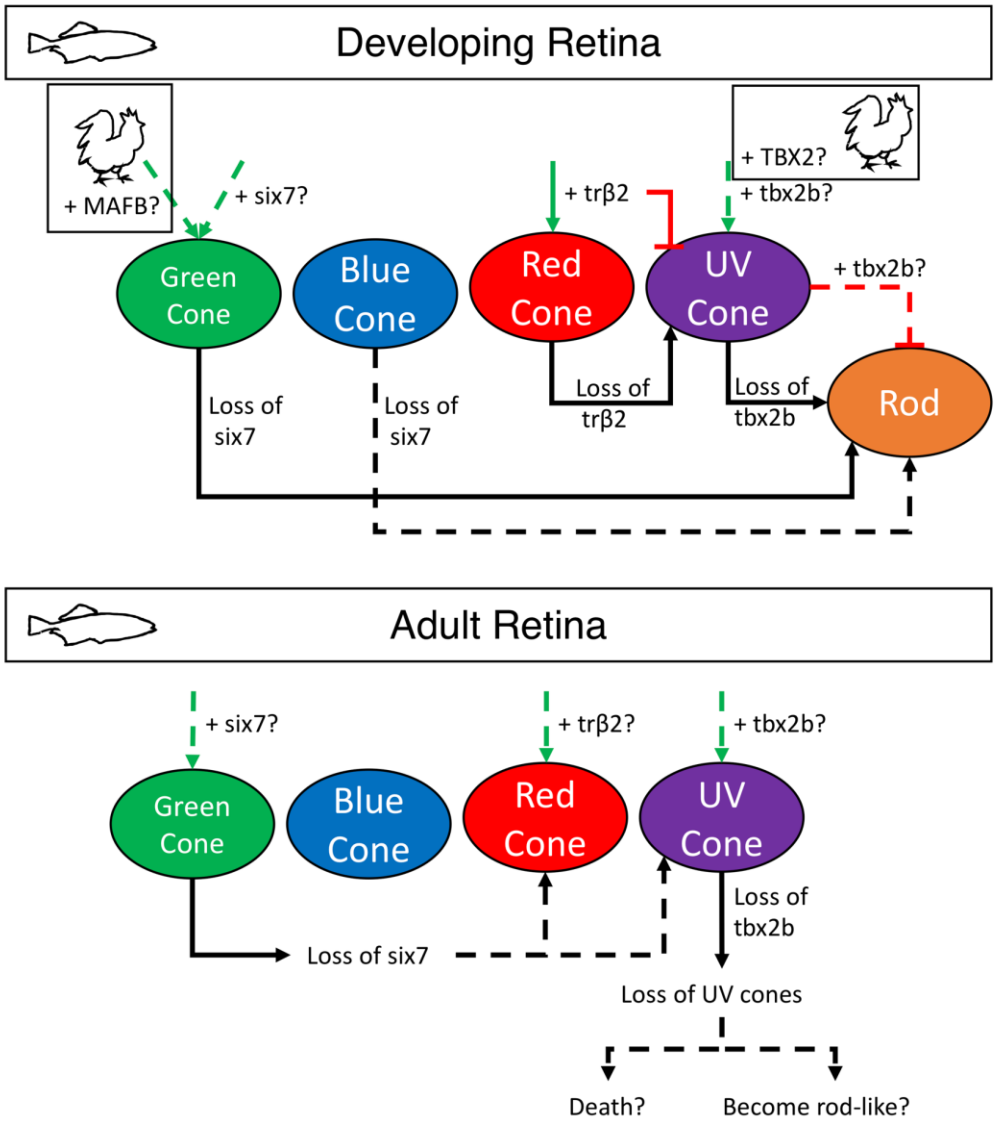

Figure 1.6: Schematic summary of the genetic network governing specification of the cone cells from a bipotent progenitor.

This information is based on literature derived from the zebrafish model, with a note about speculative roles for *MAFB* and *TBX2* in chicken where indicated. Colour scheme has been modified from Table 1.1 and Figures 1.3 and 1.4, to improve ease of comparison between the mouse (Figure 1.5) and tetrachromat cone specification schematics. Black lines indicate the broadly accepted interpretation of phenotype for a given mutation; for example, in larval zebrafish, *tbx2b* mutation has been proposed to lead to transformation of UV cone-fated cells to rods. Dashed lines indicate prediction of mechanism or phenotype, where direct demonstration is currently lacking.

1.2.1 Specifying the photoreceptor lineage

1.2.1.1 Notch

Notch is the transmembrane receptor of an eponymous paracrine signaling pathway that appears to regulate when retinal progenitor cells leave the cell cycle and begin to differentiate. Modulation of retinal Notch signaling has been accomplished by overexpression of its ligand Delta in *Xenopus laevis* (Dorsky et al., 1997), and in mouse by Cre/lox-mediated conditional ablation of the Notch receptor at various timepoints in retinal development (Jadhav et al., 2006; K. Mizeracka et al., 2013; Karolina Mizeracka et al., 2013; Yaron et al., 2006). Directly Notch-regulated downstream transcription factors have been mutated, such as *Hes1* (Tomita et al., 1996), and ectopically overexpressed, such as *Id1/3* and *Nrarp* (K. Mizeracka et al., 2013), in order to examine Notch function in retinal development. These disruptions of Notch signaling during early retinal development led to precocious birth of over-abundant cone photoreceptors (Jadhav et al., 2006) and fewer ganglion cells and horizontal cells (Yaron et al., 2006), while later disruption yielded almost exclusively rods at the expense of bipolar cells and Müller glia (K. Mizeracka et al., 2013). In the zebrafish, loss of Notch signaling impairs retinal progenitor proliferation (Uribe et al., 2012), in conservation with the findings above from mouse; Notch signaling in zebrafish has been examined predominantly from the perspective of retinal regeneration (Elsaeidi et al., 2018; Taylor et al., 2015; Wan and Goldman, 2017; Wilson et al., 2016), and it is currently not clear to what extent developmental mechanisms are recapitulated during retinal regeneration in fish.

Cumulatively, it appears that Notch signaling keeps retinal progenitors in the cell cycle, but also represses the photoreceptor fate and permits production of horizontal and bipolar cells, and eventually Müller glia. Blocking Notch signaling early, when cells can still become most cell types, causes cells to take the cone fate. Later, after the competence window for retinal progenitor cells has narrowed to just rods, bipolar cells, and Müller glia, blocking Notch leads only to over-production of rods rather than cones, at the expense of the other cell types within the competency window.

1.2.1.2 Otx2

Orthodenticle homeobox2 (*Otx2*) is a paired-like homeodomain gene which regulates the early differentiation of photoreceptors. *Drosophila orthodenticle* is expressed throughout the central nervous system during development (Finkelstein et al., 1990). The specific expression of *otd* in fly photoreceptors is regulated by an intron, and mutation of just this region allows otherwise wildtype development of the animal (Vandendries, E.R., Johnson, D., Reinke, 1996). *Otd* is involved in photoreceptor morphogenesis and directly activates two fly opsins, repressing another, and preventing their co-expression (McDonald et al., 2010). In the vertebrates, *Otx1*, *Otx2*, and *Crx* are all homologs of the single fly *Otd*. *Otx1* is primarily involved in cortical development in the mammalian CNS (Pantò et al., 2004), and not discussed further here.

In the mouse, *Otx2* is expressed in the developing anterior CNS, including the forebrain and eye. In the adult, it is expressed in the bipolar cells, photoreceptors, and retinal pigment epithelium (Samuel et al., 2014). *Otx2* expression is regulated by at least two enhancer sequences. The first promotes *Otx2* expression in photoreceptor precursors undergoing their terminal mitosis (Emerson and Cepko, 2011). The second *Otx2* enhancer is bound and repressed by Notch-induced Hes/Hey proteins, and probably stimulated by the Rax transcription factor (Muranishi et al., 2011). Complete *Otx2* knockout is embryonic lethal, but photoreceptor-specific conditional ablation of *Otx2* blocks photoreceptor development (Nishida et al., 2003). Loss of *Otx2* before photoreceptor specification, using viral transfection in early retinal progenitor cells, showed a specific depletion of rods and bipolar cells, with an increase generation of amacrine cells (Koike et al., 2007). In the production of progenitor cells which can become rods or bipolar cells, Otx2 directly induces the expression of *Blimp1* (discussed below), which negatively regulates *Otx2*, lowering but not abolishing *Otx2* expression, and promotes the photoreceptor fate (S. Wang et al., 2014). Interestingly, high levels of Otx2 instead promote *Chx10* expression and promotes bipolar cell fate; overexpression of *Otx2* in Blimp1+ (rod-fated) cells redirects them back to the bipolar cell fate, while short hairpin RNA-mediated knockdown of *Otx2* in Blimp1- cells expands the proportion of rods generated at the expense of bipolar cells (S. Wang et al., 2014). A major role of *Otx2* in specifying photoreceptors is to initiate *Crx* expression, which redundantly binds

~70% of the same targets as Otx2 in the neural retina (Samuel et al., 2014). A current model for the interplay between Otx2 and Crx is that Otx2 activates several early photoreceptor genes, including *Crx,* and then Crx eventually takes over the continual stimulation of these genes as *Otx2* expression subsides during photoreceptor maturation (Montana et al., 2011).

Otx2 appears to support photoreceptor differentiation by enabling the decision between bipolar cell and photoreceptor fate; without *Otx2*, progenitors become amacrine cells and do not reach this decision point. Factors downstream of *Otx2*, such as *Blimp1* determine whether Otx2+ cells become photoreceptors or bipolar cells. With strong *Crx* expression, the cells differentiate as photoreceptors. Mature photoreceptors express very little *Otx2*, as its role in maturing photoreceptors is eventually assumed by the closely related Crx.

1.2.1.3 Blimp1

B-lymphocyte-induced maturation protein1 (Blimp1), also known as PR domain-containing 1 (Prdm1) is a zinc finger transcription factor, and functions mainly as a transcriptional repressor, by histone deacetylation (Yu et al., 2000) and/or methylation (Ancelin et al., 2006). It is well studied in the context of germ cell (Vincent, 2005) and immune system development (Turner et al., 1994), but only lightly studied in sensory neuron biology, starting in 2004 (Roy and Ng, 2004).

Blimp1 is required transiently for the normal production of rods, and mediates a rod versus bipolar cell fate decision. *Blimp1* was first implicated in photoreceptor development by strong down-regulation in a gene expression profile of conditional *Otx2* knockout retinas, where developmentally-early *Dkk3:Cre*-mediated *Otx2* deletion blocked production of photoreceptors, among other cell types (Katoh et al., 2010). Nascent photoreceptors transiently express *Blimp1*, and *Blimp1* knockout blocks photoreceptor development and increases bipolar cell abundance (Brzezinski et al., 2010; Katoh et al., 2010), while ectopic expression of *Blimp1* inhibits the bipolar cell fate in favor of the photoreceptor fate (Brzezinski et al., 2010). Expression of *Blimp1* is directly stimulated by a combination of Rorβ and Otx2 (S. Wang et al., 2014), and blocked by Notch signaling (Karolina Mizeracka et al., 2013; S. Wang et al., 2014).

Blimp1 directly represses the bipolar cell specifier *Chx10* (Katoh et al., 2010), itself (S. Wang et al., 2014), and *Otx2* in a negative feedback loop that attenuates but does not fully extinguish *Otx2* expression (S. Wang et al., 2014).

Cumulatively, Otx2 creates a scenario where precursor cells can become either bipolar cells or rods, and *Blimp1* expression promotes the rod outcome. Rorβ can promote *Blimp1* expression, while Notch signaling can antagonize it, and *Blimp1* expression biases the rod versus bipolar cell fate decision to the rod fate, apparently by blocking bipolar cell gene expression and by lowering *Otx2* expression, permitting *Otx2* to activate *Crx*, eventually leading to photoreceptor gene expression. *Blimp1* expression is not maintained in mature photoreceptors.

1.2.1.4 Onecut

Onecut proteins are transcription factors with both homeodomains and cut domains (Nguyen et al., 2000). Cut homeodomain proteins can have multiple cut domains, which directly bind DNA. Onecut proteins have a single cut domain, and in *Drosophila*, Onecut directly activates expression of a visual opsin gene (Nguyen et al., 2000). *Onecut* is expressed in developing fly neurons, and strongly expressed in developing and mature adult retinal photoreceptors. *Onecut* is necessary but not sufficient for fly photoreceptor specification (Nguyen et al., 2000).

In mammals, *Onecut1* and *-2* likely act redundantly in the retina; single knockout mice have impaired generation of horizontal cells with extra generation of photoreceptors (Wu et al., 2013, 2012), and double knockout mice completely fail to generate horizontal cells (Emerson et al., 2013; Klimova et al., 2015; Sapkota et al., 2014). In the first phase of retinal progenitor cells exiting the cell cycle (Table 1.1), *Onecut* mutants completely fail to generate horizontal cells, while cones production is delayed but ultimately generated at 70% normal abundance (Sapkota et al., 2014). Ectopic expression of *Onecut* during normal rod generation (Phase 2, Table 1.1) induced cone and horizontal cell markers and morphology at the expense of rod markers, although these ectopic cone-like cells did not appear to complete maturation as cones (further details unclear) (Emerson et al., 2013). This indicates that *Onecut* promotes horizontal cell fate at time when retinal progenitor cells can become either

cones or horizontal cells. However, once committed to the cone fate, Onecut proteins appear to directly stimulate cone-specifying genes such as *Trβ2*, and probably antagonize rod specification indirectly through somehow inducing *Nrl* repression (Emerson et al., 2013). There is currently no evidence that Onecut proteins directly bind to *Nrl* regulatory sequence.

At this time, it appears that Onecut proteins play two roles in the specification of retinal neurons; at an early timepoint, Onecut regulates horizontal cell versus cone fate decisions, promoting horizontal cell development. Later, Onecut acts to promote cone differentiation, and possibly to repress rod differentiation, although they are neither sufficient to fully differentiate cones at the expense of rods, nor fully required for the development of cones.

1.2.1.5 Crx

Cone-rod homeobox (*Crx*) is another vertebrate homolog of *Drosophila orthodenticle*; in mammals, the three homologs are *Otx1*, *Otx2*, and *Crx*, and *otd* mutation in flies can be rescued by expression of any of these three vertebrate homologs (Terrell et al., 2012). In non-mammalians such as fish, lizards, turtles, and birds, *otx5* has been described (Gamse et al., 2002; Plouhinec et al., 2003), and mammalian *Crx* may in fact be the remaining member of an ancestral pair, *Crx* and *Otx5* (Plouhinec et al., 2003).

Crx is a master effector transcription factor required for the normal expression of many mature photoreceptor genes. It was independently discovered and published by three groups in 1997 (Chen et al., 1997; Freund et al., 1997; Furukawa et al., 1997), as a direct activator of rhodopsin expression and a locus to which many human visual diseases mapped. *Crx* mutation does not block the specification of rods and cones, but mutant photoreceptors show abnormal synaptic morphology (Morrow et al., 2005), fail to make outer segments (Furukawa et al., 1999; Morrow et al., 2005), fail to express numerous phototransduction machinery genes properly, and the photoreceptors have no electrophysiological response to light (Furukawa et al., 1999). *Crx* expression requires direct activation by Otx2 (Nishida et al., 2003), although Crx later stimulates expression of itself, and directly activates the expression of most photoreceptor

specification and phototransduction genes of both rods and cones (Corbo et al., 2010), as well as photoreceptors in the non-visual photoreceptors of the pineal gland (Rovsing et al., 2011). Interestingly, genomic sequences for which Crx has high binding affinity tend to be repressed by Crx activation; low affinity predicts activation by Crx, while high affinity binding sites together with dimerization with a binding partner like Nrl can cause normally repressive Crx action to become stimulatory (White et al., 2016).

Crx is critically important for the proper development of photoreceptors, but does not mediate specification alone. Instead, it works with rod and cone-specific genes to regulate type-specific targets that enable the terminal differentiation of the various photoreceptors.

1.2.1.6 Summary schematic of photoreceptor lineage specification

As summarized in Fig. 1.3, Notch signaling regulates when proliferative retinal progenitor cells exit the cell cycle; cells that leave the cycle during the first phase of terminal mitoses (Table 1.1) are competent to become at least cones and horizontal cells in mammals, and Onecut activity promotes the horizontal cell fate. Cells that exit the cell cycle later, during the second phase of terminal mitoses (Table 1.1, Fig. 1.3) can become at least bipolar cells or rods in mammals. *Otx2* expression supports both fates, but together with Rorβ (discussed in next section) can activate expression of *Blimp1*, which represses the bipolar cell fate, and attenuates *Otx2* expression, and then represses itself as the photoreceptors express *Crx* and mature into rods, eventually decreasing *Otx2* expression further. Notch signaling represses *Blimp1*, allowing some Otx2+ cells to maintain high levels of *Otx2* expression, and then to express bipolar cell differentiation factors such as *Chx10*.

1.2.2 Specification of rods

1.2.2.1 Rorβ

Retinoid-related orphan receptor β (*Rorβ*) is broadly expressed in the developing CNS as well as retina and pineal tissues, but has a retina and pineal photoreceptor-specific isoform, *Rorβ2* (André et al., 1998). Rorβ2 differs from Rorβ1 at the N-terminus;

the first two amino acids of the β1 isoform are replaced by 13 different ones in the β2, and these restrict what DNA sequences it binds to, but enhances the potency of activation of reporter genes (André et al., 1998). The two isoform-specific N-terminal peptide stretches are part of the DNA binding domain, the common element of which extends for a further 95 amino acids (Liu et al., 2017). Where the isoform reported in this review is not known, Rorβ is used instead of isoform-specific notation.

Rorβ2 plays a role in the differentiation of cones (discussed below), but is an important regulator of the rod fate as well, where it has been studied chiefly in the mouse. Rorβ directly binds the promoter of *Nrl* (below) (Kautzmann et al., 2011), and its promoter is itself bound by Nrl, which enhances the production of the *Rorβ2* isoform in a positive feedback loop (Fu et al., 2014). The *Nrl* promoter element bound by Rorβ is also bound by Otx2 and Crx (Montana et al., 2011), but the binding sites are not conserved in chicken or fish (Kautzmann et al., 2011), implying possible divergent mechanisms in mammals. *Rorβ* knockout mice do not make rods, and instead have overabundant, non-functional S cones (Jia et al., 2009). This phenotype can be rescued by ectopic expression of *Nrl* using a *Crx* promoter, indicating that the rod-specific role for *Rorβ* is to induce *Nrl* expression, which then induces expression the *Rorβ2* isoform. In the *Rorβ* mutant, *Crx* and *Otx2* are both downregulated (Jia et al., 2009), suggesting that Rorβ also positively regulates these genes. There is some evidence, predating the discovery of the *Rorβ2* isoform, that *Rorβ* is expressed weakly in horizontal cells and bipolar cells (Chow et al., 1998), and a later *Rorβ1*-specific knockout mouse failed to produce amacrine and horizontal cells, but still produced bipolar cells (Liu et al., 2013). *Rorβ1*-specific disruptive GFP knock-in showed specific expression in amacrine cells horizontal cells, and bipolar cells expressed the GFP knock-in (Liu et al., 2013), and thus, *Rorβ1* is expressed in cells which can become any of amacrine, horizontal, or bipolar cells, but bipolar cells do not require it. As Rorβ activates expression of *Blimp1* (discussed above), which is expressed in the shared progenitors of rods and bipolar cells and promotes the rod fate (S. Wang et al., 2014), bipolar cells probably have a developmental history of *Rorβ* expression but do not require it.

Rorβ is broadly expressed in CNS tissues including the retina. The default isoform, *Rorβ1*, is involved in the production of non-photoreceptor subtypes. The

photoreceptor-specific isoform *Rorβ2* is expressed in both cones and rods. In rods, *Rorβ* is part of the initial expression of the key rod specification gene, *Nrl*, which then specifically activates expression of *Rorβ2*, which further stimulates *Nrl* and possibly *Crx* and *Otx2* as well. Rorβ2 is possibly a binding partner for Otx2 and/or Crx, mediating expression of a suite of photoreceptor-specific genes.

1.2.2.2 Nrl

Neural retina-specific leucine zipper (*Nrl*) is a member of the Maf family of transcription factors, which belong to the basic leucine zipper (bZIP) superfamily of transcription factors. The basic leucine zipper domain has two major elements: a leucine zipper used to bind with various binding partners; and an adjacent 18 amino acid stretch of basic residues used to bind DNA (Yang and Cvekl, 2007). The Maf family of bZIP transcription factors has two groups, the large and small Mafs. The small Mafs have only the bZIP domain, while the large Mafs have an additional DNA binding domain termed the ancillary or extended homology domain, which is located near the bZIP domain. The large Mafs also have an N-terminal transactivator domain (Friedman et al., 2004), a 100 amino acid stretch enriched for serine, proline, and tryptophan (Yang and Cvekl, 2007). *Drosophila* has a single large Maf, *trafficjam*, while jawed vertebrates have four: *cMaf*, *MafA*, *MafB*, and *Nrl*. *Nrl* is encoded in mammals and in zebrafish as 4 exons, while the remaining large *Mafs* are encoded in single exons. All three large *Mafs* have a clear role in vertebrate lens development (Reza and Yasuda, 2004; Yoshida and Yasuda, 2002), and *Nrl* has weak and transient but detectable expression in the mouse lens (Liu et al., 1996).

Nrl is a central node in the rod specification pathway. The *Nrl* knockout mouse fails to make rods (Jia et al., 2009; Mears et al., 2001; Yoshida et al., 2004), and cells originally destined to become rods instead become a cone-like cell that resembles the S-cone (Daniele et al., 2005; Mears et al., 2001; Nikonov et al., 2005). *In situ* hybridization and transgenic expression of eGFP under *Nrl* regulatory sequences demonstrates it is expressed robustly and continuously in rods shortly after terminal mitosis and into adulthood (Akimoto et al., 2006). Cre expression under the same sequences demonstrates that all retinal cells with even brief *Nrl* expression become rod

photoreceptors (Brightman et al., 2016). The cone-like photoreceptors of the mutant mouse disrupt the laminar structure of the ONL (Daniele et al., 2005; Mears et al., 2001), with numerous “rosettes” of delaminated photoreceptors forming along the retina. These degenerate until late adulthood, when the remaining cone-like cells persist in a wildtype-like laminar arrangement in the retina (Roger et al., 2012). Ectopic *Nrl*, expressed under *Crx* regulatory regions, is sufficient to completely re-program all photoreceptors to rods (Oh et al., 2007), although later expression under the S-opsin promoter causes the cells to look rod-like but not to function as rods or cones, and are likely non-functional (Oh et al., 2008). Nrl exists in photoreceptors at multiple levels of phosphorylation (Kanda et al., 2007; Swain et al., 2001), requires sumoylation for its proper activity (Roger et al., 2010), and is possibly regulated by microRNAs post-transcriptionally (Sreekanth et al., 2017). Nrl has a primarily activating role, and dimerizes with Crx to directly regulate dozens of rod-specific terminally differentiated genes (Hao et al., 2012; Mitton et al., 2000), and with an E3 SUMO ligase Pias3 (Onishi et al., 2009), but also acts through four key secondary effector transcription factors, including *Nr2e3* (discussed below) (Kim et al., 2016a) which chiefly acts to suppress cone genes (Jia et al., 2009; Kim et al., 2016a; Oh et al., 2008). *Nrl* expression is directly activated by Otx2 (Kautzmann et al., 2011; Montana et al., 2011) and Rorβ (Fu et al., 2014; Jia et al., 2009; Khanna et al., 2006; Montana et al., 2011), and Nrl positively feeds back onto *Rorβ* and stimulates expression of the photoreceptor-specific *Rorβ2* isoform. Postnatally, the role for Otx2 in *Nrl* expression wanes and is replaced by the activation from the related Crx (Montana et al., 2011), which persists for the life of the photoreceptor. Nrl requires SUMOylation at two residues for activity, although this does not appear to require Pias3 (Roger et al., 2010).

In humans, *NRL* mutation is chiefly associated with retinitis pigmentosa and clumped pigment type retinal degeneration, two degenerative diseases that cause progressive loss of photoreceptors, and consequently, of vision. Dominant human *NRL* variants are not commonly associated with Enhanced S cone Syndrome (ESCS) (Acar et al., 2003), but 11 patients with homozygous recessive *NRL* variants have been identified to date (Littink et al., 2018). In two of these, rod function was reduced, while S cone function was at least normal (Nishiguchi et al., 2004); in four others, no ESCS was

reported, although they had retinitis pigmentosa, and in two more, the patients had mutations in at least one other ocular disease gene (Newman et al., 2016). The three latest identified cases of recessive *NRL* variants did show an ESCS-like phenotype, including loss of rod-mediated electrophysiological responses to light and a slightly exaggerated response to blue light, but not to a similar magnitude as in *NR2E3* variant ESCS (Littink et al., 2018). It has not been examined if these patients have rods which do not contribute to a response to light, or if they in fact have more S cones; optical coherence tomography (OCT) and fundoscopy of the patients with recessive *NRL* variants showed normal retinal layering in the macula, aside from retinopathy (Littink et al., 2018). Thus, it is not clear if a switch from rod to cone phenotype is occuring in humans with recessive *NRL* variants.

Zebrafish express *nrl* in the photoreceptor layer during development (Coolen et al., 2005; Nelson et al., 2008), but it is not obviously specific to rods, and may not persist in specified rods even in larvae (Nelson et al., 2008; Stenkamp, 2011), although the *nrl* transcript has been detected in adult rods (Sun et al., 2018). *Xenopus* retinas lipofected with human or frog *Nrl* showed enhanced production of rhodopsin, suggesting some functional conservation, but only frog *Nrl* and not human *NRL* was able to influence lens fibre development in the same experiments, implying evolutionarily divergent roles (McIlvain and Knox, 2007). The bird lineage appears to have lost *NRL*, but maintains rods, and probably relies on *MAFA* expression to specify rods (Enright et al., 2015a; Ochi et al., 2004), although this has not been directly tested. Lamprey have branched off very early in vertebrate evolution, and there is still no consensus as to whether they have homologous or convergently evolved rod-like photoreceptors. Therefore, while the role of mammalian *Nrl* is quite well-established, differing roles for *nrl* in tetrachromat eyes is plausible.

Taken together, Nrl is necessary for rod specification in mammals, without which cells become cones, and expression in developing cones is sufficient to reprogram them to rods. Nrl is primarily an activator of transcription, and pairs with Crx to directly activate expression of dozens of rod-specific genes. It is treated as the primary node of photoreceptor type specification in mammals, and indirect assays of Nrl function outside of mammals suggest it has similar activity in most vertebrates.

1.2.2.3 Nr2e3

Nuclear receptor subfamily 2 group E member 3 (Nr2e3) or photoreceptor-specific nuclear receptor (PNR) is an orphan nuclear receptor, of the steroid receptor superfamily. Nuclear receptors have DNA-binding, hinge, and ligand binding domains, as well as protein-interaction domains known as the D-box, and can bind DNA in monomers or more commonly as homo- or heterodimers (Zhao et al., 1998). Defects in the *Drosophila* homolog, *unfulfilled* (*unf*), do not specifically lead to obvious retinal photoreceptor defects, but instead to numerous other problems, including eclosion failure and subfertility (Sung et al., 2009), but specifically including coordination defects due to mushroom body neuronal specification and maturation defects. The neurons of the mushroom body fail to maintain coherent specification as a specific subtype (Bates et al., 2010; Lin et al., 2009), and the small ventral lateral neurons involved in circadian rhythm are unable to maintain a rhythm without light entrainment (Beuchle et al., 2012). Thus, the *Drosophila Nr2e3* homolog is involved in cell fate maintenance during neural development, if not in retinal photoreceptor differentiation.

In mammals, Nr2e3 is a primary downstream effector protein for Nrl, and directly represses cone gene expression in rods, and perhaps has some ability to stimulate rod genes. In humans and mice, *Nr2e3* loss of function leads to rods developing with functional S cone phenotypes; S cones are hyper-abundant in the retina, and rods are typically absent (Akhmedov et al., 2000; Cheng et al., 2011; Haider et al., 2001, 2000; Milam et al., 2002). Physiological recordings of retina function show a supernormal response to short wavelength light stimulation (an S-cone property) and almost complete lack of response to dim illumination in green light, which is the preferred wavelength for rods. M cones, which detect greenish light at brighter intensities, are not affected in *Nr2e3* mutants. The outer nuclear layer of *Nr2e3*-deficient retinas is buckled, with photoreceptor rosettes forming as described for *Nrl* mutants (Haider et al., 2001; Milam et al., 2002), and in human *NR2E3*-deficient patients, S-cone opsin-positive cells are present in the inner nuclear layer. Expression is completely dependent on Nrl direct activation (Oh et al., 2008) and is normally restricted specifically to rod photoreceptors (Cheng et al., 2004). Nr2e3 directly complexes with Nrl and Crx to mediate rod-specific

gene expression (Cheng et al., 2004; Peng et al., 2005), and its most obvious roles are repressive (Chen et al., 1999), shutting down cone gene expression in rods, rather than directly activating rod gene expression (Chen et al., 2005; Cheng et al., 2006; Corbo and Cepko, 2005; Haider et al., 2009; Oh et al., 2008). However, Nr2e3 in complex with Crx and/or Nrl may mediate some rod-specific gene activation, as Nr2e3 was physically bound to the promoters of rod genes such as rhodopsin in a ChIP assay (Peng et al., 2005), and *Crx:Nr2e3* ectopic expression in the background of an *Nrl*-null retina was able to partially rescue expression of rhodopsin, although not of rod-specific transducin alpha (*Gnat1*) (Cheng et al., 2006), further indicating at least a weak ability to activate expression of rod-specific genes. The ability of Nr2e3 to repress cone gene expression is dependent on SUMOylation by Pias3 (Onishi et al., 2009).

Work in other vertebrates has suggested Nr2e3 function in photoreceptors is conserved. On the basis of photoreceptor-specific expression, high amino acid conservation to mammalian Nr2e3, and in vitro predominantly repressive activity in luciferase assays, chicken NR2E3 was assumed to have mammal-like activity (Kobayashi et al., 2008). It is unclear whether zebrafish *nr2e3* expression is rod-specific. Zebrafish *nr2e3* appears to be specifically expressed in rods in adult fish, but perhaps also in larval cone precursors during development (Chen et al., 2005). Later literature (Khuansuwan et al., 2016) cites Morris and colleagues as replicating this in 2008 (Morris et al., 2008), but Morris *et al.* merely cited Chen *et al.*, and the work by Morris and colleagues does not support the conclusion that zebrafish *nr2e3* is expressed transiently in larval cone precursors. Subsequent *in situ* hybridization and antibody staining in larval zebrafish also failed to demonstrate *nr2e3* outside of rod photoreceptors in the retina (Alvarez-Delfin et al., 2009; Nelson et al., 2008), although it is discussed as being obviously expressed in non-rod retinal cells (Nelson et al., 2008; Stenkamp, 2011). Outside the retina, *nr2e3* is expressed in the zebrafish nonvisual pineal photoreceptors, located above the brain and which are described variously as cone and/or rod-like (Khuansuwan et al., 2016). During normal zebrafish development, a subset of pineal precursor cells migrates out of the differentiating mass to form the parapineal organ, and *nr2e3* represses this transition; moreover, *tbx2b* may repress this *nr2e3*-mediated repression (Khuansuwan et al., 2016). As zebrafish *tbx2b* has some

cone photoreceptor-specifying activity (reviewed below), this could indicate a mechanism of *nr2e3* regulation in the retina, although this has not been explored. In the Atlantic cod, generation of retinal rods is extremely delayed, taking place only as the young fish metamorphose into juveniles ~37 days after hatching, and *nr2e3* expression is undetectable until this stage, suggesting that *nr2e3* expression is in fact rod-specific (Valen et al., 2016).

Cumulatively, *Nr2e3* expression is dependent on direct activation by Nrl, and is therefore rod-specific in the mammals. Nr2e3 protein complexes with Crx and Nrl to mediate rod-specific transcriptional activity. This activity is mostly the direct binding to and repression of cone-specific genes, and requires Pias3-mediated SUMOylation (Onishi et al., 2009). Nr2e3 participates in the stimulation of some rod genes, but Nrl mediates the bulk of pro-rod gene expression.

1.2.2.4 Summary schematic of rod specification

As summarized in Fig. 1.4, the rod lineage is specified by the induction of *Nrl* expression in precursor cells. *Nrl* expression is stimulated by Rorβ and Otx2. Once *Nrl* is expressed, it pairs with Otx2 and later Crx to directly activate numerous genes expressed in terminally differentiated rod photoreceptors, thereby directly constructing the rod phenotype. It also activates expression of secondary effector transcription factors like *Nr2e3*, which pair with Nrl and Crx to repress expression of cone-specific genes; cone gene repression appears to require SUMOylation of Nr2e3 by Pias3, as does rod gene stimulation by Nrl.

1.2.3 Specification of the cones

1.2.3.1 Tbx2

The T-box (Tbx) transcription factor superfamily is named after the DNA-binding domain of the founding member T, or Brachyury, and the Tbx superfamily has 17 members in mammals, grouped in 5 families. The *Tbx2* family has four members, which derive from serial duplications in early vertebrates: *Tbx2* and *Tbx4* are paralogs, and *Tbx3* and *Tbx5* are paralogs, and both groups are paralogs of each other (Sheeba and

Logan, 2017) and linked to the same chromosome. Tbx2 acts as a monomer to repress gene transcription, probably mediated through recruiting histone deacetylators using its C-terminus (Paxton et al., 2002; Sinha et al., 2000). In the mouse, *Tbx2* homozygous knockouts die mid-gestation due to heart defects, but work in both mouse and chicken show conserved activity in patterning limb bud formation (Sheeba and Logan, 2017; Suzuki et al., 2004). In the chick limb bud, TBX2 represses *BMP2* expression, relieves repression on SHH signalling, and represses GLI3 activity, showing that TBX2 is upstream of both SHH and BMP pathways. However, TBX2 is also subject to BMP regulation, as exogenous BMP4 induces *TBX2* expression in the chick limb bud as well (Suzuki et al., 2004), and disrupting expression of the zebrafish BMP ligand *gdf6a* in the earliest stages of retinogenesis blocks *tbx2b* expression (Gross and Dowling, 2005). The conservation of these expression patterns and transcriptional activity extends to frog (Takabatake et al., 2000) and zebrafish (Ruvinsky et al., 2000) as well, which maintain the syntenic arrangement of duplicated *tbx2* family members. Nothing is known about the role of *Tbx2* in specifying cell types in the mouse eye, as the mutant pups die before the retina is well developed (Sheeba and Logan, 2017), and no eye-specific conditional alleles exist.

In zebrafish, *tbx2b* mutation appears to regulate the production of UV cones and rods. In two *tbx2b* mutants, the animals develop overtly normal retinas but larvae have very few UV cones, and instead have at least twice as many rods, leading to the phenotype designation *lots of rods* (Alvarez-Delfin et al., 2009; Raymond et al., 2014). The *tbx2b*^{lor} allele is hypomorphic and animals are viable; the *from beyond* allele *tbx2b*^{fby}, isolated by Snelson and colleagues, is a null allele and produces fewer or occasionally zero UV cones, and most homozygous animals die before reaching adulthood, and are sterile if they do (Raymond et al., 2014; Snelson et al., 2008). The extra rods produced by the *tbx2b* mutations express rod opsin and *nr2e3*, and morphologically resemble rods. Reciprocal transplants between mutants and wildtype demonstrated that the role of *tbx2b* in generating UV cones is cell autonomous. The current interpretation of the *tbx2b* mutant phenotype is that UV cone-fated cells instead develop as rods instead. However, work by Raymond and colleagues undermines this; in adult zebrafish, whose retinas show annular growth like tree rings throughout their

lives, rare adult *tbx2b*^{fby} homozygotes show that UV cones are indeed generated, and apparently at normal density in the dorsal retina of the animals (Raymond et al., 2014). These UV cones do not persist in the mutant, and are lost as the new rings of retina age; this disrupts the otherwise orderly pentameric arrangement of the cone photoreceptors, and suggests that the *tbx2b* phenotype may actually be death of UV cones coupled with hyperproliferation of rods, rather than a UV cone-to-rod fate transition. However, in the larval *tbx2b*^{lor} mutants, proliferation was not increased as assayed for by BrdU pulse chase during photoreceptor development (Alvarez-Delfin et al., 2009), and in adult *tbx2b*^{fby} animals, TUNEL assays did not label UV cones, although this could be due to the transient availability of TUNEL substrate in dying cells (Raymond et al., 2014). Thus, it is presently unclear what the genetic or developmental mechanisms of *tbx2b* are in the zebrafish retina.

The only other tetrachromat model organism in which *Tbx2* has been implicated in cone specification is the chicken; *TBX2* expression was found to be tightly correlated to UV cones in a photoreceptor subtype-specific set of parallel RNAseq experiments (Enright et al., 2015a). This suggests that *Tbx2* involvement in photoreceptor development is not fish-specific, but instead conserved across vertebrates, despite the current lack of evidence in the cone-impoverished mammalian models.

At this time, the role for *Tbx2* in photoreceptor specification is broadly interpreted to be supportive of the UV cone fate at the expense of the rod fate, as mutant zebrafish larvae fail to generate normal numbers of UV cones and instead over-produce rods. In chicken, *TBX2* is expressed in developing and potentially mature UV cones, suggesting a conserved role for *Tbx2* in UV cone development. Analysis of zebrafish adult *tbx2b* null mutants suggests that the mutant UV cone paucity and rod hyperabundance are actually separate phenotypes, but this is not acknowledged in reviews which cover *tbx2b*, and the lack of other genetic tools in zebrafish, such as an *nrl* knockout, has precluded inserting *tbx2b* into the photoreceptor differentiation pathways already known.

1.2.3.2 Six7

The vertebrate *Six* genes are homologs of the *Drosophila sine oculis (so)* homeodomain gene, with mouse *Six3/6* being considered the closest pair of homologs.

Zebrafish *six7* is one of the teleost homologs of mouse *Six3* (Seo et al., 1998), and all *Six3* homologs have retinal expression early in retinogenesis, including in the optic vesicle and lens placode (Drivenes et al., 2000). A role for *six7* in photoreceptor development has only been discovered in zebrafish at this point, although its mammalian homolog Six3 has been implicated in regulating rod opsin expression (Manavathi et al., 2007).

Zebrafish *six7* mutants show disrupted ratios of green cones and rods. Due to phenotypic similarity to *tbx2b* (discussed above), the first *six7* allele was named *lor junior* (*ljr*) (Saade et al., 2013). While UV cone abundance is not affected, Saade *et al.* found that in the *six7*^{ljr} hypomorph, rods were four times as abundant in larvae, approximately as numerous as any one of the four cone subtypes, and Ogawa and colleagues independently used TALEN-mediated targeted mutagenesis to show that *six7* null larvae over-produce rods and have a variety of cone specification perturbations (Ogawa et al., 2015). Mutant larvae had doubled *rhodopsin*, *nrl*, and rod-specific transducin alpha (*gnat1*) transcript abundance, half as much of the two cone arrestins, nearly abolished green cone opsins, and halved blue cone opsin (Ogawa et al., 2015). In adult animals, rod opsin and *gnat1* transcript abundances were unchanged from wildtype, but green cone opsin transcript was still undetectable, while the proportions of the two red cone opsins (long wavelength-sensitive 1, 2) were swapped and upregulated, blue cone opsin was unchanged, and UV cone opsin was ~50% more abundant. Normally, *lws1* is expressed only in developing red cones at the retinal periphery, and mature red cones in the rest of the retina express only *lws2* normally. In the *six7* mutants, *lws2* expression was abolished in the central retina, and *lws1* was four times as abundant as usual, and expressed throughout the retina. The authors do not report the expression levels of *trβ2* (reviewed below), a potent regulator of red cone fate and an obvious gene of interest given the phenotype. Ogawa and colleagues also do not examine *tbx2b* expression in these mutants, although this is looked at subsequently (Sotolongo-Lopez et al., 2016). Sotolongo-Lopez and colleagues evaluated the larval phenotypes in the *six7*^{ljr} allele, finding mutant rod super-abundance to be semidominant (heterozygotes have an intermediate increase in rods relative to homozygotes and wildtype siblings), and cumulative with *tbx2b* mutant rod super-abundance. This is

consistent with a scenario where *tbx2b* mutant UV cones become rods, as do *six7* mutant green cones. Refuting this scenario, however, green cone paucity varies between *six7* mutants, while the rods are invariably super-abundant. The *six7* mutants had more apoptotic cells during development as measured by TUNEL staining, suggesting that green cones are born but then die, and that rods are over-produced separately. However, the increase in number of apoptotic cells was not equal to the deficit in green cone abundance; thus, it is possible that both cell death and other mechanisms collude to generate the green cone-poor, rod-enriched phenotype.

Although *six7* function in photoreceptors has not been studied outside of zebrafish, the gene did not originate in the teleost-specific genome duplication. The gar, an ancient lobe-finned fish with a high degree of genomic conservation with chicken (Braasch et al., 2016), also has a *six7* (Ogawa et al., 2015). Turtles and snakes have an annotated *Six7* gene, but due to low conservation in peptide sequence the authors decided to leave it out of their phylogenetic tree (Ogawa et al., 2015), and birds and mammals appear to have lost *Six7*.

While not known to actually play a role in photoreceptor gene expression, Manavathi and colleagues demonstrated that Six3, a mammalian homolog of fish Six7, negatively regulates itself by recruiting MTA1 to its own promoter, which then recruits the histone deacetylation complex to repress *Six3* expression (Manavathi et al., 2007). In MTA1 knockout mice, *Six3* is expressed more highly in the ONL, and the rods had increased expression of rhodopsin. Six3 was shown to be able to stimulate luciferase reporter activity on rhodopsin promoters, and to enhance the stimulatory activity of Nrl and Crx in the same assays. Thus, it is plausible that *Six3* in mammals may play a covert role in photoreceptor subtype-specific gene expression. Moreover, it suggests that zebrafish Six7 may directly stimulate expression green cone opsin expression, which shares evolutionary origins with rod opsin (Lamb, 2013).

The present lack of information on *six7* frustrates a pithy summary. In larval zebrafish, *six7* appears to be required for the formation of green cones, without which the cells either become rods, or die and are replaced by extra rods. Other cone types may be affected by this; blue cones in the larvae, and red and UV cones in the adult. Adult expression of the green opsins is also nearly abolished in the *six7* mutant, but lack

of additional cell type markers precludes discriminating between lack of green cones, or lack of green cone opsin only. Investigation of *six7* in the context of *tbx2b* reveals a cumulative phenotype, suggesting that each gene acts in a separate pathway, and there is currently no information on the genetic interactions of *six7* and *trb2*.

1.2.3.3 Trb1/2

Thyroid hormone receptors alpha and beta (Trα, Trβ) are nuclear hormone receptors that act as repressors in the absence of ligand, or activators in the presence of it (Grimaldi et al., 2013). A retina-enriched isoform of *Trβ*, termed *Trβ2*, was first identified in the chicken, with an extra 107 N-terminal amino acids transcribed from an alternate start codon (Sjöberg et al., 1992).

In the mouse, knockout of the *Trβ2* isoform-specific transcriptional start site causes absolute lack of M cones with a corresponding increase in S cones (Ng et al., 2001). Manipulations of thyroid hormone show that M cone opsin distribution in the retina (normally graded with high density of M cones in the dorsal retina, and low/zero density in the ventral retina) is determined by thyroid hormone gradients in the retina (Glaschke et al., 2011; Roberts et al., 2006), and sensitivity to thyroid hormone availability continues into adulthood, with opsin-switching occurring in thyroidectomized mice provided varying doses of exogenous thyroid hormone (Glaschke et al., 2011). Trβ2 absolutely requires its TH-derived ligand to directly repress S cone opsin expression, and to stimulate M cone opsin expression (Applebury et al., 2007). Trβ2-mediated S opsin repression requires Rxrγ (reviewed below) as a co-factor (Roberts et al., 2005). Trβ2-mediated M-opsin expression requires SUMOylation by Pias3, while Trβ1 has a modest capacity to induce M opsin expression that does not require SUMOylation (Onishi et al., 2010). Moreover, ligand-bound Trβ2 and Rxrγ together induce *Pias3* expression in mouse M cones, which enables Trβ2-mediated M opsin expression (Onishi et al., 2010). *Trβ2* is transcriptionally regulated by promoter activity both upstream of the transcriptional start site as well as within its first intron, and its photoreceptor-specific expression is mediated by two short control regions, an “amplifier” (85bp) responsible for robust expression, and a “specifier” (115bp), responsible for photoreceptor-specific restriction of otherwise broad reporter expression

(Jones et al., 2007). We know little about the regulators of *Trβ2*, as we do not yet know what factors explicitly instruct the cone fate, but Nrl appears to bind this gene and at least S cone opsin, presumably in a repressive fashion (Oh et al., 2007), and the bHLH protein NeuroD1 binds to and activates expression of *Trβ2*, with *NeuroD1*$^{-/-}$ mice failing to generate M cones and instead making more S-cones (Liu et al., 2008). Rorα appears to repress *Trβ2* expression in S cones (reviewed below) (Fujieda et al., 2009). Cone-specific upregulation of *Trβ2* appears to be part of the function of the Onecut1/2 proteins (Section 1.2.1); they bind redundantly to a cis-regulatory module upstream of *Trβ2* transcription start site (Emerson et al., 2013), probably in partnership with Otx2. Electroporated ectopic expression of Onecut into post-mitotic retinal progenitor cells at P0, when mouse rods are beginning to terminally differentiate, boosted the proportion of cells with cone markers at the expense of rod markers. Onecut mutant mice also show decreases in *Trβ2* transcript abundance. Thus, Onecut proteins most likely act as cone-specific activators of *Trβ2* expression, in addition to their earlier role in regulating the cone and horizontal cell lineages all together (as reviewed above in Section 1.2.1).

Zebrafish *trβ2* plays a conserved role in cone photoreceptor specification, and regulates production of UV cones versus red cones. Manipulation of *trβ2* levels using morpholino knockdown or transgenic over-expression show it is necessary and sufficient to promote the red cone phenotype at the expense of the UV cone phenotype (Suzuki et al., 2013; Yoshimatsu et al., 2014). Moreover, *crx*-driven ectopic over-expression of *trβ2*, which is active during or just after the terminal mitosis of all photoreceptors, causes those photoreceptors to become red cones, while *gnat2*-driven expression, active in maturing cone photoreceptors only, causes only red cone opsin co-expression with whatever endogenous opsin that cone would have expressed (Suzuki et al., 2013). This indicates that at least red cones are specified by *trβ2* expression almost immediately after birth, and that Trβ2 continues to have a role in promoting red opsin expression postnatally, although other cones lose competence to shift fate to become red cones.

In summary, *Trβ2* is required for the specification of the longest wavelength-sensitive cone in vertebrates, which is red opsin in tetrachromats and M (greenish) opsin in the mouse. Its expression requires collaborative activity of Otx2 and Onecut1/2,

and Trb2 directly promotes transcription of that cell's ultimate opsin (red in zebrafish, M in mouse) and directly represses expression of UV (zebrafish) or S opsin (mouse). Trβ2 requires SUMOylation by Pias3 in order to stimulate opsin expression, and induces *Pias3* expression in combination with Rxrγ in nascent cone precursors. Trβ1 induces M opsin expression at a very weak level, and this is not SUMOylation-dependent. The actions of *Trβ2* relative to *Tbx2* and *Six7* have not been examined in any tetrachromat eyes.

1.2.3.4 Rorα/β

The retinoid-related orphan receptor alpha and beta1/2 isoforms (*Rorα*, *Rorβ1/2*) have a role in cone specification, as well as in rod specification (Section 1.2.2), and facilitate the cone fate and promote the S-cone phenotype. *Rorβ2* mutant mice, known for making a rodless mouse with primitive S-cone-like cells (Section 1.2.2), still express *Trβ2* and M cone opsin in some of their cones, indicating that *Rorβ2* mutation does not block the *Trβ2*-mediated specification of M cones; rather, the failure to make rods in this mutant causes the cells to develop similarly to S cones, and these outnumber the M cones and make the retina look like an S cone-only retina (Srinivas et al., 2006). Rorβ2 does have some ability to directly bind and activate S cone opsin promoter, which is potently enhanced by dimerizing with Crx (Srinivas et al., 2006).

Rorα, not known to have a role in rod gene regulation, is actively expressed in both S and M cones into adulthood, as well as in some INL neurons (Fujieda et al., 2009). *Staggerer* (*sg*) Rorα mutant mice express S cone opsin weakly, and M cone opsin a little less weakly, which suggest it is a factor in their expression but not required for it. Cone arrestin expression is also impaired in *sg* mice, and *Trβ2* expression is slightly upregulated, suggesting that *Rorα* normally antagonizes the M cone phenotype. Further, Rorα directly binds the S opsin promoter together with Crx, but not the M cone opsin promoter.

The only model for Rorα/β activity in cones that has been proposed so far suggests that Trβ2 and Rorα/β levels fluctuate, and in the fluctuations the two cones are specified in pulses, which predicts the early production of S cone opsin (robust

expression by ~P4) and later production of M cone opsin (robust expression by ~P11) in mouse (Fujieda et al., 2009). Early in cone development, Trβ2 and Rxrγ (reviewed below) together work to block expression of S cone opsin. Then *Trβ2* and *Rxrγ* expression decreases transiently while *Rorβ2* increases and promotes S cone opsin expression. Subsequently, *Trβ2* and *Rorα* transcripts both increase, and Trβ2 stimulates M cone opsin expression. Finally, *Rorα* increases in expression to its final levels and persists, while *Rorβ2* and *Trβ2* both decrease, although persist into adulthood (Fujieda et al., 2009). Nothing is presently known about the cone-specific regulation of the *Ror* subtypes, or what factors regulate this variable expression in S versus M cones.

1.2.3.5 Rxrγ

Retinoid X receptor gamma (Rxrγ) has long been used as a marker of cone cells; in chick, *RXRγ* is expressed abundantly through the developing retina, but as cells mature, expression is restricted to just the cone photoreceptors (Hoover et al., 1998), and only cone nuclei stain positively for Rxrγ in rat, cow, human, and mouse (Janssen et al., 1999; Mori et al., 2001). In the developing mouse, Rxrγ dimerizes with Trβ2 to repress S cone opsin expression, but does not participate in modulating M cone opsin (Roberts et al., 2005). Dimerized with Trβ2, Rxrγ also induces expression of *Pias3*, which SUMOylates Trβ2 and enables Trβ2 to stimulate M opsin expression (Onishi et al., 2010). In *Rxrγ* mutants, S cone opsin is expressed evenly in virtually all cones, whereas it is usually repressed in dorsal M cones where M cone opsin expression (and Trβ2 signaling) is strongest (Roberts et al., 2005). The regulators of *Rxrγ* expression have not been identified, but a short 208bp promoter sequence from chicken *Rxrγ* was able to direct robust eGFP to cone photoreceptors, and to activate a Cre-mediated lox reporter construct in cones and horizontal cells (Blixt and Hallböök, 2016). While this does not explicitly identify any regulators of *Rxrγ*, the Cre-mediated reporter activity implies *Rxrγ* is expressed at a time when cones and horizontal cells share a developmental history, and thus some candidate regulators of Rxrγ include Onecut, Otx2 (Sections 1.2.1) or even Spalt proteins (reviewed below).

In summary, Rxrγ does not clearly have a specifying role in cone photoreceptors, but is expressed in all mature cones in the mammal and probably in the chicken, and appears to mediate the anti-S cone activity of Trb2 by directly dimerizing with it to suppress S cone opsin expression. It does not appear to promote M cone phenotype.

1.2.3.6 Sall3

Spalt (*sal*) genes are zinc finger transcription factors present from nematodes and flies to vertebrates (De Celis and Barrio, 2009). In *Drosophila*, there are two paralogs of *spalt*, *spalt major* (*salm*) and *spalt-related* (*salr*). Together, they form the *spalt* complex, and *sal* mutants have defects in numerous developmental processes including wing patterning, but critically also including photoreceptor specification. The *sal* genes promote the differentiation of R7 and R8 photoreceptors, the two color vision-mediating photoreceptors in *Drosophila*; without *sal*, these photoreceptors appear to develop as R1-6 photoreceptors, which mediate dim light and visual acuity (Domingos et al., 2004a; Mollereau et al., 2001). *Sal* is also used to promote the proper planar cell polarity of R3 and R4 fly photoreceptors, but is repressed by *seven-up* (*svp*) as R3 and R4 mature; without *svp* repression, those photoreceptors eventually become ectopic R7 and R8 photoreceptors (Domingos et al., 2004b). Vertebrates have four *spalt-like* (*sall*) genes; *sall1, -2, 3, and 4* (De Celis and Barrio, 2009).

The first indication that Sall3 was involved in vertebrate photoreceptor development was that *Nrl* mutant retinas, which make no rods but extra S cone-like cells, showed increased transcript abundance for Sall3 (Yoshida et al., 2004). In a later investigation, de Melo and colleagues showed that developing S cones and horizontal cells robustly expressed *Sall3*, and some cone bipolar cells began to express *Sall3* at P7 in wildtype (de Melo et al., 2011). Ectopic *Sall3* electroporated into the retina promoted S opsin and cone arrestin expression, and also showed ectopic horizontal cells aberrantly generated within or mislocalized to the IPL. Mouse *Sall3* knockout mice die at birth, but mutant retinal explants cultured in vitro from birth did not express either S opsin or cone arrestin, and showed deficits in transcript abundance from numerous cone phototransduction genes. ChIP showed that Sall3 directly binds to at least S opsin and M opsin genes (de Melo et al., 2011); it is possible that Sall3 directly binds

numerous cone-specific phototransduction genes. It is currently unknown what regulates *Sall3* expression in cones. However, Emerson and colleagues invoke *Sall3* as a possible downstream effector of Onecut (Emerson et al., 2013), on the basis of being expressed in both horizontal cells and cones during differentiation, like *Onecut1/2* and, unlike Onecut1/2, directly binding to and activate cone genes (de Melo et al., 2011). Thus, it is possible that Onecut and/or Otx2 promote *Sall3* expression, although this has not yet been demonstrated. No genetic or physical interaction between Sall3 and Rxrγ has been documented, but as Rxrγ is expressed at similar time points as Sall3 (Blixt and Hallböök, 2016), and as Sall3 promotes the S cone phenotype while Rxrγ represses it (Roberts et al., 2005), it is possible these genes act in similar or parallel pathways.

The only examination of *Spalt* genes in tetrachromat retinas comes from a study in which subtype-specific photoreceptors were flow sorted out of the retinas of chickens, for RNAseq and then compared (Enright et al., 2015a). Both *SALL1* and *SALL3* were found to be cone-enriched relative to rods, and as in the mouse, *SALL3* was abundantly expressed in the photoreceptor nuclear layer as well as in the outer region of the inner nuclear layer, presumably in the cone bipolar cells and perhaps the horizontal cells as reported in the mouse (de Melo et al., 2011). Unlike the mouse, *SALL3* expression did not persist after hatching in chicken. *SALL1* was not studied by de Melo and colleagues, but in chicken, Enright and colleagues demonstrated weak but enduring expression in the photoreceptor nuclear layer, suggesting that the overall function of the *Spalt* genes may have conserved roles in vertebrate retinas, but that in chicken at least these roles may be split between *SALL1* and *SALL3*. Interestingly, *SALL1* showed weak and enduring expression also in the horizontal cells (Enright et al., 2015a), although this was not mentioned by the authors.

In summary, Spalt proteins play a role in promoting the terminal differentiation of cones, specifically and directly activating the expression of numerous cone phototransduction genes. Sall3 directly activates S cone opsin expression, and binds to but does not directly stimulate the M cone opsin promoter, and is not expressed strongly or at all in M cones in mammals. It may participate in promoting the cone phenotype during the period when cones and horizontal cells are differentiating from shared

progenitors, and may be regulated by Otx2 and Onecut proteins, and may prove to have an interaction with Rxrγ, which is expressed at similar time points.

1.2.3.7 Pias3

Protein inhibitor of activated Stat3 (*Pias3*) encodes an E3 SUMO ligase with transcription modulating activity expressed in both cones and rods, which is required for the transcriptional regulatory activity of numerous specifier genes. In the zebrafish, two paralogs exist, and are both expressed in developing and mature red, green, and UV cones (Onishi et al., 2010), although roles for it in regulating these cone subtypes are not known.

In the mouse rod, Pias3 is a co-activator of rod genes, and a co-repressor of cone genes (Onishi et al., 2009). In addition to physical presence at the promoters of these genes, it SUMOylates Nr2e3, and this modification is required for the cone gene-repressive functions of Nr2e3 (Section 1.2.2). It complexes with Nr2e3, Nrl, and Crx at rod-specific gene promoters, and there is SUMOylation of proteins at these promotors, including of Nrl, but it is not yet clear if Pias3 mediates the SUMOylation of these proteins. In the mouse cones, Pias3-mediated SUMOylation is associated with promoting M cone phenotype at the expense of the S cone phenotype (Onishi et al., 2010). Expression is induced in nascent cone genes by combinatorial activation by Trβ2 and Rxrγ. Pias3 then SUMOylates Trβ2; this is required for Trβ2-mediated M opsin expression. Rorα, which stimulates S opsin expression when dimerized with Crx, becomes a repressor of S opsin expression when SUMOylated by Pias3.

Cumulatively, Pias3 directly binds the promoters of various cone and rod genes, and at least in rods is a co-activator of rod genes and a co-repressor of cone genes. Moreover, the repression of cone genes by Nr2e3 requires Pias3-mediated SUMOylation, and Pias3-mediated SUMOlyation status of Trβ2 controls its ability to regulate S and M cone opsin expression.

1.2.3.8 Mafb

Maf family of transcription factors, belonging to the bZIP superfamily and comprised of Nrl, Mafa, Mafb, and c-Maf, has been described in more detail above

(Section 1.2.2). No other Maf family member has been directly implicated in the specification of the photoreceptors, but a recent synthesis has reviewed pre-existing data to infer a possible role for *Mafb* in tetrachromat green cone specification (Musser and Arendt, 2017).

The opsin expressed by rods (*Rh1*) is most related to tetrachromat green cone opsin (*Rh2*) (Lamb, 2013), and is derived from pre-existing green cone opsin. In chicken, *MAFB* is lightly and sparsely expressed in the photoreceptor nuclear layer at embryonic day 20 (E20) (Enright et al., 2015a), and in retinal explants removed from embryos at E6 and cultured for 15 days in vitro, thought to mimic E21 (hatch day), *MAFB* expression was strongly enriched solely in isolated green cones, relative to red cones, UV cones, or rods (Enright et al., 2015a). Musser and Arendt suggest that, since green cones and rods express similar opsins, perhaps both photoreceptor types utilize Maf family members for specification (*Nrl* for rods; *Mafb* in green cones) (Musser and Arendt, 2017). However, the chicken *MAFB* expression is not robust (Enright et al., 2015a), and if it is expressed in post-natal green cones, it is certainly more robustly expressed in a population of INL cells.

On the basis of green cone-enriched expression of *MAFB* in chicken, it is possible that a non-*Nrl* Maf family member, *Mafb*, has a role in specifying photoreceptors. Moreover, it is possible this is part of green cone specification.

1.2.3.9 Summary schematic of cone specification

The disconnect resulting from little overlap between literature from mammalian and tetrachromat organisms makes it difficult to present the data in a single diagram with high confidence. Fig. 1.5 shows a summary of the data from mammalian research, including information where possible from tetrachromat models, and Fig. 1.6 shows a summary of information presently specific to tetrachromat models.

As shown in Fig. 1.3, cones derive from a bipotential retinal precursor cell which can generate either horizontal cells or cones, and in mouse at least, the cone fate must first be specified before cone subtype can be determined. *Onecut* expression (reviewed above) appears to promote the horizontal cell fate, but expression lingers into post-differentiation cones, and Onecut can directly bind and activate *Trβ2* expression in

cones, so it may have dual roles in both horizontal and cone fates. Sall3 is similarly involved in the production of cones and of horizontal cells, and similarly binds cone-specific genes like S opsin directly. While Otx2 has not been explicitly studied in the context of specifying the cone lineage, it appears not to be involved in horizontal cell generation. Thus, it is possible that Onecut and Sall3 activity together promote the horizontal cell fate, while Onecut, Sall3, and Otx2 together promote the cone fate. Otx2, Onecut, and Sall3 all directly bind to and activate *Trβ2* expression in cones, and Sall3 directly binds to and activates expression of numerous cone-specific phototransduction genes. In the mouse, *Trβ2* is evenly expressed in most cones, but is only competent to stimulate gene expression when bound to its ligand; thus, most differentiating cones probably express *Trβ2*, and depending on activated thyroid hormone availability, assume the S cone or M cone phenotypes. In the presence of activated thyroid hormone ligand, Trβ2 directly binds to and stimulates M cone opsin, and in complex with Rxrγ, binds to and represses S cone opsin expression. S cone opsin expression is stimulated by Sall3, Rorβ2, and Rorα, aided by dimerization with Crx. For the life of the animal, manipulating thyroid hormone levels is sufficient to induce opsin switching between S and M opsins in most cones.

In the tetrachromat zebrafish retina, which has UV, Blue, Green, and Red cones, as well as rods, roles for *tbx2b*, *six7*, and *trb2* have been found which cannot yet be easily mapped onto the mammalian model. As shown in Fig. 1.6, zebrafish *trβ2* has a conserved role in promoting the production of the longest wavelength-sensitive cone over the shortest. However, unlike in the mouse there is a window of opportunity for this to occur, as recently post-mitotic cones forced to express *trβ2* can assume the red cone fate, but maturing photoreceptors forced to express *trβ2* only begin to co-express red opsin in addition to their endogenous opsin. Adult activity of *trβ2* has not been studied in zebrafish, but presumably it continues to mediate red opsin expression as in the mouse. UV cones fate is regulated not only by *trβ2* expression, but also by *tbx2b* activity. It appears that *tbx2b* promotes UV cone fate, as mutant larvae fail to make many UV cones and instead over-produce rods, and the most common model is that UV cones become rods in these mutants. In the adult, *tbx2b* mutant rod abundance does not appear to be higher, and UV cones are produced but then likely die, suggesting an

alternative mechanism whereby UV cone death in larvae is accompanied by a second phenotype, hyperproliferation of rods. The final gene with tetrachromat-only data is *six7*. In larval zebrafish, *six7* appears to promote green cone identity, as mutants fail to make many green cones and instead over-produce rods. Blue cone opsin transcript is also reduced, suggesting a decrease in blue cones in the larvae, with no change in UV or red cones. However, in the adult, the opposite effect on non-green cones is seen: green cone opsin is still abolished in the adult *six7* mutant, but the dominant red opsin paralog is switched, and red opsin transcript is overall more abundant, indicating that there are more red cones, or that green cones express red opsin. UV cone opsin transcript is also more abundant, suggesting that there may be more UV cones, or that green cones express UV cone opsin. Cumulatively, it could mean that adult green cones are lost and extra red and UV cones are made, or that green cones express opsins regulated by Trβ2. At the time of writing, no labs with access to *tbx2b*, *trb2* or *six7*-modulating tools (mutants, transgenics, morpholinos) have published work showing interactions between the three genes, so if these genes represent nodes in a genetic network, they have not yet been connected to each other or to nodes in the mammalian model (Fig. 1.4, 1.5). From work in the chicken, there is the suggestion that *MAFB* expression is involved in the specification of green cones, and no work to date has found any factor involved in blue cone specification.

1.3 Evolution of the photoreceptors

There is intense selective pressure on visual systems to evolve to fully meet the visual tasks faced by an organism. Consequently, the problem of mediating vision in relevant circumstances may have continually evolving solutions. In Section 1.3.1, I give a brief overview of rhabdomeric photoreceptors, which are the photoreceptor type used by virtually all invertebrates yet examined. In Section 1.3.2, I discuss current opinion on the origins of rods and cones, which represent the debut of ciliary photoreceptor-based vision among extant vertebrates. In Section 1.3.3, I discuss instances of evolutionary shifts in photoreceptor diversity in vertebrates, and finally conclude with Section 1.3.4, an introduction to the Nocturnal Bottleneck Hypothesis.

Section 1.3.1 is useful for understanding the fundamental innovation that distinguishes the visual biology of vertebrates from that of invertebrates. Sections 1.3.2-4 motivated and informed the research of Chapters 3 and 4, and the discussion of Chapter 5.

1.3.1 Invertebrate vision is mediated by rhabdomeric, not ciliary photoreceptors

Vertebrate vision is mediated through photoreceptors which use elaborated primary cilia, packed with opsin GPCRs which receive photons and transduce it to a signal (reviewed in Section 1.1.3). The functional output of ciliary opsin signaling is decreased intracellular cGMP concentration, which shuts cGMP-gated ion channels and causes hyperpolarization of the cell. However, an entirely separate photoreceptor biology exists, and mediates vision widely among the invertebrate lineages.

The visual photoreceptors used by the vast majority of invertebrates are termed rhabdomeric, in reference to the tube-like, light-funneling rhabdom structure in compound eyes where these photoreceptors were characterized (for example, (White, 1975)), and which contains the rhabdomeric photoreceptors and other cells. Densely packed arrays of microvilli extend from the surface of rhabdomeric photoreceptors. These rhabdomeric photoreceptors use opsins for photon absorption, although the split between ciliary and rhabdomeric opsins occurred more than 700 million years ago (Lamb, 2013), before the divergence of protostome and deuterostomes, and thus, a novel opsin can be readily determined to be a rhabdomeric or ciliary opsin based on its primary sequence (Pergner and Kozmik, 2017). The rhabdomeric phototransduction cascade is also wholly different from ciliary phototransduction, and to aid in the following sections, a brief overview is warranted.

To summarize a recent review (Fain et al., 2010), the *Drosophila* rhabdomeric photoreceptors have approximately forty thousand microvilli per photoreceptor. Each microvillus has approximately 1000 opsin molecules, and stimulation of the opsin activates G_q protein activation, which uses phospholipase C (PLC) to convert PIP_2 into IP_3 and DAG secondary messengers. DAG stimulates the opening of TRP ion channels, allowing inflow of sodium and calcium ions, thereby depolarizing the microvillus. The increase in intramicrovillar calcium opens more TRP channels, allowing more ion inflow,

and the cumulative increase in calcium ion concentration triggers depolarization of the whole cell. Although not in the fly, in numerous other invertebrates, the rapid gain in calcium concentration is further aided by IP_3-dependent release of stored Ca^{2+} from submicrovillar cisternae, which are positioned at the bases of the microvilli and are readily accessible to diffusing IP_3. This high gain in signal from single photons allows physiological detection, enabling vision in dim light. In higher levels of illumination, the baseline Ca^{2+} concentration is higher due to constant Ca^{2+} release from the microvilli and the submicrovillar cisternae, which blunts the gain in signal from photons but does not block phototransduction overall. Phototransduction can proceed despite high intracellular Ca^{2+}, as the microvilli are highly compartmentalized, and rapidly recover a locally low calcium concentration, allowing a single microvillus to report ten photons per second in *Drosophila*. Moreover, when 11-*cis*-retinal isomerises to all-*trans*-retinal, a second photon can isomerize it back to 11-*cis*-retinal, allowing opsins to never permanently bleach in physiological light conditions. In this way, rhabdomeric photoreceptors also mediate reliable photoreception in bright light.

To summarize the principal differences between ciliary and rhabdomeric phototransduction: **ciliary photoreceptors** manipulate levels of cGMP to modulate the open/shut status of cGMP-gated ion channels, and light-induced activity shuts these ion channels, blocking otherwise steady inflow of cations and thereby hyperpolarizing the cell. Ultimately this causes the cell to release less neurotransmitter in response to light. **Rhabdomeric photoreceptors** manipulate levels of IP3 and DAG to modulate Ca2+ concentration and cation inflow, which ultimately depolarizes the photoreceptor and causes it to release neurotransmitter in response to light.

In some invertebrates (not the fly), both rhabdomeric and ciliary photoreceptors are present (Arendt et al., 2004; Gomez and Nasi, 2000; Gotow and Nishi, 2002; Raible et al., 2006), suggesting that the ancient state was to have both types of photoreceptors, with subsequent loss of ciliary photoreceptors in the *Drosophila* lineage, and the loss of obvious rhabdomeric photoreceptors in the vertebrate lineage. In animals with both types, the current assumption is that rhabdomeric photoreceptors mediate vision, and ciliary photoreceptors play non-visual roles, such as entraining the circadian rhythm to the photoperiod (Arendt et al., 2004; Fain et al., 2010; Tosches et

al., 2014). Interestingly, the melanopsin recently discovered to be expressed in a tiny fraction of retinal ganglion cells is a rhabdomeric opsin, and these retinal ganglion cells are thought to participate in circadian rhythm entrainment, pupillary light reflex, and environmental irradiance (Guler et al., 2007; Schmidt et al., 2014). Revealed very recently, there may be a role for some melanopsin-expressing ganglion cells in peripheral retina image formation (Zele et al., 2018), which appears to be mediated by their own detection of light and not by the inputs from rods and cones. There are numerous subtypes of these photoreceptive retinal ganglion cells (Hannibal et al., 2017; Hughes et al., 2016; Reifler et al., 2015), each with diverse specialized functions. Their phototransduction cascade is not fully worked out, but it appears to be rhabdomeric, as light induces IP3 concentration increases in cultured photosensitive ganglion cells, and blocking PLC-mediated IP3/DAG messenger production stopped this (Contín et al., 2010). Furthermore, frog melanophores, which are pigment-bearing cells that darken the skin, express melanopsin and use PLC-mediated IP_3 and DAG to control the light-induced remodeling of the pigment granules (Isoldi et al., 2005), indicating the existence of intact rhabdomeric photoreceptor cascades in vertebrates. However, loss of several candidate mouse homologs to the TRP channels that mediate light-dependent Ca influx in invertebrate photoreceptors did not fully block melanopsin-mediated phototransduction in the retina (Perez-Leighton et al., 2011), indicating that the melanopsin signaling pathway is not yet understood.

1.3.2 Origins of the rods and cones

It is common to study the evolution of a trait that is characteristic of a given lineage or species by comparing it to the homologous structure of a closely-related species or lineage that lacks the trait. However, this is not feasible for vertebrate retinal photoreceptors. The closest relatives to the vertebrates are the non-vertebrate chordates, including amphioxus and the tunicates. These organisms do not have obviously homologous structures to the vertebrate retina, although amphioxus does have both rhabdomeric and ciliary photoreceptors whose homologies to vertebrate photoreceptors are not yet understood. The Amphioxus frontal eye consists of just nine

pigment cells that shade five adjacent ciliary photoreceptor-like cells and has *Otx* and c-opsin expression (Vopalensky et al., 2012). The Amphioxus lamellar body is disputed to have pineal-like qualities (Lamb, 2013; Pergner and Kozmik, 2017). However, neither putative photoreceptive organ has yet been demonstrated to respond to light electrophysiologically. Two other Amphioxus organs, the Joseph cells and the dorsal ocelli/organs of Hesse, are definitely photoreceptive and use rhabdomeric machinery (Angueyra et al., 2012). More distant relatives within the invertebrates use visual photoreceptors which are rhabdomeric. Therefore, the best chance to infer the evolutionary origins of ciliary rod and cone photoreceptors is to look at members of the oldest branching extant vertebrate lineages, evaluate the differences in rod and cone diversity between these members, and then construct a model that can account for these differences.

The earliest branching point in vertebrate evolution, for which members of both derived lineages still exist, is the split between jawless (agnathan) and jawed (gnathostome) vertebrates. The extant agnathans include only the lamprey and hagfish species, and all other vertebrates belong to the jawed lineage. The earliest branching jawed vertebrates are the cartilaginous fishes (elasmobranchs), which amongst extant groups includes the sharks, skates, rays, and chimeras. The retinas of most cartilaginous fish species examined clearly contain both rods and cones (Hart, 2004; Hart et al., 2006). This indicates that the archetypical vertebrate duplex retina, including rods and cones, was established at least as early as the evolution of the jaw. In contrast, retinas of the agnathans, including the hagfish and lamprey, show numerous differences from the consensus vertebrate archetype. The hagfish eyes are difficult to interpret; they lack lenses (Zeiss et al., 2011), and have only two obvious retinal layers, consisting of the photoreceptors and projection neurons (putative retinal ganglion cells) which the photoreceptors appear to directly contact (Holmberg, 1971). This is reminiscent of the photoreceptors in non-mammalian pineal glands, which consist of photoreceptors directly synapsing onto projection neurons, wrapped up in glia (Eakin, 1973). Hagfish also lack an obvious pineal gland, and thus, there is speculation about whether hagfish eyes are lateralized pineal glands, if they are pineal-like, if they are an evolutionarily intermediate precursor to the vertebrate camera-style eye, or if they are

degenerated from a true camera-style ancestral eye (Lamb, 2013). The lampreys, however, have a clear vertebrate-style eye, with inner, outer, and ganglion cell nuclear layers as in jawed vertebrates (Fritzsch and Collin, 1990), indicating that much of the vertebrate retina evolved before the split between lampreys and jawed vertebrates. Critically however, lamprey photoreceptors show a wealth of novel and intermediate cone/rod phenotypes that reveal much about the early evolution of the vertebrate photoreceptors.

Analysis of the photoreceptors of various lamprey species suggest that the common ancestor of lampreys and gnathostomes had 5 classes of photoreceptors, although the emergence of rods from one of these classes may have been convergently evolved in the two lineages. Analysis of cDNAs recovered by degenerate PCR showed that the common ancestor of lamprey and jawed vertebrates had the same set of five visual opsin genes: *SWS1* (UV), *SWS2* (blue), *RH2* (green), *RH1* (rod), and *LWS* (red) (Collin *et al.*, 2003; Pisani *et al.*, 2006). *Geotria australis* appears to have 5 cone-like cells, instead of 4 cones and 1 rod (Collin *et al.*, 2003; Collin *et al.*, 2004). In other lamprey, there is less photoreceptor diversity (at most two photoreceptor types), but genomic evidence for *SWS1* and *SWS2* pseudogenes in the sea lamprey *Petromyzon marinus* suggest that all lamprey but *G. australis* have simply lost most photoreceptor diversity over time (Wayne L. Davies et al., 2009). In *P. marinus* and the river lamprey *Lampetra fluviatilis*, pairs of photoreceptors exist in which one is physiologically rod-like, with single-photon detection capacity, but with cone-like morphology (Asteriti et al., 2015; Morshedian and Fain, 2017, 2015). The phototransduction cascade used by the rod-like photoreceptors featured different paralogs to mediate cone/rod-specific phototransduction; early in vertebrate evolution, before the split of the jawed gnathostomes and jawless agnathans, two rounds of whole genome duplication occurred (Lamb, 2013; Nordström et al., 2004), generating 4 copies of most genes, many of which were lost in later vertebrate history. In gnathostomes such as the mammals, two photoreceptor-specific transducin alpha subunits are retained, the cone-specific *Gnat2*, and the rod-specific *Gnat1* (Lamb, 2013). In lamprey, different paralogs were retained for photoreceptor-specific use, including at least *GNATX*, and additional

agnathan-specific paralogs for phosphodiesterase6 and the cGMP-gated ion channels have been identified (Lamb et al., 2016; Muradov et al., 2008, 2007).

Cumulatively, studies of lamprey photoreceptors suggest that the last common ancestor of lamprey and the jawed vertebrates had five visual photoreceptor types, one of which may have been physiologically rod-like. Furthermore, rod opsin is derived from a green cone opsin (Collin, 2009), suggesting that rods evolved from a cone subtype (Lamb, 2013). However it appears that the underlying molecular machinery for the rod-like cells is different from that used in gnathostomes, opening up the possibility that rod-like physiology may have independently evolved in the two lineages. In cases of disputed cell type homology between lineages, comparative molecular biology approaches may be used (Arendt, 2008, 2003; Arendt et al., 2016), which rely on comparing the transcriptional control of cell type specification between cells. Where the specification factors are orthologous between two species, the cell type is deemed homologous. In the dispute over whether lamprey and gnathostome rods are truly homologous, demonstrating that lamprey require an *NRL*-homolog to specify rods would be strong evidence for true homology, and not just convergent evolution. At this time, however, the genetic determination of photoreceptor types in the lamprey is wholly unexplored, and regulatory specifiers of photoreceptor identity are unknown. It therefore remains to be determined whether lamprey rods are homologous to gnathostome rods.

1.3.3 Photoreceptor evolution in vertebrate lineages

Photoreceptor ratios and diversity have shifted greatly in some vertebrate lineages, reflecting the importance of updating visual capacity to match emerging ecological needs over evolutionary time (Lamb, 2013). This has resulted in species losing one or more of the ancestral photoreceptor types, interconverting photoreceptor types, and/or shifting rod:cone ratios to adjust to changing levels of illumination in new habitats.

1.3.3.1 Loss and gain of photoreceptor diversity

Loss of cone photoreceptors is a common adaptation in vertebrate evolution, but subsequent gain in cone diversity has occurred as well. While there is evidence that the

cartilaginous fishes, comprised of sharks, skates, rays, and chimeras, initially had multiple cone subtypes (Hart, 2004; Hart et al., 2006), sharks typically have one cone or none (Hart et al., 2011). Snakes have lost ancestral blue and green cones, retaining UV and red cones, as well as rods (W. L. Davies et al., 2009; Simões et al., 2016b, 2016a). In the oldest branching group of mammals, the egg-laying monotremes including the platypus, the Rh2 (green) opsin was lost, as was the Sws1 opsin, with retention of Sws2, Lws, and Rh1 (rod) opsin (Davies et al., 2007). In all other mammals, Sws2 and Rh2 were lost instead (Jacobs, 2013). Marine mammals have broadly lost most cones, with all cetaceans (whales) having only Lws-expressing cones and rods (Peichl et al., 2001), and harbor seals expressing only Lws and rod opsin while bearing an apparently functional but not expressed *Sws1* gene (Newman and Robinson, 2005); interestingly, the shallow-dwelling manatees still express *Sws1* and *Lws* in addition to rod opsin (Newman and Robinson, 2005). On land, many mammals from diverse lineages have lost Sws1 opsin entirely (Jacobs, 2013). In contrast to the rampant loss of cone diversity described here, cone diversity can increase as well; the Old World primates, which includes the human, inherited *Sws1* and green-shifted *Lws* from ancestors, but then duplicated the *Lws* and red-shifted one of the resulting paralogs, thereby regaining trichromatic vision (Jacobs, 2013, 1996).

1.3.3.2 Photoreceptor transmutations

The conversion of rods to cones or cones to rods was first conceived of by Walls, who termed it *photoreceptor transmutation* (Walls, 1942). His evidence for this phenomenon derived mostly from comparing species of geckos and snakes, although there is now evidence that this has occurred in numerous lineages. The Tokay gecko is nocturnal, but has no rods and instead has adapted cones (Yokoyama and Blow, 2001) and cone-specific phototransduction machinery (Zhang et al., 2006) to replicate rod physiology. Garter snakes have lost green cones (reviewed above), but converted rods to cone-like physiology to play a green cone-like role (Schott et al., 2016); in another snake, a rod which had previously gained a host of cone-like qualities appears to be underway toward evolving a rod-like physiology once more (Bhattacharyya et al., 2017). The deep-sea pearlside fish has both rods and cones, but all cones have been

converted to a rod-like physiology, essentially producing an all-rod retina (de Busserolles et al., 2017). The tiger salamander has evolved a second type of rod, the so-called green rod, which expresses *Sws2* opsin and is sensitive to blue light (Isayama et al., 2014; Mariani, 1986; Zhang and Wu, 2009), although these salamanders retain a dedicated *Sws2*-expressing cone as well. Photoreceptor transmutations appear to be a viable solution to increasing or shifting photoreceptor diversity as needed over evolutionary time. At the start of my thesis research in 2012, no case of transmutation had been reported in mammals (discussed further in Chapter 3).

1.3.4 The Nocturnal Bottleneck Hypothesis: mammalian departure from the rest of the vertebrates

A nocturnal period of evolution, through which the early ancestors of all mammals first passed, was proposed by Walls in order to explain a series of characteristics specific to mammals (Walls, 1942). These appear to be adaptations which would enable nocturnal lifestyles, and yet persist in presently diurnal modern species such as humans (Gerkema et al., 2013; Heesy and Hall, 2010). These adaptations include the loss of most non-visual photoreceptive inputs; outside of mammals, photoreceptors exist in the pineal gland, the hypothalamus, and are part of the “third eye” or parietal eye of lizards, and appear to have involvement in circadian rhythm regulation and other non-visual tasks (Bellingham et al., 2006; Foster, 1998). The evolution of endothermy, or warm-bloodedness, and the loss of UV light-mediated photolyase DNA repair pathway are additional mammal-specific characteristics that appear to have emerged in ancient mammals. The loss of mammalian Sws2 (blue) and Rh2 (green) opsin-expressing cones (Jacobs, 1993) appears to date back to this time (Borges et al., 2018). Furthermore, mammalian retinas have been widely described as “rod-dominated” due to the high proportion of photoreceptors which are rods (Borges et al., 2018; Gerkema et al., 2013; Heesy and Hall, 2010). In the diurnal human, instead of producing cone-dominant retinas we instead produce all our cones in a small central area of the retina (Curcio et al., 1991). While the loss of Sws2 and Rh2 opsins in mammals could be explained by accumulation of inactivating mutations, as happened later for elements of

the cone phototransduction machinery in marine mammals (Springer et al., 2016), no mechanism had yet been proposed to explain the origin of the rod-dominated photoreceptor proportion in mammals when I started my thesis research in 2012.

1.4 Goals and structure of the thesis

Our understanding of the generation of cone and rod photoreceptors in vertebrate retinas is incomplete, and biased by mammalian derived models of photoreceptor differentiation. Mammals have, at most, half the photoreceptor diversity of other vertebrates, and possess numerous other features not found in the other vertebrate lineages. Thus, a complete understanding of vertebrate photoreceptor specification requires input from model organisms with the full diversity of photoreceptors. Genes such as *tbx2b* and *six7*, currently only studied in the tetrachromat zebrafish, have homologs that are expressed in the mammalian retina, with potentially hidden conserved roles despite cone loss in mammals. Moreover, work from chicken and zebrafish hint at conserved roles for *TRβ2/trβ2* and *MAFA/nrl* in photoreceptor specification. Cumulatively, this suggests that insights from conserved tetrachromat specification pathways will be able to merge with the mammalian literature, to ultimately enable a model of vertebrate photoreceptor specification. In constructing such a model, lineage-specific differences should become apparent, granting insight into the genetic mechanisms governing evolution of photoreceptor diversity.

The aim of my PhD thesis was to understand vertebrate photoreceptor differentiation from a non-mammalian perspective, and to use this information to bridge the gap between literatures derived from mammalian and non-mammalian models. This work was done in the zebrafish because it is a vertebrate with the full ancestral complement of photoreceptor subtypes (Allison et al., 2010). The zebrafish retina also has strong structural and functional conservation to mammalian retinas (Fadool and Dowling, 2008). Zebrafish have a published genome, a fast-growing genetic toolkit that includes inexpensive methods to reliably achieve stable transgenesis (Kwan et al., 2007) and an eternally optimistic community continually developing an array of genetic knockdown (Nasevicius and Ekker, 2000) and knockout tools (Fleisch et al., 2013;

Hwang et al., 2013; Meng et al., 2008; Pillay et al., 2013). Furthermore, zebrafish have generation times as short as one month, and produce hundreds of eggs per spawning pair, which are immediately accessible to manipulation at the one-cell stage. Finally, they produce all photoreceptor types within 96 hours of fertilization (Allison et al., 2010), and which participate in visually-mediated behaviour within a week of fertilization (Gestri et al., 2012; Neuhauss, 2003). Other tetrachromat models are valuable, but have problems which disqualify them as models for this work. The infrastructure for the chicken is not currently suitable for the stable generation and maintenance of numerous transgenic and loss of function genotypes, and certain photoreceptor genes such as red cone opsin have not yet been mapped in the chicken genome (Enright et al., 2015a). *Xenopus laevis*, the African claw-toed frog, has a generation time of more than a year and is an allotetraploid (Session et al., 2016), and both facts complicate conventional genetic assays. Thus, zebrafish are the only viable tetrachromat model for extensive genetic investigations of the photoreceptor specification pathway.

At the start of my thesis research, *tbx2b* was the first gene identified that was thought to mediate production of UV cones at the expense of rods; *tbx2b* mutant zebrafish had very low or no UV cone abundance, and instead dramatic overabundance of rods (Alvarez-Delfin et al., 2009). A role for *tbx2b* in producing other cone subtypes had not been directly tested for, and no regulators were known for it. At other stages of retinogenesis, loss of the BMP ligand *gdf6a* abolished *tbx2b* expression during eye field patterning (Gosse and Baier, 2009). This suggested that *gdf6a* could be genetically upstream of *tbx2b* during rod/cone precursor specification as well. We hypothesized that *gdf6a* homozygous mutants, which make small, degenerate eyes but still produce photoreceptors (Asai-Coakwell et al., 2013), would display the *tbx2b* mutant phenotype.

In Chapter 2 (Michèle G. DuVal et al., 2014), I tested whether the *tbx2b* phenotype was present in *gdf6a* mutant larval zebrafish, and found no evidence of changes in the ratio of rods to UV cones. However, my colleagues and I demonstrated that *gdf6a* homozygous mutants could evoke the normally strictly recessive *tbx2b* phenotype in *tbx2b* heterozygotes, indicating a genetic interaction between *gdf6a* and *tbx2b*. Moreover, we demonstrated that *gdf6a* mutants have reduced abundance

specifically of blue (*sws2*-expressing) cones, implicating *gdf6a* as the first and so far only known factor in blue cone development.

Previous gene expression profiling from developing mouse rods had suggested transient cone gene expression in rod precursors (Akimoto et al., 2006), and the M cone-inducing gene *Trβ2* is co-expressed with *Nrl* in very early, nascent rods (Ng et al., 2011). In light of the current understanding that rods ultimately evolved from cones (Section 1.3.2), this prompted the hypothesis that rods not only evolved from cones, but that they still develop from cone-fated precursors in extant vertebrates. This predicted that there would be traces of cone gene expression in all nascent and developing rod photoreceptors, across vertebrates.

In Chapter 3 (Kim et al., 2016b), my colleagues and I tested whether rods develop from cone-specified cells in two vertebrate models, the mouse and the zebrafish. My colleagues demonstrated that most, but not all mouse rods robustly but transiently express numerous cone genes, then develop into typical rods, using novel lineage tracing tools. I developed and used two lineage tracing technologies to test for the same in zebrafish, but found no evidence for rods ever expressing two candidate cone markers. On the basis of traits acquired by mammals during the Nocturnal Bottleneck (Walls, 1942) (Section 1.3.4), I proposed that in the mouse, the ancient rod population, of similar developmental origins as in zebrafish, was augmented by recruitment of S cones to the rod fate, perhaps initiated in mammals by changes in the activity of Nrl, a transcription factor known to be able to convert cones to rods. My colleagues corroborated this by demonstrating that Nrl peptide sequence and local non-coding *cis*-regulatory sequences of *Nrl* are tightly conserved among mammals, but less so in other vertebrate lineages.

My colleagues and I previously suggested that Nrl activity in the retina may have changed in some way in mammals relative to an ancestral function (Kim et al., 2016b). This may involve changes in the peptide activity, as the peptide sequence of mammalian Nrl is tightly conserved in mammals but not in other vertebrate lineages (Kim et al., 2016b), and *Xenopus* Nrl but not human Nrl can induce lens fibre differentiation (McIlvain and Knox, 2007). *Nrl* may instead or additionally have changed its expression domain in mammalian evolution, as the local non-coding genomic

sequence surrounding *Nrl* is highly conserved in mammals, but not in other vertebrate lineages (Kim et al., 2016b), and zebrafish nrl was previously reported to have retinal *nrl* expression outside of rods (Nelson et al., 2008). Furthermore, we previously showed that the avian *MAF* genes do not include *NRL* (Kim et al., 2016b); however, birds still make rods (Ochi et al., 2004), suggesting the requirement for *Nrl* to make rods may not be absolute in non-mammalians. Thus, a formal examination of the role of nrl in tetrachromat photoreceptor specification is missing from the literature.

In Chapter 4 (Oel *et al.*, in prep), I tested whether zebrafish require *nrl* to make rods. I found that *nrl* is a conserved requirement for rod production in larvae, and that it is sufficient to direct already specified cones to a rod-like phenotype. I also found that *nrl* is not required for the production of overtly normal rods in adult zebrafish, although I found some ultrastructural nuclear and synaptic similarities to cones. This indicates that non-mammals have access to an *nrl* involved in rod development, but the requirement for rods in this process varies over ontogeny. I also tested whether a small panel of *nrl* homologs, representing mammalian *Nrl*, avian *MAFA*, and agnathan *MAFBA*, and the *Drosophila* long Maf *trafficjam*, were capable of inducing elements of the rod phenotype in zebrafish. I found that all vertebrate *nrl* homologs could induce at least one candidate rod phenotype, but that invertebrate *trafficjam* was unable to do this. This suggests conservation of peptide function in vertebrate Nrl homologs, and suggests further that these organisms may use an *nrl* homolog-utilizing pathway in rod development.

In Chapter 5, I summarize the results of Chapters 2-4 of this thesis, and then introduce three groups of novel hypotheses to support future investigations of *tbx2b*, *gdf6a*, and *nrl*. These are based on work described in Chapters 2 and 4, as well as relevant recently published works from other groups. I then discuss some of the implications of my work in Chapter 4 on understanding the evolution of photoreceptor diversity in vertebrates. Finally, I conclude with a summary of unresolved questions and propose an immediate next experiment to begin to address many of them.

CHAPTER 2:

GDF6A IS REQUIRED FOR CONE PHOTORECEPTOR SUBTYPE DIFFERENTIATION AND FOR THE ACTIONS OF *TBX2B* IN DETERMINING ROD VERSUS CONE PHOTORECEPTOR FATE

Chapter 2 was published as:

Michèle G. DuVal, **A. Phillip Oel**, and W. Ted Allison. 2014. “gdf6a *Is Required for Cone Photoreceptor Subtype Differentiation and for the Actions of* tbx2b *in Determining Rod Versus Cone Photoreceptor Fate*”. PLOS One 9, e92991.

Author contributions: All authors conceived, designed, and performed the experiments, and analyzed the data, and edited the manuscript. MGD and WTA wrote the manuscript. I was an equal contributor to 6 of the 9 major experiments, and to 6 of 12 total figure elements.

The text of this manuscript has been modified slightly for formatting consistency with the rest of this thesis.

2.1 Introduction

The genetic regulation of cone photoreceptor differentiation from retinal progenitor cells is a critical knowledge gap hindering stem cell therapy as a feasible solution for clinical vision restoration. Such therapies promise treatment in patients with a breadth of retinal disease including retinitis pigmentosa and macular degeneration. Identifying pathways that promote cone photoreceptor fates, rather than rod photoreceptor fates, is particularly critical due to the reliance of the human visual system on cones for its most important functions: daytime vision, colour discrimination and high visual acuity. Apart from this, current efforts to refine stem cell therapy more prominently include the identification of intrinsic genetic factors that regulate progenitor fate. Sorting of photoreceptor progenitor cells for implantation is the most efficient contemporary approach, employing expression of photoreceptor lineage-specific genes (e.g. *Nrl*, *Crx*, and *NeuroD*) to facilitate the isolation of progenitor cells destined to develop into the photoreceptors of interest (Lakowski et al., 2011, 2010; MacLaren et al., 2006; Mansergh et al., 2010; Mears et al., 2001; Seko et al., 2012). From this perspective, the current list of genes with roles in cone development remains too short for the purpose of development of functional cones that can integrate into an existing retinal structure, thereby sufficiently restoring functional daytime vision. This list consists largely of *Trβ1/2, Rxrγ, Rorα/β, Coup-TF*, (Fujieda et al., 2009; Roberts et al., 2005; Satoh et al., 2009; Seko et al., 2012; Srinivas et al., 2006) and *tbx2b* (Alvarez-Delfin et al., 2009).

The functions of photoreceptor genes have largely been investigated in mice, especially in the context of degenerative disease (Mears et al., 2001; Milam et al., 2002; Ng, 2001; Sharon et al., 2003), however the innately low cone photoreceptor density in murine models has meant that an understanding of cone photoreceptor specification has lagged behind that of rod photoreceptors. A complementary animal model promises to expand the list of genes and regulatory pathways in cone photoreceptor development: the zebrafish. The retina of zebrafish is structurally and functionally conserved to that of humans, and, due to the diurnal nature of zebrafish, it is cone-rich akin to the human macula. Zebrafish possess rods and four cone spectral subtypes (ultraviolet- (UV-), blue-, green- and red-sensitive cones), which are spatially arranged in a highly regular heterotypical mosaic (Allison, 2004; Allison et al., 2010, 2004,

Raymond et al., 1995, 1993; Takechi, 2005; Vihtelic et al., 1999). In addition, zebrafish undergo external development, allowing for ease of observation and experimental manipulation, supported by a diverse genetic toolbox (e.g. mutants and transgenics). Of particular benefit to the study of stem cell therapy is the robust intrinsic regenerative capacity of the zebrafish CNS, which is the target of enthusiastic scrutiny (Becker et al., 1997; Fleisch et al., 2011; Kaslin et al., 2008; Kroehne et al., 2011; Lamba et al., 2008; Senut et al., 2004). In further pursuit of understanding this regenerative capacity, we have recently engineered conditional ablation of cone photoreceptors and argue that spatial cues of the remaining photoreceptor cells have substantial influence on the identity of regenerating photoreceptors (Fraser et al., 2013).

Considering the great promise of zebrafish to become the premier model of photoreceptor regeneration, it is surprising that few regulatory factors in photoreceptor development are yet to be characterized in fish. One example is thyroid hormone, which initiates UV cone death and regeneration in trout (Allison et al., 2006a, 2006b; Browman and Hawryshyn, 1994; Veldhoen et al., 2006) and modulates the maximal wavelength sensitivity of cones in zebrafish (Allison, 2004). Building on this, thyroid hormone receptor b has been shown to effect cone specification in mice (Ng, 2001; Ng et al., 2011) and more recently in zebrafish (Suzuki et al., 2013). We proposed that, during trout cone photoreceptor regeneration, thyroid hormone modulates a switch in progenitor specification very much akin to that described below, wherein UV cones are produced at the expense of rod photoreceptors (Allison et al., 2006a).

Another regulator of photoreceptor fate described in zebrafish is *tbx2b*, a transcription factor of the T-box family homologous to the mammalian gene *Tbx2*. *tbx2b* is required for neuronal differentiation in early retinal development and for maintaining dorsal retina identity during patterning of the dorsal-ventral axis (Gross and Dowling, 2005). Mutation of *Tbx2* in mice results in microphthalmia (Behesti et al., 2009). This is in agreement with its position downstream of bone morphogenetic protein 4 (*Bmp4*), mutations in which cause microphthalmia in humans and mice. Of great interest herein, *tbx2b* plays a role in promoting UV cone fate vs. rod fate late in zebrafish retinal development, as demonstrated by excess rods and few UV cones (denoted as the ‘‘lots-of-rods’’ phenotype) in *tbx2b* mutant fish (Alvarez-Delfin et al., 2009). One recessive

allele, *tbx2b*^{fby} (also known as *tbx2b*^{c144}), is reasonably considered to be a null allele due to a nonsense mutation in the sequence encoding its DNA-binding T-box domain (Snelson et al., 2008). Homozygous mutants of *tbx2b*^{fby} exhibit a severe form of the lots-of-rods phenotype, wherein few or no UV cones can be detected. A second recessive allele is *tbx2b*^{lor} (also known as *tbx2b*^{p25bbtl}), presumed to be a hypomorph because it generates a less severe form of the lots-of-rods phenotype, exhibiting a substantial reduction in the abundance of UV cones compared to wild type fish, but not to the degree observed in *tbx2b*^{fby} mutants. The location and nature of the *tbx2b*^{lor} mutation is unknown; however, based on linkage analysis and its failure to complement the *tbx2b*^{fby} allele, it is inferred to be near the coding region for *tbx2b*, but not within it (see (Alvarez-Delfin et al., 2009) and Results herein).

In recent studies, we and others identified *gdf6a* as a candidate regulator of cone photoreceptor development and disease (Asai-Coakwell et al., 2013; Gosse and Baier, 2009; Zhang et al., 2012). *Gdf6a* is a BMP gene in the transforming growth factor b (TGFb) ligand super-family; *gdf6a* induces dorsal retina fate during ocular morphogenesis, lying upstream of other dorsal patterning genes. Disruption of human *GDF6* and homologs in mice, *Xenopus* or zebrafish produces anophthalmia, microphthalmia and coloboma with varying degrees of penetrance and severity (Asai-Coakwell et al., 2013, 2007; Michéle G. DuVal et al., 2014; French et al., 2009; Gosse and Baier, 2009; Hanel and Hensey, 2006). The recessive *gdf6a* null allele used in this study, *gdf6a*^{s327}, causes microphthalmia in homozygous zebrafish mutants. Zebrafish knock-downs and mutants of *gdf6a* have down-regulation of *tbx2b* early in retinal development (French et al., 2013, 2009; Gosse and Baier, 2009), while over-expression of *gdf6a* likewise increases expression of *tbx2b* in the developing zebrafish retina (Gosse and Baier, 2009), indicating a tight regulation of *tbx2b* transcription by *gdf6a*. Based on this evidence, *gdf6a* is upstream of *tbx2b* in a pathway of dorsal retina patterning; however zebrafish mutants of *tbx2b* (*tbx2b*$^{lor/lor}$ and *tbx2b*$^{fby/fby}$) do not exhibit microphthalmia.

Mutations in *GDF6* were recently found to be associated with age-related macular degeneration and Leber's congenital amaurosis, both representing photoreceptor degenerative disease (Asai-Coakwell et al., 2013; Zhang et al., 2012).

Further, we demonstrated that the retinas of zebrafish *gdf6a*$^{s327/s327}$ mutants exhibit photoreceptor deficits (Asai-Coakwell et al., 2013), together indicating that disruption of *GDF6* leads to photoreceptor degeneration, which marks *gdf6a* as a potential regulatory factor in the differentiation and/or maintenance of cone photoreceptors. These commonalities between *gdf6a* and *tbx2b*, including both in early ocular morphogenesis and photoreceptor differentiation/maintenance, led us to hypothesize that *gdf6a* may also modulate *tbx2b* during the regulation of UV cone and/or rod photoreceptor fate specification. Establishing this type of genetic pathway in photoreceptor development would impact the direction of future studies by offering a much-needed springboard toward uncovering further signaling pathways and genetic interactions specific to cone photoreceptors. With such knowledge, stem cell therapy can be refined to procure more cone photoreceptors than using current methods, thereby enhancing functional, daytime vision restoration.

In this study we examined the relationship between the roles of *gdf6a* and *tbx2b* in photoreceptor development. We determined that these two genes do not share a genetic interaction in microphthalmia. Further, while disruption of *gdf6a* does not in itself lead to the predicted disruption of UV cone and rod abundances, *gdf6a* loss-of-function reduces the threshold for *tbx2b* mutations to manifest photoreceptor phenotypes.

2.2 Results

2.2.1 *gdf6a* and *tbx2b* do not genetically interact in any apparent way regarding the microphthalmic phenotype

Loss of function in homologues of *GDF6* induces microphthalmia in zebrafish, mice and humans (Asai-Coakwell et al., 2009, 2007; den Hollander et al., 2010; Gonzalez-Rodriguez et al., 2010; Okada et al., 2011). Further, mutation of *Tbx2* in mice likewise causes microphthalmia (Behesti et al., 2009). Considering that *gdf6a* is upstream of *tbx2b* during early eye morphogenesis in zebrafish (Gosse and Baier, 2009), we hypothesized that simultaneous disruption of both these genes would interact to increase the rate or severity of microphthalmia. We had anticipated that establishing the nature of the genetic interaction between *gdf6a* and *tbx2b* in early eye

morphogenesis might be important to provide direction to, or potentially confound, our investigations of *gdf6a* and *tbx2b* in cone photoreceptor differentiation, which occurs later in retinal development.

Microphthalmia is apparent in homozygous *gdf6a*$^{s327/s327}$ larvae by 3 days post-fertilization (dpf), but is not observed in mutants for *tbx2b*$^{lor/lor}$ or *tbx2b*$^{fby/fby}$ through any age (Fig. 2.1A, Fig. 2.2A). Microphthalmic eyes in *gdf6a*$^{s327/s327}$ fish persist to adulthood, exhibiting variably small eyes (or none at all), while eyes in *tbx2b* mutants develop normally. Paraffin sections demonstrate the microphthalmic eyes as they are positioned in the heads of *gdf6a*$^{s327/s327}$ adult fish, with developed but irregularly-shaped lens and a lack of retinal lamination (Fig. 2.1B, C, D), consistent with our recent studies (Asai-Coakwell et al., 2013).

Concerted disruption of both genes is the most sensitive test of the hypothesis that *gdf6a* and *tbx2b* share a genetic interaction in the early stages of eye development. *gdf6a*$^{s327/s327}$ and *tbx2b*$^{lor/lor}$ (or, where noted in figures, *tbx2b*$^{fby/fby}$) mutants were crossed to produce compound heterozygous, [*gdf6a*$^{+/s327}$*;tbx2b*$^{+/lor}$] mutants, which were then in-crossed to procure a full range of genotypic combinations, including compound homozygous mutants. The proportion of resulting offspring exhibiting microphthalmia did not significantly deviate from 25%, suggesting that mutation in *tbx2b* does not affect the rate of microphthalmia in a *gdf6a*$^{+/s327}$ background (Fig. 2.2B). Genotyping these fish revealed that every microphthalmic larva had a *gdf6a*$^{s327/s327}$ genotype, and all combinations of *tbx2b* alleles (*tbx2b*^{lor} and wildtype alleles) existed among these microphthalmic larvae, supporting the null hypothesis that *gdf6a* mutation independently causes microphthalmia in the compound mutants. The eye size-to-body ratio of this pool was assessed to detect possible changes in phenotype severity. Both a microphthalmic population and a normophthalmic population were present and distinct from each other (Fig. 2.2C). The values in the normophthalmic population were statistically normal in their distribution (Shapiro-Wilk Normality test, W = 0.9888, p=0.6532), further arguing against multiple populations of eye size being present. For confirmation, the eye-to-body ratios were also measured in an in-cross of [*gdf6a*$^{+/s327}$*; tbx2b*$^{+/fby}$] mutants, with similar results (Fig. 2.S3B). Only a single population of eye size was observed in in-

crosses of *tbx2b*$^{+/lor}$ mutants (Fig. 2.S1A). We did not explicitly test if combined mutations affected the severity of the microphthalmic phenotype (though no such difference is obvious in the data), because the manner in which data was collected did not support that analysis (we lacked foresight whilst collecting data to anticipate comparing between clutches of fish, which would require identical husbandry and timing of dechorionation: eye and body length are not allometric), though the data regarding rate of phenotype (from within a clutch) is robust and similar between all genotypes. We conclude that although *gdf6a* regulates *tbx2b* expression during early eye morphogenesis (Gosse and Baier, 2009), they do not genetically interact to cause microphthalmia in any obvious manner.

2.2.2 *gdf6a* regulation of cone differentiation differs from predictions derived from phenotypes of tbx2b mutants

tbx2b is proposed to regulate UV cone-versus-rod fate, based on homozygous *tbx2b*$^{lor/lor}$ and *tbx2b*$^{fby/fby}$ mutants which present with a paucity of UV cones and an excess of rod photoreceptors (Alvarez-Delfin et al., 2009). Because *tbx2b* is downstream of *gdf6a* during the previously examined stages of retinal development, we hypothesized that the two genes may share a genetic pathway in a likewise fashion during photoreceptor development. This hypothesis predicts that UV cone and rod development should be disrupted in *gdf6a*$^{s327/s327}$ mutants, similar to observations in *tbx2b*$^{-/-}$ mutants.

Abundance of *gdf6a* expression during early ocular morphogenesis correspondingly affects expression levels of *tbx2b* (Gosse and Baier, 2009). We investigated whether this direct relationship still held later on in development, when the eye is developed and photoreceptors are assuming their respective fates. At 72hpf *gdf6a*$^{s327/s327}$ mutants appear to have less *tbx2b* expression in their retinas compared to wild type siblings, similar to the apparently low *tbx2b* expression in *tbx2b*$^{lor/lor}$ mutants of the same age (Fig. 2.3). In wild type retina *tbx2b* expression was not excluded from any of the retinal layers, but was perceived to be most abundant in the ganglion cell layer

and vitreal half of the inner nuclear layer. Qualitatively, the latter tissue layer was the one with the greatest reduction of *tbx2b* abundance in the *gdf6a*$^{s327/s327}$ mutants.

We examined UV cone and rod photoreceptors in *gdf6a*$^{s327/s327}$ larvae and, contrary to our expectations, they did not show a lots-of-rods phenotype; UV cones and rods in microphthalmic *gdf6a*$^{s327/s327}$ eyes had normal relative abundance and distribution compared to wild type and to normophthalmic sibling eyes (Fig. 2.4A, B). Therefore, despite that *gdf6a* appears to regulate the abundance of *tbx2b* transcript during times of development when photoreceptors are specified (Fig. 2.3), disrupting *gdf6a* alone does not recapitulate phenotypes observed from disrupting *tbx2b* with regards to UV cone-versus-rod fate. This suggests that the downstream reductions in *tbx2b* resulting from mutation of *gdf6a* are insufficient in magnitude, or too different in their timing, to measurably produce effects upon UV cone or rod photoreceptor cell fate.

Assessing these phenotypes using a second metric was warranted because microphthalmia, a defect in early organogenesis, could have confounded potential differences in rod:cone ratios that are established later in development. Thus the abundance of UV cones in 6dpf *gdf6a*$^{s327/s327}$ larvae was also compared to the abundance of blue cones. We counted the number of UV and blue cones expressing GFP and mCherry, respectively, in transgenic fish (see Methods Section 2.6). This provided confirmation that UV cones were not reduced in abundance. However, the number of cones of the blue spectral subtype was dramatically reduced and often distributed in a patchy pattern in *gdf6a*$^{s327/s327}$ retinas compared to normophthalmic siblings (Fig. 2.4C, E). It was of interest to determine if this difference between genotypes was observable earlier in development, when cones are first detectable. Quantifying relative cone abundance in these transgenic fish at 4 dpf confirmed the difference between genotypes arises early (Fig. 2.4C). This was further confirmed at 3 dpf after identifying cones using UV and blue opsin riboprobes via *in situ* hybridization (Fig. 2.4C, D). This suggests that *gdf6a* signaling alone does not regulate cone-versus-rod development in the same fashion that *tbx2b* does, but instead appears to be acting in the differentiation of cone spectral subtypes.

2.2.3 Specificity and utility of rat monoclonal antibody 10C9.1 for labeling UV cones

To better detect UV cones and phenotypes of interest, we isolated a novel monoclonal antibody raised in rat and characterized its ability to specifically detect UV-sensitive opsin (product of *opn1sw1*, ZFIN ZDB-GENE-991109-25). The clone giving rise to antibody 10C9.1 was derived from a rat injected with a peptide antigen equivalent to the 20 amino-terminal amino acids of trout UV opsin (Fig. 2.S2E), and polyclonal sera from this rat had previously been shown to label UV cones in trout (Allison et al., 2006a) and zebrafish (Allison, 2004). 10C9.1 was isotyped to an IgG2c.

Application of 10C9.1 to cryosections of adult zebrafish retina, and counterstaining of lipid-rich material using BODIPY-TMR, revealed that 10C9.1 labels the outer segments of photoreceptors with a single cone morphology (Fig. 2.S2A). Restriction of the labeling to the cone outer segment is consistent with labeling of an opsin because in healthy eyes opsins are abundant only in this cellular compartment. Considering UV cones are one of only two spectral subtypes that exhibit a single cone morphology (along with blue cones, and in contrast to the green and red cones that are fused into a double cone morphology), the labeling also suggested that 10C9.1 was detecting either UV or blue cones. Simultaneous labeling using 10C9.1 and a well-characterized anti-blue opsin antibody (Vihtelic et al., 1999) demonstrated that 10C9.1 labels a population of single cone photoreceptors that is distinct from the blue cones (Fig. 2.5A). Further, the 10C9.1 labeling was localized to cone cells with a short single cone morphology with the outer segments in a more vitreal (basal) position than that of blue cone outer segments (Fig. 2.5A), and this is exactly consistent with the morphology of UV cones as identified via in situ hybridization (Raymond et al., 1995; Raymond and Barthel, 2004; Stenkamp et al., 1996), immunohistochemistry (Vihtelic et al., 1999), and microspectrophotometry (Allison, 2004; Allison et al., 2004). Simultaneous labeling of 10C9.1 and zpr1 antibody that labels the entire plasma membrane of red/green double cones demonstrated no apparent overlap in labeling (Fig. 2.5A).

The specificity of antibody 10C9.1 was assessed using two additional strategies. First, we noted that no such labeling was apparent when the 10C9.1 primary antibody was excluded or when it was substituted by another rat IgG2c primary antibody (Fig.

2.S2C). Second, we noted that very few cells were labeled when 10C9.1 was applied to retinas that are known to have few UV cones, i.e. retinas from adult *tbx2b*$^{lor/lor}$ mutants (Fig. 2.S2C, see also top row of Fig. 2.6B for the same approach on retinas from normophthalmic larvae).

We further confirmed that 10C9.1 is labeling UV cones by its co-localization with an established anti-UV opsin antibody raised in rabbit (Vihtelic et al., 1999) (Fig. 2.S3). Finally, we applied 10C9.1 to adult double transgenic zebrafish that we recently characterized as expressing GFP throughout their UV cones and expressing mCherry throughout their blue cones Tg(-5.5opn1s- w1:EGFP)kj9;Tg(-3.5opn1sw2:mCherry)ua3011 (Duval et al., 2013; Fraser et al., 2013; Takechi et al., 2003). This labeling again revealed localization of 10C9.1 exclusively to the outer segments of UV cones (Fig. 2.5B and Movie 2.S1).

In sum, the specificity of the antibody 10C9.1 for labeling UV cones was determined by its localization to the expected cellular compartment (photoreceptor outer segment) and only within the cone cells of the expected morphology (short single cones); this was complemented by co-localization of 10C9.1 with well-characterized antibodies and transgenes that label UV cones, and exclusion from similar markers that label other cones. Further, 10C9.1 labeling was greatly reduced when applied to retinas with few UV cones. The utility of 10C9.1 is enhanced by being a stable monoclonal source of reagent. Further, because the host animal was rat, 10C9.1 can be used in multi-label experiments with the large selection of available antibodies raised in rabbit and mouse. The latter includes that one can, for the first time we are aware of, simultaneously distinguish each of the cone subtypes of zebrafish using immunohistochemistry (Fig. 2.5A''). 10C9.1 is available from the corresponding author or from Immunoprecise Antibodies Inc (Victoria BC, Canada www.immunoprecise.com; antibody name ''UVop-10C9.1'').

2.2.4 A subtle interaction between *gdf6a* and *tbx2b* modulates the lots-of-rods phenotype

Based on the lack of a lots-of-rods phenotype in *gdf6a*$^{s327/s327}$ mutants (Fig. 2.4A, B), it had appeared that *gdf6a* might not regulate cone-versus-rod development. However, a more sensitive test to detect the presence of an interaction is concerted disruption of both genes. To determine whether *gdf6a* and *tbx2b* interact in photoreceptor development, we examined UV cone and rod photoreceptors in the progeny of compound heterozygous [*gdf6a*$^{+/s327}$*;tbx2b*$^{+/lor}$] in-crosses (and [*gdf6a*$^{+/s327}$*;tbx2b*$^{+/fby}$] in- crosses). We hypothesized that if there were a less linear, subtler interaction between *gdf6a* and *tbx2b*, disrupting both genes simultaneously would reveal it, by resulting in a synergistic phenotype or occurrence of phenotypes among larvae whose genotypes predict none.

Microphthalmic eyes from the aforementioned in-crosses showed an elevated rate of the lots-of-rods phenotype (48% of microphthalmic eyes showed a lots-of-rods phenotype among [*gdf6a*$^{+/s327}$*;tbx2b*$^{+/lor}$] in-crosses, a significantly greater proportion than the predicted 25%; X^2 p,0.001). This contrasted eyes from normophthalmic siblings wherein the rate of the lots-of-rods phenotype (29%) did not statistically differ from the expected Mendelian rate (Fig. 2.6A, B). The elevation in lots-of-rods phenotypes among microphthalmic larvae also differed significantly from rates in *tbx2b*$^{+/lor}$ in-crosses (without gdf6a mutation), where 27% of embryos exhibited the lots-of-rods phenotype, which was also statistically consistent with predicted Mendelian inheritance (Fig. 2.6A).

To better define the genetics of this system, we repeated the in-crosses of *gdf6a* $^{-/-}$ and *tbx2b*$^{lor/lor}$ mutants in a fashion that allowed us to track genotypes via single nucleotide polymorphisms (SNPs) within the *tbx2b* gene. The use of SNPs was necessitated by the fact that the *tbx2b*^{lor} mutation remains undefined. Screening a panel of potential SNPs (see Methods Section 2.6) on several fish of each genotype allowed us to identify homozygous *tbx2b*$^{lor/lor}$ and *gdf6a*$^{s327/s327}$ founders wherein each had a different homozygous SNP in the *tbx2b* gene (in the first exon, Fig. 2.6E). These were bred to generate compound heterozygous fish [*gdf6a*$^{+/s327}$*; tbx2b*$^{+/lor}$] within which we could reliably track the inheritance of the *tbx2b*^{lor} allele.

To test if the elevated rates of the lots-of-rods phenotype accords with a partial loss of *tbx2b* function, as predicted from a genetic interaction, 35 microphthalmic larvae

from the aforementioned in-cross were genotyped. All larvae were *gdf6a*$^{s327/s327}$, as expected from their microphthalmic phenotype. Amongst these, we expected a 25% (i.e. 9/35 larvae) rate of the lots-of-rods phenotype based on a recessive pattern of inheritance (see ‘‘Expected’’ column in Table 2.1). We also expected all 9 of these larvae to have a *tbx2b*$^{lor/lor}$ genotype through SNP analysis. But we observed the previously mentioned increase in rate of the lots-of-rods phenotype; 13/35 or 37% of the larvae had the phenotype (‘‘Observed’’ column in Table 2.1). Genotyping revealed that 4 of these 13 lots-of- rods phenotypic larvae were, in fact, heterozygous *tbx2b*$^{+/lor}$ (unexpected), whereas 9 were homozygous *tbx2b*$^{lor/lor}$ (matching the expected rate of homozygosity). This indicates that the lots-of- rods phenotype can occur in a subset of heterozygous *tbx2b*$^{+/lor}$ fish, but only when both copies of *gdf6a* are mutated. Genotyping also revealed that normophthalmic individuals with the lots-of-rods phenotype were all homozygous *tbx2b*$^{lor/lor}$. Therefore, the slightly elevated rate of the lots-of-rods phenotype (29%, not significantly different from Mendelian 25%, see above) in these normophthalmic eyes likely resulted from reduced survival of other genotypes. This might be expected if toxic mutations were not yet bred out following random chemical mutagenesis.

Because the rate of lots-of-rods among microphthalmic larvae (48%) does not reflect any classical Mendelian ratio that may explain such elevated rates, we examined the effect of the stronger null *tbx2b*^{fby} allele in the same context with *gdf6a* mutation, with the suspicion that introducing a null *tbx2b* mutation may induce a more severe phenotype. An in-cross of [*gdf6a*$^{+/s327}$*;tbx2b*$^{+/fby}$] showed similar results to [*gdf6a*$^{+/s327}$*;tbx2b*$^{+/lor}$] in-crosses, with the lots-of-rods phenotype occurring in 44% of microphthalmic eyes again significantly (X^2 $p = 0.007$) more than siblings (20.5%) (Fig. 2.5C, D).

2.3 Discussion

Efforts to model vision regeneration using stem cells are stymied by the difficulties procuring progenitors for cone photoreceptors, the cells required for daytime vision, in established murine models. One of the obstacles in this respect is a limited knowledge

of the genetic regulation of cone development from retinal progenitor cells. To complement and utilize our novel zebrafish cone regeneration model (Fraser et al., 2013), we are investigating candidate regulatory factors of cone and cone subtype development. In this paper, we explored the potential interaction between two genes with recently realized connections to photoreceptor development and degeneration. To this end we demonstrated that these genes, *gdf6a* and *tbx2b*, unexpectedly regulate development of spectral subtypes of cones and interact in the development of UV cones and rod photoreceptors, specifically.

tbx2b is one of the most recently recognized regulatory genes directing cone and rod differentiation (Alvarez-Delfin et al., 2009). Human and mouse *GDF6/Gdf6* (and the zebrafish homolog *gdf6a*) was selected as a candidate regulator of cone development because deficits in its function cause photoreceptor degeneration, as identified through panels of LCA patients, complemented by murine and zebrafish models (Asai-Coakwell et al., 2013). These developments, in synergy with the established regulatory relationships between *gdf6a* and *tbx2b* in early retinal development (French et al., 2013; Gosse and Baier, 2009), led us to speculate that *gdf6a* signaling also regulates cone photoreceptor development.

2.3.1 *gdf6a* signaling has a conserved role in ocular morphogenesis that does not appear to depend on *tbx2b* activity

The genetic interactions between *gdf6a* and *tbx2b* in zebrafish eye development are not as linear as we had assumed. Although *Tbx2* knockout mice display microphthalmia (Behesti et al., 2009), akin to *gdf6a* loss-of-function models in various vertebrate homologs (Asai-Coakwell et al., 2013; Duval et al., 2013; French et al., 2013; Raymond and Barthel, 2004; Stenkamp et al., 1996), and *gdf6a* signaling has been previously demonstrated to positively regulate *tbx2b* expression during ocular morphogenesis (Gosse and Baier, 2009), our data indicate that in zebrafish disruption of *tbx2b* is not sufficient to augment the pathology of microphthalmia observed upon *gdf6a* disruption. This was revealed both by the lack of a microphthalmic phenotype upon *tbx2b* loss of function, and the lack of change in rate or apparent severity of

microphthalmia when *gdf6a* and *tbx2b* null mutations were combined. This data ruled out an alternative explanation for the genetic interdependence we observed regarding photoreceptor development, demonstrating that alterations in microphthalmia cannot explain the increased rates of photoreceptor-related phenotypes we noted during concerted gene disruption. Towards a broader relevance of this data, *gdf6a* and *tbx2b* have both been demonstrated to play roles in cell proliferation and establishing dorsal retina identity, though in different animal models (Behesti et al., 2009; Bilican and Goding, 2006; Chi et al., 2008; French et al., 2013, 2009; Gosse and Baier, 2009; Gross and Dowling, 2005; Martin et al., 2012; Snelson et al., 2008; Vance et al., 2005). Our observations of *tbx2b* disruption in zebrafish contrast that of the mouse homolog *Tbx2*, which is also downstream of ocular BMP signaling, and mutations in this pathway produce a microphthalmic phenotype in mice (Behesti et al., 2009). It may be that *tbx2b* and *Tbx2* do not share the same role in early retinal development, that *tbx2b* has different spatiotemporal kinetics, or that redundancy with other genes (*tbx2a*, *gdf6b* or others) can compensate in zebrafish.

2.3.2 Differential role for gdf6a amongst the spectral subtypes of cone photoreceptors

We had speculated that *gdf6a* mutants would present with phenotypes similar to *tbx2b* mutants (lots of rods and few UV cones). This speculation was borne upon observations that *tbx2b* specifies rod versus UV cone fate, and *gdf6a* is a positive upstream regulator of *tbx2b* expression. Instead, the data revealed that gdf6a mutants do not exhibit the anticipated phenotype; rather, our observations indicate that *gdf6a* signaling promotes development or maintenance of blue-sensitive cones. This is uniquely promising, suggesting a set of novel regulatory actions in a stage of photoreceptor development that has not been adequately explored in zebrafish before: that of cone opsin spectral subtype specification. It is not yet clear whether *gdf6a* serves a role in cone specification, differentiation and/or survival, but one avenue of investigation will be modulating *gdf6a* signaling during proliferation and cone photoreceptor differentiation as replicated in our regeneration model (Fraser et al.,

2013). Pursuing *gdf6a* effects in the regenerative context is especially intriguing since recent work shows that the proliferative response in Müller glia requires regulation of Tgfβ signaling (Lenkowski et al., 2013).

It remains undetermined the extent to which the blue cone-specific requirement for *gdf6a*, established herein, is mechanistically similar to the apparent UV cone-specific requirement of *tbx2b* (Alvarez-Delfin et al., 2009). At the cellular level, a notable difference in phenotypes is that *tbx2b* mutants present with an excess of rod photoreceptors (Alvarez-Delfin et al., 2009), which we did not observe in *gdf6a* mutants. With respect to cellular sites of action for these genes in determining cell fate, it is not clear whether UV and blue cones are products of a common pool of progenitor cells; although UV cones and blue cones are together the last photoreceptor types to differentiate during retinal development (based on the sequential appearance of detectable opsin transcript in goldfish (Stenkamp et al., 1997)), the terminal divisions seem to rely upon separate/dedicated progenitor pools (Suzuki et al., 2013). Regardless, it is tempting to speculate that common molecular signaling pathways might lead to a low abundance of blue and UV cones, in *gdf6a* and *tbx2b* mutants respectively, especially considering the epistatic relationship of these genes during both early and late retinal development (see below).

2.3.3 *gdf6a* and *tbx2b* genetic interdependence in UV cone and rod photoreceptor differentiation

Considering the disparate ocular phenotypes observed between their respective mutants, during both early and late retinal development, the genetic interaction between *gdf6a* and *tbx2b* is neither simple nor linear. But interpreting this relationship is made more complex by the low UV cone abundance and high rod abundance (the lots-of-rods phenotype) observed in high rates among compound mutant larvae. Some of these larvae were found to display the recessive *tbx2b* phenotype despite being genetically heterozygous for the *tbx2b* mutation (which alone does not yield the lots-of-rods phenotype). *gdf6a* appears to modulate *tbx2b* indirectly, suggestive of a genetic interdependence in a UV cone fate decision. One hypothesis to this end is that *gdf6a*

and *tbx2b* both promote a common activity, perhaps via being in the same pathway (as per Fig. 2.3). Thus a lack of *gdf6a* signaling would reduce the efficacy of *tbx2b* to promote a UV cone fate, causing the assumption of a lots-of-rods phenotype or a wild type phenotype to become more random. Alternatively, *tbx2b* expression may have a minimum threshold for activity that is sensitive to perturbations (including disrupted *gdf6a* signaling) affecting *tbx2b* mRNA transcript levels. Alternatively, *gdf6a* signaling may alter the timing of cell cycle exit of photoreceptor progenitors, as has been established for *gdf11* (Kim, 2005); thus with altered *gdf6a* there may be increased probability that progenitors undergo specification/ differentiation and invoke *tbx2b* expression at an inappropriate time, thereby shifting cell fates.

2.4 Conclusion

Further exploration into pathways utilizing *tbx2b* and *gdf6a* would clarify the order or pattern of photoreceptor specification, which will also provide insight into zebrafish cone mosaic formation and photoreceptor regeneration following injury. Zebrafish possess latent stem cells within the retina and have a robust neural regenerative capacity. Because of these properties, zebrafish are a promising in vivo model to study not just photoreceptor development, but also regulation of cone photoreceptor regeneration and integration. With zebrafish as an impressive model of functional regeneration, stem cell therapy for restoring daytime vision can become a reality.

2.5 Figures

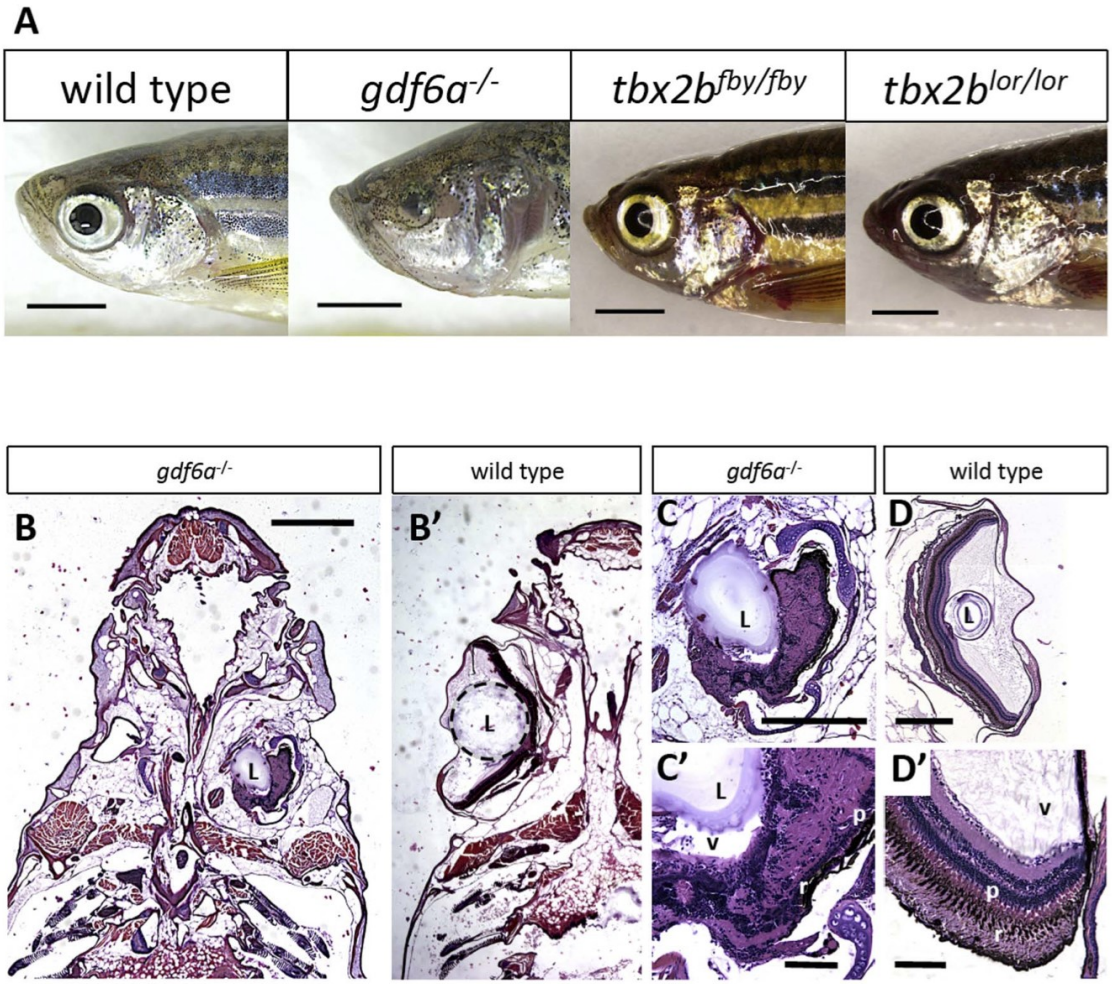

Figure 2.1. *gdf6a* and *tbx2b* mutants do not share the microphthalmic phenotype, despite a shared pathway in early eye development.

(**A**) *gdf6a*$^{s327/s327}$ mutants (labeled *gdf6a*$^{-/-}$ in figures) exhibit microphthalmia to varying degrees of severity during development and throughout adulthood, unlike their wild type and heterozygous siblings. *tbx2b* mutants do not exhibit microphthalmia, and their eyes develop normally. Scale bars 2 mm. B, C, D. Coronal sections of adult zebrafish heads, comparing microphthalmic *gdf6a*$^{s327/s327}$ (**B**) and wildtype fish (B9). Microphthalmia and anophthalmia present variably in *gdf6a*$^{s327/s327}$ fish (e.g. right and left eyes in B, respectively) and eyes are often noted to possess a lens (L), though in this instance the right eye is inverted such that the anterior segment is oriented towards the midline. RPE

(r) and a thin layer of photoreceptors (p) are discernable in *gdf6a*$^{s327/s327}$ fish (**C'**), though other retinal layers are not recognizable due to multiple tissue infoldings. In panel **D**, the lens was presumably displaced away from the iris during dissection/fixation. Note **C** is at higher magnification compared to **D**. Scale bar in B 1 mm; C, D is .5 mm; C9, D9 is .1 mm. L, lens; v, vitreous; r, RPE layer; p, photoreceptor layer.

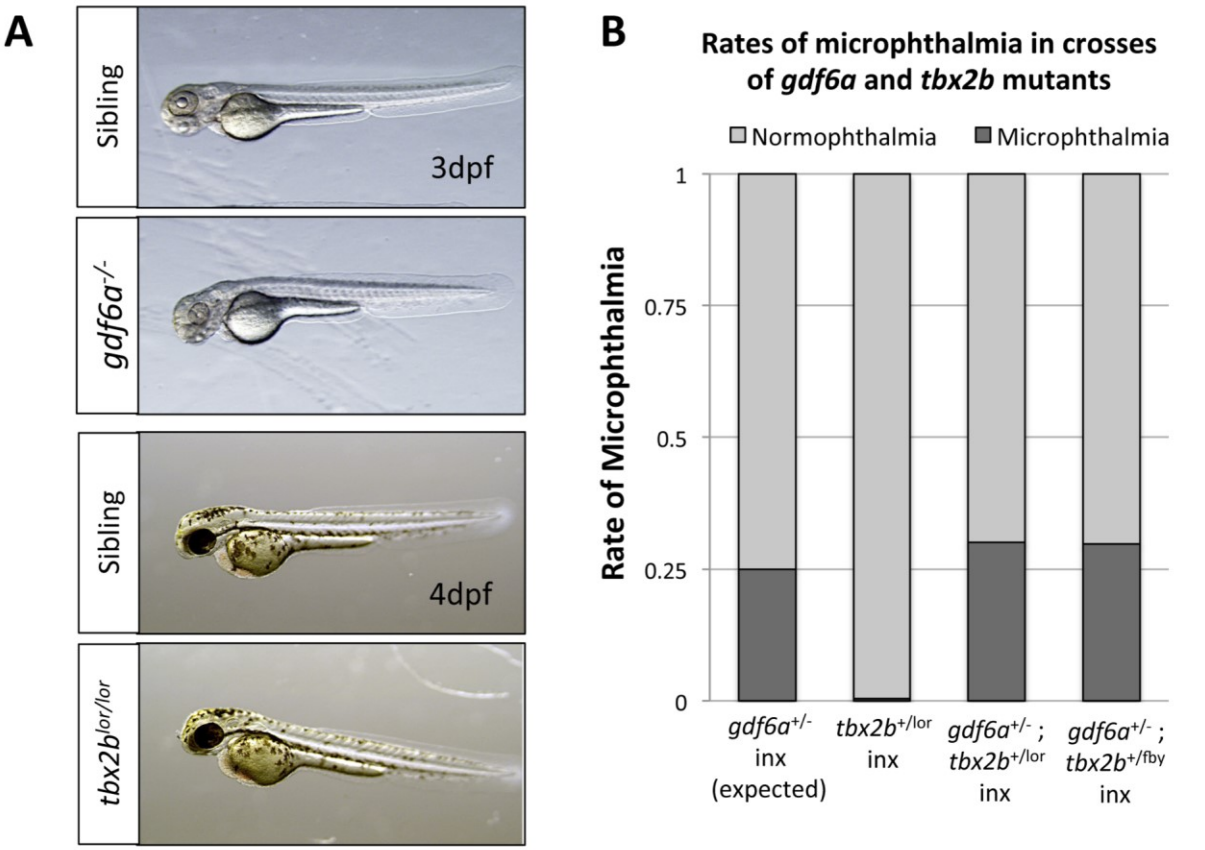
A
Sibling
3dpf
gdf6a-/-
Sibling
4dpf
tbx2blor/lor
B
Rates of microphthalmia in crosses of gdf6a and tbx2b mutants
Normophthalmia
Microphthalmia
Rate of Microphthalmia
1
0.75
0.5
0.25
0
gdf6a+/- inx (expected)
tbx2b+/lor inx
gdf6a+/- ; tbx2b+/lor inx
gdf6a+/- ; tbx2b+/fby inx
C
Distribution of Eye Size in [gdf6a+/- ; tbx2b+/lor] in-crosses
n= 89
n= 29
Number of fish per Bin
25
20
15
10
5
0
44-45
46-47
48-49
50-51
52-53
54-55
56-57
58-59
60-61
62-63
64-65
66-67
68-69
70-71
72-73
74-75
76-77
78-79
80-81
82-83
84-85
86-87
88-89
90-91
92-93
94-95
1000X eye length/body length

Figure 2.2. Disruption of *tbx2b* does not modify the gdf6a microphthalmic phenotype.

(**A**) *gdf6a*$^{s327/s327}$ mutants exhibit microphthalmia (observed at 3dpf) but *tbx2b*$^{-/-}$ mutants (lor and fby) do not, indicating that disruption of *tbx2b* does not interfere with identical pathways as *gdf6a* in early eye development. (**B**) Microphthalmia is rarely observed in *tbx2b* mutant in-crosses (inx) alone (*tbx2b*$^{+/lor}$ in-cross shown, n = 220) compared to in-crosses of *gdf6a*$^{+/s327}$, which yield 25% with microphthalmia (following Mendelian ratios of inheritance and recessive phenotype). When [*gdf6a*$^{+/s327}$;*tbx2b*$^{+/lor}$] or [*gdf6a*$^{+/s327}$;*tbx2b*$^{+/fby}$] compound heterozygous mutants are in-crossed (n = 121 and 195 respectively, both at 6dpf), rates of microphthalmia do not increase significantly from rates expected of in-crosses of *gdf6a*$^{+/s327}$ alone (X^2 p = 0.873 and p = 0.137, respectively). (**C**) The eye size compared to body length (shown as ratio) of a [*gdf6a*$^{+/s327}$;*tbx2b*$^{+/lor}$] in-cross does not reveal a subset of intermediate eye sizes, but remains bimodal, with the normophthalmic curve (right curve) showing a normal distribution (Shapiro-Wilk Normality test, W = 0.9888, p = 0.6532) (n = 118, 4dpf).

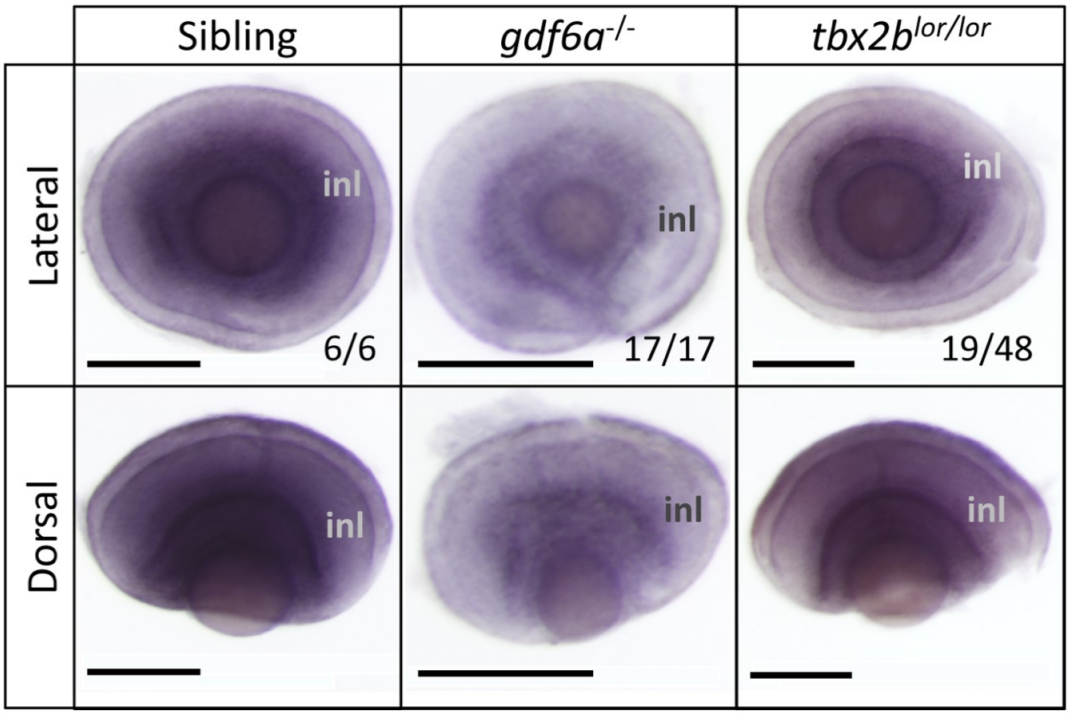

Figure 2.3. *gdf6a* positively modulates the abundance of *tbx2b* transcript during stages of retinal development when photoreceptors differentiate.

All panels show in situ hybridization using *tbx2b* riboprobe. *gdf6a*$^{s327/s327}$ mutants have less *tbx2b* expression at 3 days post- fertilization (dpf) compared to normophthalmic siblings, akin to tbx2blor/lor mutants. Fractions represent proportion of clutch represented by image shown. Scale bars 100 mm; inl, inner nuclear layer.

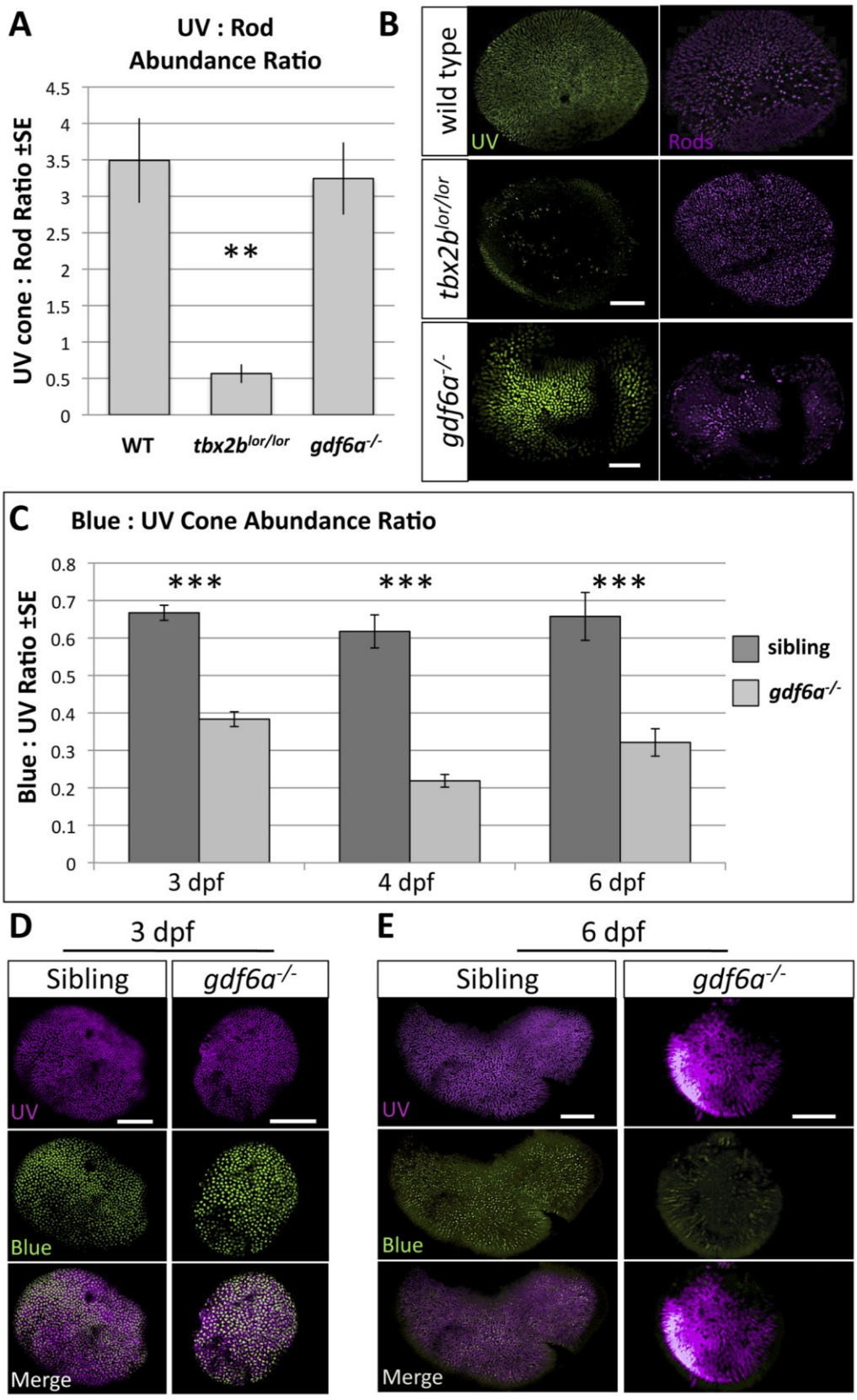
A
UV : Rod
Abundance Ratio
UV cone : Rod Ratio ±SE
4.5
4
3.5
3
2.5
2
1.5
1
0.5
0
**
WT
tbx2b lor/lor
gdf6a -/-
B
wild type
tbx2b lor/lor
gdf6a -/-
UV
Rods
C
Blue : UV Cone Abundance Ratio
Blue : UV Ratio ±SE
0.8
0.7
0.6
0.5
0.4
0.3
0.2
0.1
0
***
***
***
3 dpf
4 dpf
6 dpf
sibling
gdf6a -/-
D
3 dpf
Sibling
gdf6a -/-
UV
Blue
Merge
E
6 dpf
Sibling
gdf6a -/-
UV
Blue
Merge

Figure 2.4. Mutation in *gdf6a* does not disrupt *tbx2b* function in UV-versus-rod photoreceptor specification, but *gdf6a* rather plays a role in blue cone specification.

(**A, B**) *tbx2b*$^{lor/lor}$ mutants have fewer UV cones and more rods than wildtype fish (the lots-of-rods phenotype) (Kruskall-Wallis ANOVA, **p,0.005), but *gdf6a*$^{s327/s327}$ mutants have a normal abundance ratio and distribution of UV cones and rods (n = 10 wildtype, 8 *tbx2b*$^{lor/lor}$, and 7 *gdf6a*$^{s327/s327}$; UV cones expressing GFP and rods were labeled with antibody 4C12). Scale bars 30 mm and 80 mm, respectively. (**C**) Larval *gdf6a*$^{s327/s327}$ mutants have a unique cone photoreceptor phenotype in which there are significantly fewer blue cones relative to UV cones at all ages examined (which is not observed in *tbx2b*$^{lor/lor}$ or *tbx2b*$^{fby/fby}$ mutants- not shown) (Kruskall-Wallis ANOVA, ***p,0.001) Sample sizes at 3 days post-fertilization (dpf) are n = 17 larvae per genotype quantifying cells visualized via opsin in situ hybridization (Panel **D**); at 4 dpf data are from n = 9 wild type and n = 13 mutants assessed via GFP and mCherry transgene expression in cones; at 6dpf data are from 2 replicates of n = 4+7 wild type and n = 5+6 mutants assessed via transgene expression in cones (Panel E). (**D**) UV and blue cones identified in 3 dpf by in situ hybridization against their respective opsins (Scale bars are 100 mm). (**E**) UV and blue cones identified in transgenic lines at 6dpf by expression of GFP and mCherry, respectively (Scale bars are 60 mm and 40 mm in sibling and mutants, respectively).

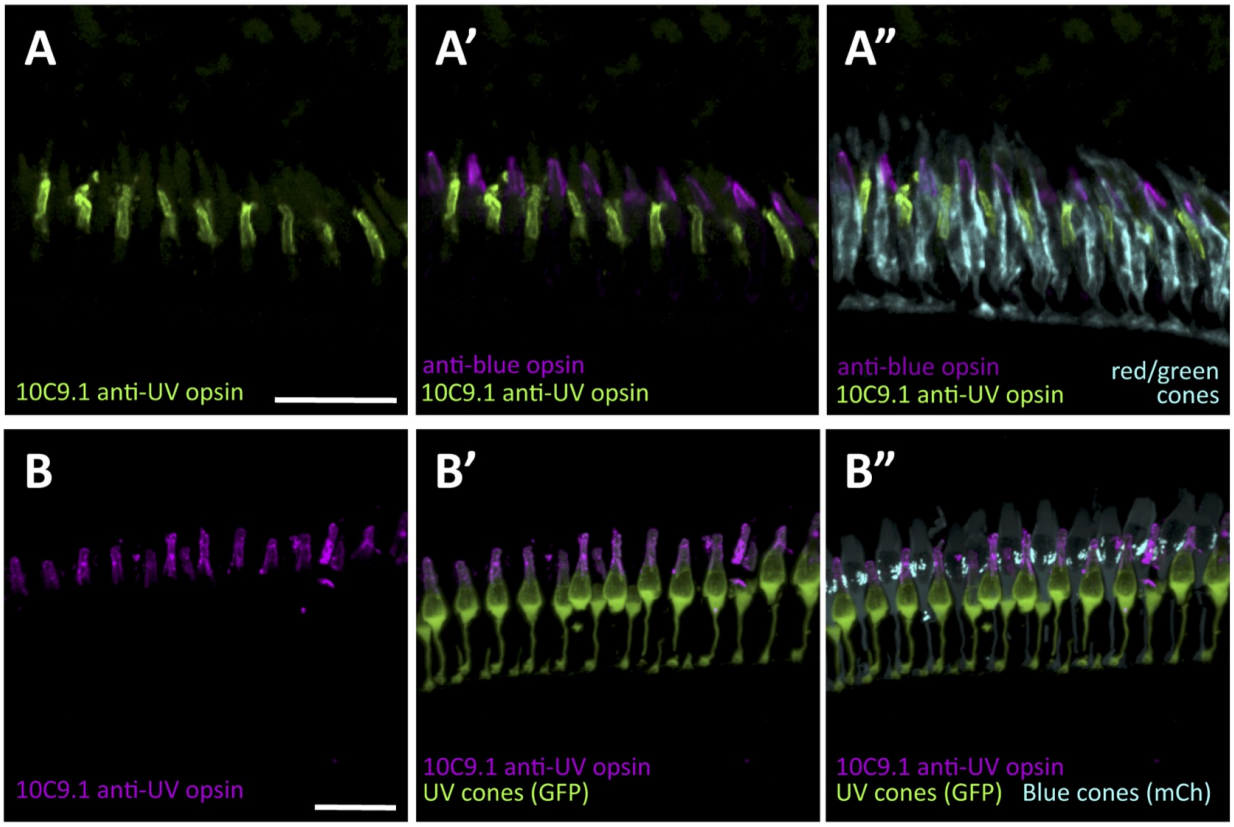

Figure 2.5. A monoclonal antibody raised in rat (10C9.1) labels zebrafish UV cone outer segments, allowing all cone subtypes to be simultaneously labeled by immunohistochemistry.

Antibody 10C9.1 specifically labels the outer segments of a class of short single cones in the adult zebrafish retina (Fig. 2.S1 panel **A**). 10C9.1 specificity is supported (see Fig. 2.S1 panels **B–D**), including by a dramatic decrease in number of cells labeled when 10C9.1 is applied to retinas from zebrafish mutants (*tbx2b*$^{lor/lor}$) that have a paucity of UV cones. (**A**) The population of single cones labeled by 10C9.1 is the UV cones, because established antibodies against the other single cone class, the blue cones, labels a distinct cone population (**A'**). 10C9.1 enables an unprecedented combination of antibodies raised in different species that simultaneously label and distinguish all cone photoreceptor subtypes (**A''**). E. Further evidence that 10C9.1 labels UV cone outer segments comes from its co-localization with UV cones filled with green fluorescent protein (GFP), and its exclusion from blue cones filled with mCherry (mCh) in transgenic zebrafish (Tg(-5.5opn1sw1:EGFP)kj9;Tg(-3.5opn1sw2:mCherry)ua3011). Panel **B** is available as Movie 2.S1. Scale bars 30 mm.

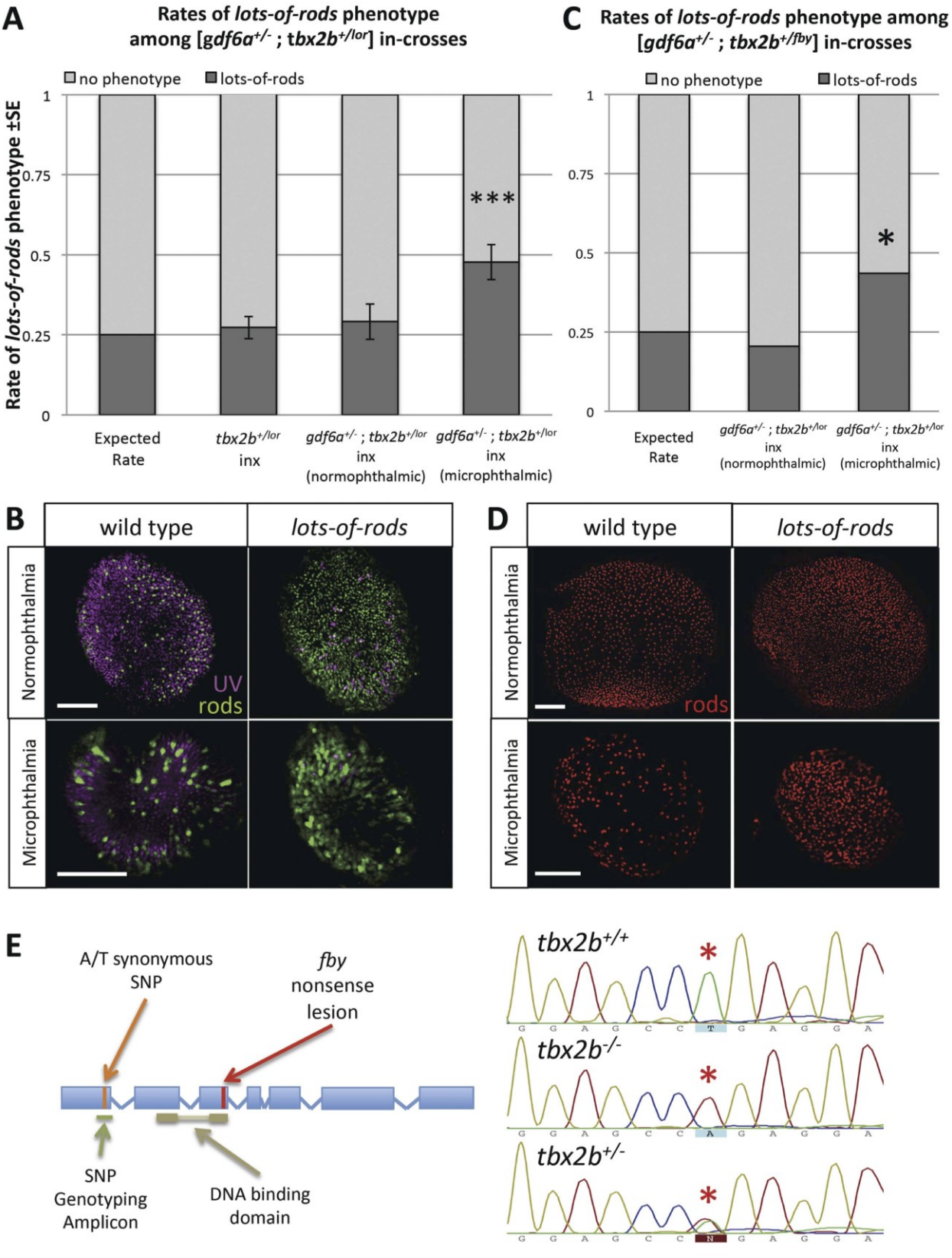
A
Rates of lots-of-rods phenotype among [gdf6a+/- ; tbx2b+/lor] in-crosses
no phenotype
lots-of-rods
Rate of lots-of-rods phenotype ±SE
1
0.75
0.5
0.25
0
***
Expected Rate
tbx2b+/lor inx
gdf6a+/- ; tbx2b+/lor inx (normophthalmic)
gdf6a+/- ; tbx2b+/lor inx (microphthalmic)
C
Rates of lots-of-rods phenotype among [gdf6a+/- ; tbx2b+/fby] in-crosses
no phenotype
lots-of-rods
1
0.75
0.5
0.25
0
*
Expected Rate
gdf6a+/- ; tbx2b+/lor inx (normophthalmic)
gdf6a+/- ; tbx2b+/lor inx (microphthalmic)
B
wild type
lots-of-rods
Normophthalmia
Microphthalmia
UV rods
D
wild type
lots-of-rods
Normophthalmia
Microphthalmia
rods
E
A/T synonymous SNP
fby nonsense lesion
SNP Genotyping Amplicon
DNA binding domain
tbx2b+/+
tbx2b-/-
tbx2b+/-
G G A G C C T G A G G A
G G A G C C A G A G G A
G G A G C C N G A G G A

Figure 2.6. *gdf6a* modulates *tbx2b* regulation of UV cone and rod development. (**A, B**) When [*gdf6a*$^{+/s327}$;*tbx2b*$^{+/lor}$] compound heterozygous mutants are in-crossed (inx), a disproportionate fraction of microphthalmic offspring exhibit the lots-of-rods phenotype compared to normophthalmic siblings, *tbx2b*$^{+/lor}$ in-crosses, and to predicted Mendelian ratios of the recessive lots-of-rods phenotype (X^2 ***p,0.001; 3 replicates of n = 17, 19, 35 microphthalmics; 6dpf). UV cones and rods were labeled using antibodies 10C9.1 and 4C12 displayed in magenta and green, respectively. A portion of microphthalmic larvae with the lots-of-rods phenotype has a *tbx2b*$^{+/lor}$ genotype (see Table 2.1). (**C, D**) When [*gdf6a*$^{+/s327}$;*tbx2b*$^{+/fby}$] compound heterozygous mutants are in-crossed, the lots-of-rods phenotype is again observed at higher rates in microphthlamic eyes compared to normophthalmic eyes (X^2 *p = 0.007; 1 replicate, n = 39 microphthalmics, 6 dpf). Panel **D** shows rod opsin in situ hybridization (red). Scale bars are all 50 mm. (**E**) Genotyping for the lor mutation was performed via linkage analysis using an A/T synonymous SNP located before the DNA binding domain of *tbx2b* in lor and non-lor alleles, respectively. *gdf6a*$^{s327/s327}$ mutants with a corresponding SNP of T were used in crossing of the mutant lines.

		Expected				**Observed**			
Phenotype		wildtype	Lots-of-rods			wildtype	Lots-of-rods		
	Raw #/35 total	26	9			22	13		
	%	75%	25%			63%	37%		
			Lots-of-rods				Lots-of-rods		
tbx2b			+/+	+/-	-/-		+/+	+/-	-/-
genotype	Raw #/35 total		0	0	9		0	4	9
	%		0%	0%	**25%**		0%	12%	25%

Table 2.1. Identification of compound [*gdf6a*$^{s327/s327}$*; tbx2b*] mutants with mismatched phenotype and genotype regarding *tbx2b*.

SNP	Fwd primer	Rev primer	Size (bp)
rs40785418	TGC GCT TGA ATG GAC ATC CGC A	AAG GCG AGA GCA GAC AGC GG	196
rs40952575	**CGG ACC ATA CCC TGG CCG GA**	**TGG TCC CAT AGA TCC TTC GCT TCC A**	**160**
rs41094432	CTG CCG ACG ACT GCC GCT AC	TCC CCA GTA GCT GGG CTA TCC G	115
rs41247043 rs40724179	CCG CAT TGC CAA GCG GCC TA	TGA CGA AGT CTC CCG CTG GCT	194

Table 2.2. Primers used to identify single nucleotide polymorphisms (SNPs) for *tbx2b* genotyping.

SNP names from http://www.ncbi.nlm.nih.gov/snp/ ; the SNP ultimately used for genotyping in this study is in bold.

A

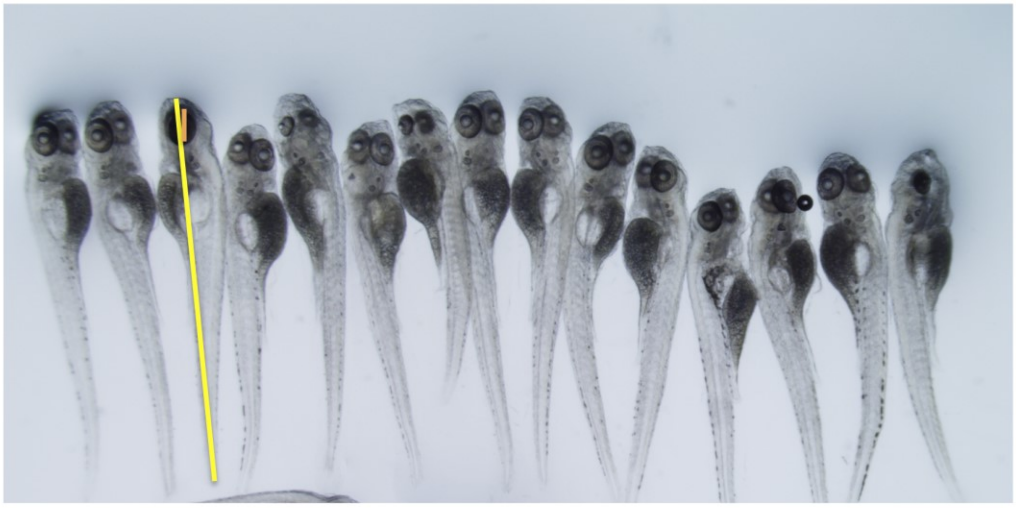

B

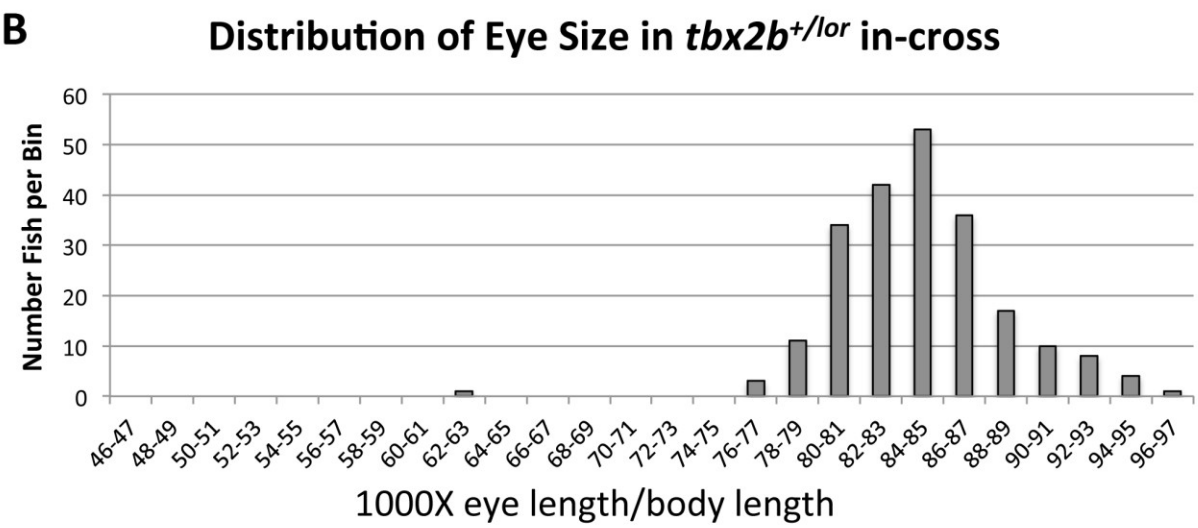
Distribution of Eye Size in tbx2b+/lor in-cross
Number Fish per Bin
0
10
20
30
40
50
60
46-47
48-49
50-51
52-53
54-55
56-57
58-59
60-61
62-63
64-65
66-67
68-69
70-71
72-73
74-75
76-77
78-79
80-81
82-83
84-85
86-87
88-89
90-91
92-93
94-95
96-97
1000X eye length/body length

C

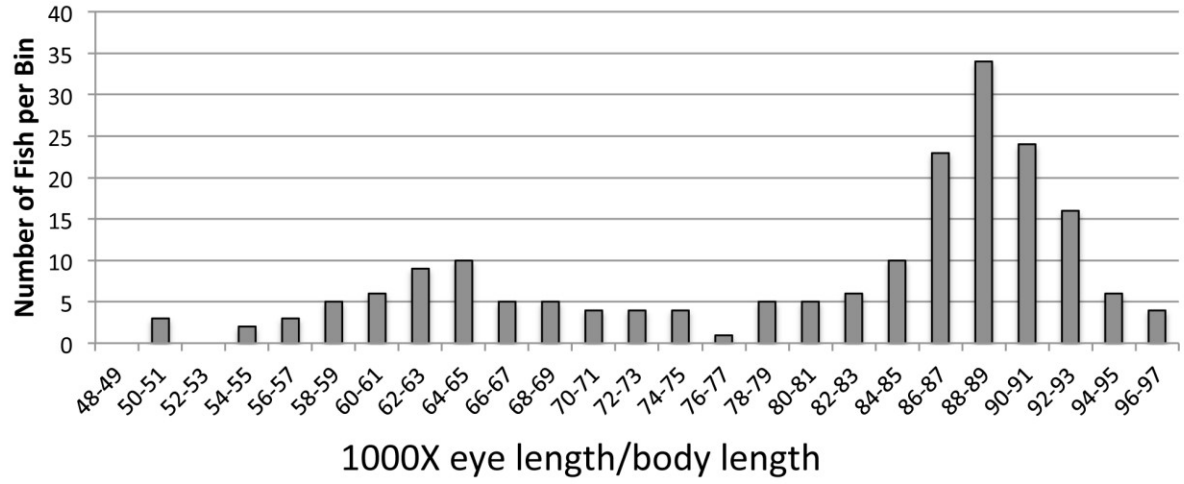
Distribution of Eye Size in
[gdf6a+/s327 ; tbx2b+/fby] in-cross
Number of Fish per Bin
0
5
10
15
20
25
30
35
40
48-49
50-51
52-53
54-55
56-57
58-59
60-61
62-63
64-65
66-67
68-69
70-71
72-73
74-75
76-77
78-79
80-81
82-83
84-85
86-87
88-89
90-91
92-93
94-95
96-97
1000X eye length/body length

Figure 2.S1: Eye size in various compound mutants shows no obvious change in severity of the microphthalmia phenotype (compare to Fig. 2.1C).

(**A**) Eye diameter along the anterior-posterior axis (orange line) was measured at 6dpf and normalized to body length (not including tail fin) (yellow line). Both normophthalmic and microphthalmic larvae are shown. (**B**) Ratios of eye length to body length among the progeny of an in- cross of *tbx2b*$^{+/lor}$ fish show no obvious difference from wild type fish, (n = 220). (**C**) The same ratios among the progeny of an in- cross of [*gdf6a*$^{+/s327}$; *tbx2b*$^{+/fby}$] fish show the expected Mendelian abundance of ~25% microphthlamic fish (see also Fig. 2.3**B**). The normophthalmic fish have eye sizes distributed in a normal fashion (Shapiro-Wilk Normality test, p.0.05). Among the microphthalmic progeny, there is also a normal distribution of eye size (Shapiro-Wilk test, p.0.05) (n = 194).

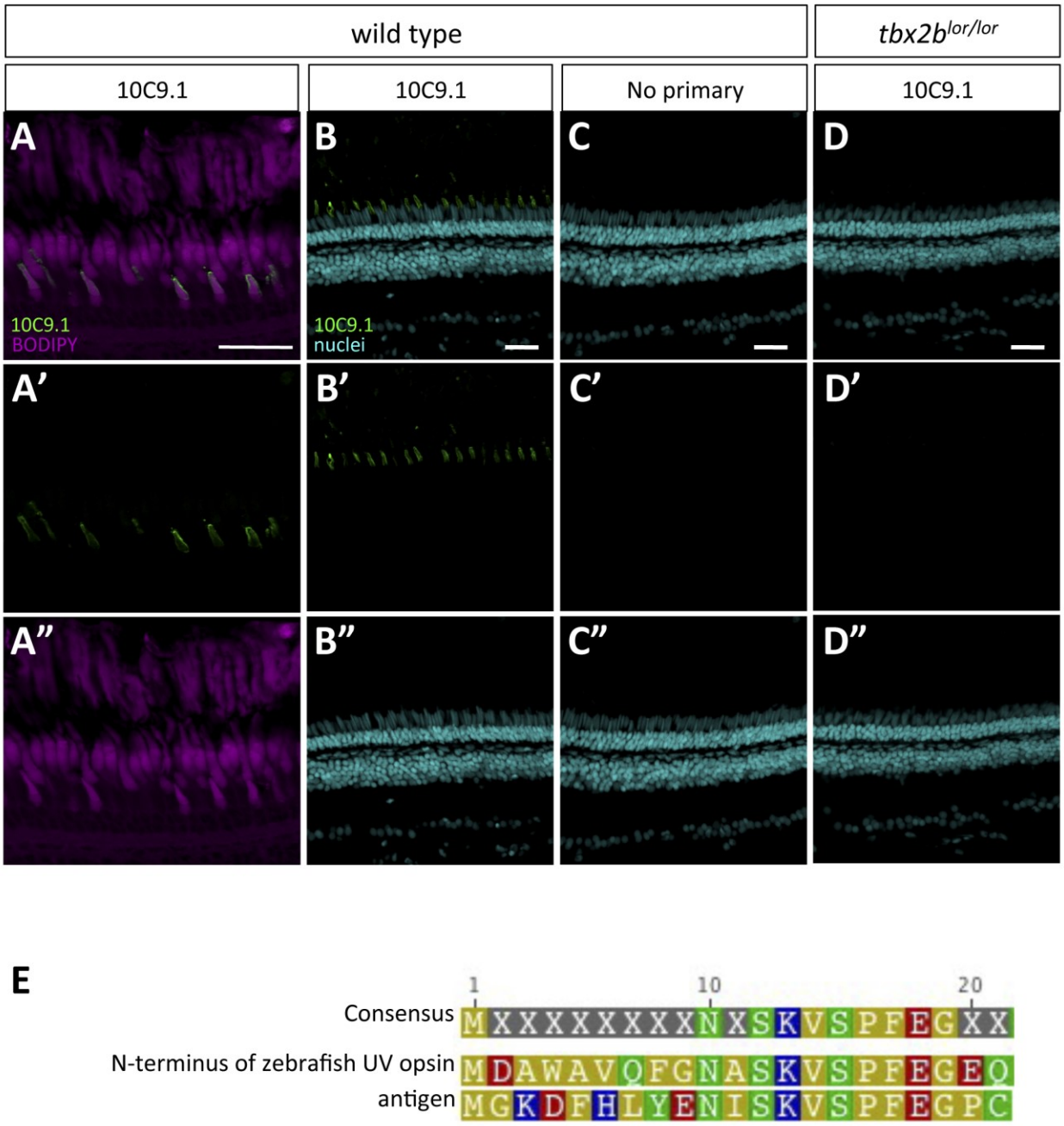

Figure 2.S2: Antibody 10C9.1 specifically labels the outer segments of a class of short single cones in the adult zebrafish retina, as seen in Fig. 2.5.

(**A**) Localization of 10C9.1 labelling to single cone outer segments as clarified by Bodipy counterstain of lipid-rich photoreceptor cell bodies and outer segments. (**B–D**) 10C9.1 specificity is supported by localized labeling in the adult retina (**B**), a lack of labeling when adjacent retinal cryosections are treated identically except for omission of primary antibody (**C**), and by a dramatic decrease in number of cells labeled when 10C9.1 is

applied to retinas from adult zebrafish mutants (*tbx2b*$^{lor/lor}$) that have a paucity of UV cones (**D**). Other negative controls included applying other rat IgGs as primary antibody, and these produced equivalent results to panel **C**. Retinas in panels **B** and **D** were treated identically including equivalent application of 10C9.1 antibody, and simultaneous processing of tissue by inclusion in the same tissue block prior to cryosectioning. The specificity of 10C9.1 is supported by the paucity of labeling in *tbx2b*$^{lor/lor}$ retinas (**D**), which are known to have few UV cones. Scale bars 30 mm. ‘‘rods’’ indicates rod outer segments; dc, double cones; ipl; inner plexiform layer; onl, outer nuclear layer; inl, inner nuclear layer; rgc, retinal ganglion cell layer. (**E**) An alignment of the antigen used to raise 10C9.1 in rats, which represents the 20 N-terminal amino acids from rainbow trout UV opsin plus a C-terminal cysteine to enable linkage of the peptide to the carrier protein keyhole limpet hemocyanin.

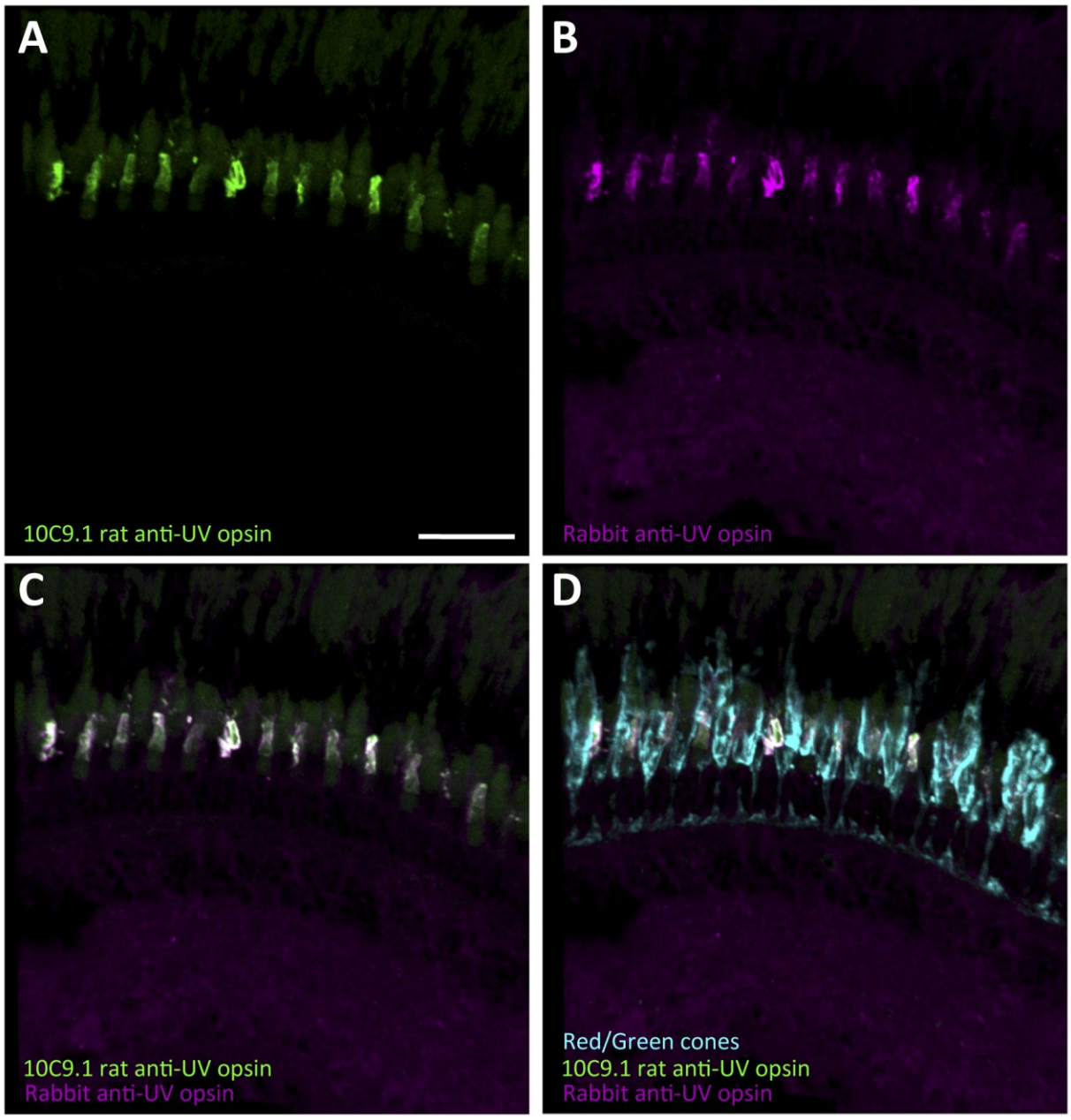

Figure 2.S3: 10C9.1 colocalizes with existing rabbit anti- UV antibody

Scale bar 30 mm. Both the 10C9.1 rat anti-UV and Hyde rabbit anti-UV are somewhat over-exposed to demonstrate background/autofluorescent labeling (existing rabbit anti-UV antibody was provided by David Hyde, University of Notre Dame).

(Movie can be accessed at PloS ONE: http://journals.plos.org/plosone/article?id=10.1371/journal.pone.0092991#s6)

Movie 2.S1: A new monoclonal antibody raised in rat (10C9.1) labels zebrafish UV cone outer segments.

Coordinate with Figure 5E. Further evidence that rat monoclonal antibody 10C9.1 (pseudocoloured magenta) labels UV cone outer segments. 10C9.1 co-localizes with UV cones filled with green fluorescent protein (GFP, pseudocoloured green), and is excluded from blue cones filled with mCherry (mCh, pseudoco- loured cyan) in transgenic zebrafish (Tg(-5.5opn1sw1:EGFP)kj9; Tg(-3.5opn1sw2:mCherry)ua3011). Scale bars 30 mm.

2.6 Methods

2.6.1 Ethics statement

Fish care and protocols were approved by the Animal Care and Use Committee: Biosciences at the University of Alberta. Rat care and protocols were approved by the Animal Care Committee at the University of Victoria. In each instance protocols and care were in accordance with the Canadian Council on Animal Care.

2.6.2 Animal care and establishment of mutant crosses

Zebrafish (Danio rerio) were raised and maintained according to standard procedures (Westerfield, 2000). Larvae were kept at 28ºC in E3 media. *Gdf6a*$^{s327/+}$ (Gosse and Baier, 2009) (ZFIN ID ZDB-ALT-050617-10), *tbx2b*$^{p25bbtl/p25bbtl}$ (ZFIN ID ZDB-GENO-080920-2, referred in text and figures as *tbx2b*$^{lor/lor}$) (Alvarez-Delfin et al., 2009), and *tbx2b*$^{c144/+}$ (ZFIN ID ZDB- GENO-130130-6, referred in text and figures as *tbx2b*$^{fby/+}$) (Clanton et al., 2013; Snelson et al., 2008) fish were gifted from Andrew Waskiewicz (University of Alberta), James Fadool (Florida State University), and Josh Gamse (Vanderbilt University), respectively. These lines were crossed to create [*gdf6a*$^{+/s327}$; *tbx2b*$^{+/lor}$] and [*gdf6a*$^{+/s327}$; *tbx2b*$^{+/fby}$] compound heterozygous mutants, which were subsequently in-crossed to acquire [*gdf6a*$^{s327/s327}$; *tbx2b*$^{lor/lor}$] and [*gdf6a*$^{s327/s327}$; *tbx2b*$^{fby/fby}$] compound homozygous mutants along with siblings of various genotypic combinations. The *gdf6a*$^{s327/s327}$ and *tbx2b*$^{lor/lor}$ lines were also crossed with transgenic lines: Tg(-5.5opn1sw1:EGFP)kj9 (Takechi, 2005) and Tg(-3.5opn1sw2:mCherry)ua3011 (Duval et al., 2013; Fraser et al., 2013) expressing fluorescent proteins in UV and blue cones, respectively.

2.6.3 Assessing phenotypes, genotyping and linkage analysis

Larvae from the above-described mutant lines were assessed for phenotype and, where noted, subsequently genotyped. *Gdf6a*$^{s327/s327}$ larvae were identified by their microphthalmic phenotype starting at 3dpf. Where relevant, eye size-to-body length

ratios were calculated to check for an intermediate eye size phenotype (details below). To identify putative *tbx2b*^{lor} or *tbx2b*^{fby} homozygous mutants, larval retinas were removed from the heads, flatmounted, imaged on a Zeiss Axio Observer.Z1 microscope with AxioCam software (Carl Zeiss MicroImaging, Oberkochen), and thereby screened for the lots-of-rods phenotype, characterized by an abnormally large population of rod photoreceptors and a small population of UV cones, which is exacerbated in *tbx2b*$^{fby/fby}$ mutants (Alvarez-Delfin et al., 2009). Heterozygous mutant and wildtype gdf6a and *tbx2b* siblings, which do not have a phenotype, were identified by genotyping.

Genomic DNA was isolated as described previously (Meeker et al., 2007). Genotyping for *gdf6a*^{s327} was done by restriction fragment length polymorphism (RFLP) analysis. Primers designed by Gosse and Baier (Gosse and Baier, 2009) amplify a 280 bp region including the *gdf6a*^{s327} locus. This PCR product was either digested with *SfaNI* restriction enzyme and run on a gel, or sequenced with a BigDye v3.1 kit (Invitrogen, Carlsbad, Cat. # 4337455) and submitted to Molecular Biology Services Unit at the University of Alberta. *Tbx2b*^{fby} was genotyped through RFLP analysis; primers used were designed previously (Snelson et al., 2008) and amplify a 318 bp region featuring the *tbx2b*^{fby} locus. The PCR product was digested with *MseI* restriction enzyme and run on a gel.

The lesion of the *tbx2b*^{lor} allele has been linkage-mapped to the region of *tbx2b* (Alvarez-Delfin et al., 2009), but has not yet been identified. Therefore, genotyping fish for *tbx2b*^{lor} required developing a single nucleotide polymorphism (SNP) genotyping assay, and inferring the *tbx2b* genotype. We explored six SNPs annotated in the zebrafish *tbx2b* gene in the Ensembl database; using Geneious software, we designed primers to amplify each of the SNPs to genotype via sequencing (performed at Molecular Biology Service Unit, University of Alberta) (Table 2.2). Each SNP was amplified from representative adult male *tbx2b*$^{lor/lor}$ fish, and from representative adult female *gdf6a*$^{s327/s327}$ fish, and examined for homozygosity at each SNP. While several homozygous SNPs were identified, only two were different between the two populations, and one synonymous SNP (bold text in Table 2.2) was chosen based on the reliability of PCR amplification and sequencing (Fig. 2.6E). Thus, the presence of an

‘‘A’’ in this SNP implied inheritance of the parental *tbx2b*^{lor} allele, while presence of a ‘‘T’’ implied the parental WT allele (in fish with mutation in *gdf6a*). These adult fish were crossed, and all resulting [*gdf6a*$^{+/s327}$*; tbx2b*$^{+/lor}$] fish were confirmed to be heterozygous at the relevant SNP. In-crossing these compound heterozygotes and genotyping the resultant normophthalmic progeny confirmed that the SNP genotyping assay consistently predicts the lots-of-rods phenotypes.

2.6.4 Generation of rat monoclonal against UV opsin

Generation of rat monoclonal antibodies against UV opsin was performed by Immunoprecise Antibodies Ltd (Victoria BC, Canada) using standard intraperitoneal injection method. Two F344 female rats were immunized with a recombinant antigen designed to mimic the N-terminus of trout UV opsin (NCBI accession NP_001117793.1) (Allison et al., 2003; Levin et al., 2004), see Fig. 2.S2E. Sera from hyperimmunized rats had been found to be specific against both trout and zebrafish UV opsin in immunohistochemistry and/or Western blots (Allison, 2004; Allison et al., 2006a). Lymphocytes were harvested from the spleen of the best responding rat and fused with rat myeloma YB2/0 to generate the hybridomas. Supernatants from a panel of clonal cells were screened for robust and specific labeling of zebrafish UV cones, and a successful clone was subcloned to generate line 10C9.1.

2.6.5 Immunocytochemistry and in situ hybridization

Immunocytochemistry was performed on larval zebrafish and retinal sections as previously described (Fraser et al., 2013) to label relevant structures. Briefly, larvae were fixed in 4% paraformaldehyde with 5% sucrose made in PO_4, pH 7.4 (PFA) overnight at 4ºC. Following fixation, washes of 1.0 M PO_4/5% sucrose, 1% Tween/H2O (pH 7.4), and acetone were performed. Blocking was done for 90 minutes with 10% NGS/PBS^{3+} (PBS^{3+}— phosphate buffered saline with 1% Tween, 1% Triton-X and 1% DMSO, pH 7.4), followed by incubation in antibody in 2% NGS/PBS^{3+} overnight at 4ºC. Primary antibodies and dilutions are as follows: 4C12 anti-rod opsin (ZFIN ID: ZDB-

ATB-090506- 2, 1:200) (Morris et al., 2005), zpr-3 anti-rod opsin (ZFIN ID: ZDB-ATB-081002- 45, 1:200); zpr-1 anti-arrestin3a labels double cones (ZFIN ID: ZDB-ATB-081002-43); and 10C9.1 anti-UV opsin (generated herein as described above, 1:100). Larvae were then incubated in secondary antibody in 2% NGS/PBS^{3+} overnight at 4uC Secondary antibodies used are as follows: Alexafluor anti-mouse 555 (Invitrogen, Carlsbad, Cat. #A-31570) (1:1000), Alexafluor anti-rabbit 488 (Invitrogen, Carlsbad, Cat. #A-21441) (1:1000). Deviations from the above protocol include using PBS/0.01% Tween in lieu of PBS^{3+} and omitting the 1.0 M PO_4/5% sucrose wash. Retinas were dissected from the head and flatmounted for imaging. Immunohistochemistry on retinal sections followed the same protocols applied instead to 10 mm cryosections of adult eyes prepared as described previously (Duval et al., 2013; Fraser et al., 2013).

In situ hybridization for photoreceptor opsins and *tbx2b* expression was performed as previously described (Allison et al., 2010) using DIG- and FLR-labeled riboprobes against blue-sensitive cone opsin (*opn1sw2*, 1424 bp, Accession No. AF109372, ZFIN ID: ZDB-GENE-990604-40), UV-sensitive cone opsin (*opn1sw1*, 1777 bp, Accession No. NM_131319, ZFIN ID: ZDB-GENE- 991109-25), rod opsin (1584 bp, Accession No. NM_131084, ZFIN ID: ZDB-GENE-990415-271), or *tbx2b* (1144 bp) (French, 2010) (2616 bp, Accession No. NM_131051, ZFIN ID: ZDB-GENE- 990726-27). Briefly, larvae were fixed in 4% PFA overnight at 4ºC, then permeabilized in MeOH overnight at 22ºC. Larvae underwent 30 minutes of digest in Proteinase K at 37ºC and were incubated in Hauptmann's prehybridization solution at 65ºC for between 2 hours and overnight, depending on the riboprobes used. Subsequently larvae were hybridized with riboprobe for at least one night at 65ºC. Blocking with Maleate Tw/2% DMSO/ 2% RMB was done for 2 hours prior to riboprobe detection using either 1:100 anti-digoxigenin-POD (Roche, Quebec, Cat. # 11 207 733 910) or 1:100 anti-fluorescein-POD (Roche, Quebec, Cat. #11 426 346 910) overnight at 4ºC. Larvae were then incubated in tyramide-conjugated fluorochrome according to manufacturer's instructions (Invitrogen, Carlsbad, Cat. #T-20912; T-30954).

Imaging was performed with a Zeiss Axio Observer.Z1 microscope with AxioCam software (Carl Zeiss MicroImaging, Oberkochen). Images were manipulated for channel colour and brightness in AxioCam (Carl Zeiss MicroImaging, Oberkochen), Imaris 664

(version 7.4.0, Bitplane, Badenerstrasse), or Adobe Photoshop CS5 Extended (Adobe Systems Inc., San Jose).

2.6.6 Histology

Paraffin sections of adult zebrafish heads fixed in PFA were prepared using standard protocols. Staining of sections with hematoxylin and eosin occurred after dewaxing. Sections were imaged on an Axioscope A.1 microscope (Carl Zeiss MicroImaging, Oberkochen) using a 12-bit, 2 megapixel MacroFIRE colour camera (Optronics, Goleta CA).

2.6.7 Data analysis

Photoreceptor abundance was measured in flatmounted retinas by counting labeled cells within a 100mm x 100mm area dorsal to the optic nerve head or, if this location was not obvious, sampling an area containing a minimum of 100 cells of each labeled photoreceptor type. Eye-to-body ratios were calculated using values from measuring the largest width of the eye, and the body length from nose to end of notochord. Cell counts and eye-to-body measurements were performed in ImageJ 1.45 (Wayne Rasband, National Institutes of Health, Bethesda; http://rsbweb.nih.gov/ij/ index.html) and statistical analysis was performed in SYSTAT 12 (Systat Software Inc., Chicago) and R (Robert Gentleman and Ross Ihaka, University of Auckland; http://www.r-project.org).

CHAPTER 3:

RECRUITMENT OF ROD PHOTORECEPTORS FROM SHORT-WAVELENGTH-SENSITIVE CONES DURING THE EVOLUTION OF NOCTURNAL VISION IN MAMMALS

Chapter 3 was previously published as:
Jung-Woong Kim[1], Hyun-Jin Yang[1], **Adam Phillip Oel[1]**, Matthew John Brooks, Li Jia, David Charles Plachetzki, Wei Li, William Ted Allison[2], and Anand Swaroop[2]. 2016. "*Recruitment of Rod Photoreceptors from Short-Wavelength-Sensitive Cones during the Evolution of Nocturnal Vision in Mammals*". Developmental Cell 37, 520-532.
[1]Co-first authors; [2]co-corresponding authors.

Author contributions: JK: mouse experiments, data analysis, evolutionary analysis, next-gen sequencing analysis, original draft. HY: mouse experiments, data analysis, next-gen sequencing analysis, original draft. **APO:** data analysis, and zebrafish experiment conceptualization, performance, and analysis. MJB: next-gen sequencing experiments, data curation, and analysis, and evolutionary analysis. LJ: mouse resource generation. DCP: next-gen sequencing analysis, and phylogenetic analysis. WL: mouse resource generation. **WTA**: zebrafish experiment conceptualization, data analysis, supervision. AS: data analysis, supervision, project administrator. JK, HY, APO, MJB, DCP, WL, WTA, and AS reviewed and edited the manuscript.

The text of this manuscript has been modified slightly for formatting consistency with the rest of this thesis.

3.1 Introduction

The duplex retina in vertebrates consists of specialized cone and rod photoreceptors (Fain et al., 2010; Lamb et al., 2007; D.-G. Luo et al., 2008a). Cones mediate non-quenching, rapid responses to photons with high acuity in daylight, whereas rods allow maximum sensitivity and energy conservation at the expense of spatial and temporal resolution. Cone photoreceptors also enable color discrimination by combining outputs of visual pigments (opsins) having distinct peak wavelength sensitivity (Nathans, 1999). How and when the duplex retina evolved, however, remains a long-standing mystery (Schultze, 1866; Walls, 1942).

Short-wavelength-sensitive (S) and long-wavelength-sensitive (L) cone opsins were present in the last common ancestor of jawed and jawless vertebrates (Okano et al., 1992), while rod visual pigment Rh1 (rhodopsin) and other cone opsin classes emerged subsequently by duplication of an ancestral, likely short-wavelength, opsin gene (Pisani et al., 2006). In concordance, rods first appear as an intermediate form in agnathan species (i.e., jawless vertebrates) such as lampreys and become more evident in gnathostomes (i.e., jawed vertebrates) (Lamb, 2013) (Fig. 3.1A). Despite functional specialization, rod morphology and phototransduction machinery are similar to those of cones (Fain et al., 2010; Morshedian and Fain, 2015), and rod signals piggyback on cone pathways in retinal circuitry (Oesch et al., 2011; Strettoi et al., 1992). On the basis of phylogenetic and anatomical analyses, rod photoreceptors were proposed to have originated from ancestral cone-like photoreceptors (Lamb et al., 2009, 2007).

In the mammalian retina, the generation of rods and cones is controlled by the combined actions of two transcription factors, Maf-family neural retina leucine zipper protein (Nrl) and thyroid hormone receptor b2 (Trβ2) (Ng et al., 2011; Swaroop et al., 2010), and S cones are proposed to be the default fate of post-mitotic photoreceptor precursors (Hunt and Peichl, 2014; Swaroop et al., 2010). In mice, loss of *Nrl* results in a retina with predominantly S cones in place of rods (Mears et al., 2001), and ectopic expression of *Nrl* in cone precursors is sufficient to induce rod differentiation (Oh et al., 2007). *Nrl* is expressed in rod photoreceptors shortly after the final mitosis, as indicated by GFP expression directed by a 2.5-kb *Nrl* promoter (Akimoto et al., 2006), consistent

with antibody immunostaining studies (Ng et al., 2011). Furthermore, mice lacking *Trβ2* have S cones but no medium-wavelength-sensitive (M) cones (Ng et al., 2001), and replacement of *Nrl* by *Trb2* produces M cones instead of rods (Ng et al., 2011). Transcriptional control of rod photoreceptor birth is less well resolved in cone-dominant vertebrates such as teleosts (Stenkamp, 2011), especially with respect to *nrl*, whose expression is not limited to rods in zebrafish (Nelson et al., 2008). Notably, the loss of T-box transcription factor *tbx2b* in zebrafish results in rod generation from UV cone precursors (Alvarez-Delfin et al., 2009; Michèle G. DuVal et al., 2014). In addition, thyroid hormone treatment affects photoreceptor development in trout (Allison et al., 2006b), and *thrb2* modulates the generation of different cone subtypes in zebrafish (Suzuki et al., 2013; Yoshimatsu et al., 2014).

A typical mammalian retina accommodates a great abundance of rods with a paucity of cones; few exceptions include rare cone-dominant retinas of a subset of diurnal species and highly specialized regions (such as fovea) in primate retinas (Gerkema et al., 2013). On the contrary, most non-mammalian vertebrates possess abundant cone photoreceptors in multiple spectral subclasses. This stark difference in retinal composition may reflect a ‘‘nocturnal bottleneck’’ hypothesized to have occurred early in the evolutionary history of mammals, wherein early mammals adapted to novel scotopic (dim light) niches (Gerkema et al., 2013; Heesy and Hall, 2010). We were curious as to how a rod-dominant duplex retina evolved in a relatively short time span. We hypothesized that the abundance of rod photoreceptors in the mammalian retina originated from, and at the expense of, S cones with the co-emergence of an *Nrl*-centered, rod-specific, regulatory network and that developing rods would therefore carry vestiges (‘‘footprints’’) of S cones (Fig. 3.1B). Here, we provide multiple lines of evidence that developing rods in mouse retinas show a well-defined molecular footprint of S cones, whereas rods in zebrafish, representing an outgroup to tetrapods and having a cone-rich retina, do not. While alternative explanations are possible, our studies argue in favor of the recruitment of S cones to augment rods in mammalian retinas and suggest a developmental mechanism involving *Nrl* that facilitated the adaptation to scotopic ecological niches during a ‘‘nocturnal bottleneck’’ experienced by the ancestors of extant mammals.

3.2 Results

3.2.1 Developing Mouse Rod Photoreceptors Have a Molecular Footprint of S Cones

To test our hypothesis, we examined whether rod photoreceptors showed a signature of gene expression similar to S cones during development. We took advantage of an *Nrl*p-GFP transgene to obtain pure populations of rods from wild-type mouse retinas and of S-cone-like photoreceptors from *Nrl* mutant retinas (Akimoto et al., 2006; Ng et al., 2011). Transcriptome profiling, using RNA sequencing (RNA-seq) of fluorescence-activated cell sorting (FACS)-purified rods from *Nrl*p-GFP retinas revealed a progressive increase in the expression of rod-specific phototransduction genes, including rhodopsin (*Rho*), as the rods reached anatomical and functional maturity (Fig. 3.2A). As predicted, absolutely no known rod-specific gene was expressed in *Nrl*p-GFP photoreceptors from the rod-less *Nrl* mutant retinas (Fig. 3.2A). Interestingly, we noted strong expression of S-opsin (*Opn1sw*), but not M-opsin (encoded by *Opn1mw*), and of many cone-specific phototransduction genes, well above the median gene expression values, in the developing rods from wild-type *Nrl*p-GFP retinas (Fig. 3.2B). The expression of cone genes diminished with rod maturation in wild-type *Nrl*p-GFP retinas but not in photoreceptors of *Nrl* mutant retinas (Fig. 3.2B). Expression of several progenitor genes was also detected in rods at postnatal day2 (P2) and P4, but rapidly declined as rod birth was completed and maturation began (Fig. 3.S1), reflecting the likely contribution of GFP^+ rods that just exited terminal mitosis (Akimoto et al., 2006). Genes specifically expressed in other retinal cell types (ganglion, bipolar, amacrine, and horizontal cells) were barely detectable in the rod transcriptome data (Fig. 3.S1). As a low level of opsin expression was recently reported in cultured human epidermal skin cells (Haltaufderhyde et al., 2015), we examined S-opsin expression in ENCODE data-sets (Yue et al., 2014) to ensure the specificity of *Opn1sw* expression as an S-cone marker. S-opsin expression was not detected in any non-retinal human/mouse tissue or cell type (including epidermal cells) for which expression data were available (Fig. 3.S2).

To validate RNA-seq results, we performed qPCR analysis using RNA purified from 50 manually collected *Nrl*p-GFP$^+$ cells each at P2 (peak of newborn rods) and P28 (mature rods). As predicted, rhodopsin expression increased dramatically in P28 rods compared with P2 rods, whereas S-opsin expression was undetectable in mature rods (Fig. 3.2C).

We then examined the expression of S-opsin in dissociated *Nrl*p-GFP$^+$ retinal cells at P2 and P28 (Fig. 3.3A and 3.S3). Consistent with the RNA-seq and previously published P0 immunohistochemistry data (Ng et al., 2011), S-opsin immunostaining was clearly detectable in GFP$^+$ rods at P2 but not at P28. Quantification by FACS analysis demonstrated that 13.8% of GFP$^+$ cells were also positive for S-opsin at P2, but double-positive cells were negligible at P28 (Fig. 3.3B). In addition, FACS analysis of Nrl and S-opsin double-immunostained wild-type retinal cells revealed 26.4% Nrl$^+$ cells being S-opsin$^+$ at P2, while double-positive cells decreased to almost none by P28 (Fig. 3.3C). We then estimated the number of S-opsin$^+$ and S-opsin/GFP double-positive cells at different developmental stages. P2 retina contained a greater number of total S-opsin$^+$ cells compared with P28 retina (Fig. 3.3D). A majority (72%) of S-opsin$^+$ cells at P2 (on an average ~141,000) was also positive for GFP; however, the number of S-opsin/GFP double-positive cells was negligible by P28. The number of cells that were positive for only S-opsin remained remarkably constant (Fig. 3.3D).

To further validate the preceding results, we performed FACS analysis of photoreceptors from an independent *Opn1sw*p- Venus transgenic mouse line where the S-opsin promoter was used to drive the expression of the Venus reporter gene. Consistent with the above data, Nrl immunostaining was detectable in 85.6% of Venus$^+$ cells at P2, and Venus and Nrl double-positive cells accounted for 12% of Nrl$^+$ cells in the developing retina; however, the number of double-positive cells was negligible in the P28 retina (Fig. 3.3E).

Taken together, our findings exclude the possibility of S-opsin$^+$ rods being an artifact of the transgenic mouse line. Our data thus demonstrate the expression of S-opsin and other cone phototransduction genes in mouse rod photoreceptors during early stages of development.

3.2.2 Chromatin State in Developing Mouse Rods Favors Cone Gene Expression

Our hypothesis that mammalian rods derive from cells fated as S cones further predicts that developing rods would exhibit a chromatin state concordant with S-cone characteristics. To address this, we performed reduced representation bisulfite sequencing (RRBS) and histone modification chromatin immunoprecipitation sequencing (ChIP-seq) using flow-sorted rod photoreceptors at three key stages of development: P2, P10, and P28 (see Fig. 3.2). We also analyzed DNase I hypersensitivity sequencing (DNase-seq) data from developing mouse retinas (Vierstra et al., 2014). In P2 rods, chromatin state was unfavorable for active *Rho* transcription as indicated by the high degree of DNA methylation (meDNA), limited enrichment of active histone mark H3 lysine 4 trimethylation (H3K4me3) at the promoter, and low chromatin accessibility (indicated by lack of DNase- seq signal) (Fig. 3.4). In contrast, *Opn1sw* promoter exhibited hallmarks of active chromatin state in P2 rods; these include the absence of meDNA, accumulation of H3K4me3, chromatin accessibility, and a low level of repressive H3K27me3 marks (Fig. 3.4). Rod-specific epigenetic architecture was acquired by P10 and maintained thereafter with concurrent accumulation of repressive chromatin marks in Opn1sw (Fig. 3.4). The observed chromatin dynamics were specific to opsin gene loci and other rod- and cone-specific genes (data not shown). The promoters of photoreceptor-specific transcription factors including *Nrl* (Fig. 3.4) and of constitutively expressed genes possessed active chromatin architecture at all stages of rod development, whereas genes specifically expressed in non- neuronal tissues exhibited repressed chromatin state (data not shown). Overall, the state of chromatin in newly post-mitotic rods, but not in mature rods, is favorable for expression of S-opsin and other cone genes.

3.2.3 Lineage Tracing Shows History of S-Opsin Expression in Mouse Rods

To further test whether rod photoreceptors in mice originated from S cones, we performed lineage tracing using the *Opn1sw*p-Cre mouse (Akimoto et al., 2004) by breeding it to ROSA26-iAP reporter line (Badea et al., 2009) (Fig. 3.5A). Here, active

Opn1sw promoters permanently tag the cell by inducing alkaline phosphatase (AP) expression (Fig. 3.5A), allowing inference of lineage history. Cell bodies of most, but not all, rods and cones in the outer nuclear layer showed heavy AP activity in the P28 retinas (Fig. 3.5B and 3.S4), demonstrating the expression of S-opsin in rods at an early stage in their development. Immunostaining with antibodies against markers of mature photoreceptors revealed stronger AP staining in S cones and further confirmed the history of S-opsin promoter activity in rods (Fig. 3.S4D and 3.S4E). Similar experiments using *Opn1mw*p-Cre mouse, which expresses Cre recombinase under the control of M-opsin promoter (Akimoto et al., 2004), demonstrated no overlap between rod and M-cone lineage (Fig. 3.5C and 3.S4C). Occasional ganglion cell staining was detected in both *Opn1sw* and *Opn1mw* lineage tracing experiments (Fig. 3.S4C). Detection of the history of *Opn1sw* expression in most mature mouse rods was further validated by an independent lineage tracing experiment using BAC transgenic *Opn1sw*p- Cre and Z/EG fluorescence reporter lines (Fig. 3.5D). In accordance with the results above, GFP lineage tracer was detected in both cones and most rods in mature retinas even though Cre and S-opsin immunoreactivity was observed only in mature cones (Fig. 3.5E and 3.5F). Robust lineage tracer labeling of S cones in most but not all rods, and not of any other retinal neuron, in the BAC transgenic *Opn1swp*-Cre mice strongly argues in favor of the derivation of rods from S-cone lineage.

3.2.4 Rods Do Not Show UV Cone Opsin *sws1* Lineage in Zebrafish

Next we examined whether rods in a cone-dominated, teleost retina were also specified from a cone lineage. Teleosts branched earlier than mammals in the evolutionary history of vertebrates. To address this, we engineered a lineage-tracing zebrafish line with two genetic constructs that constituted a positive-feedback mechanism (‘‘Kaloop’’ technology, Fig. 3.6A). We used this line to permanently label cells with the history of expression of UV cone opsin *sws1*, a zebrafish homolog of mouse *Opn1sw*. We characterized 4,024 cells that had expressed *sws1* opsin at some point in development from ten retinas of 4 dpf (days post fertilization) zebrafish larvae. The vast majority of lineage-traced cells (4,021 of 4,024; 99.92%) unambiguously

lacked immunolabeling by 4C12 (a rod marker), whereas three cells (0.08%) found among two individuals were ambiguously labeled (i.e., they probably were not rods, though we cannot formally exclude this possibility) (Fig. 3.6B). Lineage tracing of an mCherry transgene in each cell, where image resolution permitted assessment, was tightly associated with immunolabeling by the UV cone marker 10C9.1 antibody (Fig. 3.6B). Although *sws1* is the closest homolog of mouse Opn1sw, we also traced the lineage of zebrafish blue cone opsin *sws2* to exclude the possibility that rods may have derived from the other S-cone class. As with *sws1* lineage-traced cells, we did not find any rods with *sws2* lineage (Fig. 3.S5). Therefore, the cells with a history of *sws1* or *sws2* expression exclusively differentiate into UV or blue-sensitive cones, respectively.

3.2.5 Advent of Nocturnal Mammals Coincides with the Acquisition of Novel Regulatory Elements, Rod-Specific Expression, and Deep Conservation of NRL

Our data describe a novel developmental origin of rod abundance in mouse (a representative placental mammal) compared with zebrafish (an earlier branching, non-amniotic vertebrate with a cone-dominant retina), encouraging us to determine a mechanistic explanation. We first compared genomic sequences spanning the *Nrl* gene in selected vertebrates. DNA sequences in the coding region of *Nrl* are highly conserved in all vertebrates (Fig. 3.7A). Strikingly, however, we observed extensive conservation of genomic sequences upstream and downstream of *Nrl* in mammals as well as in the intronic regions and UTRs of selected loci (Fig. 3.7A). We also noted the gradual evolution of conserved genomic sequences spanning *Nrl* from the egg-laying platypus to the pouched and placental mammals, consistent with the appearance of rod-dominant duplex retina and the pivotal role of Nrl in mammalian rod cell fate determination.

Next, we explored the phylogeny of Nrl and related Maf proteins from a range of vertebrate genomes including jawless agnathans, cartilaginous and bony fishes, terrestrial vertebrates, and representatives of each major lineage of mammals (Fig. 3.7B). Our results show that Nrl and other closely related Maf paralogy classes have

each originated among the jawed vertebrates, with a single distant ortholog being present in the earlier branching agnathan (*Petromyzon*) genome. Furthermore, each of these Maf paralogy classes, including Nrl, demonstrates dynamic histories of loss among taxa. Strikingly, while we infer that Nrl has been lost from several non-mammalian taxa, Nrl loci are retained in all mammalian genomes included, in contrast to each of the other paralogy classes. Furthermore, the mammalian Nrl genes are separated from non-mammalian paralogs by the longest internal branch in our tree, indicating a burst of molecular evolution. Together, our results suggest an evolutionary history for mammalian Nrl whereby rapid molecular innovations in the lineage leading to mammals are followed by strong conservation and gene retention.

We also evaluated Nrl and other Maf protein sequences across vertebrate species (Fig. 3.S7). Transactivation and DNA binding domains were highly conserved in all vertebrate species including zebrafish and mouse. Protein sequence comparison revealed a high degree of conservation between all chicken long MAFs and vertebrate Nrl homologs in both transactivation and DNA binding domains (Fig. 3.S7). To test for functional conservation, we introduced the chicken *MAFA* gene, which is expressed in avian rods and a few other retinal neuronal types but not in cones (Ochi et al., 2004), in cone-only *Nrl* mutant mouse retina (Mears et al., 2001) (Fig. 3.8). Chicken *MAFA*, but not GFP empty vector, induced the expression of rhodopsin (Fig. 3.8B) and characteristic single synaptic ribbon observed in rods (Carter-Dawson and Lavail, 1979), as opposed to cone opsin expression and multiple ribbons present in cones (Fig. 3.8C and 3.8D). Chicken *MAFA*-induced cone-to-rod transformation was confirmed by expression of rod-specific genes including *Nr2e3*, *Gnat1*, and *Cnga1*, but not cone genes such as *Arr3* and *Gnat2*, in *MAFA*-expressing *Nrl* mutant mouse retina (Fig. 3.8E). Thus, chicken *MAFA* induces rod development akin to the actions of mouse *Nrl* when expressed ectopically in *Nrl* mutant mouse retinas.

3.3 Discussion

Current concepts regarding the behavioural and organismal ecology of early mammals propose that the evolution of a rod-dominant retina was a landmark event,

central to the persistence and success of the lineage. Extant mammalian lineages first diverged during the Jurassic when dinosaurs were dominant and diurnal predators in most terrestrial habitats. During this period, predation pressures forced early mammals to adapt to a nocturnal life-style (termed the nocturnal bottleneck), permitting them to exploit a novel scotopic ecological niche (Davies et al., 2012; Heesy and Hall, 2010; Menaker et al., 1997; Walls, 1942). How these early mammals survived and prospered during this nocturnal bottleneck, and attained the capacity for high-sensitivity photon capture in night vision, has defied explanation. Here, we provide strong evidence in support of the hypothesis that a subset of S cones was transformed to rods by ectopic expression of *Nrl* early in the evolutionary history of mammals. We suggest that this extreme dominance of rods is retained in the retinas of most extant mammals.

Our understanding of photoreceptor evolution has been continuously revised since Schultze initially considered cones to be a more derived photoreceptor type than rods (Schultze, 1866), based on their capacity to detect highly specific wavelengths of light. A more detailed histological examination (Dickson and Graves, 1979) and phylogenetic analysis of opsin genes (Okano et al., 1992; Pisani et al., 2006) predicted the opposite scenario. Inspired by recent technical advances, we revisited the question of rod origins, specifically their vast abundance in mammals. Global transcriptome and epigenome analysis of pure photoreceptor populations enabled us to detect prominent footprints of S cones in developing mouse rods. Further validation at single-cell type resolution and fate-mapping analyses allowed us to conclude that most, but not all rod photoreceptors in mice are derived from the S-cone lineage. Conversely, lack of direct evidence supporting the origin of rods from the S-cone lineage in zebrafish indicates that the derivation of most rods from S cones might be a developmental innovation of mammals, one that serves to contrast two distinct phases of rod origins: (1) the initial origin of unambiguous rods in early gnathostomes and (2) the later shift to rod-dominated retinas in mammalian species. It remains feasible that this lack of direct evidence supporting the origin of rods from S cones in zebrafish represents loss of this character in fish taxa, or could be attributable to the developmental phase examined; e.g., lineage tracing to examine rod development in post-larval zebrafish may be warranted. Importantly, the rod population without a detectable S-cone footprint (Fig. 3.5B

and 3.5F) in the mouse retina may represent a more ancient cellular lineage of rods homologous to those of earlier branching, non-mammalian taxa including zebrafish.

Our finding of two distinct rod populations in the mouse retina is intriguing and requires further explanation. Although not as explicit as the distinct rod populations reported in amphibian retinas (Sherry et al., 1998), some evidence indicates that mouse rods are not a homogeneous cell type. For example, a subpopulation of rods forms direct synaptic contacts with cone bipolar cells, whereas others only synapse with rod bipolar cells (Tsukamoto et al., 2001). In addition, two phases of rod differentiation are reported in developing rat retinas (Morrow et al., 1998). Although there is no evidence of physiological or morphological difference between early- and late-born rods, rods born prior to embryonic day 19 (E19) exhibit the onset of rhodopsin expression that is further lagged and more synchronized than those born on and after E19 (Morrow et al., 1998). Whether the rod sub- groups with distinct synaptic pathways and differential temporal expression of rhodopsin can be related to the rods with or without a history of *Opn1sw* expression would be an interesting and testable future direction.

Multiple lines of evidence validate the expression of *Opn1sw* and other cone genes in developing rods. Though not emphasized as such, *Nrl*p-GFP cells in P0 mouse retina are documented to express S-opsin (Ng et al., 2011). Both transcriptome and epigenome analyses demonstrate the robustness of co-expression of *Nrl* and *Opn1sw* in isolated mouse rod photoreceptors. We used flow-sorted rods of purity of over 96% (>99% for most samples) for all next-generation sequencing (NGS) experiments; thus, S-cone contamination in purified rod samples cannot explain the expression values (fragments per kilobase of exon per million fragments mapped [FPKM]) in our samples. We note that the genes associated with inner retina show no to negligible expression in flow-sorted rods (see Fig. 3.S1). Although some progenitor genes were detected in early developing rods (P2 and P4), it is not surprising given that *Nrl* expression commences during or immediately after the final mitosis (Akimoto et al., 2006). Furthermore, qRT-PCR analysis of manually picked GFP^+ cells, where no contamination is allowed, confirmed high *Opn1sw* expression in P2 rods compared with P28 rods (see Fig. 3.2C). Multiple independent experiments, including immunocytochemistry and flow cytometry using distinct combinations of reporter mouse

lines (see Fig. 3.3), point to *Opn1sw* expression in immature rods. Lineage-tracing experiments using two different S-opsin Cre lines and phylogenetic analysis provide additional strong support of our hypothesis.

Evolutionary innovations are enabled by changes in gene-regulatory networks that consist of transcriptional regulators and their cognate DNA binding elements (Koentges, 2008). Comparative genomic analysis of *Nrl*, a hub of the transcriptional regulation circuits regulating rod development (Swaroop et al., 2010), provides insights into the underlying mechanism of rod recruitment from S cones. At the level of protein sequence, functional domains of Nrl are highly conserved throughout vertebrates (see Fig. 3.S7) and functional equivalency exists among different Maf paralogs when expressed in a suitable context. For example, ectopic expression of mouse *Nrl* (Ng et al., 2011; Oh et al., 2007) or chicken *MAFA* (see Fig. 3.8) is sufficient to convert cones to rods in the mouse retina. Notably, ectopic expression of human *NRL* led to an increased number of rods at the expense of cones in the *Xenopus* retina, whereas *Xenopus Nrl* induced the differentiation of both rods and lens fiber cells (McIlvain and Knox, 2007). Thus, the function of Nrl as a rod differentiation factor seems to be well conserved across amniotes despite the additional function(s) *Nrl* homologs may have outside of mammals. Given that rod photoreceptors, broadly defined, likely originated in ancient (jawless) vertebrates, it is reasonable to hypothesize that the development of these early rods involved a long Maf homolog, such as the single locus present in the lamprey (Fig. 3.7B). In contrast, novel regulatory sequences at the *Nrl* locus later evolved within the mammalian lineage (see Fig. 3.7A) giving rise to a novel gene-regulatory network and a second, independent origin of rods. Additional independent origins of rods have also been noted in nocturnal birds (Martin et al., 2004) and deep-sea fish (Landgren et al., 2014), although the developmental basis for these transitions remains an open question.

Developmental plasticity can support the evolution of novel traits by providing the raw materials (i.e., phenotypic variation) necessary for rapid adaptation (Müller, 2007), and vertebrate photoreceptors are known to demonstrate such plasticity. In humans, opsin expression is plastic over the course of development. S-opsin expression precedes L-/M-opsin expression, and the number of cones expressing both increases

during development, followed by their decrease at later stages (Szél et al., 1994; Xiao and Hendrickson, 2000). Similarly, mouse genetic studies have demonstrated the developmental plasticity of post-mitotic photoreceptor precursors (Ng et al., 2011; Oh et al., 2007). Thus, it is reasonable to predict that the recruitment of S cones to augment rod photoreceptors in mammalian retinas via the plastic redeployment of *Nrl* enabled the rapid adaptation of early mammals to the nocturnal niche. Notably, loss of *Sws2* and *Rh2* as well as a shift in spectral sensitivity of Sws1 also coincided with this critical period (Jacobs, 2013). Thus, multiple lines of evidence suggest a fundamental reorganization of the mammalian retina during the nocturnal bottleneck.

Despite their nocturnal origin, extant mammalian species have adapted to diverse activity patterns such as nocturnal, diurnal, crepuscular, and cathemeral habits (Gerkema et al., 2013). Paradoxically and with few exceptions, rods remain the dominant photoreceptor type in most mammalian retinas (Peichl, 2005). Why is rod dominancy retained in diurnal mammals? It is interesting to note that patients with retinal degeneration and 90% cone loss in the fovea had sufficient visual acuity (Geller and Sieving, 1993). Considering the low energy-consumption rate of rods compared with cones (Okawa et al., 2008), it is conceivable that maintaining rod abundance in diurnal mammals is adaptive because it allows energy efficiency without compromising visual acuity. In addition, rods may have additional functions beyond scotopic light detection. Chemical and electrical rod:cone coupling can mediate mesopic vision (Abd-El-Barr et al., 2009; Asteriti et al., 2014; Hornstein, 2005; Pang et al., 2012; Ribelayga and Mangel, 2010). Rods also drive circadian photoentrainment (Altimus et al., 2010) and horizontal cell-mediated surround inhibition of cone signal (Szikra et al., 2014). Furthermore, trophic factor(s) released by rods can enhance cone survival in degenerating retina (Aït-Ali et al., 2015). Thus, the integration of numerous functions in mammalian rods may have represented a pleiotropic constraint against a reversion to cone dominance in the retinas of diurnal mammalian taxa.

We recognize that our proposed mechanism for the transition from cone-dominant to rod-dominant retinas in early mammals does not provide a complete explanation for the developmental transformation of mammalian retinas that took place during the nocturnal bottleneck. In addition to their cellular composition, rod-dominant

retinas also have a greatly increased proportion of photoreceptors. Thus, an explanation is also required for the increase in progenitor proliferation and cell number. How cell number is modulated in developing retinas is largely unclear, although the myoblast oncogene Myb has been implicated in determining cone photoreceptor number (Whitney et al., 2011).

In conclusion, we propose that the evolutionary origin of the majority of mammalian rods occurred by their developmental recruitment from the S-cone lineage, a phenomenon not observed in non-mammalian vertebrates. We further hypothesize that this process was predicated on the origins of novel regulatory sequences of *Nrl* that restrict its expression to rod photoreceptors in mammals. We show that the origins of novel *Nrl* regulatory sequences coincide with a period of punctuated visual system evolution early in mammalian evolution known as the nocturnal bottleneck, followed by strong conservation and stasis in extant mammalian species. Our study provides critical mechanistic details underlying the rapid adaption to the scotopic light environment that was the driving force behind the profound cone-to-rod transformation that occurred during the nocturnal bottleneck, and reveals how the evolutionary history of a neuronal cell type can be revealed by comparative molecular and ontogenetic analysis.

3.4 Figures

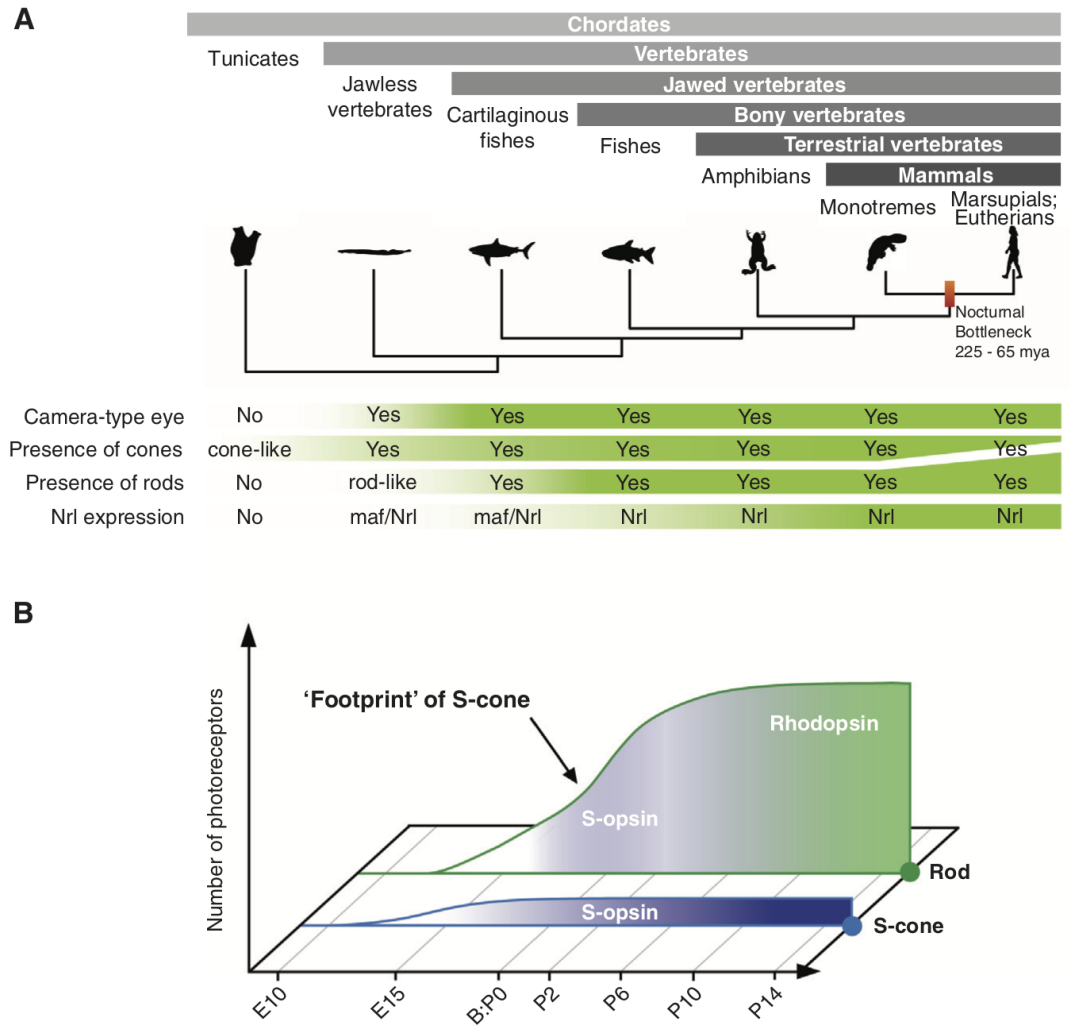

Figure 3.1: Developmentally Conserved Vestiges during Rod Photoreceptor Evolution

(**A**) Co-emergence of rod photoreceptors and *Nrl* during vertebrate evolution. True functional rod photoreceptors exist only among jawed vertebrates in the evolutionary tree of Chordata (D.-G. Luo et al., 2008b), but *Nrl*-like *Maf* gene is encoded in the lamprey genome (Fig. 3.7**B**) and may be expressed in RhA (rod visual pigment) expressing rod-like cone photoreceptors (Morshedian and Fain, 2015). Red bar indicates the time period that corresponds to nocturnal bottleneck during mammalian evolution. The tapering down and thickening of second and third rows of the table

indicates a decrease in cone abundance and an increase in rod abundance observed in most mammals, respectively. Time-calibrated tree was redrawn from Hedges et al. (Hedges et al., 2015). mya, million years ago; Monotremes, egg-laying mammals; Marsupials, pouched mammals; Eutherians, placental mammals. (**B**) Hypothesis being tested in the present study. Green and purple curves represent cumulative rod and cone number, respectively. The respective shades indicate opsin expression. X axis indicates developmental stages of mouse retina. E, embryonic day; B, birth; P, postnatal day.

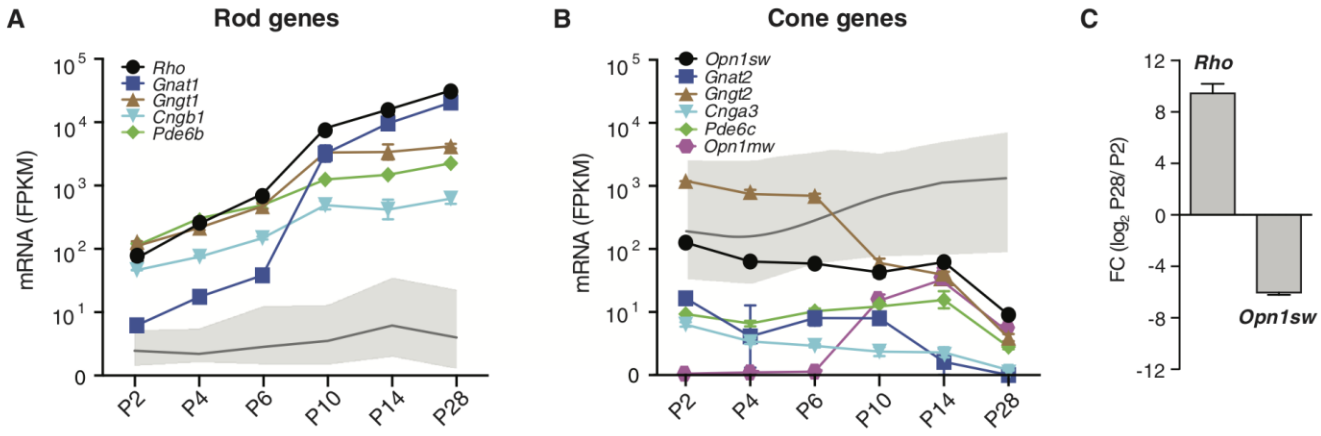

Figure 3.2: Molecular ‘‘Footprint’’ of S Cones in Developing Mouse Rod Photoreceptors

(**A** and **B**) Gene-expression profiles of selected (**A**) rod-specific and (**B**) cone-specific phototransduction genes in the rod photoreceptors purified from *Nrl*p-GFP mouse retina. Developmental time points are indicated on the x axis; y axis shows FPKM ± SEM from RNA-seq data. Gene expression in photoreceptors from *Nrl*p-GFP;*Nrl*$^{-/-}$ retina is shown as mean by dark gray lines and range of five indicated genes as gray shading. The six time points selected for RNA-seq analyses represent key stages of mouse rod development: P2, peak of post-mitotic rod generation; P4, robust increase in phototransduction gene expression; P6, rod outer segment discs beginning to form; P10, outer segment elongation and synaptogenesis; P14, eye opening and outer segment/synapse formation completed; P28, rods fully mature. (**C**) qRT-PCR validation of *Rho* and *Opn1sw* expression from 50 manually collected GFP^{+} rods. Data are normalized to P2 expression level and presented as mean of fold change (FC) ± SEM.

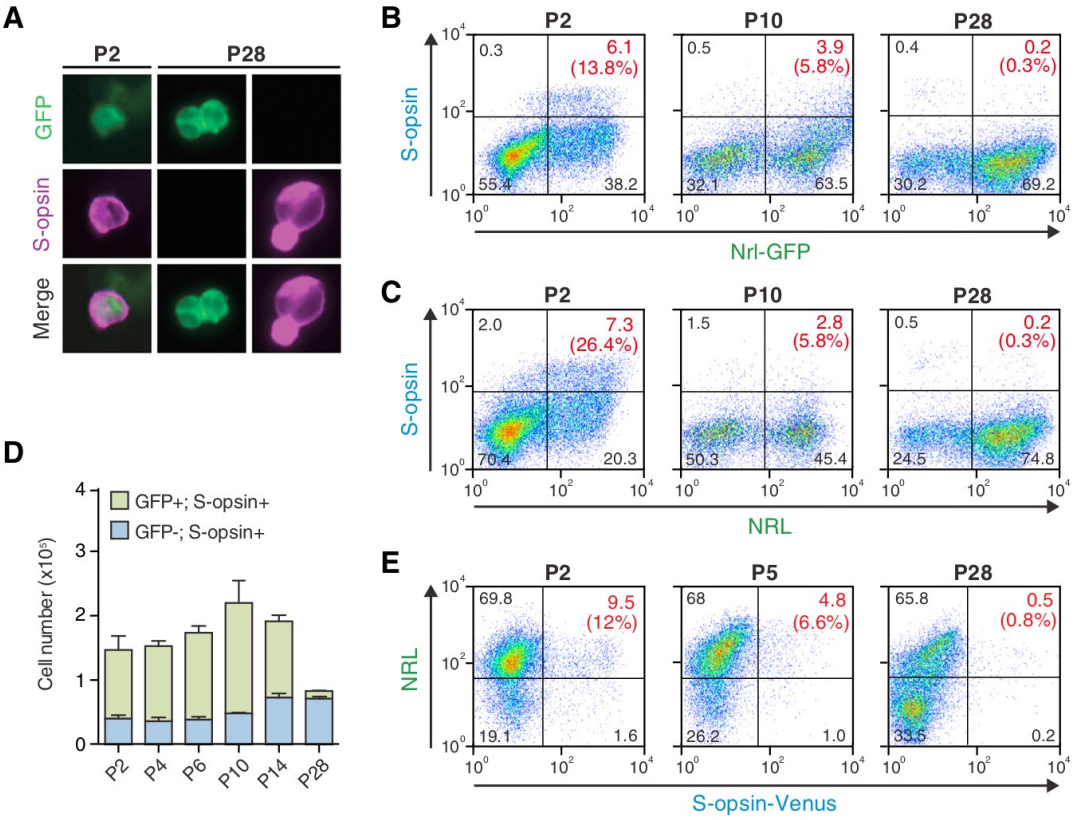

Figure 3.3: S-Opsin Expression in Developing Mouse Rod Photoreceptors

(**A**) Immunocytochemistry of dissociated *Nrl*p-GFP retinal cells. S-opsin (purple) and GFP (green) double-positive cells were detected at P2 but not P28. (**B**) Quantification of S-opsin$^+$ rod photoreceptors by flow cytometry. Percentage of cells in each quadrant relative to total counted cells is indicated in the dot plots, and percentage of S-opsin$^+$ cells among GFP$^+$ rods is shown in parentheses. (**C**) Quantification of S-opsin and NRL double-positive cells by immunostaining followed by flow cytometry. Percentage of cells in each subpopulation is indicated. Percentage of S-opsin$^+$ cells among NRL population is shown in parentheses. (**D**) Quantification of S-opsin$^+$ and GFP/S-opsin double-positive photoreceptors per retina. Percentage of each cell population determined by flow cytometry of *Nrl*p-GFP retina was multiplied by total retinal cell number at the corresponding stage. y Axis indicates mean cell number (310^5) ± SEM. (**E**) Quantification of NRL-expressing S cones at indicated time points by flow cytometry of *Opn1sw*p-Venus mouse retina. Proportion of cells in each subpopulation is indicated as

a percentage relative to total cells, and percentage of Venus$^+$ cells among NRL$^+$ rods is shown in parentheses.

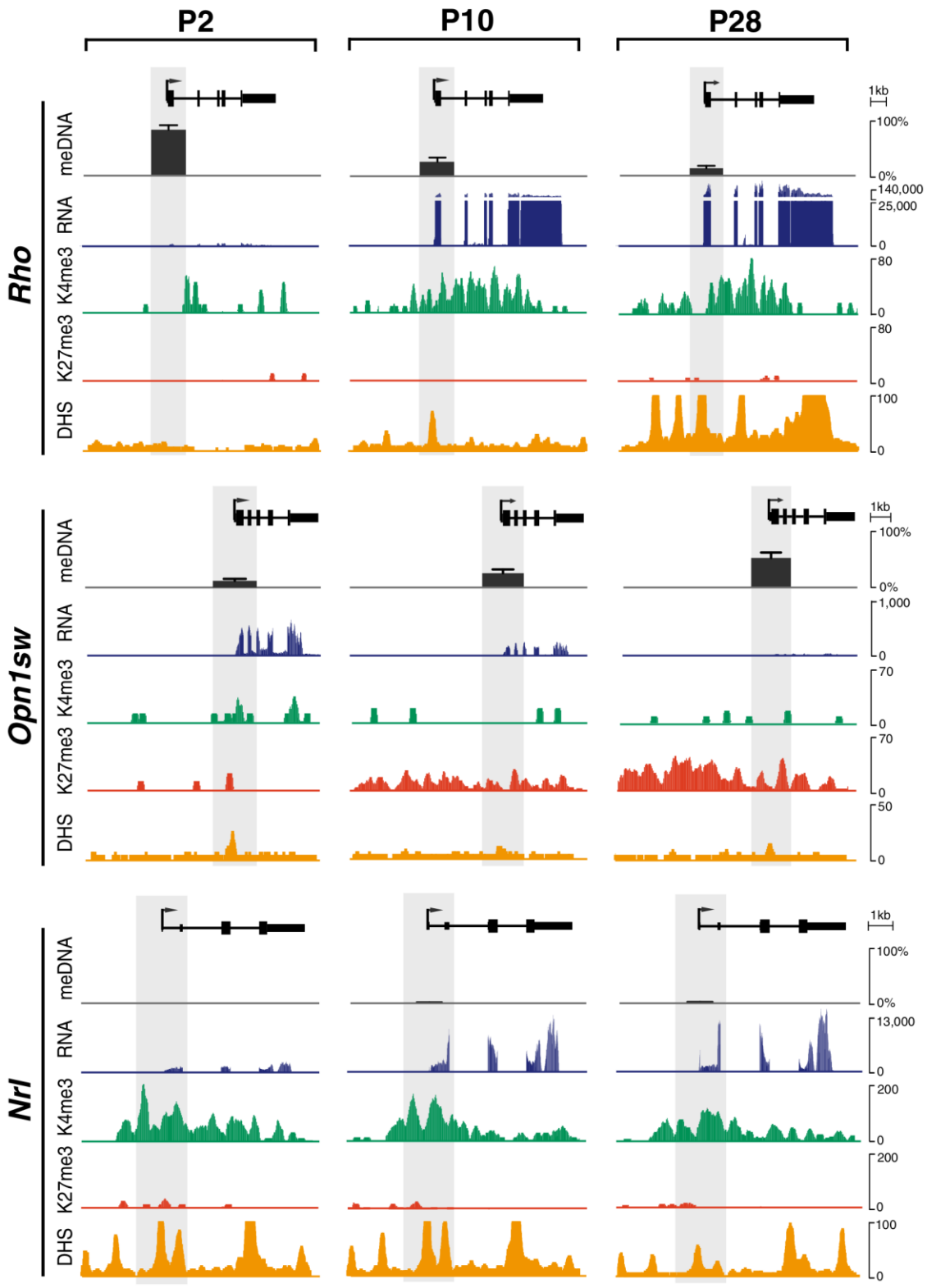
P2
P10
P28
Rho
Opn1sw
Nrl
meDNA
RNA
K4me3
K27me3
DHS
1kb
100%
0%
140,000
25,000
80
1,000
70
50
13,000
200
100

Figure 3.4: Epigenetic Vestiges of Cones in the Developing Rod Photoreceptors in Mouse Retina

Epigenetic state on *Rho*, *Opn1sw*, and *Nrl* genes were revealed by reduced representation bisulfite sequencing (RRBS; DNA methylation profiling), H3K4me3 and H3K27me3 ChIP-seq, and DNase I hypersensitivity sequencing (DNase-seq) at indicated developmental stages. Data were generated using flow-sorted rod photoreceptors from *Nrl*p-GFP mouse retina, except for retina DNase-seq data that were downloaded from the mouse ENCODE project (Vierstra et al., 2014). Percentage ± SEM of methylated cytosine in the promoter regions is indicated as bar graphs. Aligned sequencing reads for mRNA expression (dark blue), H3K4me3 (green, active mark) and H3K27me3 (red, repressive mark) enrichment, and DNase hypersensitivity sites (orange) are shown as histograms. Promoter of each gene, defined as 1 kb to +1 kb from the transcription start site, is highlighted with gray shading.

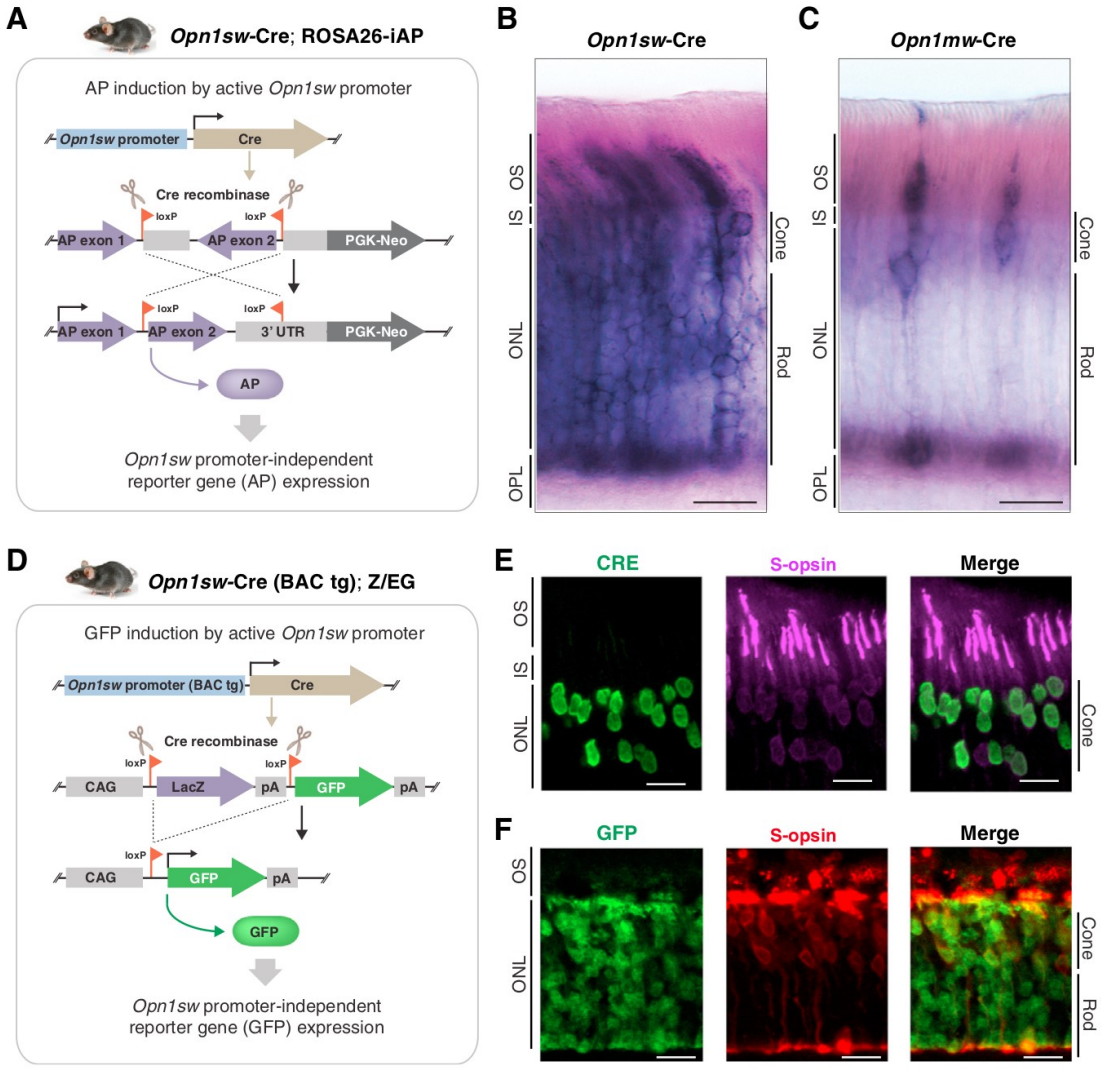

Figure 3.5: History of S-Opsin Expression in Mature Mouse Rod Photoreceptors

(**A**) Lineage tracing strategy in mouse. *Opn1sw*p- Cre mouse line was crossed with ROSA26-iAP line. In this line, cells with active *Opn1sw* promoter express Cre recombinase, which brings alkaline phosphatase (AP) gene back to the correct configuration by inverting the DNA piece surrounded by two loxP sites in head-to-head orientation. Once recombined, a constitutive promoter in the ROSA locus drives AP reporter gene expression even when cells no longer have *Opn1sw* promoter activity. (**B** and **C**) Lineage tracing of S-opsin-expressing cells using *Opn1sw*p-Cre; ROSA26-iAP (**B**) or tracing of M-opsin lineage cells using *Opn1mw*p- Cre; ROSA26-iAP mouse lines (**C**). Shown is AP staining (purple) in the photoreceptor layer of adult (P28) retina

of respective genotype. OS, outer segment; IS, inner segment; ONL, outer nuclear layer; OPL, outer plexiform layer; Cone, outer portion of ONL where cone nuclei are located; Rod, inner ONL with rod nuclei. Scale bar, 20 mm. (**D**) Lineage tracing strategy using BAC transgenic mouse line. *Opn1sw*p-Cre BAC transgenic mouse line was crossed with Z/EG reporter line. Cells with active *Opn1sw* promoter express Cre re-combinase, which permanently activates GFP expression in all progeny of the cells that once expressed *Opn1sw*. (**E** and **F**) Lineage tracing of S-opsin-expressing cells using *Opn1sw*p-Cre (BAC tg); Z/EG mouse line. (**E**) CRE (green) and S-opsin (magenta) immunoreactivity in the outer portion of ONL. Note that S-opsin signal is strong in outer segments, and only weak S-opsin immunoreactivity can be detected in inner segments and cell bodies (merged image). (**F**) GFP^+ cells (green) are found both in outer and inner layers of ONL (i.e., cone and rod nuclei layers, the upper and lower half of ONL in the micrograph, respectively), while S-$opsin^+$ cones (red) are located only in the outer portion of ONL. OS, outer segment; IS, inner segment; ONL, outer nuclear layer; Cone, outer portion of ONL where cone nuclei are located; Rod, inner ONL with rod nuclei. Scale bar, 20 mm.

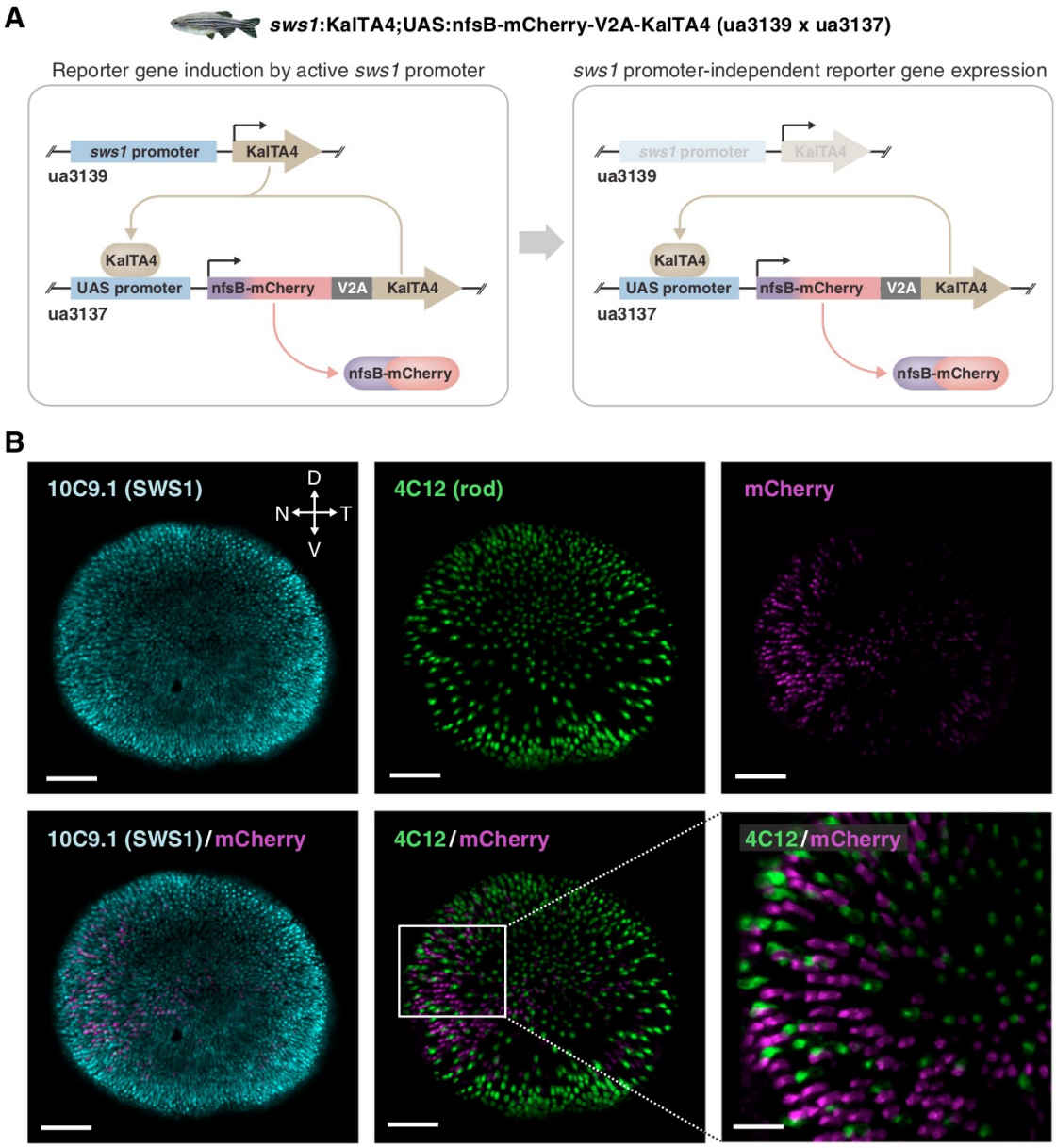

Figure 3.6: Absence of *sws1* Opsin Expression History in Zebrafish Rod Photoreceptors

(**A**) Lineage tracing strategy in zebrafish. Lineage tracing in zebrafish was accomplished using a feedforward system that has been previously designated as "Kaloop" (Distel et al., 2009) (see Fig. 3.S6). Two constructs, Tg[*sws1*:KalTA4] and Tg[UAS:nfsB-mCherry-V2A-KalTA4] (ua3139 and ua3137, respectively), were independently inserted to generate the transgenic zebrafish. In ua3137, a fluorescent reporter protein mCherry is

fused in-frame to a bacterial nitroreductase gene (nfsB), and the fusion protein is connected via the labile linker peptide V2A to a second copy of the KalTA4 transcription factor. (**B**) Lineage tracing of *sws1*-expressing cells using *sws1*:KalTA4; UAS:nfsB-mCherry-V2A- KalTA4 zebrafish line. The UV-sensitive cones (cyan, 10C9.1) and rods (green, 4C12) of 4-dpf zebrafish were labeled using immunohistochemistry. Representative images from 1 of 10 left eyes. D, dorsal; V, ventral; N, nasal; T, temporal. Scale bar, 50 mm in low-magnification images and 20 mm in high-magnification image (bottom right).

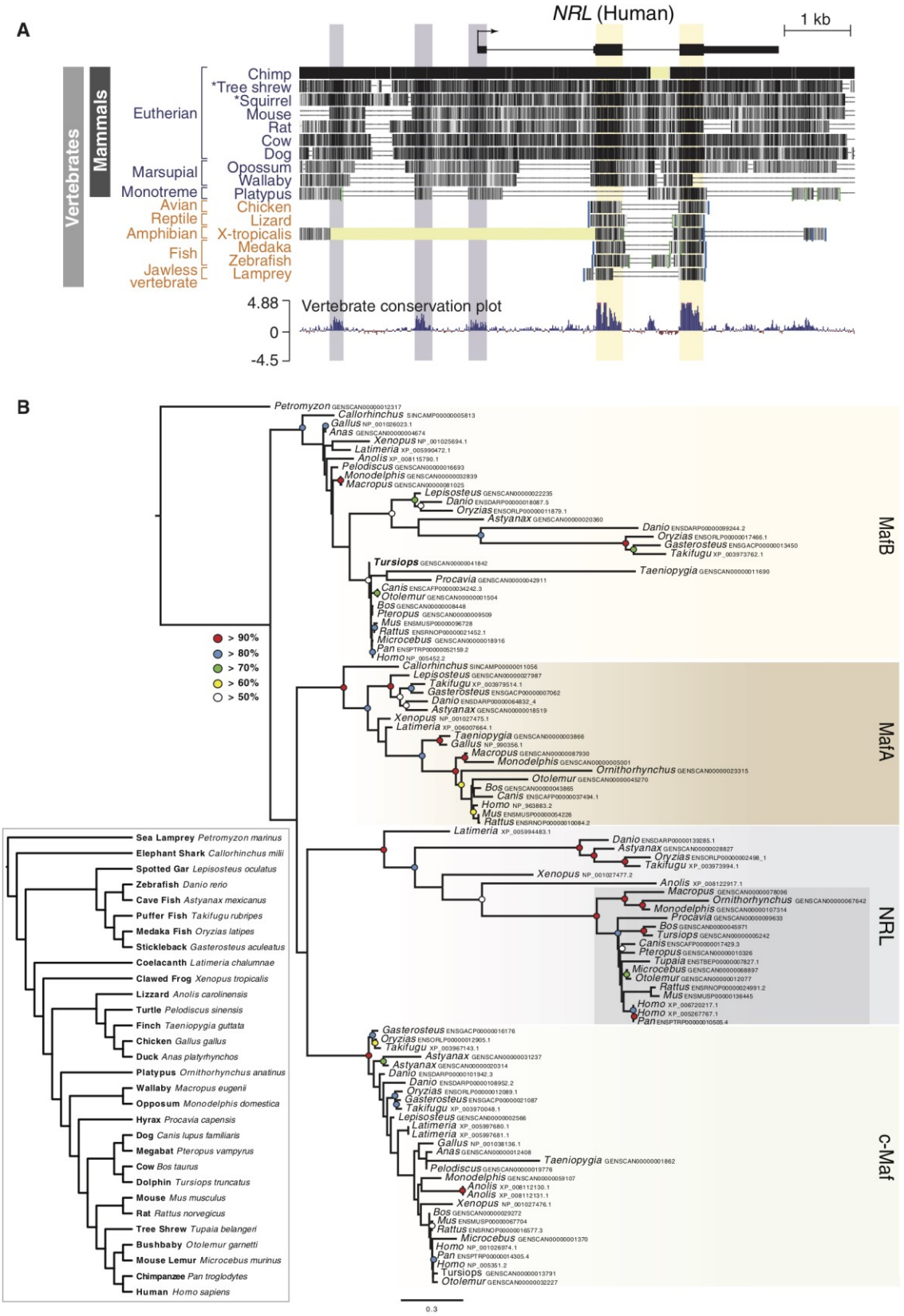
A
NRL (Human)
1 kb
Vertebrates
Mammals
Eutherian
Marsupial
Monotreme
Avian
Reptile
Amphibian
Fish
Jawless vertebrate
Chimp
*Tree shrew
*Squirrel
Mouse
Rat
Cow
Dog
Opossum
Wallaby
Platypus
Chicken
Lizard
X-tropicalis
Medaka
Zebrafish
Lamprey
4.88
0
-4.5
Vertebrate conservation plot
B
> 90%
> 80%
> 70%
> 60%
> 50%
MafB
MafA
NRL
c-Maf
0.3
Sea Lamprey Petromyzon marinus
Elephant Shark Callorhinchus milii
Spotted Gar Lepisosteus oculatus
Zebrafish Danio rerio
Cave Fish Astyanax mexicanus
Puffer Fish Takifugu rubripes
Medaka Fish Oryzias latipes
Stickleback Gasterosteus aculeatus
Coelacanth Latimeria chalumnae
Clawed Frog Xenopus tropicalis
Lizzard Anolis carolinensis
Turtle Pelodiscus sinensis
Finch Taeniopygia guttata
Chicken Gallus gallus
Duck Anas platyrhynchos
Platypus Ornithorhynchus anatinus
Wallaby Macropus eugenii
Opposum Monodelphis domestica
Hyrax Procavia capensis
Dog Canis lupus familiaris
Megabat Pteropus vampyrus
Cow Bos taurus
Dolphin Tursiops truncatus
Mouse Mus musculus
Rat Rattus norvegicus
Tree Shrew Tupaia belangeri
Bushbaby Otolemur garnetti
Mouse Lemur Microcebus murinus
Chimpanzee Pan troglodytes
Human Homo sapiens

Figure 3.7: Advent of Nocturnal Mammals Coincides with the Acquisition of Novel Regulatory Elements and Rod-Specific Expression of NRL

(**A**) Comparison of genomic sequences within and flanking areas of *Nrl*. Yellow shading highlights a high degree of DNA sequence homology across all vertebrate species in the protein-coding region of *Nrl*, and purple shading indicates additional conserved domains including upstream regulatory sequences and UTRs. (**B**) Phylogenomic analysis of *Nrl* and related *Maf* genes among vertebrates. A single homolog is present in the genome of the agnathan *Petromyzon* while other Maf paralogs, including *Nrl*, originated in the lineage leading to gnathostomes. Mammalian *Nrl* loci are shaded in gray. Colored circles indicate bootstrap support for nodes greater than 50%. Inset: species relationships of the 30 vertebrate genomes included in this analysis.

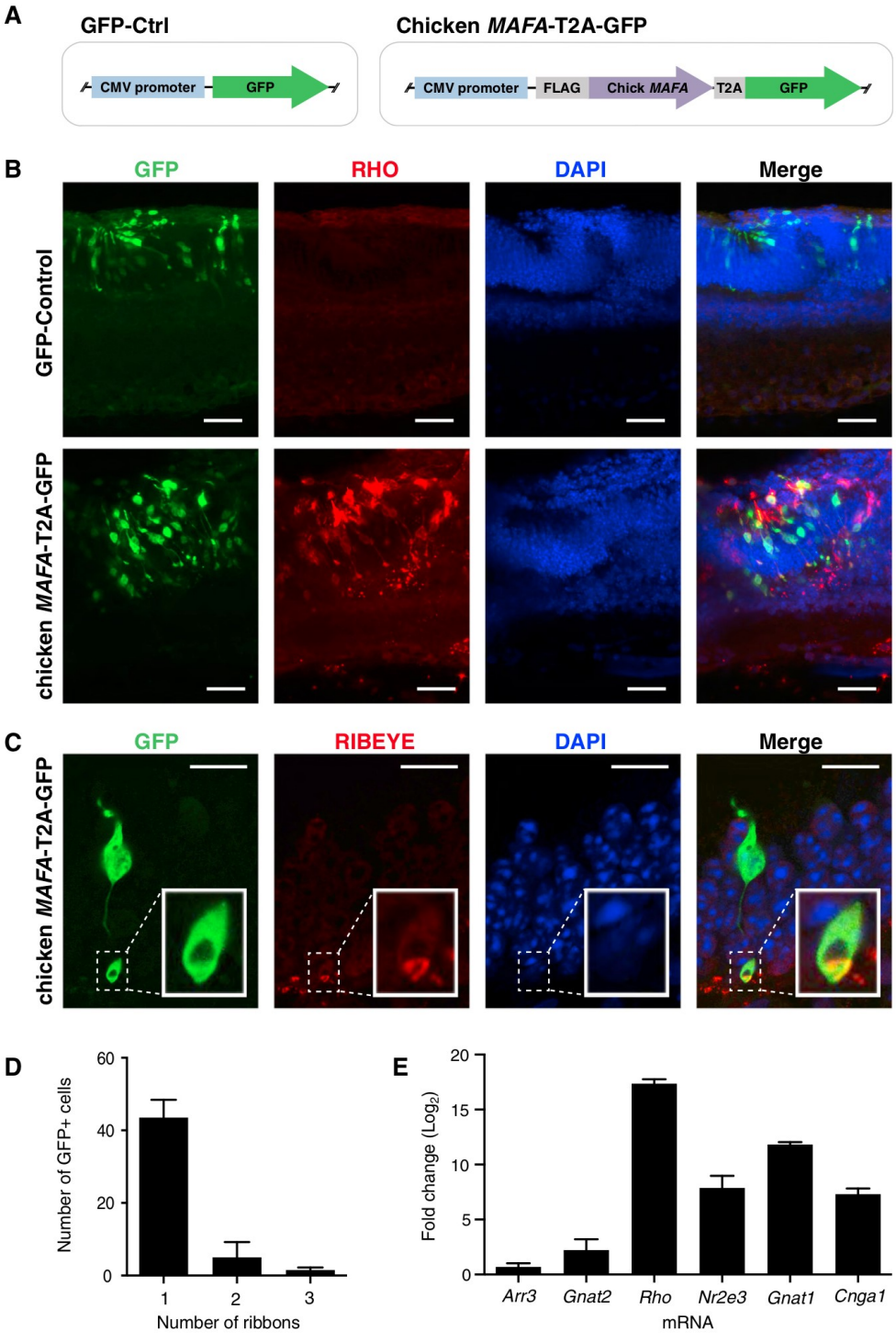
A
GFP-Ctrl
CMV promoter
GFP
Chicken MAFA-T2A-GFP
CMV promoter
FLAG
Chick MAFA
T2A
GFP
B
GFP
RHO
DAPI
Merge
GFP-Control
chicken MAFA-T2A-GFP
C
GFP
RIBEYE
DAPI
Merge
chicken MAFA-T2A-GFP
D
Number of GFP+ cells
60
40
20
0
1
2
3
Number of ribbons
E
Fold change (Log2)
20
15
10
5
0
Arr3
Gnat2
Rho
Nr2e3
Gnat1
Cnga1
mRNA

Figure 3.8: Cone-to-Rod Transformation in *Nrl* Mutant Mouse Retina by Chicken *MAFA*

(**A**) Chicken *MAFA* expression vector design. GFP or FLAG-tagged chicken *MAFA*-T2A-GFP was placed under cytomegalovirus promoter. *MAFA* expression vector or empty control vector was introduced by in vivo electroporation into dividing progenitor cells in P2 *Nrl*$^{-/-}$ mouse retina. (**B**) GFP signal (green; marks electroporated cells) and rhodopsin (RHO) immunoreactivity (red) of electroporated *Nrl*$^{-/-}$ retina at P21. DAPI counterstains all nuclei. Merged images are shown in the rightmost column. Scale bars, 50 mm. (**C**) GFP signal (green) and RIBEYE immunoreactivity (red) in electroporated *Nrl*$^{-/-}$ retina at P21. DAPI counterstains all nuclei. Insets in each micrograph show a high-magnification image of synaptic area of the transfected cells as outlined with the dotted line. Merged image is shown in the rightmost micrograph. Scale bar, 20 mm. (**D**) Bar graph summarizing the number of ribbons per chicken *MAFA*-expressing cell (indicated by GFP). Error bars indicate SEM. (**E**) qRT-PCR analysis of the transfected retina. Expression of selected cone-specific (*Arr3* and *Gnat2*) and rod-specific (*Rho*, *Nr2e3*, *Gnat1*, and *Cnga1*) genes in chicken *MAFA*-expressing *Nrl*$^{-/-}$ retina was assayed by qRT-PCR and compared with the respective expression in *Nrl*$^{-/-}$ retina transfected with an empty control vector. Error bars indicate SEM.

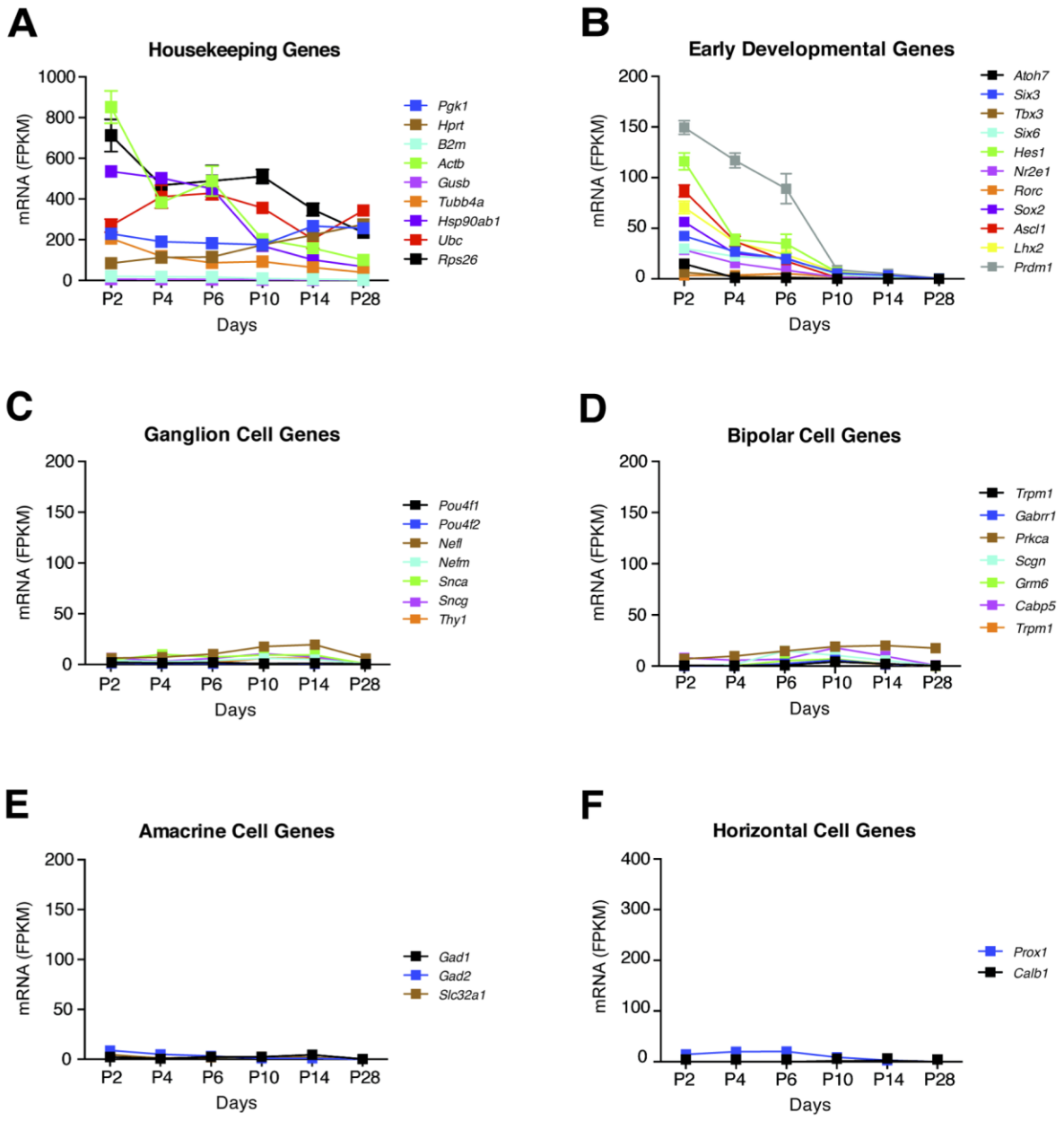

Figure 3.S1: Expression Pattern of Non-photoreceptor Genes in Developing and Mature Mouse Rod Photoreceptors, related to Figure 3.2.

Rod photoreceptor gene profiles (described in Fig. 3.2**A** and 3.2**B**) do not show appreciable expression of non-photoreceptor genes. X-axis shows the developmental stage of isolated rods. Y-axis represents mRNA expression level in FPKM (fragments per kilobase of exon per million fragments mapped) ± SEM. Expression profiles of (**A**) housekeeping genes and (**B**) early development eye field transcription factors. Note that

the expression of a commonly used housekeeping gene b-actin (*Actb*) is reduced during rod maturation. Expression of all early eye field transcription factors is undetectable in mature rods. (**C**-**F**) Expression pattern of genes specific to retinal neuronal cell types: (**C**) retinal ganglion cells, (**D**) bipolar cells, (**E**) amacrine cells, and (**F**) horizontal cells.

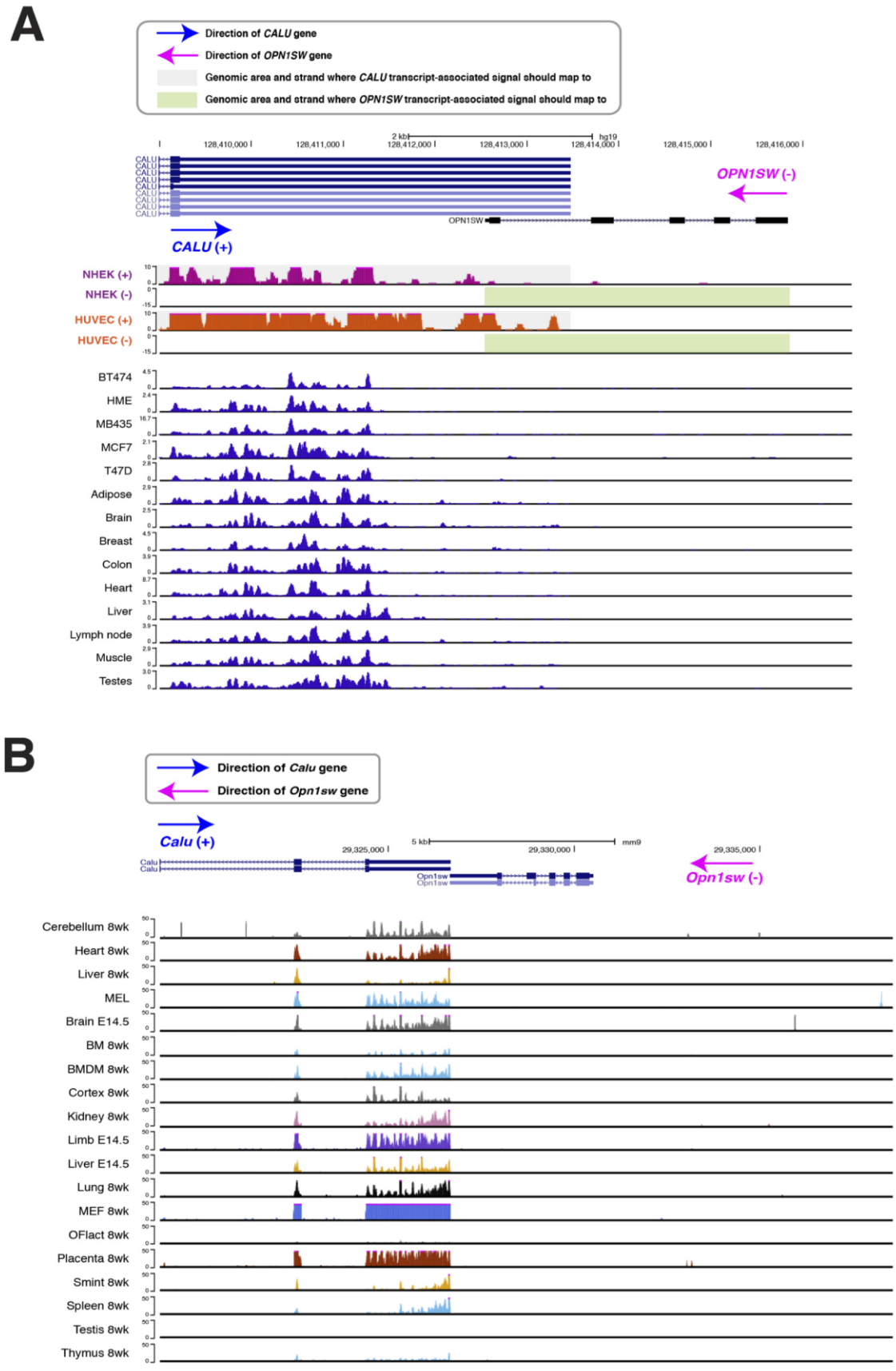
A
Direction of CALU gene
Direction of OPN1SW gene
Genomic area and strand where CALU transcript-associated signal should map to
Genomic area and strand where OPN1SW transcript-associated signal should map to
128,410,000
128,411,000
128,412,000
128,413,000
128,414,000
128,415,000
128,416,000
hg19
OPN1SW (-)
OPN1SW
CALU (+)
NHEK (+)
NHEK (-)
HUVEC (+)
HUVEC (-)
BT474
HME
MB435
MCF7
T47D
Adipose
Brain
Breast
Colon
Heart
Liver
Lymph node
Muscle
Testes
B
Direction of Calu gene
Direction of Opn1sw gene
Calu (+)
29,325,000
29,330,000
29,335,000
mm9
Opn1sw (-)
Cerebellum 8wk
Heart 8wk
Liver 8wk
MEL
Brain E14.5
BM 8wk
BMDM 8wk
Cortex 8wk
Kidney 8wk
Limb E14.5
Liver E14.5
Lung 8wk
MEF 8wk
OFlact 8wk
Placenta 8wk
Smint 8wk
Spleen 8wk
Testis 8wk
Thymus 8wk

Figure 3.S2: Absence of *OPN1SW* Expression in Non-retinal Human and Mouse Tissues, related to Figure 3.2.

(A) ENCODE RNA-seq datasets show complete lack of *OPN1SW* expression in non-retinal human tissues, thereby demonstrating *OPN1SW* expression being an appropriate S-cone photoreceptor-specific maker. RNA-seq read coverage plots of indicated human tissues are shown in a genomic area of *OPN1SW* and its neighboring gene *CALU*. Despite a slight overlap, the two genes are located on complementary DNA strands (indicated by blue and magenta arrows). Thus, strand-specific RNA-seq data can differentiate to which gene the individual sequence reads belong. All human tissues examined express varying level of *CALU* but no *OPN1SW*. Occasional sequence reads detected in the overlapping region of the two genes clearly map to the DNA strand (highlighted in grey shades for NHEK and HUVEC RNA-seq data) where *CALU* transcript-associated reads should map to, while no reads are detected from the opposite strand that *OPN1SW*-associated reads should map to (highlighted in green shades). NHEK, normal human epidermal keratinocyte; HUVEC; human umbilical vein endothelial cell; BT474, breast carcinoma cell line; HME, human mammary epithelial cell; MB435, melanoma cell line; MCF7, mammary gland adenocarcinoma; T47D, epithelial cell line derived from a mammary ductal carcinoma. **(B)** Mouse ENCODE RNA-seq datasets reveal a complete absence of *Opn1sw* expression in non-retinal mouse tissues, validating S-cone specific expression of *Opn1sw*. RNA-seq read coverage plots of indicated mouse tissues are shown in the genomic area including *Opn1sw* and its neighboring gene *Calu*. Although most tissues express *Calu*, no *Opn1sw*-associated signal is detected. MEL, leukemia cell line (K562 analog); BM; bone marrow, BMDM, bone marrow derived macrophage; MEF, mouse embryonic fibroblast; OFlact, olfactory bulb; Smint, small intestine.

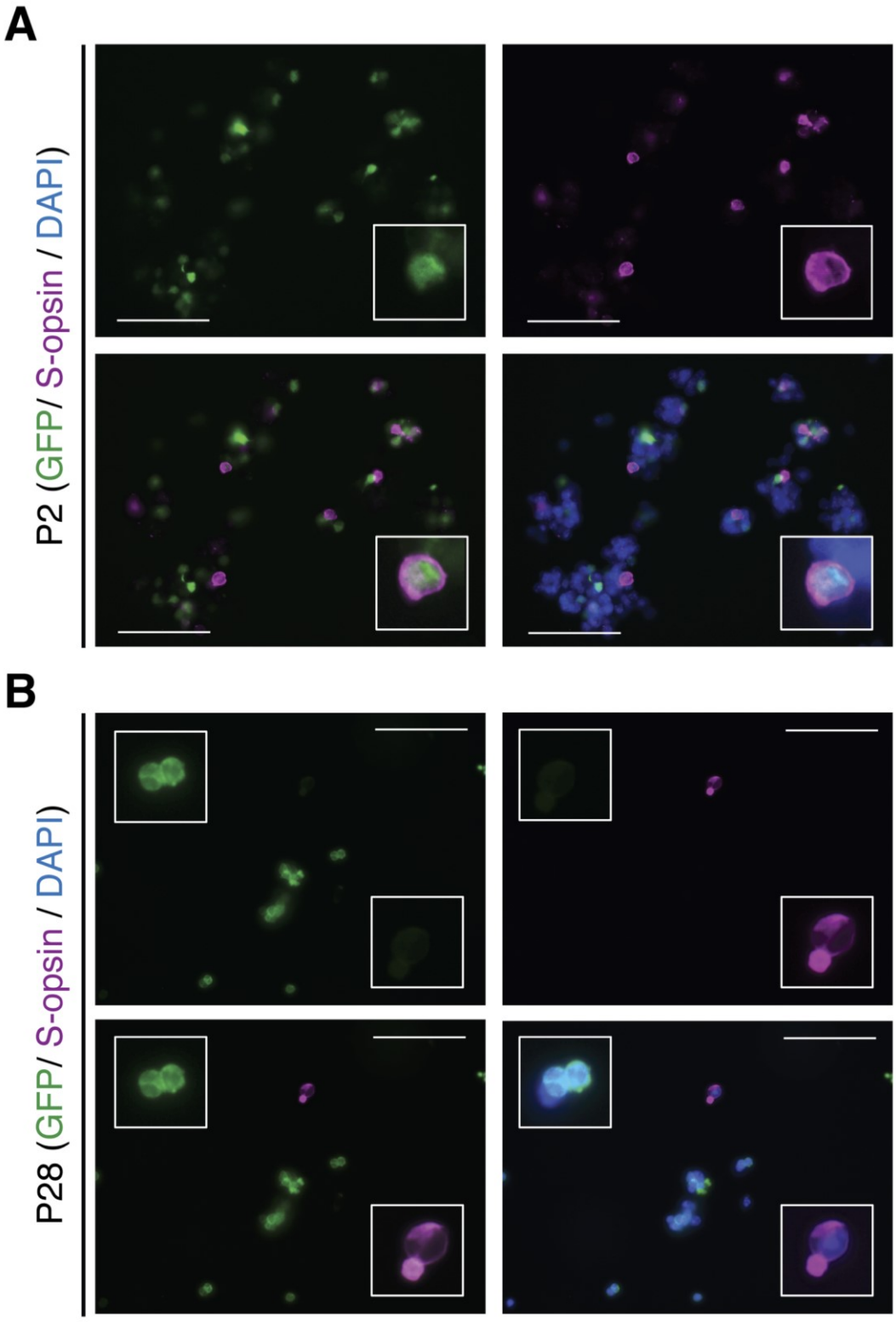
A
P2 (GFP/ S-opsin / DAPI)
B
P28 (GFP/ S-opsin / DAPI)

Figure 3.S3: S-opsin Expression in Developing Mouse Rod Photoreceptors, related to Figure 3.3.

Cells dissociated from the retina of (**A**) P2 and (**B**) P28 *Nrl*p-GFP mice were immunostained with anti-S-opsin antibody. Micrographs of single channels or merged images are shown for each time point. Enlarged pictures in insets have been used in Figure 3.3. Scale bar: 100 μm.

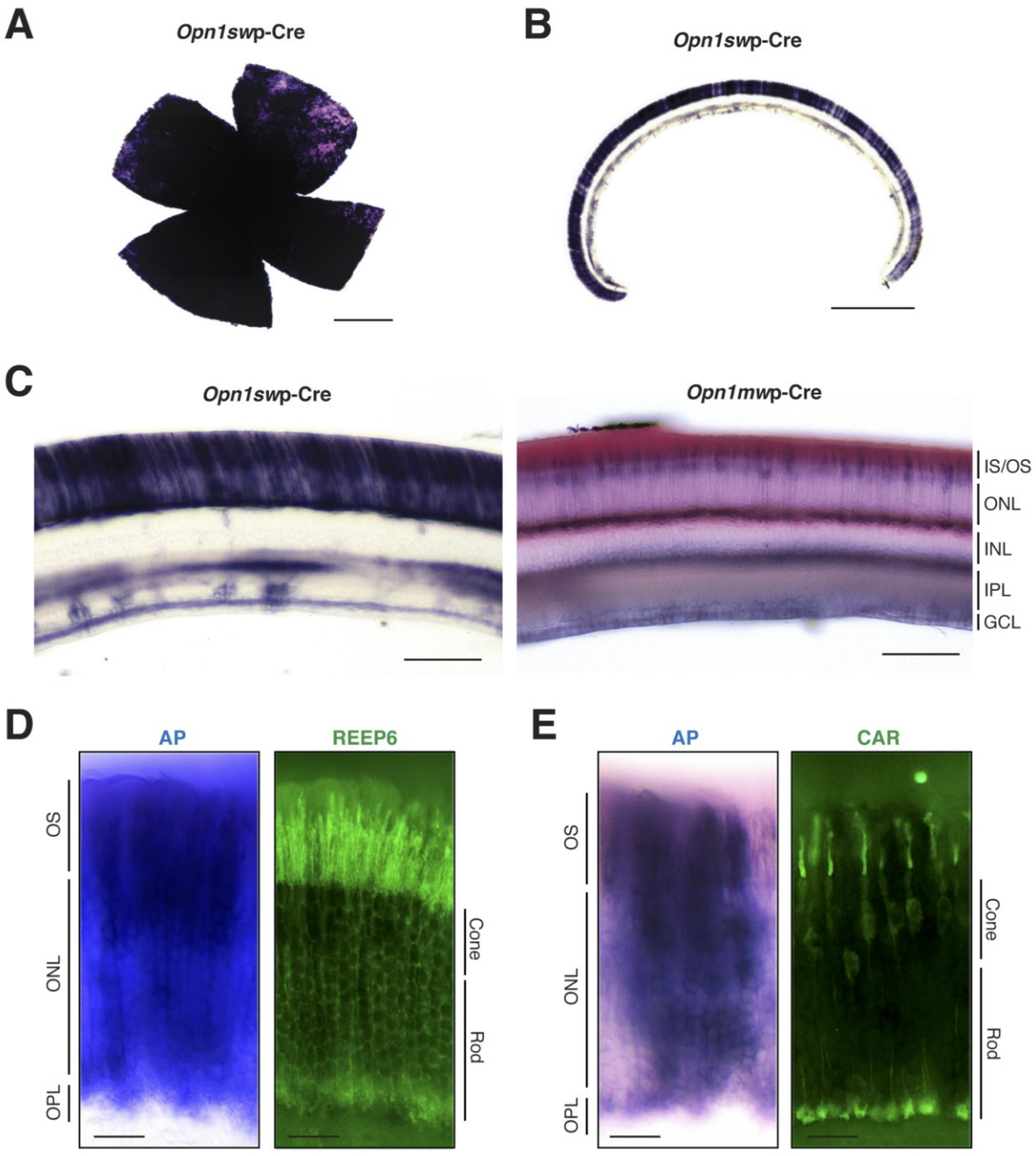

Figure 3.S4: Distribution of Alkaline Phosphatase (AP) Stained Cells in S-opsin-Cre and M-opsin-Cre Mouse Retina, related to Figure 3.5.

(**A**) Flat mount and (**B**) cross-section of the adult (P28) *Opn1sw*p-Cre;ROSA26-iAP mouse retina, stained with NBT/BCIP for detection of AP activity. Scale bar: 1 mm. (**C**) Enlarged view of the cross-section of AP-stained P28 *Opn1sw*p-Cre;ROSA26-iAP and

*Opn1mw*p-Cre;ROSA26-iAP mouse retina. OS, outer segment; IS, inner segment; ONL, outer nuclear layer; INL, inner nuclear layer; IPL, inner plexiform layer, GCL, ganglion cell layer. Scale bar: 100 μm. (**D** and **E**) AP staining (left) and immunohistochemistry (right) using REEP6 (**D**) and cone-arrestin (CAR; **E**) antibodies demonstrated the identity of AP-stained rod and cone photoreceptors, respectively. OS, outer segment; ONL, outer nuclear layer; OPL, outer plexiform layer. Scale bar: 20 μm.

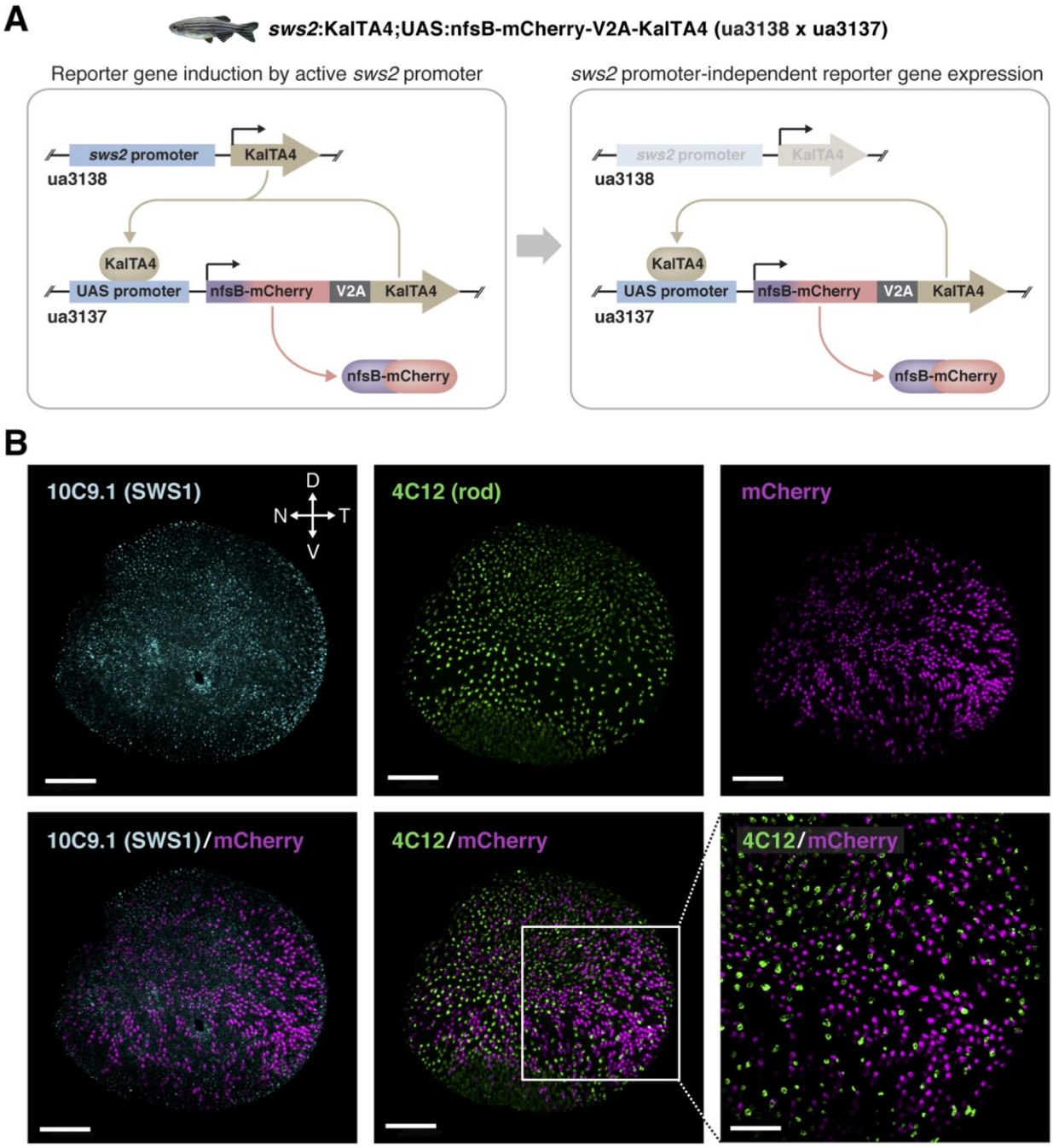

Figure 3.S5: Absence of *sws2* Opsin Expression History in Zebrafish Rod Photoreceptors, related to Figure 3.6.

(**A**) *sws2* opsin lineage tracing strategy in zebrafish. Lineage tracing was performed using a Kaloop feedforward system. Two constructs Tg[*sws2*:KalTA4] and Tg[UAS:nfsB-mCherry-V2A-KalTA4] (ua3138 and ua3137, respectively) were

independently inserted to generate the transgenic zebrafish. In ua3137, a fluorescent reporter protein mCherry is fused in-frame to a bacterial nitroreductase gene (nfsB), and the fusion protein is connected via the labile linker peptide V2A to a second copy of the KalTA4 transcription factor. (**B**) Lineage tracing of *sws2*- expressing cells using *sws2*:KalTA4; UAS:nfsB-mCherry-V2A-KalTA4 zebrafish line. The UV-sensitive cones (cyan, 10C9.1) and rods (green, 4C12) of 4 dpf zebrafish were labeled using immunohistochemistry. Representative images are shown for 1 of the 10 left eyes. A vast majority of lineage-traced cells (4,273 of 4,278; 99.88%) clearly lack immunolabeling by 4C12 (a rod marker), whereas 5 of the cells (0.12%) showed somewhat ambiguous (unclear detection) labeling. D, dorsal; V, ventral; N, nasal; T, temporal. Scale bar: 50 μm in low magnification images, and 20 μm in the high magnification image.

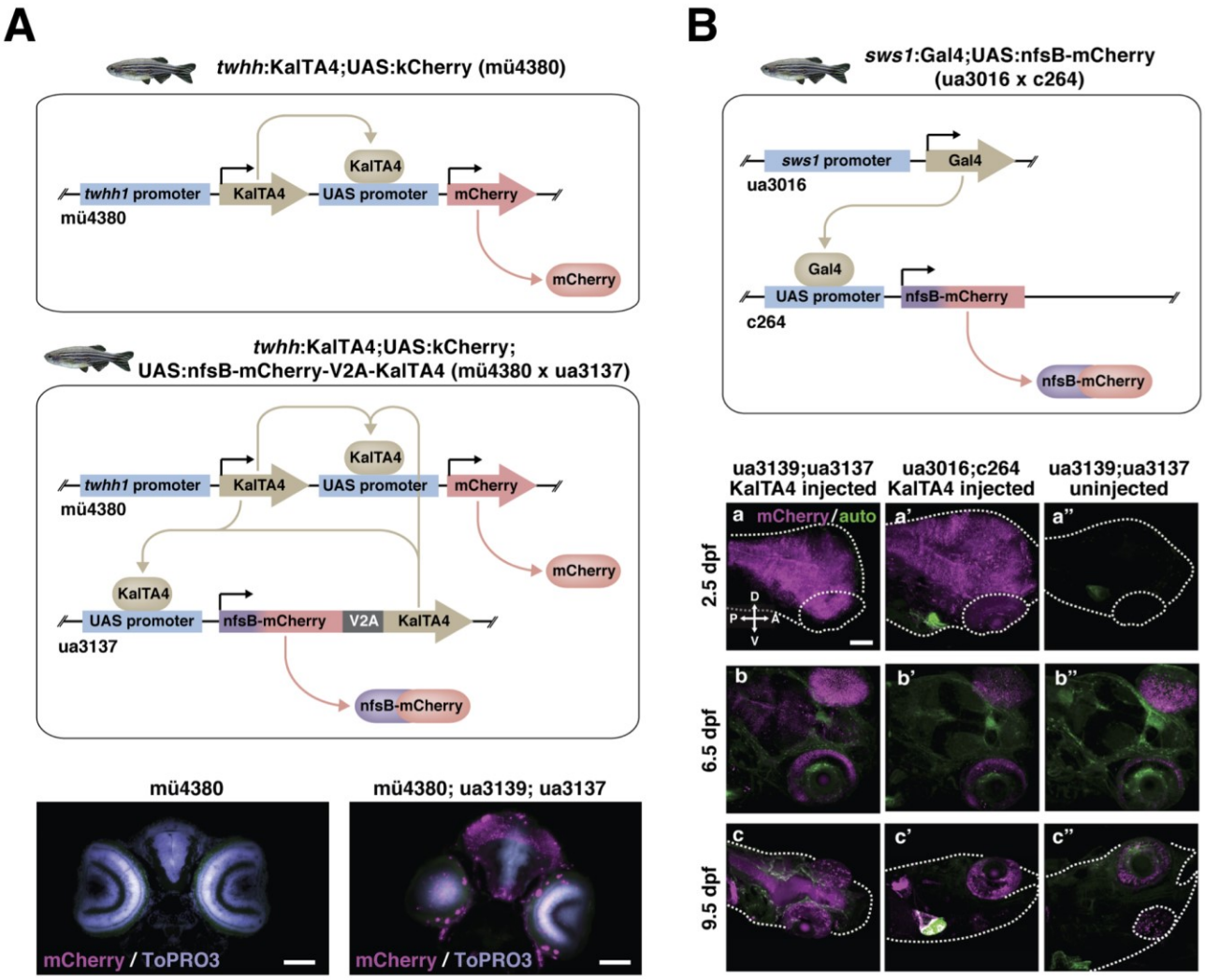

Figure 3.S6: Validation of the Kaloop System, related to Figure 3.6.

The expression of *efna5a* activates *twhh1* promoter, which in turn would induce transgene under UAS. (**A**) The mü4380 zebrafish line was initially recovered from an enhancer trap screen (Distel et al., 2009). In mü4380, developmentally early (20-30 hpf) activation of the nearby endogenous *efna5a* gene induces *twhh*-driven production of KalTA4, which acts upon the UAS promoter to drive expression of the reporter fluorescent protein mCherry. This source of KalTA4 can also act upon the reporter element of the ua3137 construct. Cryosections of 13 dpf mü4380 or mü4380 x ua3137 larvae were imaged. The regions of magenta fluorescence detected only in the mü4380 x ua3125 larvae provide one line of validation for the lineage tracing function of the

Kaloop construct. Cyan shows nuclear stain by ToPRO3. Scale bar: 40 μm. (**B**) Larval *ua3139;ua3137* (Kaloop; see Figure 6A) and *ua3016;c264* zebrafish were injected with KalTA4 mRNA as single-celled zygotes shortly after fertilization, and the level of global mCherry fluorescence is shown at three time points, most visible in the brain. Fluorescence is maintained over time in the Kaloop line but not the ua3016;c264 line, providing further validation that the Kaloop construct has lineage-tracing functionality. In green is manually enhanced autofluorescence, to provide a landmark in each image. In the some cases, extra green fluorescence can be seen in the heart; this is a reporter gene built into the inserted construct which serves only to identify carriers of the [*sws1:KalTA4*] or [*sws1:Gal4*] transgene. In the c264, there is an additional red heart marker which can be seen in some images, which identifies carriers of the [*UAS:nfsb-mCherry*]^{c264} transgene. dpf, days post fertilization; D, dorsal; V, ventral; T, temporal; N, nasal. Scale bar: 50 μm.

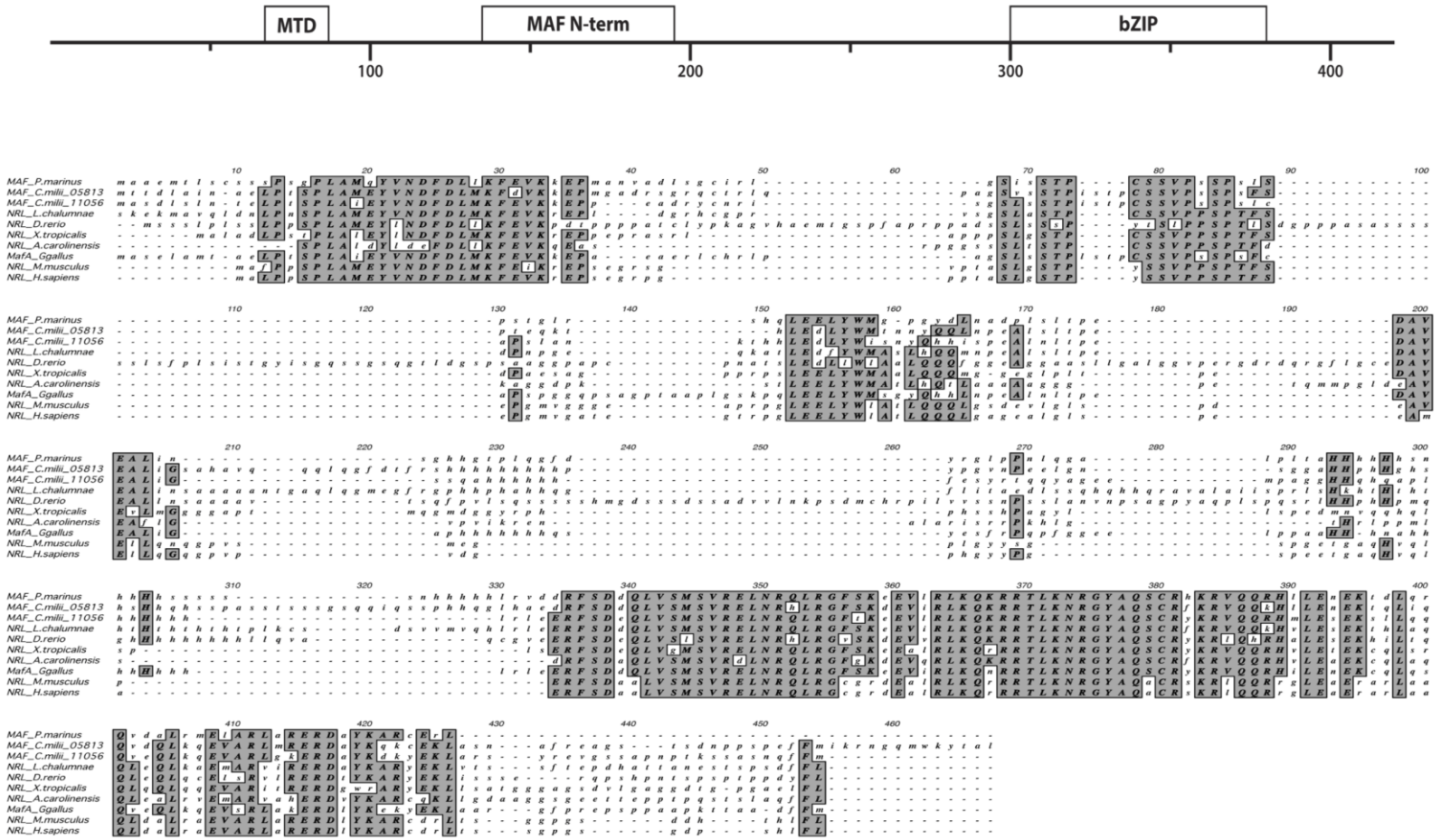
MTD
MAF N-term
bZIP
100
200
300
400
MAF_P.marinus
MAF_C.milii_05813
MAF_C.milii_11056
NRL_L.chalumnae
NRL_D.rerio
NRL_X.tropicalis
NRL_A.carolinensis
MafA_Ggallus
NRL_M.musculus
NRL_H.sapiens

Figure 3.S7: Sequence Alignment of Maf and Nrl Proteins from Sea Lamprey to Human, related to Figure 3.7.

Sequence alignments of Maf and Nrl from indicated species show high degree of homology in jawless vertebrate lamprey (*Petromyzon marinus*) and jawed vertebrates. Protein sequences were obtained from NCBI RefSeq or Ensembl protein databases and aligned by ClustalW using MacVector 12.0.2. MAF and NRL protein alignment: northern hemisphere lamprey (*Petromyzon marinus*, ENSPMAP00000004970), Australian ghostshark (*Callorhincus milii*, SINCAMP00000005813), African coelacanth (*Latimeria chalumnae*, ENSLACP00000018168), zebrafish (*Danio rerio*, NP_001035421.1), western clawed frog (*Xenopus tropicalis*, NP_001027477.2), American green anole (*Anolis carolinensis*, ENSACAP00000015884), house mouse (*Mus musculus*, NP_001258846.1), and human (*Homo sapiens*, NP_006168.1).

Species Name	Common Name	Link
Anas platyrhynchos	Mallard Duck	ftp://ftp.ensembl.org/pub/release-83/fasta/anas_platyrhynchos/pep/
Anolis carolinensis	Carolina Anole	ftp://ftp.ensembl.org/pub/release-83/fasta/anolis_carolinensis/pep/
Astyanax mexicanus	Cave Fish	ftp://ftp.ensembl.org/pub/release-83/fasta/astyanax_mexicanus/pep/
Bos taurus	Cow	ftp://ftp.ensembl.org/pub/release-83/fasta/bos_taurus/pep/
Callorhinchus milii	Elephant Shark	http://esharkgenome.imcb.a-star.edu.sg/download/
Canis familiaris	Dog	ftp://ftp.ensembl.org/pub/release-83/fasta/canis_familiaris/pep/
Ciona intestinalis	Sea Squirt	ftp://ftp.ensembl.org/pub/release-83/fasta/ciona_intestinalis/pep/
Danio rerio	Zebrafish	ftp://ftp.ensembl.org/pub/release-83/fasta/danio_rerio/pep/
Gallus gallus	Chicken	ftp://ftp.ensembl.org/pub/release-83/fasta/gallus_gallus/pep/
Gasterosteus aculeatus	Stickleback	ftp://ftp.ensembl.org/pub/release-83/fasta/gasterosteus_aculeatus/pep/
Homo sapiens	Human	ftp://ftp.ensembl.org/pub/release-83/fasta/homo_sapiens/pep/
Latimeria chalumnae	Coelacanth	ftp://ftp.ensembl.org/pub/release-83/fasta/latimeria_chalumnae/pep/
Lepisosteus oculatus	Spotted Gar	ftp://ftp.ensembl.org/pub/release-83/fasta/lepisosteus_oculatus/pep/
Macropus eugenii	Wallaby	ftp://ftp.ensembl.org/pub/release-83/fasta/macropus_eugenii/pep/
Microcebus murinus	Mouse Lemur	ftp://ftp.ensembl.org/pub/release-83/fasta/microcebus_murinus/pep/

Monodelphis domestica	Opposum	ftp://ftp.ensembl.org/pub/release-83/fasta/monodelphis_domestica/pep/
Mus musculus	Mouse	ftp://ftp.ensembl.org/pub/release-83/fasta/mus_musculus/pep/
Ornithorhynchus anatinus	Platypus	ftp://ftp.ensembl.org/pub/release-83/fasta/ornithorhynchus_anatinus/pep/
Oryzias latipes	Medaka Fish	ftp://ftp.ensembl.org/pub/release-83/fasta/oryzias_latipes/pep/
Otolemur garnettii	Bushbaby	ftp://ftp.ensembl.org/pub/release-83/fasta/otolemur_garnettii/pep/
Pan troglodytes	Chimpanzee	ftp://ftp.ensembl.org/pub/release-83/fasta/pan_troglodytes/pep/
Pelodiscus sinensis	Turtle	ftp://ftp.ensembl.org/pub/release-83/fasta/pelodiscus_sinensis/pep/
Petromyzon marinus	Sea Lamprey	ftp://ftp.ensembl.org/pub/release-83/fasta/petromyzon_marinus/pep/
Procavia capensis	Hyrax	ftp://ftp.ensembl.org/pub/release-83/fasta/procavia_capensis/pep/
Pteropus vampyrus	Megabat	ftp://ftp.ensembl.org/pub/release-83/fasta/pteropus_vampyrus/pep/
Rattus norvegicus	Rat	ftp://ftp.ensembl.org/pub/release-83/fasta/rattus_norvegicus/pep/
Taeniopygia guttata	Zebra Finch	ftp://ftp.ensembl.org/pub/release-83/fasta/taeniopygia_guttata/pep/
Takifugu rubripes	Puffer Fish	ftp://ftp.ensembl.org/pub/release-83/fasta/takifugu_rubripes/pep/
Tupaia belangeri	Tree Shrew	ftp://ftp.ensembl.org/pub/release-83/fasta/tupaia_belangeri/pep/
Tursiops truncatus	Dolphin	ftp://ftp.ensembl.org/pub/release-83/fasta/tursiops_truncatus/pep/
Xenopus tropicalis	Clawed Frog	ftp://ftp.ensembl.org/pub/release-83/fasta/xenopus_tropicalis/pep/

Table 3.S1. Species and genome databases used in phylogenomic analysis, related to Figure 3.7

Purpose	Primer name	Primer sequence
To create mCherry insert for pDestTol2CR2 vector	pmCherry.F11	5'-GGT AAC GCG TGC CAC CAT GGT GAG CAA GGG CGA GGA-3'
	pmcherry.R1	5'-CAC TGA TAT CTT ACT TGT ACA GCT CGT CCA T-3'
To create pDestTol2CR2 vector	pDestTol2CR24 104.F1	5'-AGG TAC GCG TGG TCA CTG TCT GCT TTG CTG-3'
	pDestTol2CR2-3383.R1	5'-CAC AGA TAT CAG CGG CCC CTC TCG AGC-3'
To create T2AKalTA4 entry vector	attB2-Viral T2A forward	5'-GGG GAC AGC TTT CTT GTA CAA AGT GGC TGA GGG AAG AGG AAG TCT GCT GAC C-3'
	attB3-Kal TA4 reverse	5'-GGG GAC AAC TTT GTA TAA TAA AGT TGC TTA GTT ACC CGG GAG GA T GTC CAG-3'

Table 3.S2: Primers used to clone zebrafish constructs

3.5 Experimental Procedures

3.5.1 Mouse and Zebrafish Strains

All procedures involving the use of mice were approved by the Animal Care and Use Committee of the National Eye Institute of the NIH. *Nrl*p-GFP and *Nrl*p-GFP;*Nrl*$^{-/-}$ were described previously (Akimoto et al., 2006). *Opn1sw*p- Cre (BP-Cre) and *Opn1mw*p-Cre (RGP-Cre) (Akimoto et al., 2004) mice were crossed with ROSA26-iAP line (Badea et al., 2009) for the lineage tracing. *Opn1sw*p-Cre (BAC tg) mice were crossed with Z/EG line (The Jackson Laboratory) to generate *Opn1sw*p-Cre (BAC tg);Z/EG for lineage tracing. Zebrafish were maintained and bred in accordance with the approved protocols of the University of Alberta's Animal Care and Use Committee: BioSciences. Details of the strains are provided in Section 3.6 Supplemental Experimental Procedures.

3.5.2 FACS Isolation of Mouse Rod Photoreceptors, and Next-Generation Sequencing

P2, P4, P6, P10, P14, and P28 *Nrl*p-GFP transgenic mouse retinas were dissected and retinal cells were dissociated by incubating in Accutase (Life Technologies) or Papain (Worthington Biochemical) at 37 C for 10 min followed by trituration. GFP^{+} cells were isolated by FACS using FACS Aria II (Bec- ton Dickinson). After sorting, these samples were also reanalyzed to check its purity. Only samples showing over 96% purity were used for strand-specific RNA-seq, ChIP-seq, and RRBS, and a majority had 99% or more GFP^{+} cells. Strand-specific RNA-seq was performed as previously described (Brooks et al., 2012), and data quantification was performed at transcript level using Ensembl v73 transcriptome annotation (Kaewkhaw et al., 2015). Modifications were made to standard methods (Barski et al., 2007; Brooks et al., 2012) for ChIP-seq and RRBS using isolated photoreceptors. ChIP-seq and RRBS reads were aligned using the Genomatix Mapper v3.7.5 (Genomatix), and the aligned RRBS reads were further analyzed using the methylKit package in R (Akalin et al., 2012). Details of experimental protocols are provided in Section 3.6 Supplemental Experimental Procedures. The dynamics of rod transcriptome during development and network analysis will be

published elsewhere. NGS data reported here are available under Gene Expression Omnibus accession numbers GEO: GSE74660 (RNA-seq), GSE81099 (Methyl DNA), and GSE81953 (ChIP-seq).

3.5.3 Immunostaining and Flow Cytometry Analysis of Dissociated Retinal Cells

Retinal cells were dissociated as described above and fixed in 1% paraformaldehyde for 15 min at room temperature. Fixed cells were incubated with anti- S-opsin or NRL antibodies. After washing with PBS, cells were incubated in a 1:200 dilution of secondary antibodies. Stained cells were mounted on slide glass for fluorescence microscopy or analyzed by FACSCalibur (Becton Dickinson). One retina from an *Nrl*p-GFP mouse was dissociated by trypsin (Life Technologies) and counted using a hemocytometer to obtain the total retinal cell count. Details are provided in Section 3.6 Supplemental Experimental Procedures.

3.5.4 Lineage Tracing and Immunohistochemistry

Enucleated eyes from the indicated lineage tracing mouse lines were pre- immersed in 4% paraformaldehyde for 15 min at room temperature. After AP staining, tissues were washed three times in PBS with 0.1% Tween 20 for 20 min each and post-fixed in 4% paraformaldehyde overnight. The AP-stained retinas were sectioned at 70 mm and processed for immunofluorescent staining as needed. See Section 3.6 Supplemental Experimental Procedures for details.

3.5.5 Phylogenomic Analyses

Whole genomes from 30 taxa representing the major lineages of vertebrates were selected for analysis (Table 3.S1). Protein models for each genome were searched using BLAST (Altschul et al., 1997) and known NRL query sequences. Redundant hits were removed using cd-hit (Li and Godzik, 2006), sequences were aligned in MAFFT (Katoh and Standley, 2013), and regions of the alignment that contained less than 20%

sequence coverage were removed using trimAl (Capella-Gutiérrez et al., 2009). Phylogenetic analysis was conducted using RAxML 8.2 (Stamatakis, 2014) under the bestfit model using 20 random starts and 1,000 bootstrap replicates. Reconciled tree analysis was conducted using NOTUNG 2.6 (Chen et al., 2000).

3.6 Supplemental Materials and Methods

3.6.1 Mouse Strains

All procedures involving the use of mice were approved by Animal Care and Use Committee of the National Eye Institute (NEI), National Institutes of Health, USA. *Nrlp*-GFP transgenic mice and *Nrlp*-GFP;*Nrl*$^{-/-}$ were back- crossed over 10 times to C57BL/6 strain and have been described previously (Akimoto et al., 2006). *Opn1sw*p-Cre (BP-Cre) and *Opn1mw*p-Cre (RGP-Cre) (Akimoto et al., 2004) mice were crossed with ROSA26-iAP line (Badea et al., 2009) to generate *Opn1sw*p-Cre;Rosa26-iAP and *Opn1mw*p-Cre;Rosa26-iAP progenies for lineage tracing of S- opsin- and M-opsin-expressing photoreceptor precursor cells, respectively. *Opn1sw*p-Cre (BAC tg) mice were crossed with Z/EG line (The Jackson Laboratory, Stock number 004178) to generate *Opn1sw*p-Cre (BAC tg); Z/EG for lineage tracing of S-opsin expressing photoreceptor precursor cells.

3.6.2 Zebrafish Strains

Zebrafish were reared and maintained using standard protocols with a 14:10 light:dark cycle of fluorescent lights in briny fresh water (1350±100 µS conductivity). Several novel transgenic zebrafish lines were generated (see below) in a background of AB crossed to WIK strains, and these were bred to the existing transgenic strains Tg(*sws1*:Gal4-VP16)ua3016;Tg(UAS-E1b:NfsB-mCherry)c264 (ZFIN ID ZDB-GENO-130328-4) that express Gal4 and mCherry in UV-sensitive cones as described previously (Fraser et al., 2013). An enhancer trap line Et(shhb:KalTA4,UAS- E1b:mCherry)zf265^{mü4380} (ZFIN ID ZDB-ALT-120220-4) was used that expresses KalTA4 (a zebrafish-optimized Gal4 derivative) and mCherry apparently under the enhancer/promoter of the ephrin gene

efna5a (Distel et al., 2009). Zebrafish were maintained and bred in accordance with the approved protocols of the of the University of Alberta's Animal Care and Use Committee:BioSciences, which operates under the auspices and mandate of the Canadian Council on Animal Care.

3.6.3 Generation of *Opn1sw*p-Venus and *Opn1sw*p-Cre (BAC tg) Mice

Venus (a variant of YFP) and Cre were inserted in the endogenous *Opn1sw* locus on a BAC clone (bMQ-440P15) at NEI Genetic Engineering Core Facility. DNA from the recombined clone was injected into fertilized mouse pronuclei to generate transgenic mice at Transgenic Core Facility at National Institute of Mental Health. Founders that highly expressed the Venus gene in S-cones were selected. Only 30% of the anti-S-opsin antibody positive cells expressed the Venus reporter gene.

3.6.4 Genotyping for Mice

Mouse tail biopsies were digested with proteinase K in DirectPCR tail buffer (Viagen Biotech, CA, USA) at 55°C for 16 h followed by heat inactivation of the enzyme at 85°C for 45 min. After centrifugation, 1 ml of supernatant was analyzed by PCR using the following primers: *Nrl*p-GFP forward 5'-TGA TCT CAG GGA ACC AGT CC-3' and reverse 5'-AAG TCG TGC TGC TTC ATG TG-3'; *Opn1sw*p-Venus forward 5'-TGC TGT AGG GAA GGG TGA TAG-3' and reverse 5'-CGT CGT CCT TGA AGA AGA TGG-3'; *Opn1sw*p-Cre forward 5'-AGG AGG GTG CTG TAG GGA AG-3' and reverse 5'-GAA CGA ACC TGG TCG AAA TC-3'; *Opn1mw*p-Cre forward 5'-AAT GGG AAC AGT GGT GTG TG-3' and reverse 5'-GAA CGA ACC TGG TCG AAA TC-3'; ROSA26-iAP forward 5'-GGC AAC GAG GTC ATC TCC GTG ATG AA-3' and reverse 5'-GGT TGC CTG GGT CTG AGC TAG TGC C-3'.

3.6.5 Isolation of Mouse Rod Photoreceptors

Postnatal day (P) 2, P4, P6, P10, P14 and P28 *Nrl*p-GFP transgenic mouse retinas were dissected in Hank's Balanced Salt Solution (HBSS; Life Technologies, NY, USA),

and retinal cells were dissociated by incubating in Accutase (Life Technologies) at 37°C for 10 min followed by trituration. Cell clumps were removed by filtration, and dissociated cells were washed thoroughly with 4 ml of PBS (GIBCO, Life Technologies), collected by centrifugation at 1,000 RPM for 5 min and re-suspended in 1 ml of PBS. GFP-positive cells were isolated by fluorescence-activated cell sorting (FACS) using FACS Aria II (Becton Dickinson, CA, USA). Stringent precision setting was employed to eliminate contamination from different retinal cell types. After sorting, collected samples were re-analyzed to check purity, and only those samples with over 97% of purity were used for further analysis (RNA-seq and RRBS). For histone modification ChIP-seq, cells from *Nrl*p-GFP mouse retinas were dissociated using papain (Worthington biochemical, NJ, USA) supplemented with DNase I, superoxidodismutase, catalase, D- alpha-tocopherol acetate, and gentamycin at 28°C for 8 min. Dissociated cells were fixed in 1% formaldehyde for 15 min at room temperature before flow-sorting. These samples were also re-analyzed to check its purity.

3.6.6 Immunostaining and Flow Cytometry Analysis of Dissociated Retinal Cells

Retinal cells were dissociated as described above and fixed in 1% paraformaldehyde for 15 min at room temperature. Fixed cells were incubated with anti-S-opsin (SC-14363, Santa Cruz Biotechnology, TX, USA) or custom-made anti-NRL antibodies diluted to 1:100 in permeabilization buffer (0.1% Saponin, 0.1% BSA, 75 mM Sodium Acetate and 25 mM HEPES, pH 7.2) for 20 min at room temperature. After wash, cells were incubated in 1:200 dilution of secondary antibodies. Donkey anti-goat or rat IgG antibodies conjugated to AlexaFluor dyes (1:200; Life Technologies) were used for immunocytochemistry and donkey anti-goat or rat antibody conjugated with APC (Jackson ImmunoResearch, PA, USA) for flowcytometry. Stained cells were mounted on slide glass for fluorescence microscopy or analyzed by FACS Calibur (Becton Dickinson) and BD Cell Quest Pro software. To obtain total retinal cell count, one retina from *Nrl*p-GFP mouse at desired developmental stages was incubated in 0.1% trypsin (Life Technologies) for 15-20 min at 37°C and fully dissociated by trituration after

addition of 0.1 mg/ml DNase I and 10% fetal bovine serum, and dissociated cells were counted using a hemocytometer.

3.6.7 Single Cell Collection and Quantitative RT-PCR

Fifty GFP(+) cells from dissociated P2 and P28 *Nrl*p-GFP mouse retinal cells were isolated by micromanipulator. Total RNA was isolated from three independent samples for each time point using TRIzol (Invitrogen, Life Technologies) and used for first strand cDNA synthesis using SuperScript II reverse transcriptase (Invitrogen, Life Technologies) according to manufacturer's instruction. RT-qPCR was then performed using SYBR Green-based detection of gene expression (Applied Biosystems, 7900HT, Life Technologies). Data analysis employed the DDCt method.

3.6.8 Strand-specific RNA Sequencing

GFP-positive cells flow-sorted from *Nrl*p-GFP and *Nrl*p-GFP; *Nrl*$^{-/-}$ mice were lysed with TRIzol LS (Invitrogen), and total RNA was isolated following manufacturer's instruction. RNA quality was assessed using Bioanalyzer RNA 6000 Pico assay (Agilent technologies, CA, USA). Strand-specific mRNA sequencing libraries were generated from 20 ng of total RNA using TruSeq RNA Sample Prep Kit-v2 (Illumina, CA, USA) with modified protocol as described previously (Brooks et al., 2012) and sequenced on Genome Analyzer IIx platform (Illumina). Transcript quantitation was performed with eXpress v1.3.1 (Roberts et al., 2013) by streaming pass filter reads to Bowtie2 v2.1.0 (Langmead and Salzberg, 2012) for alignment to GRCm38.p2/Ensembl v73 annotation. This study utilized the high-performance computational capabilities of the Biowulf Linux cluster at NIH (http://biowulf.nih.gov).

3.6.9 Reduced Representation Bisulfite Sequencing (RRBS)

Previously published RRBS protocol (Gu et al., 2011) was modified to create a streamlined workflow optimized for smaller sample sizes and for sequencing on Illumina platform. Genomic DNA was isolated from flow-sorted rod photoreceptors of *Nrl*p-GFP

mouse at indicated time points using Purelink gDNA isolation kit (Invitrogen, Life Technologies), and 50 ng of genomic DNA was digested with 1 ml of 20 U/ml MspI restriction enzyme (New England Biolabs, MA, USA) in NEB Buffer 4 in a total reaction volume of 50 ml. The reactions were performed at 37°C for varied digestion times - 5 min, 10 min, 30 min and 60 min to retrieve diverse gDNA length, and 150 ml TE buffer (10 mM Tris-HCl, pH 8.0 and 1 mM EDTA) and equal volume (200 ml) of UltraPure phenol/chloroform/isoamyl alcohol (Life Technologies) was added. Then, the four gDNA samples digested for different amount of time were pooled into one tube. Fragmented DNA in the aqueous phase was isolated by ethanol precipitation (100% ethanol, 100 mM NaCl, 20 ng of Glycogen). Sequencing libraries were prepared using TruSeq DNA sample preparation kit (Illumina). We followed the manufacturer's instruction to blunt the ends of the fragmented DNA, to add 3'-A overhang, and to ligate 1/10 dilution of TruSeq index adapters. Using diluted adapters significantly reduced the chance of having access adapter-adapter dimers. Adapter ligated DNA fragments were size selected using 2% agarose gel and gel extraction kit (MinElute; Qiagen, Hilden, Germany). Then, bisulfite modification was performed using Epitech kit (Qiagen). For library amplification, we used KAPA Uracil+ 2X polymerase mixture (KAPA Biosystems, MA, USA) using Illumina primer kit. Eighteen cycles of PCR amplification were performed as recommended by the manufacturer. Sequencing was performed on Genome Analyzer IIx (Illumina) platform.

3.6.10 Chromatin Sample Preparation and Chromatin Immunoprecipitation Sequencing (ChIP-seq)

Flow-sorted fixed cells were lysed by 10 min incubation in cold lysis buffer (50 mM HEPES-KOH, pH 8, 1 mM EDTA, 0.5 mM EGTA, 140 mM NaCl, 10% glycerol, 0.5% nonidet P-40, 0.25% Triton X-100 with proteinase inhibitors) followed by homogenization using Dounce tissue grinder (VWR international, PA, USA). Lysed cells were retrieved by centrifugation at 2,500g for 5 min and washed first in washing buffer

(10 mM Tris-HCl, pH 8, 1 mM EDTA, 0.5 mM EGTA, 200 mM NaCl, proteinase inhibitors) followed by second wash in shearing buffer (10 mM Tri-HCl, pH 8, 2 mM EDTA, 0.1% SDS, proteinase inhibitors). Cells resuspended in shearing buffer were processed for sonication using Covaris S220 focused-ultrasonicators (20% duty cycle, intensity 8, 200 cycles per burst, 60 seconds per cycle) to obtain chromatin fragments with the average size of 150-200 bp. Chromatin solutions were centrifugated at 16,000g for 10 min to remove pelleted insoluble material. Cleared chromatin fragments were then reconstituted to 500 ml of RIPA buffer (10 mM Tris-HCl, pH 8, 1 mM EDTA, 0.5 mM EGTA, 140 mM NaCl, 1% Triton X-100, 0.1% Sodium deoxycholate, 0.1% SDS, proteinase inhibitors). Before proceeding to ChIP, chromatin solutions were incubated with Protein A conjugated Dynabeads (Invitrogen) with constant rotation at 4°C for 2 hrs to remove any chromatin fragments that bind beads via nonspecific interaction. Pre-cleared chromatin solution was then incubated with anti-H3K4me3 (ab8580, Abcam, MA, USA), anti-H3K27me3 (07-449, Millipore, MA, USA) or normal IgG (12-370, Millipore) with constant rotation at 4°C overnight. Antibody-chromatin complexes were then incubated with 10 ml beads at 4°C for 4 hrs. Free antibodies and chromatin fragments and nonspecific antibody-chromatin binding were washed away with following wash solutions: 10 min in RIPA buffer; 10 min in RIPA with 500 mM NaCl; 10 min in LiCl wash buffer (10 mM Tris-HCl, pH 8, 1 mM EDTA, 0.5 mM EGTA, 250 mM LiCl, 1% Triton X-100, 1% Sodium deoxycholate, proteinase inhibitors); TE, pH 8. Thoroughly washed immunoprecipitation complexes were then digested, and the cross-link was reversed by incubation in 50 ml of TE, pH 8 supplemented with 0.3% SDS and 1 mg/ml proteinase K at 65 °C for 6 hrs. The supernatant was transferred to new tubes, and TE containing 0.5 M NaCl was used to rinse the remaining beads and combined with initial 50 ml solution. The carried-over RNA was digested by 1 hr incubation at 37°C with RNase cocktail (Ambion, Life Technologies), and the immunoprecipitated DNA was then purified using Agencourt AMPure XP beads (Beckman Coulter, CA, USA). Sequencing libraries were prepared using TruSeq DNA sample preparation kit (Illumina) with multiple adjustments, which include usage of 1/100 dilution of TruSeq adapters and gel-free DNA size selection using AMPure XP beads. Libraries were PCR-amplified for 18

cycles and sequenced on Genome Analyzer IIx (Illumina) platform following manufacturer's protocol.

3.6.11 Alkaline Phosphatase Staining and Immunohistochemistry

Enucleated eyes from the indicated lineage tracing mouse lines were pre-immersed in 4% paraformaldehyde for 15 min at room temperature. Extra ocular tissues were then removed leaving only the retina and lens, which were fixed for an additional hour. Fixed retinas were heated to 65°C in water bath for 1 hour to inactivate endogenous AP activity, and incubated in the AP substrates, 0.34 mg/ml nitroblue tetrazolium (NBT) and 3.4 mg/ml 5-bromo-4- chloro-3-indolyl-phosphate (BCIP; Boehringer Mannheim, IN, USA) in 0.1 M Tris, 0.1 M NaCl, 50 mM $MgCl_2$, pH 9.5, for 1 ~ 2 hours at room temperature with mild agitation. After staining, tissues were washed three times in PBS with 0.1% Tween 20 for 20 min each and post-fixed in 4% paraformaldehyde overnight. The AP stained retinas were sectioned at 70 mm on a Vibratome (VT1000S, Leica Biosystems, IL, USA). Some of the AP-stained retinal sections were further processed for immunofluorescent staining with the following primary antibodies: custom-made rabbit polyclonal antibody against REEP6 (1:1000 dilution) and mouse monoclonal antibody against CAR (1:500; Millipore, AB15282). AlexaFluor 488 dye-conjugated donkey antibodies against rabbit or mouse IgG (1:200; Life Technologies) was used to detect the primary antibodies. Retinal sections were imaged using Olympus BX50 fluorescence microscope.

3.6.12 Engineering Transgenic Zebrafish

Primers for zebrafish cloning to make these constructs are found in Table 3.S2. Constructs for delivery to engineer transgenic zebrafish were engineered with multisite Gateway Cloning and Tol2 systems as described (Fraser et al., 2013; Kwan et al., 2007). A novel Destination vector was generated, pDestTol2CR2, which is a modified version of pDestTol2CG2 that replaces GFP with mCherry such that fluorescent red heart muscle serves as a marker of successful transgenesis. Thus fish could be identified that were transgenic for both of the requisite constructs, as they would

possess both red and green hearts. This vector was made by PCR amplifying a fragment of pDestTol2CG2 that was 7kb and lacked eGFP, whereas mCherry was PCR amplified from existing plasmids, both using primers in the table below. Both products were then digested with EcoRV and MluI, the former product was treated with CIAP (Calf Intestinal Alkaline Phosphatase), and it was ligated to the latter mCherry product using T4 ligase and confirmed via sequencing.

A Kaloop vector enabling lineage tracing, inspired by the one previously validated by Distel et al (Distel et al., 2009), was recombined into pDestTol2CR2. A middle entry vector pME-nfsB-mCherryΔSTOP was generated by BP cloning a product from existing plasmids (Davison et al., 2007; Fraser et al., 2013), in order to remove the terminal stop codon using primers in Table 3.S2. This was recombined with vectors p5E-4X-uas and a novel p3E-T2a- KalTA4 vector created by BP reaction using primers in Table 3.S2 amplifying off existing plasmids (Distel et al., 2009). The product of the cognate LR reaction, pDestTol2CR2.4UAS:kozak-nfsB-mCherry^DAV-T2A.KalTA4.pA, expresses an mCherry fusion protein and KalTA4 as separate peptides whenever KalTA4 or Gal4 is present to initiate expression. The KalTA4 feeds back upon itself (“Kaloop”) to maintain expression of the construct, permitting lineage tracing to determine the fate of cells that expressed the initial Gal4, even if said Gal4 was expressed transiently.
A construct to drive KalTA4 under control of the *sws1* (UV-senstitive opsin) promoter was generated by using an LR reaction to recombine the well-characterized (Allison et al., 2010; Duval et al., 2013; Fraser et al., 2013; Takechi et al., 2003) UV-opsin promoter (our p5E-*sws1* plasmid containing 5.5 kB of the *sws1* promoter (Fraser et al., 2013)), with pME-KalTA4 (Distel et al., 2009), p3E-pA and pDestTol2CG2 (Kwan et al., 2007) to generate pDestTol2CG2.*sws1*:KalTA4. These constructs were delivered to zebrafish embryos, which were screened for red or green heart fluorescence as appropriate and grown to adulthood. Stable transgenic carriers were identified by screening progeny of these fish for robust expression of mCherry in UV cones, including in adult fish by fluorescent fundoscopy (Duval et al., 2013), thereby isolating novel transgenic lines Tg(*sws1*:KalTA4)ua3139 and Tg(4X- UAS:nfsb-mCherry-V2A-KalTA4)ua3137.

3.6.13 Kaloop Method and Validation

In these fish, expression of *sws1* drives expression of the transgenic transcription factor KalTA4, derived from the more classical Gal4 of yeast genetics, which then acts upon any transgene with the promoting upstream activating sequence (UAS). In cells that are currently expressing or had previously been expressing KalTA4 transcription factor, mCherry fluorescent fusion protein and a second copy of the KalTA4 transcription factor are expressed, thereby maintaining activity of the reporter construct independent of *sws1* activity (see Fig. 3.6A).

To ensure the positive feedback construct was capable of self-maintenance after the initial source of KalTA4 ceased activity, we performed two independent validations. First, we crossed the fish line with the feedback construct to the enhancer trap line mü4380 (Distel et al., 2009). mü4380 features a minimal form of the *twhh* promoter to drive expression of KalTA4 under the influence of the nearby endogenous *efna5a* locus, and also contains a UAS promoter driving the fluorescent reporter protein mCherry (see Fig. 3.S4A). The mü4380 enhancer trap activates by 28 hours post fertilization, and manifests as fluorescence within the dorsal-nasal retina, the midbrain, and part of the hindbrain (Fig. 3.S4A). When mü4380 was crossed to the positive feedback transgenic fish line ua3137, we observed much brighter fluorescence in perhaps more areas of the brain and retina, compared to the mü4380 line alone (Fig. 3.S4A). This increased fluorescence confirms that the positive feedback aspect of the lineage-tracing construct is functional, but because the mü4380 fish still have fluorescence at the assayed age (13 dpf), it is possible we observe simply strengthened signal, and not true tracing of lineage.

To distinguish between these possibilities, we tested whether a temporary source of KalTA4 could enduringly activate the reporter fluorescence. We injected KalTA4 mRNA, transcribed *in vitro*, into one-cell embryos bearing either the ua3137 construct, or the c264 construct, which lacks the second copy of KalTA4 (see Fig. 3.S4B) and is therefore incapable of self-maintenance of expression. KalTA4 mRNA is capable of inducing fluorescence in fish with either the ua3137 or c264 constructs (Fig. 3.S4B), visible at 2.5dpf, but by 6.5dpf the fluorescence in the larvae with c264 is restricted to the retina, where the *sws1:Gal4* (ua3016) construct provides continual activation of the

UAS-driven reporter construct. In contrast, mCherry is still visible in the brains of injected larvae bearing ua3137 by 6.5 dpf. By 9.5 dpf, a collapsed z-stack image series of injected ua3137-bearing larvae shows that the brain in particular still robustly expresses fluorescent protein, which is not the case for the injected ua3016;c264 larvae.

3.6.14 Immunohistochemistry and Visualization for Zebrafish

As per recent descriptions (Duval et al., 2014), UV cones and rods were detected with 1:100 rat and mouse monoclonal antibodies 10C9.1 and 4C12, respectively (ZFIN IDs ZDB-ATB-140728-2 and ZDB-ATB-090506-2). Secondary antibodies anti-rat-AlexaFluor647 and anti-mouse-AlexaFluor488 (Invitrogen, Carlsbad, Cat. #A-21472 and A-21202) were diluted 1:1000. Antibodies were diluted in 2% normal goat serum in phosphate buffered saline (pH 7.4) with 0.1% Tween-20, and applied overnight to whole 4dpf larvae that had been fixed in 4% paraformaldehyde. Following rinses, enucleated eyes were flatmounted and visualized on a Zeiss Axio Observer.Z1 with LSM 700 confocal microscope and ZEN 2010 software (version 6.0, Carl Zeiss MicroImaging, Oberkochen). Images were manipulated linearly for brightness and/or channel colour in Imaris x64 (version 7.4.0, Bitplane, Badenerstrasse), Zen 2010 (Carl Zeiss MicroImaging, Oberkochen) and/or Adobe Photoshop CS5 Extended (Adobe Systems Inc., San Jose) and compiled for presentation in PowerPoint. To examine potential co-localization of mCherry lineage tracer with rod-specific antibody 4C12, a z-stack of confocal images was browsed using the orthogonal plane view of the ZEN 2010 confocal imaging software.

3.6.15 Chicken *MAFA* Expression Vector Construction

Chicken retina was harvested at postnatal day (P)10 and lysed with TRIzol LS (Invitrogen). Total RNA was isolated following manufacturer's instruction. Chicken retinal cDNA was synthesized using Superscript II (Invitrogen). Chicken *MAFA* cDNA was then amplified by PCR using the following primers: forward primer 5'- GAA TTC ATG GAC TAC AAA GAC GAT GAC GAC AAG GCC TCG GAG TTG GCC AT-3' that

includes EcoRI site and a FLAG tag, and reverse primer 5'- CGT CGA CTT TGC AAG GGC CGG GAT TCT CCT CCA CGT CAC CGC ATG TTA GAA GAC TTC CTC TGC CCT CCA TGA AGA AGT CA-3' that includes a T2A cleavage site and SalI site. The amplified PCR product was introduced into the pCRII-TOPO vector (K4650; Invitrogen) and subcloned into GFP-N1 vector using EcoRI and SalI restriction enzymes. The FLAG-chick MAFA-T2A-GFP clone was verified by DNA sequencing.

3.6.16 *In Vivo* Electroporation in Mouse Retina and Analysis of Photoreceptor Markers

Control GFP vector or chicken *MAFA* expression vector (0.2 µl of 1 mg/ml) was injected into subretinal space of rodless P2 *Nrl*$^{-/-}$ mouse retinas. Tweezer electrodes were placed over the head of the injected pups with the positive electrode covering the injected eye and the negative covering the other eye. Five square pulses at 80 V, each with 50 msec duration and 800 msec interval, were applied to deliver the injected DNA into outer neuroblastic layer of the retina. Electroporated retinas were harvested at P14 and P21 and processed for downstream analysis. Total RNA from harvested retina was used for quantitative PCR analysis of rod- and cone-specific genes. For immunohistochemistry, enucleated eyes were pre-immersed in 4% paraformaldehyde for 15 min at room temperature and dissected retina was then fixed for 4 hours at room temperature. Retinal sections of 100 mm thickness (generated by vibratome (VT1000S, Leica Biosystems, IL, USA) were stained with the following primary antibodies: mouse monoclonal antibody against Rib-eye (CTBP2) (1:1000 dilution; BD Transduction Laboratories, 612044), and mouse monoclonal antibody against cone arrestin (CAR) (1:500; Millipore, AB15282). AlexaFluor 555 dye-conjugated donkey antibodies against mouse IgG (1:200; Life Technologies) was used to detect the primary antibodies. Retinal sections were imaged using Carl Zeiss LSM 700 confocal microscope.

3.6.17 Phylogenomic Analyses of NRL and related Maf Proteins

Whole genomes from 30 taxa representing the major lineages of vertebrates were selected for analysis (Table 3.S1). Protein models for each genome were searched

using BLAST (Altschul et al., 1997) with an e value of 0.1 using the known NRL sequences from mouse (NP_032762.1) and human (BAJ84046.1) as queries. The top twelve sequences from each BLAST search were retained for each species and hits were concatenated into a single file. Redundant sequences were then removed using cdhit (Li and Godzik, 2006). Sequences were aligned in MAFFT (Katoh and Standley, 2013) under the auto setting and regions of the alignment that contained less than 20% sequence coverage were removed using trimal (Capella-Gutierrez et al., 2009) using the –gt 0.2 option. Phylogenetic analysis was conducted using RAxML 8.2 (Stamatakis, 2014). First, the best fitting model (LG+I+G) was determined and then trees were searched using 20 random starts and 1000 bootstrap replicates. Gene duplication and loss events were estimated using reconciled tree analysis in NOTUNG 2.6 (Chen et al., 2000) under default settings.

CHAPTER 4:

REQUIREMENTS FOR NRL IN PRODUCING ROD PHOTORECEPTORS VARY OVER ZEBRAFISH ONTOGENY

A version of this chapter has been prepared for submission as:

A. Phillip Oel[1], Spencer Balay, Keon Collett, Emily Dong, and W. Ted Allison[2], 2018. "*Requirements for* nrl *in producing rod photoreceptors vary over zebrafish ontogeny.*"
[1]First author, [2]author for correspondence.

Author contributions: SB developed, performed, and analyzed the qPCR experiments of Fig. 4.1E, 4.4C, 4.S24 and 4.S25, and edited the manuscript. KC helped establish transgenic zebrafish used throughout, and aided in generating morpholino data for Fig. 4.S4. ED developed, performed and analyzed the *in situ* hybridization for Fig. 4.4D-G, and edited the manuscript. **APO** and WTA conceived the experiments, analyzed the data, and wrote the manuscript. All other work in this chapter is my own.

4.1 Introduction

Rods and cones are the ciliary photoreceptors used by vertebrates to mediate vision in a broad range of circumstances. Rod photoreceptors can detect even single photons of light, supporting vision in dim conditions, while cone photoreceptors convey colour-specific information and enable high acuity in brightly lit environments. Retinas that possess both rods and cones are known as duplex retinas, and the basic features of the duplex retina are present even among some of the oldest vertebrates, the lampreys (Asteriti et al., 2015; Collin and Trezise, 2004; Morshedian and Fain, 2015). In many extant vertebrate lineages, rod and cone diversity has been continually modulated as organisms adapt to changing environments. However, the basic genetic regulation of vertebrate photoreceptor diversity remains poorly understood, and how this regulation has been modified in evolution is unexplored. Comparing photoreceptor development across vertebrates will be critical to addressing this knowledge gap.

The development of the visual photoreceptors is most studied in the mouse, although cone specification has also been examined in zebrafish and chicken. In the mouse, as a photoreceptor precursor cell of a developing retina exits its terminal mitosis, expression of the bZIP transcription factor *Nrl* will direct it to a rod fate; without *Nrl* expression, it will develop as a cone (Daniele et al., 2005; Mears et al., 2001; Nikonov et al., 2005). With high activity of the thyroid hormone receptor Trβ2, the presumptive cone will develop into the medium (green) wavelength light-sensitive M-cone (the ancestral red cone). Without Trβ2 activity, it becomes a short (UV/blue) wavelength light-sensitive S-cone (the ancestral UV cone) (Ng et al., 2001). This efficient two-factor specification pathway is sufficient to generate all photoreceptor diversity in mammals, which have lost the ancestral blue and green light-sensitive cone subtypes (Ng et al., 2011). In other taxa, blue and green cone specification remains unexplained. Moreover, the regulation of rod-versus-cone fate appears to be more nuanced in tetrachromats, as zebrafish lacking *tbx2b* overproduce rods at the expense of UV cones specifically (Alvarez-Delfin et al., 2009; Michèle G. DuVal et al., 2014); it is currently unclear whether mammalian *Tbx2* has a role in developing photoreceptors, as *Tbx2* knockout is lethal before photoreceptor generation (Sheeba and Logan, 2017). However, chicken violet cones (ancestral UV cones) show enriched expression of *TBX2*

(Enright et al., 2015a), suggesting that a role for *TBX2* is ancestral. Recently, zebrafish *six7*, a homolog of mammalian *Six3*, was shown to regulate green cone versus rod abundance in larvae (Ogawa et al., 2015; Sotolongo-Lopez et al., 2016), and does so independently from the actions of *tbx2b* in regulating UV cone versus rod abundance (Sotolongo-Lopez et al., 2016). *TRB2* has been associated with red cone development in chicken as well (Enright et al., 2015a), and *trβ2* regulates red cone versus UV cone fate in zebrafish (Suzuki et al., 2013), demonstrating the conservation of the photoreceptor specification program in tetrachromats. However, we do not yet know a genetic pathway that integrates these genes. *trβ2* regulates UV and red cone abundance, and *tbx2b* and *six7* appear to modulate UV and green cone abundance relative to rods; the ability to directly manipulate rod development in zebrafish will be invaluable to constructing a genetic network for specifying tetrachromat photoreceptors. One candidate factor for this would be zebrafish *nrl*, although it has not yet been tested whether the role of *nrl* in rod development is conserved outside of mammals.

Previous work has shown *nrl* to be expressed in or near the rod photoreceptors of zebrafish larvae (Coolen et al., 2005; Nelson et al., 2008), and Xenopus embryos expressing lipofected Xenopus *Nrl* showed rhodopsin immunoreactivity in lipofected cells (McIlvain and Knox, 2007). This provides tentative support for *nrl* playing a role in photoreceptor development outside of mammals. However, while mouse *Nrl* is expressed in lens tissue (Liu et al., 1996), lipofected human *NRL* did not promote lens fibre cell differentiation as did Xenopus *Nrl* (McIlvain and Knox, 2007), suggesting divergent activities for *Nrl* across taxa. Underscoring this, the avian lineage has apparently lost *NRL* (is not recognizable in any available genome), and possibly relies on the *NRL*-related gene *MAFA* for rod specification (Ochi et al., 2004), which is expressed also in non-photoreceptor retinal cells (Enright et al., 2015a) as well as lens tissues (Ochi et al., 2004). In the Atlantic cod, larvae have cone-only retinas until metamorphosis, at which point they begin to produce rods, but recent transcriptomic analysis of metamorphic cod retina shows that cod *nrl* is not expressed during the onset of adult rod specification (Valen et al., 2016). Furthermore, many lamprey species have duplex retinas featuring a photoreceptor with physiological rod characteristics (Asteriti et al., 2015; Govardovskii and Lychakov, 1984; Morshedian and Fain, 2017, 2015;

Teranishi et al., 1982), but lamprey do not appear to have *NRL* (Kim et al., 2016b). Therefore a critical question for vertebrate photoreceptor specification is whether *nrl* is indeed a conserved requirement for rod development outside of mammals.

We and colleagues recently proposed a new hypothesis that ancient mammals began to convert a large proportion of cone-fated cells to the rod fate (Kim et al., 2016b), as part of the mammalian adaptation to a nocturnal life, call the Nocturnal Bottleneck (Heesy and Hall, 2010; Walls, 1942). We speculated that changes in *Nrl* expression or function may have been involved in re-directing cone cells to the rod fate; a burst of evolutionary change in Nrl peptide sequence, well conserved among mammals but less so outside the clade (Kim et al., 2016b), supports a change in Nrl function, as does the differing capacity for *Xenopus Nrl* versus human *NRL* to induce lens fibre differentiation in the frog (McIlvain and Knox, 2007). Thus Nrl may have altered its function across these taxa; however, it is daunting to consider testing the pro-rod capacity of ancient mammalian Nrl using extant mammals. The amniote avians, our closest related group, have entirely lost NRL; and the tetrapod *Xenopus* has very recently undergone genome hybridization between two species (~18 MYA) (Session et al., 2016). As such, the high retention of duplicate genes thwarts classical genetic functional analysis. Zebrafish are well-positioned to address this, being a tetrachromat model of retinal development and vision. Despite a teleost-specific genome duplication event occurring 350 MYA, only 26% of zebrafish genes persist as ohnologous pairs (Howe et al., 2013), and *nrl* is not one (Coolen et al., 2005; Kim et al., 2016b). Therefore, by examining the role of *nrl* in zebrafish photoreceptor development, we can begin to infer whether mammalian *Nrl* has diverged in function or expression from the ancestral condition.

We examined whether *nrl* is a conserved requirement for rod development outside of mammals, and directly tested the hypothesis that the functional role of *nrl* has changed between mouse and zebrafish. To do this, we examined the outcome of loss of *nrl* on zebrafish photoreceptors in both developing and adult eyes. To test if *nrl* has changed in its overall function across taxa, we exploited the observation that ectopic mouse *Nrl* can override an established cone-specified phenotype in favor of a rod phenotype, and drove the expression mouse and zebrafish *nrl* in fish cones; by

assessing whether non-mammalian *nrl* homologs share this capacity, we assessed whether phylogenetically diverse *nrl* homologs have pro-rod activity. We interpret the results in light of evolution of photoreceptor specification, and conclude that while *nrl* has an ancient role in rod development, it is not fundamentally required for the production of all rods in vertebrates.

4.2 Results

4.2.1 Larval zebrafish require *nrl* to make rod photoreceptors

Zebrafish Nrl is the sole zebrafish ortholog to mammalian NRL (Coolen et al., 2005; Kim et al., 2016b). Because we investigated the activities of multiple vertebrate *nrl* homologs in this study, we closely evaluated their sequence conservation at the level of the whole peptide, and especially within key domains (Fig. 4.S1A-C). Overall conservation of zebrafish Nrl peptide versus human NRL is low (32.1% identity; Fig. 4.S1B,C, and Fig. 4.S2), but the bZIP domain is well conserved, with 63% identity. Moreover, the amino acids which constitute the Maf_N (pfam081831) domain, easily detected in human and mouse Nrl, chicken MAFA, and lamprey MAFBA, are present in zebrafish, but spaced out with inserted amino acids such that the domain is interrupted three times (Fig. 4.S1C). Therefore, despite its low apparent conservation to mammalian NRL orthologs, and to other vertebrate long Maf peptides, it appeared zebrafish Nrl has the potential to share the function of its homologs and we proceeded with investigating whether the zebrafish *nrl* gene is necessary and sufficient for rod development.

Mammalian *Nrl* is required for the production of rods (Mears et al., 2001), and if its function is conserved in zebrafish, we predicted that disruption of *nrl* would preclude rod development. We used CRISPR/Cas9 targeted mutagenesis to generate two frameshift alleles in *nrl*, leading to early disruption of the peptide (Fig. 4.1A, Fig. 4.S3). The first 51 residues from these alleles are predicted to remain wildtype. In allele ua5009, the frameshift predicts production of 23 nonsense residues before an induced stop codon, and in allele ua5014, 19 nonsense residues were predicted before a stop codon (Fig. 4.S3). In both alleles, the peptide sequence diverged from normal Nrl sequence immediately upstream of the start of the minimal transactivation domain

(MTD) (Friedman et al., 2004), and 83 residues upstream of the Maf_N domain (Fig. 4.1A). These alleles lacked all major domains of mammalian Nrl, and thus are predicted to be nulls. All following work used the allele *nrl*^{ua5009}.

nrl^{ua5009} mutant zebrafish do not have rods at 4 days post fertilization (dpf) (Fig. 4.1B, C), contrasting with wild type larvae that have consistently produced a large abundance of rods by this time point. When examined using the rod-specific 4C12 antibody, or the rh1:eGFP transgene, which drives GFP expression under the rhodopsin promoter (Hamaoka et al., 2002), we found that *nrl* mutant zebrafish consistently contain zero rods within the entirety of the larval retina. A splice-blocking morpholino targeted to the end of the first coding exon of *nrl* and the following intron also reduced the abundance of rod photoreceptors (Fig. 4.S4) in injected wildtype animals. This independently demonstrates that the absence of rods in the *nrl* mutant is specific to loss of *nrl* function. The specificity of the nrl mutation is further supported by rescue of the phenotype with transgenes described in the next section. Characterizing mutant transcript by 5' rapid amplification of cDNA ends (5' RACE) analysis showed that mutant and wildtype larvae each produced a single prominent *nrl* transcript, and the mutant transcript contained the frameshift lesion (Fig. 4.S5). We attempted to stain for Nrl protein using a battery of previously-published antibodies (Kataoka et al., 2002; Kim et al., 2012; C. Wang et al., 2014), and commissioned a custom-designed antibody against zebrafish Nrl bZIP domain, but were unable to find Nrl-specific staining in adult or larval frozen sections or Western Blots (data not shown).

In mammals, lack of *Nrl* causes overproduction of an S-cone-like photoreceptor (Mears et al., 2001). To assess if one or multiple of the zebrafish cone subtypes are more abundant, we quantified the relative abundance of photoreceptors in 4 day old animals. We again found that rods were consistently absent in *nrl* mutants (n = 37), whereas in wildtype larvae, within a 100x100μm region of interest (ROI), there were consistently more than one hundred rods (n = 29) (Fig. 4.1D). Within the same ROI, we found that UV cones were significantly more abundant in mutants (mutants n = 8, wildtype n = 14, $p < 0.001$) (Fig. 4.1D). The increase in UV cone abundance in nrl mutants was approximately equivalent to normal abundance of rods in wildtype larvae, suggesting that cells otherwise fated to become rods exclusively become UV cones

without *nrl*. Consistent with this, we did not detect a significant difference in blue cone or red cone abundance in *nrl* mutants (Fig. 4.S6).

We next compared the abundance of rod-associated genes between the published mouse knockout and our nrl mutant zebrafish. In the mouse, *Nr2e3* and rhodopsin expression are abolished in *Nrl* mutants, and S opsin is upregulated (Mears et al., 2001), and *Nrl* is downstream of, but positively feeds back on, *Rorβ* expression (Fu et al., 2014). We found that *crx* and *rorb* transcripts were significantly less abundant, while *nr2e3* appeared less abundant, but this was not significant (Fig. 4.1E). Rhodopsin transcripts were undetectable in *nrl* mutants. Interestingly, *nrl* transcript abundance was increased in our *nrl* mutants. UV cone opsin (*sws1*; homolog of mouse S cone opsin) transcript abundance was not significantly different. Since *nrl* mutant larvae have more UV cones and less rods than wildtype (Fig. 4.1D), and because this is the opposite phenotype of *tbx2b* mutation (Alvarez-Delfin et al., 2009; Michèle G. DuVal et al., 2014), we quantified *tbx2b* transcripts and found they were unchanged between *nrl* mutant and wildtype larvae (Fig. 4.1E).

The phenotypes in *nrl* mutants appeared to be limited to photoreceptors, displaying no other overt ocular phenotypes (Fig. 4.S3C), with one exception. By 2dpf, mutant zebrafish could be routinely distinguished from heterozygous or wildtype siblings by the presence of an occlusion in the lens (shown at 3dpf, Fig. 4.S7B). Zebrafish *nrl* has previously been detected as highly expressed in the developing lens fibre cells (Coolen et al., 2005). Adult *nrl* mutant zebrafish had a small occlusion in the centre of the lens, presumably leftover from the larval stage (Fig. 4.S7C, D).

4.2.2 Zebrafish *nrl* is sufficient to convert UV cones to a rod-like fate

NRL is necessary (Mears et al., 2001) and sufficient (Oh et al., 2007) to drive photoreceptors to the rod fate in mice. Recently, our collaborative efforts led to the hypothesis that ancient mammalian NRL became more potently pro-rod, capable of over-riding a previous commitment to the cone phenotype by cone precursor cells (Kim et al., 2016b) and therefore enabling mammals to direct cone precursors to the rod fate. We therefore assessed if zebrafish *nrl* (a non-mammalian *nrl*) is capable of inducing a rod-like fate in cells already specified and maturing to become cones.

To test if zebrafish *nrl* is sufficient to induce rod photoreceptor fate, we transgenically expressed it in zebrafish UV cones. We engineered transgenic zebrafish using regulatory sequences upstream of the *sws1* gene, previously characterized as expressed exclusively in UV cones (Michèle G. DuVal et al., 2014; Fraser et al., 2013; Kim et al., 2016b), to drive expression of the coding DNA sequence of zebrafish *nrl*. At 4 dpf, zebrafish with UV cones that expressed *nrl* showed 4C12 immunostaining (normally specific to rods) that colocalized with UV cones, as stained by anti-UV cone opsin (Fig. 4.2A, B). Thus zebrafish *nrl* is sufficient to produce rod photoreceptors.

To evaluate the morphology of UV cones expressing *nrl*, we compared fluorescent cells in the dorsal regions of radial sections of 7dpf larval retinas nrl mutants and sibling heterozygotes (Fig. 4.2C-E). UV cones and rods were easily differentiated in sibling larvae based on their morphology (Fig. 4.2C versus D). UV cones expressing ectopic *nrl* express rh1:GFP and adopt a rod-like morphology, although their synapses apparently maintained a cone-like pedicle morphology (Fig. 4.2C and E, arrows). In adult transgenic zebrafish expressing *nrl* in UV cones, UV cones were only detected near the CMZ (Fig. 4.3A, B). This could be due to the death of the UV cone, or to its conversion to rod and the cessation of UV opsin production.

To follow the fate of UV cones that express *nrl* into adulthood, we used genetically encoded lineage tracing. We cloned Cre recombinase downstream of *gnat2* regulatory sequences, which promote reporter expression in all subtypes of post-mitotic cones (Kennedy et al., 2007), and used two lox-mediated reporter lines, Zebrabow (Pan et al., 2013) (Fig. 4.3C) and ubi:Switch (Mosimann et al., 2011; Solek et al., 2017) (Fig. 4.S8), to test if sws1:nrl induced UV cones to become rods. In wildtype fish, cells expressing gnat2:cre-mediated fluorescent reporter, including UV cones, did not become rods (1/2 Zebrabow, 7/7 ubi:Switch) (Fig. 4.3D). In contrast, the same lineage tracing on fish expressing sws1:nrl abundantly showed lineage reporter expression in rods (8/8 Zebrabow) (Fig. 4.3E, arrowheads), consistent with conclusion that these had been sws1:nrl cones that were converted to rod fate by *nrl* expression. In 1 of 2 wildtype lineage tracing fish with Zebrabow reporter, we found a total of 27 lineage trace reporter-positive rods, in 5 clumps, between the CMZ and optic nerve head (Fig. 4.S9A shows the largest clump, of 9 rods). In contrast, lineage reporter-positive rods were

abundant and evenly spaced along the stretch in one representative lineage tracing fish with sws1:nrl (see Fig. 4.S9B, C for representative images). Moreover, there was expression of lineage reporter in other cell layers, including bipolar cells (Fig. 4.S9B) and ganglion cells (not shown). We suggest the clumps of lineage-traced rods in the single wildtype fish, and the rare labeling of other cell types, equally derive from spurious expression of the transgenic construct. Incidentally, we found no rods with gnat2:cre lineage tracing in 5 day old wildtype larvae (6/6 retinas examined) (Fig. 4.S10), consistent with our previous finding using a GAL4/UAS-derived lineage tracing technology (Kim et al., 2016b).

In summary, zebrafish *nrl* was sufficient to respecify maturing cone photoreceptors into a rod-like fate that is ultimately difficult to discern from natural rods.

4.2.3 Adult zebrafish produce rods without *nrl*

The adult zebrafish retina contains rod and cone photoreceptors with mature morphology and in their final relative proportions. Moreover, the cone photoreceptors are arranged into a repeating crystalline mosaic in adults, but not in larvae (Allison et al., 2010). We examined the photoreceptor composition of adult nrl mutant fish, to assess the impact of the mutation upon these features. Surprisingly, zebrafish adults with homozygous *nrl* mutation produce abundant rod photoreceptors which looked similar to wildtype rods (Fig. 4.4A, B), in sharp contrast to our observations on larval *nrl* mutant fish (Fig. 4.1). In the mouse, $Nrl^{-/-}$ retinas do not produce rods (Daniele et al., 2005; Mears et al., 2001; Nikonov et al., 2005), but we did not see an overt cone-like phenotype of adult zebrafish *nrl* mutant rods.

We first examined whether there was an enduring molecular phenotype of *nrl* mutation in adult retinas. The larval mutants had showed clear disruptions in the photoreceptor specification pathway (Fig. 4.1E). In adult mutants, the *nrl* transcript was significantly more abundant as in the larvae, while *nr2e3* transcript abundance was decreased (Fig. 4.4C). In the mouse, *Nr2e3* expression is completely dependent on activation by Nrl (Oh et al., 2008); this suggests that zebrafish Nrl is a conserved requirement for *nr2e3* expression. The adult expression of *crx*, *rorb*, and *rhodopsin* were unchanged from wildtype, unlike in larvae. In situ hybridization showed the expression

domain of *nrl* was unchanged from wildtype in frozen sections (Fig. 4.4D, E), and confirmed that mutant rods expressed rhodopsin (Fig. 4.4F, G). We considered the possibility that the adult zebrafish could produce an alternative transcript of *nrl* that bypassed the lesion. This would not be consistent with the alterations in transcript abundance observed for *nr2e3* (Fig. 4.1C). Further, 5' RACE analysis showed only a single dominant *nrl* transcript in adult wildtype and mutant retinas, and sequencing it showed that the mutant transcript still contained the frameshift lesion (Fig. 4.S5). Thus, *nrl* mutant zebrafish had rhodopsin-expressing photoreceptors despite transcript abundance perturbations in *nrl* and *nr2e3*, which are considered critical regulators of the rod phenotype in mouse.

We next examined histological sections, to assess if there was an overt phenotype in the structure or composition of the retina, as *Nrl* mutant mice have decreased photoreceptor abundance, and bigger photoreceptor nuclei (Daniele et al., 2005). We found that adult *nrl* mutant zebrafish retinas did not have any delamination defects, and looked overtly wildtype (Fig. 4.S11). We then examined whether the central retina abundances of the major classes of retinal cell types were perturbed in the adult nrl mutants. We were able to count cones and rods, as the nuclei of blue, red, and green cones are spatially segregated from UV cone and rod nuclei, and UV cone nuclei are morphologically distinct from rod nuclei. We also quantified the abundance of horizontal cells, inner nuclear layer cells (besides horizontal cell), and ganglion cells; We found no difference in the abundance of any of these major cell types between *nrl* mutant and wildtype zebrafish retinas (Fig. 4.S12A). We considered that, in zebrafish, retinas continue to grow throughout adulthood, and new retinal neurons are constantly added at the CMZ (Allison et al., 2010). However, it is not clear if rods are derived from the stem cells of the ciliary marginal zone (Stenkamp, 2011), and it was possible that quantifying the abundances of the newest-born cells may reveal differences between adult wildtype and nrl mutant zebrafish. We repeated our examination in a region of retina abutting the ciliary marginal zone, but found no differences in any cell type (Fig. 4.S12B). Finally, we assessed if the adult *nrl* mutant rod nuclei were bigger than wildtype rod nuclei, as in the mouse (Daniele et al., 2005). We measured the area of rod nuclei in each genotype, and found that there was no statistical differences overall (Fig.

4.S13A). However, the areas measured for the mutant rod population were bimodal, with a larger subpopulation (Fig. 4.S13B).

While the rod opsin-expressing cells of the *nrl* mutant zebrafish appeared rod-like in our histological preparation (Fig. 4.4B), we next examined whether there were ultrastructural similarities to cones, because the mouse *Nrl* knockout produced cells with cone-like phenotypes at the ultrastructural level. A key difference between rod and cone outer segments is that cones use extensive plasmalemma invaginations to produce high membrane surface area within the outer segment; rods instead have free-floating discs of membrane which are consistently separate from and enclosed by the cell membrane (Tarboush et al., 2012). The rod outer segments in both wildtype and *nrl* mutant were highly tortuous, and we could not reliably use length of segment as the basis for quantification. However, wildtype and mutant rod outer segments appeared similarly long and slender (Fig. 4.S14), and we did not find invaginations of the plasma membrane, nor membrane discs that were continuous with it, in the mutant rod-like outer segments (Fig. 4.S15). This suggests that rod-like photoreceptors of the adult *nrl* mutant zebrafish have wildtype-like rod outer segments. We next looked at the nuclei of these cells; in wildtype mouse and zebrafish, rod nuclei have an electron-dense, heterochromatin-rich chromatin arrangement, while cone nuclei are electrolucent and show clumping of mixed eu- and heterochromatin (Hughes et al., 2017; Tarboush et al., 2012). Moreover, the mouse *Nrl* knockout photoreceptors lose this distinction, and all photoreceptor nuclei have cone-like chromatin arrangement (Daniele et al., 2005). We found that rods in adult *nrl* mutant zebrafish had cone-like clumping of chromatin but remained electron dense (Fig. 4.S16A, B), while mutant cones remained indistinguishable from wildtype cones (Fig. 4.S16C, D).

We then examined the ultrastructure of synapses of wildtype and mutant adult zebrafish photoreceptors. Wildtype cone and rod synapses were easily distinguished. Cone synapses were relatively larger and electrolucent, with numerous synaptic ribbons per synapse (Fig. 4.S17A). Wildtype rod synapses were smaller, more electron-dense, contained a single synaptic ribbon per synapse, and were positioned slightly sclerad to the cone synapses in the synaptic layer (Fig. 4.S17C). Adult *nrl* mutant cone-like synapses (Fig. S17B) were abundant, but we found only a single wildtype-like rod

synapse (Fig. 4.S17D). In one of two mutants but in neither wildtype animal, we found several “white” synapses interdigitated between cone-like synapses (Fig. 4.S17E). These “white” synapses were extremely electrolucent, and had multiple synaptic ribbons per synapse; in that animal, approximately half of the obviously non-rod-like synapses were “white” synapses (4/9 assessed); we speculated that these cone-like “white” synapses might represent the rod synapses that were absent from the *nrl* mutants (despite the presence of rod cell bodies described above). We compared the density of synaptic vesicles among these synapses (Fig. 4.S18): wildtype cones had significantly higher vesicle density than wildtype rods, while mutant cone-like synapses had an intermediate density, significantly different from both wildtype cones and wildtype rods. The sole wildtype-like mutant rod synapse, and the “white” synapses had dramatically lower densities than the wildtype rod synapses. We also compared the lengths of synaptic ribbons in the various synapses (Fig. 4.S19), as previous work has shown that wildtype rod synaptic ribbons are approximately twice as long as cone ribbons in wildtype zebrafish (Tarboush et al., 2012). We confirmed this in wildtype synapses, and we also found that the cone-like and “white” synapses had ribbons of statistically non-different length to wildtype cone ribbons (Fig. 4.S19). The sole wildtype-like rod synapse ribbon was of similar length to wildtype rod ribbons. Cumulatively, this data suggests that the rod-like photoreceptors of adult *nrl* mutant zebrafish have rod-like outer segments, but cone-like nuclei and synapses.

The histological characterizations in Fig. 4.S12 suggested the total cone population was unchanged in *nrl* mutants, but we considered whether the cone subtype abundances had shifted. The well-characterized (Allison et al., 2010) cone mosaic pentamer had previously been shown to become disarrayed with loss of a cone subtype during ontogeny (Raymond et al., 2014), so we first assessed whether the cone pentamer was intact in adult *nrl* mutant zebrafish. We found intact repeating groups of five nuclei in the cone nuclear layer (Fig. 4.4H, I), which matched the wildtype fish. In wildtype animals, this pentamer consists of green, red, blue, red, green (GRBRG) cones. The outer pairs of cones, the red and green cones, are physically paired as double cones in zebrafish, and express cone *arrestin 3a* (*arr3a*), which blue and UV cones do not (Ile et al., 2010; Larison and Bremiller, 1990). We found that the outer

pairs of cones in the *nrl* mutant pentamers stained positive for Arr3a (Fig. 4.S20), suggesting they are double cones. The central cone of the pentamer did not stain positive for Arr3a, suggesting it is a blue cone. The mutant fish also had overtly normal distributions of cones which stained positive for red opsin (Fig. 4.S21), indicating red cones are present. Moreover, there are similar numbers of red cones in mutant and wildtype adults (Fig. 4.S21). Importantly, there were not twice as many red cones in mutants as in wildtype; because Arr3a stains green and red cones, and did not stain differently in the mutant and wildtype fish, and because there were similar numbers of red cones in both genotypes, we deduce these Arr3a+, red opsin- cones to be green cones. Typical UV cone opsin staining is evident in *nrl* mutant adults (Fig. 4.4A, B), indicating that the mutants have UV cones. Thus, there four distinct classes of cone photoreceptor present in the *nrl* mutant retina (UV cones, red cones, non-red cone member of double cones, and non-Arr3a+ pentameric cones), and we therefore conclude that adult *nrl* mutant zebrafish rods were not produced at the expense of one or more cone subtypes.

We next considered when during ontogeny rods first begin to populate the maturing *nrl*$^{-/-}$ retina. To observe rod development *in vivo*, we bred an rh1:eGFP rod reporter into the *nrl*^{ua5009} line. Screening for the rh1:eGFP transgene in larvae based on rod expression was not feasible in *nrl* mutants, since they do not have rods. However, we noted that the rh1:eGFP transgene drives a brief pulse of eGFP expression in the developing pineal gland at 1-2 dpf, sufficient to identify transgene carriers (Fig. 4.S22). By 11 dpf, most rh1:gfp *nrl* mutant larvae monitored had developed several GFP-expressing cells in their retinas (Fig. 4.4K). The abundance and location of these rods was apparently random, because the locations of these GFP+ rods differed between larvae, and differed between the two eyes within individuals (see Fig. 4.4K, Fish 2 and 3). Thus, *nrl*$^{-/-}$ rods begin to populate the zebrafish retina around 11 dpf, increasing over time until adult rod abundance was apparently normal (Fig. 4.S12).

Finally, in light of the difference in requirement for *nrl* in larvae versus adults, and the putative role of *maf* genes in photoreceptor development in other vertebrates (see Introduction), we next considered if another *maf* gene might be redundant with *nrl* in older animals, thereby rescuing rod production. We therefore evaluated a panel of *maf*

homologs i) with some documented expression in or near the eye in zebrafish larvae (Fig. 4.S23), ii) for changed expression between nrl mutants and wildtype over the second week of development, and iii) with a spike in expression during the time (~11 dpf) when the first *nrl*$^{-/-}$ mutant rods emerge. *mafba* and *mafbb,* paralogs of mammalian *Mafb,* were the only two Maf family members that exhibited significant transcript abundance differences (Fig. 4.S24) between genotypes. The abundance of *mafba* transcript was transiently increased at 7 and 9 dpf in mutants, but not at later ages, and possibly due more to narrow error values than to meaningful changes in abundance. *mafbb* was approximately 3-fold more abundant at 8dpf and 2-fold more abundant at 9dpf (Mann-Whitney U test, $p < 0.01$, both time points). However, *mafbb* transcript abundance was not significantly changed from wildtype in adults (Fig. 4.S25). None of this expression analysis compelled us to prioritize these *maf* orthologs for extensive further analysis.

In summary, adult zebrafish *nrl* mutants had wildtype numbers of rod-like photoreceptors, which emerged in late larval development. The production of these rod-like cells did not appear to be at the expense of other cell types in the retina, including the cone subtypes which appeared to be normally distributed. The presence of rods in adult mutants was unexpected, as it is in sharp contrast to what is observed when *nrl* is absent in larval fish or adult mice.

4.2.4 An *nrl*-mediated rod specification program is conserved across vertebrates

We reasoned that if zebrafish Nrl could stimulate the rod program in UV cones, we could use this paradigm to assess the pro-rod inductive capacity of diverse Nrl homologs. In the mouse, Nrl directly binds to the promoters of dozens of rod-specific genes, including rod-specific phototransduction genes (Hao et al., 2012). This indicates that Nrl is not just a rod-specifying factor, but actually a primary effector (“master regulator”) of the rod cell phenotype. We reasoned that if cones could be induced to assume a rod phenotype by expression of *nrl* homologs, this would be highly suggestive of a conservation between the rod specification program of zebrafish and the candidate homolog donor species. As zebrafish *nrl* is necessary (Fig. 4.1) and sufficient (Fig. 4.2,

3) to induce expression of rh1:eGFP and 4C12 antigen, we used these criteria to evaluate the functional conservation of various *nrl* homologs.

We cloned *nrl* homologs from an array of organisms selected on the basis of their informative positions relative to vertebrate phylogeny. Mouse *Nrl* was cloned because it has been previously shown that mammalian Nrl peptide sequence has diverged from that of other vertebrate lineages during the nocturnal bottleneck, and we recently proposed that this might have led to a more potent role in mammalian rod development (Kim et al., 2016b). We predicted mouse *Nrl* would robustly promote the rod phenotype in zebrafish cones. Chicken *MAFA* was selected because it has previously been suggested to fulfill the role of *NRL* in birds (Ochi et al., 2004) before, but this has not been tested. Recently, electroporated *MAFA* was shown to be correlated with rhodopsin expression in *Nrl* knockout mice (Kim et al., 2016b). We therefore predicted that chicken *MAFA* expression would stably induce at least rod opsin expression in UV cones. We selected sea lamprey *MAFBA* on the basis of a phylogenetic tree constructed in a recent analysis of Nrl evolution (Kim et al., 2016b). Lamprey make rod-like photoreceptors (Asteriti et al., 2015; Morshedian and Fain, 2015), but only a single Maf family member has been detected in *Petromyzon marinus* the genome to date (Kim et al., 2016b), and there is no information as to whether it is involved in development of their rods or where it is expressed. Moreover, the evolutionary cell homology of rods in lamprey and jawed vertebrate is not yet clearly resolved, and recent molecular comparisons suggest lamprey may have convergently evolved rod physiology (Lamb et al., 2016; Muradov et al., 2008, 2007). Finally, we selected the sole long Maf gene of *Drosophila melanogaster*, *trafficjam* for our comparison. It was previously shown that *trafficjam* is a key factor in specifying the fruit fly pR8 photoreceptor (Jukam et al., 2013), and that a primary cofactor of Trafficjam is Orthodenticle, which is the homolog of vertebrate Otx2/5/Crx. Crx is a primary binding partner of Nrl in mammals (White et al., 2016). We predicted that expression of *trafficjam* would be sufficient to induce expression of at least rhodopsin, as it directly regulates opsin expression in the fly (Jukam et al., 2013) and is an *nrl* homolog.

We established transgenic animals which expressed tagged lamprey *MAFBA*, chicken *MAFA*, mouse *Nrl*, or *Drosophila trafficjam* under UV cone opsin regulatory

sequences, and assessed the capacity of these constructs to promote the rod phenotype in UV cones by 6 days post fertilization. We found that all three vertebrate-derived *Nrl* homologs were capable of inducing zebrafish UV cones to express a rod-specific antigen (4C12; Fig. 4.5, C-E), similar to the capacity of zebrafish *nrl*, demonstrating that the various peptides are capable of activating the rod specification program in zebrafish. Interestingly, mouse *NRL* and lamprey *MAFBA,* but not chicken *MAFA*, induced expression of the *rh1:eGFP* transgene in UV cones at the age examined (Fig. 4.S26), suggesting a weaker ability to override the zebrafish UV cone fate in favour of the rod fate. Finally, we found that Drosophila *trafficjam* did not induce expression of the 4C12 antigen in UV cones (Fig. 4.5F), nor cause the cones to express rh1:eGFP transgene (Fig. 4.S26). The *trafficjam* construct was expressed abundantly in UV cones, as the entire cell bodies of UV cones were immunopositive for the N-terminal FLAG tag we cloned onto the *trafficjam* N-terminus (Fig. 4.S27).

In summary, the expression of zebrafish rod-specific marker 4C12 could be launched in UV cones by *nrl* homologs from mouse, chicken, and lamprey. Mouse and lamprey *nrl* homologs could induce expression of an eGFP reporter driven by rod opsin regulatory sequences. *Drosophila trafficjam*, the fly *nrl* homolog, induced expression of neither reporter in UV cones. This suggests a deep conservation of rod-inductive capacity of Maf family members across vertebrates (Fig. 4.5G).

4.3 Discussion

In this study, we demonstrated that zebrafish require *nrl* to make rods during larval retinogenesis. Without it, zebrafish overproduce UV cones in an apparent 1-to-1 fashion with absent rods, suggesting that the previously rod-fated cells do not die, but become UV cones, and not other cone types. Despite the absence of *nrl*, zebrafish begin to generate rod-like photoreceptors in late larval development, during the phases of continued retinal growth generating adult tissue, and by adulthood have overtly normal rod/cone ratios. This is a very surprising result, because mice lacking *Nrl* are infamous for lacking rods, a fact that has been exploited for many labs to investigate cone physiology and proposed as a clinical gene therapy to cure blindness (Yu et al., 2017). The rods present in adult *nrl* mutants have gene expression and ultrastructural

differences from normal rods, including cone-like nuclei and synapses, indicating that *nrl* is involved in, but not solely responsible for, rod specification in adult zebrafish. We also evaluated the capacity for a non-mammalian *nrl* to over-ride the cone specification program in maturing cones, and found that the erstwhile UV cones eventually adopted an unambiguous rod-like phenotype, indicating a conserved capacity for zebrafish *nrl* to induce rod characteristics. Indeed this capacity to induce a rod phenotype was indistinguishable in transgenic fish expressing mouse or zebrafish homologs of *Nrl*. Finally, we evaluated the capacity of other *nrl* homologs to induce the rod program in cone photoreceptors. In line with previous work, mouse *Nrl* induced a rod phenotype in UV cones, and chicken *MAFA* induced at least one rod-like characteristic as well. Lamprey *MAFBA* also induced rod phenotype in UV cones, indicating that even 550 MYA, ancient vertebrates had a retinal Maf protein capable of activating elements of a modern gnathostome rod program. This suggests that *Maf*-based photoreceptor specification, as deployed in vertebrates, is at least as ancient as the role of vertebrate rods.

4.3.1 Molecular phenotypes of mouse vs. zebrafish *nrl* knockouts

There are numerous comparisons to be made between the qPCR results from the *nrl* mutant zebrafish (Fig. 4.1E larvae, Fig. 4.4C adult) and the *nrl* mutant mouse.

First, *nrl* transcript abundance was increased in the larval and adult *nrl* knockout zebrafish. Mouse Nrl is part of a positive feed-back loop with Rorβ (Fu et al., 2014). It appears that zebrafish *nrl* may participate in negative feedback regulation, although the mechanisms are not clear. In *Drosophila*, *trafficjam* plays a role in gonadogenesis, as well as in directing retinal photoreceptor phenotypes, where it partners with fly Crx ortholog Orthodenticle to silence one opsin and to facilitate the expression of another (Jukam et al., 2013). In the fly, this interaction forms a feedforward loop, not a feedback loop. In its role in gonadogenesis, *Drosophila trafficjam* plays two roles in silencing retrotransposons: the 3’ untranslated region of its transcript is the site of transcription for numerous piRNAs, which together with Piwi and Argonaute proteins silence retrotransposons in the germline (Saito et al., 2009). Trafficjam also directly induces expression of *piwi* in germline cells (Saito et al., 2009). In flies with *piwi* mutant follicle

clones, the protein abundance of Trafficjam is increased, suggesting that the *trafficjam* transcript may be a target of piRNA repression (Robine et al., 2009). It is therefore feasible that vertebrate Nrl may be the subject of small RNA-mediated repression. Recent work has suggested that Nrl translation may be reduced by microRNAs that are possibly induced by Nrl (Sreekanth et al., 2017). If so, then the loss of functional Nrl would reduce production of these microRNAs, which would relax regulation of *Nrl* transcript abundance, consistent with what we see in the zebrafish. This would not have been detected in the mouse, as the *Nrl* knockout widely used is a full-gene deletion (Mears et al., 2001), which deleted dozens of Crx binding sites in three clusters of binding sites positioned upstream of the first two exons, and within the third intron (Montana et al., 2011), as well as much or all of the 3' untranslated region. Some of these binding sites may be sites of repression by unidentified factors active in rods. In the zebrafish *nrl* mutant we report here, the lesion is a frameshift in the first coding exon, and nearby noncoding sequences are wildtype. Thus, loss of functional Nrl protein would still allow unidentified factors to bind the *nrl* gene and induce expression, while Nrl-facilitated negative regulators would be unable to attenuate the abundance of *nrl* transcripts. It is possible that even mouse Nrl negatively regulates its own transcription; in a paired ChIP-seq experiment documenting Nrl and Crx binding sites within the mouse genome, the majority of Nrl-bound reads originated within the introns of the *Nrl* gene, as with Crx (Hao et al., 2012).

The abundance of *nr2e3* transcript was significantly lower in the adult retina of *nrl* mutant zebrafish, and non-significantly but potentially lower in the larval retina. In the mouse, expression of *Nr2e3* is absolutely dependent on Nrl-mediated stimulation (Oh et al., 2008). As zebrafish *nrl* mutants had lower *nr2e3* transcript abundance in adult, we infer a conserved requirement of Nrl for zebrafish *nr2e3* expression. This may also be true for larvae. It has previously been suggested that *nr2e3* is expressed in cone precursor cells transiently during early larval retinogenesis (Chen et al., 2005; Nelson et al., 2008), but the evidence for this was indirect. We provide another line of indirect evidence for this, as some unidentified factor was able to promote expression of *nr2e3* in larvae without *nrl*. Interestingly, pineal expression of the rh1:eGFP transgene was observable in *nrl* mutants (Fig. 4.S22), although larval rods were not present later in

slightly older larvae (Fig. 4.1B). In the development of the pineal and parapineal organs, parapineal-destined cells migrate out of the presumptive pineal gland, and *nr2e3* antagonizes this migration (Khuansuwan et al., 2016). If Nrl is required for *nr2e3* expression in all instances, then *nrl* mutants should have parapineal development phenotypes. If they do not, it would suggest that *nr2e3* expression is induced by alternative factors, which may be the same as in the retinas of *nrl* mutant larvae. Finally, because zebrafish larvae are so small, we performed *nr2e3* qPCR on total RNA isolated from 10 whole larvae per replicate. Extraretinal sources of *nr2e3* may therefore overwhelm/disguise a local retinal decrease in *nr2e3* transcript abundance. In the adults, we extracted total RNA from isolated neural retina, without RPE, lens, or scleral tissue, and thus, there was little opportunity for extraretinal *nr2e3* to bias our adult qPCR analysis.

Abundance of *sws1* transcript was not perturbed in either larvae or adult mutant retinas. In the mouse, the homologous S cone opsin is dramatically upregulated in Nrl mutants, and in Nr2e3 mutants (Chen et al., 2005; Mears et al., 2001; Nikonov et al., 2005; Oh et al., 2008). This divergence in phenotype between mouse and zebrafish may be due to the relative photoreceptor abundances. In the mouse, 97% of photoreceptors are rods (Young, 1984), and the conversion of these to S opsin-expressing cells represents a 33-fold increase. In the 4 day old larval zebrafish, there are approximately 1000 rods in the whole retina of one eye, and approximately 4000 UV cones (unpublished observations). Thus, conversion of every rod to UV cone-like phenotype, as the relative abundances of these photoreceptors indicate (Fig. 4.1D, 4.S6), represents a 25% increase in UV cones, which might not be sufficient to elicit a significant increase in *sws1* opsin transcript with n = 6 replicates. Alternatively, in the mouse Nrl does not directly repress S opsin expression; rather, it recruits Nr2e3 to silence transcription of cone genes (Chen et al., 2005; Cheng et al., 2006; Corbo and Cepko, 2005; Haider et al., 2009; Oh et al., 2008; Onishi et al., 2009). It could be that *nrl*-independent *nr2e3* expression in the larvae attenuated the excess production of *sws1* transcripts, although there was no obvious variation in staining intensity of the UV cones counted for Fig. 4.1D and 4.S6 (intensity data not shown).

Rod opsin transcripts were undetectable in the larval nrl mutants at 4 dpf, yet were abundant in the adult retinas. Ectopic *nrl* supplied by the sws1:nrl transgene was able to rescue this loss (Fig. 4.2E), indicating that the loss of *rh1* transcription was specific to loss of *nrl*. Moreover, rh1:eGFP transgene was expressed in the pineal in 2dpf *nrl* mutants (Fig. 4.S22). The source of *nrl*-independent transcription from the rod opsin gene in adults and transgene in larval pineal glands is of great interest, as there is no known paralog of *nrl* in zebrafish. If there is not a paralog of *nrl* to mediate this expression, then it suggests that another factor can promote rod opsin expression. It appears that larval opsin expression in rods is at least entirely dependent on *nrl*, which is conserved with mammalian rods.

Abundance of *rorβ* transcript was down in *nrl* mutant larvae, but not in adult *nrl* mutants. In the mouse, Rorβ is upstream of, and directly stimulates *Nrl* expression (Fu et al., 2014; Kautzmann et al., 2011), but Nrl feeds back on *Rorβ* and stimulates expression of the *Rorβ2* isoform, constituting a positive feedback loop. We infer that this feedback loop is conserved in larval rods, but not in adult rods.

Abundance of *tbx2b* transcript was not affected by mutation of *nrl* in larvae or adults. In the zebrafish, *tbx2b* mutation causes reduced UV cones and over-abundant rods, and the wildtype protein has been interpreted to mediate a developmental decision promoting UV cones at the expense of rods (Alvarez-Delfin et al., 2009; Sotolongo-Lopez et al., 2016). In the chicken, *TBX2* expression is enriched in UV cones, suggesting a conserved role for promoting UV cone phenotype. The mechanism of action for *tbx2b* in mediating UV versus rod abundances has not been identified; however, work in pineal versus parapineal precursor specification suggests *tbx2b* promotes the parapineal fate, while *nr2e3* antagonizes the parapineal fate. Both transcription factors are well-characterized as inhibitors of expression (Khuansuwan et al., 2016). If *tbx2b* is active in nrl-expressing rod-directed precursors, and normally acts to redirect cells to a cone fate, then its expression should be decreased in *nrl* mutants. We did not find this, and therefore *tbx2b* is not genetically downstream of *nrl* in rod-fated cells. This suggests that *tbx2b* is active earlier in a shared pathway with *nrl*, or in a different pathway all together. The *TBX2* UV cone-enriched expression in chicken (Enright et al., 2015a) favours the latter option.

Finally, *crx* transcript abundance was significantly reduced in the larval mutants, but not in the adult mutants. This suggests that Nrl may regulate *crx* expression. Crx has been well-documented to act upstream of, and to directly stimulate mouse *Nrl* (Hao et al., 2012; Kautzmann et al., 2011; Montana et al., 2011). Nrl participates in a positive feedback loop with Rorβ, its own inducer, so it is possible that Nrl feeds back onto *crx* in a positive feedback loop as well. To our knowledge, this has not been demonstrated in the mouse, and a recent ChIP-seq publication in mouse did not describe Nrl occupancy sites in *Crx* regulatory regions (Hao et al., 2012).

In the end, the molecular phenotypes of *nrl* mutation in larval zebrafish rods demonstrate conservation of the rod specification pathway in vertebrates, and generates new hypotheses about the regulation of key specification genes; critically, this includes the possibility that Nrl may regulate *crx* in a positive feedback loop, and that Nrl may regulate its own transcript abundance. We note that the greatest discrepancy between zebrafish and mouse rod transcript dynamics was in the adult zebrafish rods, which do not appear to require *nrl* for a rod-like phenotype. This suggests that molecular work intended to apply to mammalian rods should be focused on larval, not adult rods in the zebrafish.

4.3.2 Zebrafish rods do not express cone genes during development

We previously demonstrated that, in contrast to mice, larval zebrafish rods do not have a history of *sws1* expression (Kim et al., 2016b), using a Gal4/UAS-derived technology. Zebrafish silence the UAS promoter as they age and over generations (White and Mumm, 2013), precluding the use of that arrangement of genetically encoded lineage tracing constructs for this study. We found that another cone gene, *gnat2*, also did not report expression in any rod in zebrafish larvae (Fig. 4.S10), using a Cre/Lox lineage tracing system (Fig. 4.4C, C'), consistent with the previous study (Kim et al., 2016b), which concluded that larval zebrafish rods do not exhibit a history of expressing cone genes. In the previous study, we used UV and blue cone opsin regulatory sequences to test for one-time cone expression; in this study, we use a gene expressed in all cones. If rods could routinely derive from cones, feasibly they might derive from green opsin-expressing cones, as rod and green opsins are derived from an

ancestral opsin (Lamb, 2013). Our gnat2:cre lineage tracing extends our previous findings, and suggests no cone genes are expressed during the normal development of zebrafish rods.

While the *gnat2:cre* lineage tracer robustly reported rods in conjunction with ectopic *nrl* expression in UV cones (Fig. 4.4E), we noted 5 clusters of lineage-traced rods, along the length of a retinal section from CMZ to optic nerve head, in one animal without transgene-induced ectopic *nrl* expression (Fig. 4.S9A, arrowheads). In animals of both genotypes, we noted occasional labeling of other cell types (e.g., Fig 4.S9B, a bipolar cell). Transgenic reporters do not always perfectly recapitulate endogenous gene expression (Hans et al., 2009), and while re-creation of a construct using CRISPR-mediated reporter-integration into endogenous loci (Kesavan et al., 2018) or BAC recombineering are options for reducing off-target expression (Fuentes et al., 2016), we consider it likely that the 5 clusters of lineage traced rods represent 5 clonal populations of rods with one-time spurious expression of *gnat2:cre* during their development. Indeed, adult zebrafish continually generate clones of rods throughout the retina, from dedicated precursor stem cells derived from Müller glia (Bernardos et al., 2007). If 5 isolated Müller glia spuriously expressed the gnat2:cre transgene, all rod-fated daughter cells would integrate clonally into the photoreceptor layer and remain as clusters of reporter-positive rods.

Other potential explanations for the five clusters of lineage reporter-positive rods in the single wildtype animal include the possibility that very few rods in zebrafish in fact do emerge from cone-fated cells, in conflict with our previous report (Kim et al., 2016b). Alternatively, some rods may express *gnat2* at low levels. Finally, material transfer between photoreceptors has been recently reported in mammalian retinas (Ortin-Martinez et al., 2017; Pearson et al., 2016; Santos-Ferreira et al., 2016; Singh et al., 2016), and while such a lapse in non-cell-autonomous cellular discipline has not been observed in fish at this time, it is possible the five clusters of lineage-traced rods represent isolated instances of this phenomenon.

4.3.3 Capacity of Nrl to direct a rod-like fate and over-ride a cone program

We and colleagues previously suggested that Nrl could have played a role in the origins of the mammalian rod-dominated retina, presumably by acting in nascent developing cone progenitors to convert them to rods (Kim et al., 2016b). Nrl protein sequences are tightly conserved among the mammals, but vary considerably outside the clade; together with differing functional outcomes between human *NRL* and Xenopus *Nrl* mRNAs in lipofected frog retina (McIlvain and Knox, 2007), this suggested that if Nrl had a role in the conversion of nascent cones to rods, changes in peptide activity were perhaps involved (i.e. Nrl then would have gained new functions). In the present study, we demonstrated that zebrafish Nrl, with only 32% identity to human Nrl (Fig. 4.S2), had the capacity to override the established cone phenotype of UV cones and to induce a rod-like phenotype that was ultimately difficult to distinguish from natural rods. Previous work using an ectopic *Nrl* expression paradigm in mice used *Crx* promoter sequence, active in the precursors of all photoreceptors, to induce the rod fate before obvious cone specification had taken place (Oh et al., 2007), and S opsin regulatory sequences driving expression of mouse Nrl produced mixed phenotype cells with coexpression of S and rod opsins, although a reduction in overall S opsin-expressing cells coupled with lineage tracing suggests some cells may have slipped into a stronger rod-like phenotype (Oh et al., 2007). To interpret this data with optimism, it suggests that mammalian Nrl can transform other photoreceptors into rods. In Xenopus, *Nrl* transcript was lipofected into developing retinas, and transformed clones were analyzed later, after photoreceptor development took place (McIlvain and Knox, 2007). We used *sws1* promoter sequences, expressed solely by maturing UV cones (Michèle G. DuVal et al., 2014; Kim et al., 2016b; Takechi, 2005), to drive zebrafish *nrl* expression after specification. The difference in timing is known to affect the ability of a transcription factor to modulate phenotype; *trb2* modulation by transgenic expression under *crx* (early acting) or under *gnat2* (late acting) indicated that early, but not late expression of *trb2* could reprogram all cones to red cones (Suzuki et al., 2013). Taken together, our data on ectopic *nrl* expression suggest that ancient mammals had access to an Nrl that was sufficiently potent to over-ride the cone program in nascent cones. If ancient Nrl indeed played a role in the evolution of the rod-dominated retina (at the

expense of cones), our data suggest this may have been enabled by changes in expression, more so than changes in Nrl activity.

4.3.4 Speculation about the specification of adult *nrl*$^{-/-}$ rods in zebrafish

The presence of cells robustly expressing rhodopsin (Fig. 4.4C, G) in the adult *nrl*$^{-/-}$ zebrafish retina was surprising, given the strong rod-free phenotype of the larval mutants, and given the permanently rod-free phenotype of *Nrl*$^{-/-}$ mice. While zebrafish are well known for their widely duplicated genes owing to the teleost-specific whole genome duplication (TSD), in reality only 26% of zebrafish genes are paralogous pairs from the TSD (Howe et al., 2013), and a paralog of zebrafish *nrl* has been sought (Coolen et al., 2005; Kim et al., 2016b), but not found. Alternatively, instead of an *nrl* paralog, a related gene of the *maf* family could feasibly rescue *nrl* mutation. Nrl belongs to the Long Maf peptide family, characterized by the pfam08383 Maf_N domain paired with a bZIP domain. There are several non-*nrl* Long Maf genes identified in zebrafish; we compiled a subset of *maf* genes with previously documented expression even remotely near the eye in zebrafish (Fig. 4.S23), and screened for suggested changes in *maf* expression as larvae aged, including through the time period where the adult *nrl*$^{-/-}$ rod-like cells begin to emerge (Fig. 4.4K; Fig. 4.S24). Only *mafbb*, a homolog of mammalian *Mafb*, had suggestive expression changes during larval maturation, but it was not significantly changed in adult mutant animals (Fig. 4.S25). We attempted to analyze somatic mutation in mosaic adult animals, by injecting a CRISPR directed against *mafbb* into *nrl* mutant*; rh1:eGFP* fish, but we did not observe any changes in the eGFP+ cell population in inspected adult injectees (n > 30). The effectiveness of this CRISPR remains uncharacterized, and a detailed *maf* mutagenesis screen is beyond the scope of this study. Nevertheless, the possibility of another *maf* rescuing the *nrl* mutation remains real, as *MAFA* has been suggested to fulfill the role of missing *NRL* in birds (Enright et al., 2015a; Ochi et al., 2004); moreover, a recent transcriptome profile of chick photoreceptors found a brief but suggestive association of *MAFB* with developing green cones, which express the rhodopsin-related green opsin, *RH2* (Enright et al., 2015a).

We highlight the brief pineal expression of the *rh1:eGFP* transgene, at 1dpf, in both wildtype and *nrl*$^{-/-}$ larvae (Fig. 4.S22). Nrl has been shown to directly bind to and activate expression of rhodopsin in the mouse (Hao et al., 2012; Mitton et al., 2000), and *nrl*$^{-/-}$ larvae did not express rhodopsin detectably at 4dpf (Fig. 4.1E); whatever factor briefly induced expression of the *rh1:eGFP* reporter transgene in the pineal of the mutant larvae might also be the source of *rh1* stimulation in adult mutants (Fig. 4.4C, G).

Recent work in Atlantic cod suggest that *nrl*-independent rod specification may occur in nature (Valen et al., 2016). Valen and colleagues characterized the ontogeny of photoreceptors in the cod, which lives for 30 days as a pre-metamorphic cone-only larvae, and develops its first rods during metamorphosis between 30 and 53 days post hatching. Valen and colleagues performed comparative RNAseq experiments from various time points, and *nrl* transcripts are not abundant beyond the first days of life in these fish. Later, *nrl* transcript abundance actually *decreases* at the time when rod cells are most rapidly generated (37 days post hatching). Nrl and the other Maf family transcription factors have been implicated in lens development (Coolen et al., 2005; Reza and Yasuda, 2004), and our mutants display lens development defects (Fig. 4.S7). It is possible that in the Atlantic cod, *nrl* has played a role in lens or other development only, and that cod have lost larval *nrl*-mediated rod production. This suggests that at least in fish, there is a bona fide *nrl*-independent pathway to specify rods, deployed in adult but not larval animals.

4.3.5 Zebrafish *nrl*$^{-/-}$ rod ultrastructural similarities to mouse *Nrl* knockout suggest a role for *nrl* in adult rods

Close examination by electron microscopy of the adult *nrl*$^{-/-}$ rods suggested apparently normal outer segments, but subtle cone-like phenotypes in the nuclear and synaptic ultrastructure indicate that nrl is not entirely dispensable for the complete rod phenotype in adult zebrafish rods. Over two mutant animals, we found a single synapse that was clearly rod-like: electron dense relative to neighbouring photoreceptors, a single synaptic ribbon that was longer than nearby ribbons, and placed slightly sclerally within the synaptic layer, in line with previous zebrafish rod synapse characterization

(Tarboush et al., 2012) (Fig. 4.S17). The remaining synapses, which presumably include many *nrl*$^{-/-}$ rod synapses, all had ultrastructure morphology indistinguishable from cone synapses, apart from the “white” synapses of one mutant animal. The “white” synapses were positioned like cones within the synaptic layer, interspersed among other synapses. We only found 4 among a local total of 9, which may not be sufficient to fully account for the lack of obvious rod-like synapses; perhaps most of the *nrl*$^{-/-}$ rods had more overtly cone-like synapses. If these mutant rods produce cone-like synapses, this then is reminiscent of the synapses of lamprey photoreceptors. Therefore, unlike the mouse *Nrl* knockout, zebrafish *nrl* adults make an overtly rod-like phenotype; however, there are subtle cone-like phenotypes in the nucleus and synapses, similar to the mouse *Nrl* knockout (Daniele et al., 2005). It is likely that *nrl* has a function in adult rods, although it may not be required to specify them. This is consistent with a recent finding that adult zebrafish rods express *nrl* (Sun et al., 2018).

4.3.6 Evidence for homology between lamprey and gnathostome rods

A looming problem for comparative molecular biological studies is whether a given cell phenotype, found in two organisms, is shared as a result of being present in the last common ancestor (a homologous cell type) (Arendt, 2003), or whether it was convergently evolved in the two lineages to solve a similar problem. In investigations of the ultimate origins of rods and cones, the basal-branching vertebrate lamprey has been an invaluable model (Lamb et al., 2016), but until recently the genome was partially obscured by programmed genome rearrangement (Smith et al., 2018), and the multiyear development of the lamprey precluded deep genetic interventions to explore photoreceptor genetics. It is now very clear that some lamprey species have rod-like photoreceptors capable of responding to single photons of light (Asteriti et al., 2015; Morshedian and Fain, 2017, 2015), a trademark rod ability shared with gnathostome rods. However, there is also ample evidence that lamprey rods have cone-like morphologies. Moreover, it appears that the lamprey and gnathostome lineages split shortly enough after the last shared genome duplication that lamprey have used alternative phototransduction gene paralogs to facilitate vision (Lamb et al., 2016; Muradov et al., 2008, 2007). The last common ancestor of lampreys and gnathostomes

thus possessed at least 5 photoreceptor types, which in gnathostomes became the four cones and single rod (Lamb, 2013). It is possible that lamprey have convergently evolved rod physiology from a cone-like precursor. A solution to resolve such situations was recently proposed, based on testing whether candidate homologous cell types utilize the same core regulatory complex of transcription factors (Arendt et al., 2016). At this time, lamprey are not highly genetically manipulable model organisms, and a rigorous dissection of their photoreceptor genetics is still not practical.

We were able to use our UV cone heterologous expression paradigm to assess the rod-inductive capacity of a suite of *nrl* homologs. Mouse *Nrl* was previously shown to promote the rod phenotype in mouse cones (Oh et al., 2007), and we were able to demonstrate this in zebrafish as well, indicating that this heterologous expression paradigm could detect rod phenotype induction. *Drosophila* Trafficjam cooperates with orthologs of vertebrate photoreceptor specifying genes such as Orthodenticle (vertebrate Otx2/Otx5/Crx) to direct fly photoreceptor phenotypes, but did not promote the rod phenotype in zebrafish UV cones. This indicated that heterologous expression of *nrl* homologs in UV cones could discriminate between Maf-family generic transcriptional activity and probable roles in rod development (fruit flies do not have rod-like photoreceptors). Only a single long Maf transcription factor has been identified in the sea lamprey genome (Kim et al., 2016b), and we expressed it in zebrafish larval UV cones. Similar to mouse and zebrafish *nrl* homologs, lamprey *MAFBA* induced the two phenotypes we tested for (4C12 antigen and rh1:eGFP expression) (Fig. 4.5E, 4.S26E), suggesting that lamprey *MAFBA* was able to induce the rod phenotype in zebrafish UV cones. In fact, it did this better than the chicken homolog, which only induced one of the two target phenotypes (Fig. 4.5D, and Fig. 4.S26D). This may spur investigations into whether avian rods are homologous to the rods of other vertebrates, or at least provide additional reason to characterize avian photoreceptor genetics. For the lamprey, that the rod phenotype could be generated in zebrafish, which have been separated from sea lamprey by more than 500 million years of evolution and which occupy very different ecological niches, suggests that lamprey *MAFBA* is used to promote the rod phenotype (Fig. 4.5G). This is only one element of the rod core regulatory complex, which would also include at least Otx2/Crx, Rorβ, and Nre2e3 as reviewed above, but

by the criteria proposed by Arendt and colleagues for determining cell type homology (Arendt et al., 2016), our data provide missing regulatory evidence that lamprey rods are homologous to gnathostome rods. Ideally, this will become feasible to confirm in lamprey in the future.

4.4 Conclusions

We identified a conserved role for *nrl* in zebrafish larval rod development, and show that it is necessary for larval rod production, and that it is sufficient for rod production in larvae and adults. In contrast, we demonstrated that adult zebrafish unexpectedly access an *nrl*-independent pathway to generate rod-like photoreceptors. These rod-like photoreceptors have subtle ultrastructural similarities to cones, indicating that *nrl* still plays a role in adult rods; this was supported by transcriptional phenotypes of mutant adult retinas. By comparing the transcriptional phenotypes of larval and adult *nrl* mutants to the *Nrl* knockout mouse, we found that that larval zebrafish rods are developmentally more similar to mouse rods than adult zebrafish rods. We were able to exploit this new understanding of zebrafish photoreceptor specification to address an evolutionary question, adding an important new layer of evidence that lamprey rods and gnathostome rods are homologous.

4.5 Figures

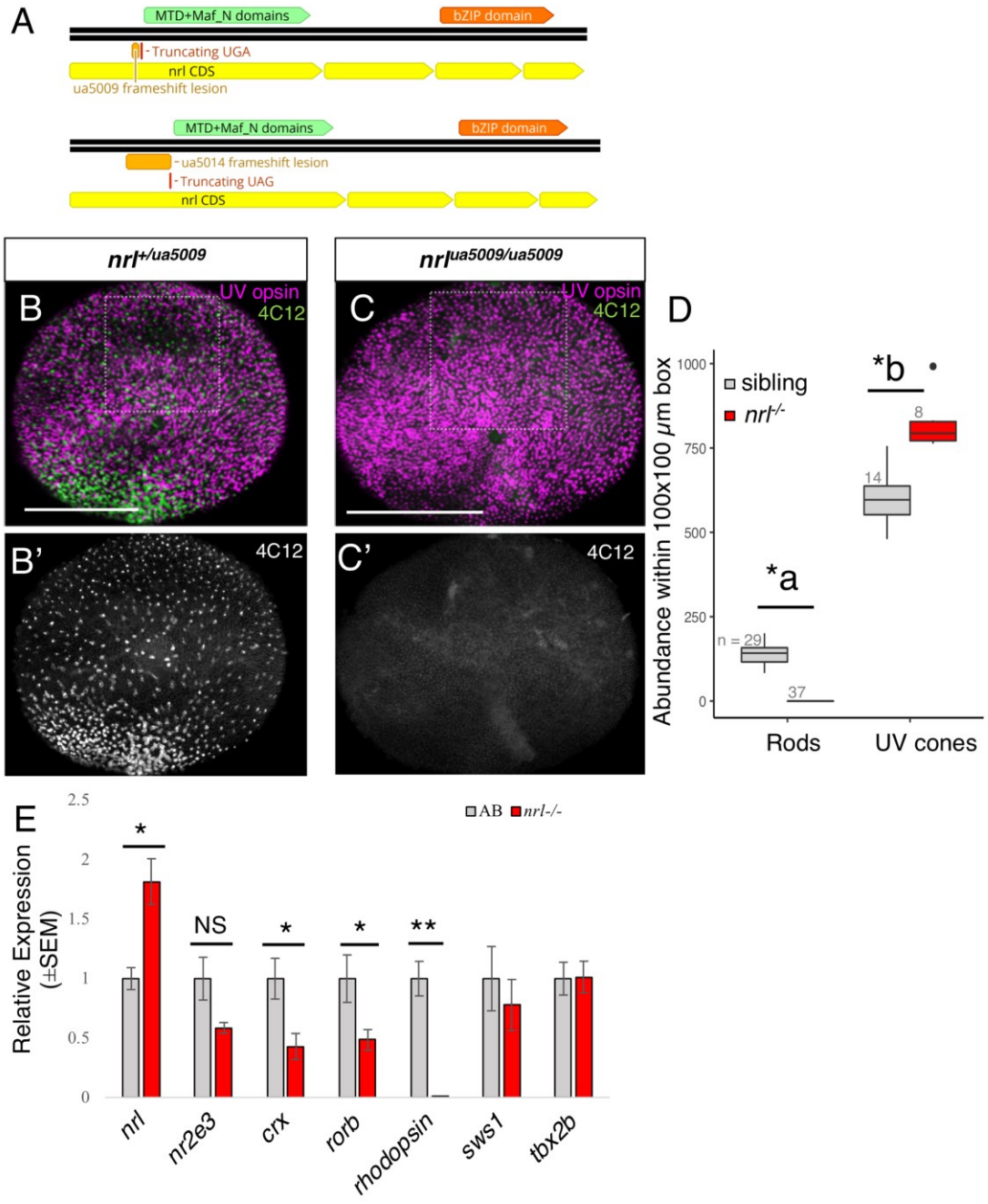

Figure 4.1. Zebrafish *nrl* is a conserved requirement for rod development in larval retina.

(**A**) Allele schematic showing the two mutant nrl alleles generated for this study. See also Figure 4.S3. (**B-C'**) Homozygous *nrl* mutant zebrafish larvae lack rods in their retinas, compared to sibling larvae that have abundant rods. Wholemount retina of 4 days post-fertilization zebrafish larvae heterozygous (**B-B'**) or homozygous (**C-C'**) for *nrl*^{ua5009}, a putative null allele. Mutant animals did not produce rods. Magenta is 10C9.1 antibody staining (anti-UV cone opsin), and green is 4C12 antibody staining (against a rod-specific antigen). Scale bar is 100 um. (**D**) Photoreceptor quantification shows UV cone photoreceptors are more abundant in *nrl* mutant zebrafish, per Mann-Whitney U (MWU) test (*a: rods, U = 0, p = 2.36e-14; *b: UV cones, U = 112, p = 0.0001512; floating dot is a statistical outlier). See also Supplemental Figure S6. (**E**) Relative transcript abundance of various opsins and transcription factors previously implicated in photoreceptor development, performed on 6 replicates 4dpf wildtype and *nrl*$^{-/-}$ whole larvae. ** $p < 0.01$; * $p < 0.05$, MWU.

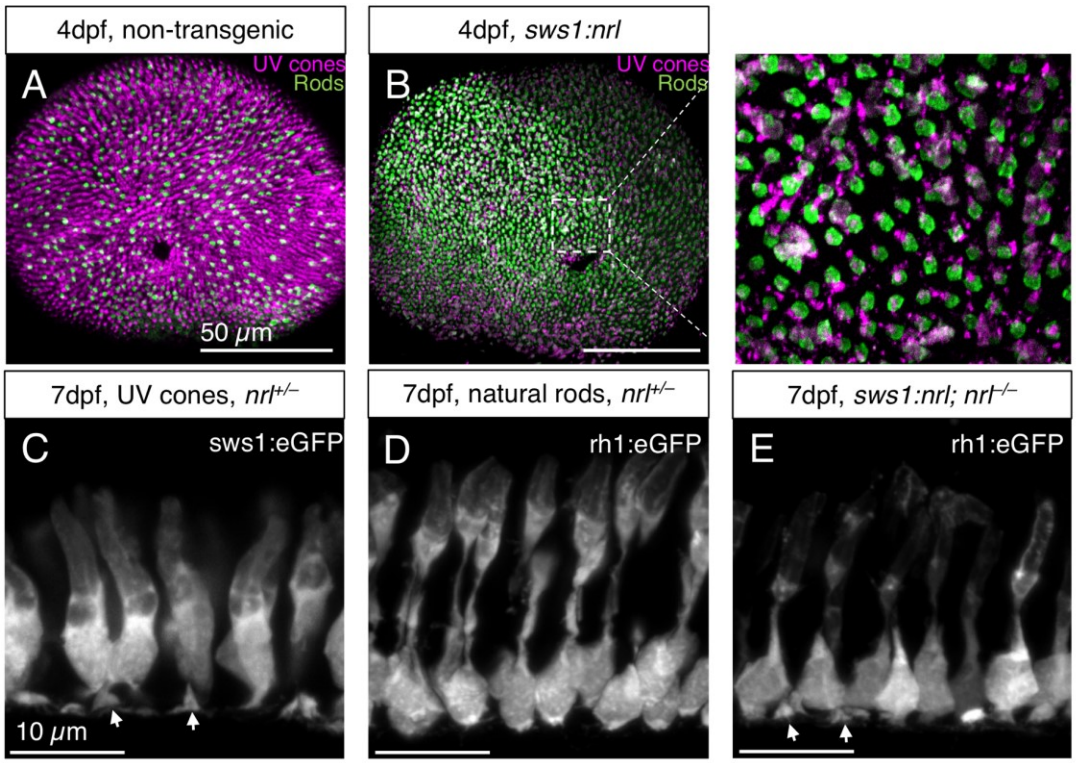

Figure 4.2: Zebrafish *nrl* is sufficient to convert UV cone photoreceptors to a rod-like cell fate.

(**A, B**) Ectopic expression of zebrafish *nrl* in UV cones led to appearance of rod markers. Wholemount retinas of 4 day old zebrafish larvae, wildtype (**A**) and transgenic (**B**), stained with 4C12 antibody against rods (green) and 10C9.1 antibody against UV cones (magenta). In transgenics, the rod-specific 4C12 antibody colocalized with UV cone-specific 10C9.1 antibody, which detects Sws1 opsin. In contrast, non-transgenic siblings do not show co-labeling of 4C12 and 10C9.1. Scale bars are 50 μm. (**C-E**) Ectopic expression of zebrafish *nrl* in UV cones led these cells to take on a rod morphology. Natural UV cones (**C**), and natural rods (**D**) from a 7 days post-fertilization sibling $nrl^{+/ua5009}$ larva expressing GFP in UV cones or rods with the transgenes sws1:GFP or rh1:GFP, respectively. (**E**) UV cones ectopically expressing zebrafish *nrl*, from a 7dpf $nrl^{ua5009/ua5009}$ larvae that also expressed GFP with rh1:GFP transgene; these UV cones have a rod-like morphology. White arrowheads: pyramidal cone or cone-like synapses. Scale bars are 10 μm.

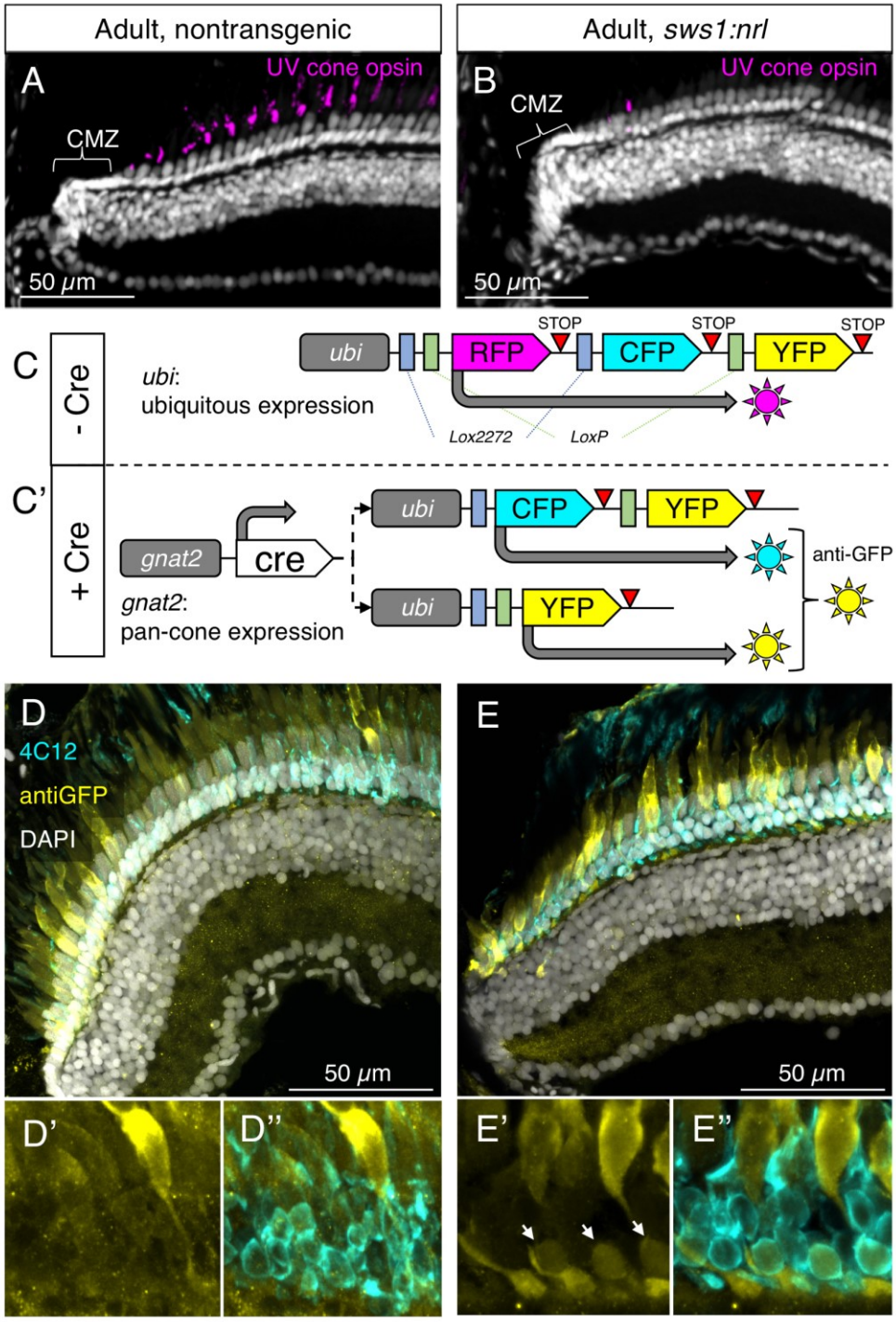

Figure 4.3: Zebrafish UV cones can be converted to a rod-like fate by ectopic expression of zebrafish *nrl*.

(**A, B**) In adult transgenic zebrafish retina, UV cones that ectopically express *nrl* disappear from the retina as they mature. Radial sections of adult zebrafish retina,

either wildtype (**A**) or transgenic driving expression of *nrl* in UV cones (**B**), with DAPI nuclear stain and anti-UV opsin staining. The ciliary marginal zone (CMZ) is a site of proliferation for new retinal cells; in B, a young UV cone mature enough to express UV cone opsin is visible, but no older UV cones are detected among older cells further along the section. Scale bars are 50 μm. (**C, C‘**) Schematic of Cre/lox-based lineage tracing permanently marks all cells that ever expressed *gnat2* (all cone photoreceptors) with a fluorescent marker that is pseudocoloured yellow. Without Cre recombinase (**C**), the Zebrabow reporter construct produced red fluorescent protein (RFP) in all cells of the zebrafish. In the presence of Cre driven by a cone-only promoter (**C‘**), the Zebrabow locus was randomly recombined to produce either cyan or yellow fluorescent protein, permanently. Variable fluorescence intensities between cells resulting from multiple Zebrabow loci per animal were mitigated by uniting the CFP and YFP channels into one using an anti-GFP antibody. (**D**) Lineage tracing faithfully marks all cones, and only cones, in zebrafish with unperturbed *nrl*. Radial section of an adult zebrafish retina, with the transgene *gnat2:cre* and the Zebrabow construct. In 2 of 2 adult animals of this genotype examined, no lineage tracing-positive rods were detected within 300 μm of the CMZ in sections that include the optic nerve head, sectioned parallel to the nasal-temporal axis (Fig. 4.S9 for schematic); D’-D’’ show representative lack of lineage tracing in rods at the 100 μm position. (**E**) Lineage tracing reveals that the UV cones with ectopic *nrl* are transmuted into rods; thus they are not detectable as UV cones after maturation because they stop expressing UV opsin and become rods. Radial section of an adult zebrafish, with the transgenes gnat2:cre, sws1:nrl, and the Zebrabow construct. In 7 of 8 adult animals of this genotype, lineage tracing-positive rods were detected within 100 μm of the CMZ; E’-E’’ show representative lineage-traced rods (arrows) at the 100 μm position. See also Figures 4S.8 and 4.S9.

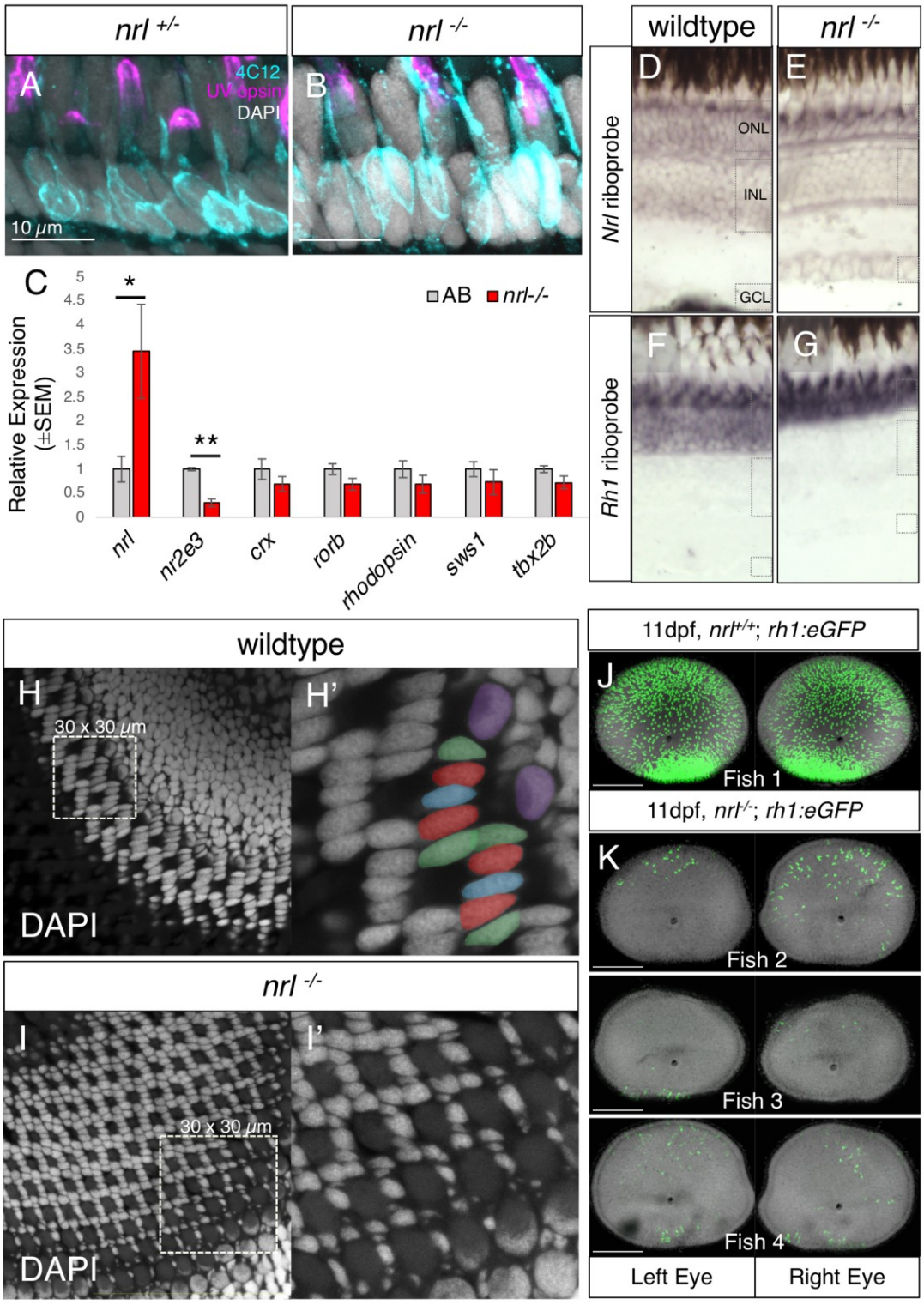

Figure 4.4: Adult zebrafish make abundant rods despite *nrl* mutation.

No difference in rod abundance was apparent in adult zebrafish homozygous for *nrl* mutation compared to siblings. 10 μm radial sections of adult zebrafish retina

heterozygous (**A**) or homozygous (**B**) for *nrl*^{ua5009}, showing no overt difference in rod abundance between heterozygotes and mutants. Cyan is 4C12 staining, magenta is 10C9.1 staining, and grey is DAPI nuclear stain. Scale bar is 10 μm. (**C**) *nrl* and *nr2e3* had disrupted transcript abundances in adult *nrl* mutant neural retina. Relative quantitation of transcripts isolated from adult neural retina of n = 5 animals per genotype, from dark-adapted animals at 6:00pm. ** $p < 0.01$; * $p < 0.05$, MWU. (**D-G**) *in situ* hybridization on frozen sections of adult retina comparing wildtype (**D, F**) and *nrl*$^{-/-}$ retinas (**E, G**), showing no overt changes in the area of *nrl* or of rhodopsin (*rh1-1*) expression. ONL, INL, GCL are outer nuclear layer, inner nuclear layer, and ganglion cell layer. (**H, I**) Cone photoreceptors have no apparent alteration in abundance in adult *nrl* mutants. Cryosections of adult wildtype (**H**) or *nrl* mutant (**I**) eyes, highlighting the well-described cone pentamer (DAPI-stained nuclei hand-pseudocoloured green, red, blue, red, green to match cone type) with space for UV cones between each pentamer. Adult *nrl* mutants have wildtype-like cone pentamer arrangements, indicating no deficit in cone subtypes. See also Figure 4.S12, 4.S20 and 4.S21. (**J, K**) Pairs of eyes from 11 dpf zebrafish larvae bearing rh1:eGFP transgene, mounted to display rods (green) and retinal nuclei (gray) from ToPRO3 stain. (**J**) a pair of representative wildtype retinas; (**K**) three pairs of representative *nrl*$^{-/-}$ retinas. Despite a synchronized hour of birth, mutant larvae display various numbers of rods between individuals, and often between eyes within one single larva. Not shown: numerous siblings without obvious rods. Scale bars are 100 μm.

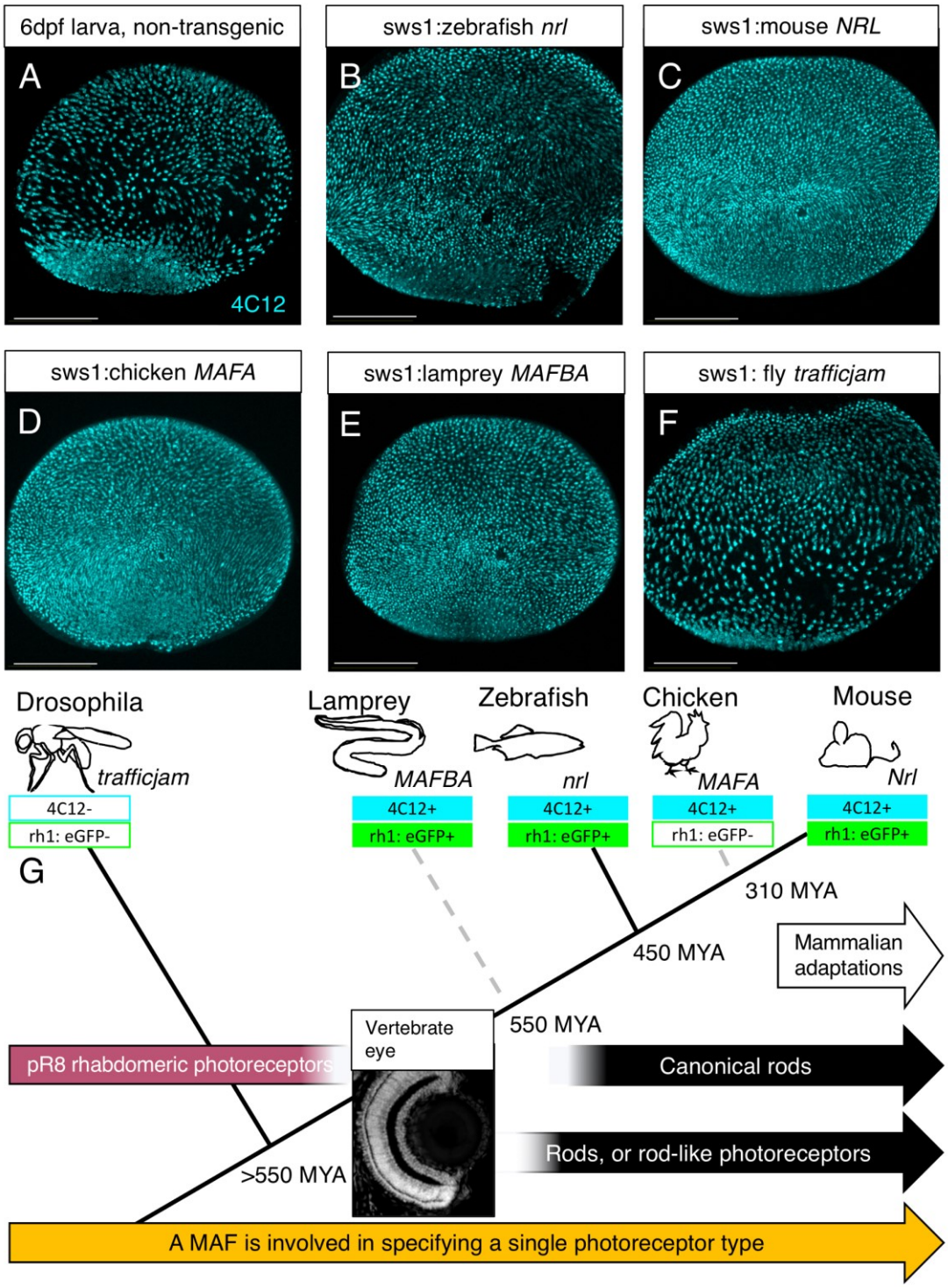

Figure 4.5: The zebrafish rod program can be initiated in UV cones by various vertebrate orthologs of *nrl*.

(**A-F**) 6 day old larval zebrafish with rods shown by 4C12, detecting rods. All expression constructs indicated use zebrafish *sws1* gene regulatory sequence to drive

the indicated N-terminal FLAG-tagged gene solely in UV cones and represent stable transgenic insertions. (**A, F**) 4C12 signal is restricted to rods in the non-transgenic and sws1:FLAG-trafficjam panels, despite abundant *trafficjam* expression in UV cones in (**F**) (Fig 4.S27 flag stain). Scale bars are 100 μm. (**B-E**) zebrafish Nrl, mouse NRL, chicken MAFA, and sea lamprey MAFBA are each capable of inducing a rod-like phenotype in UV cones. (**G**) Schematic phylogeny indicating the ancient role for Mafs in photoreceptor specification. Among the vertebrates, of the one rod and four cone visual photoreceptors, only the rod specification program appears to be driven by a Maf transcription factor. In *Drosophila*, whose visual system is based on rhabdomeric photoreceptor biology, a single photoreceptor type appears to rely on the sole *Drosophila* long Maf family member, *trafficjam*. See also Figure 4.S26. Coloured boxes featuring 4C12 and rh1:eGFP reporter status summarize data from this figure and from Figure 4.S26.

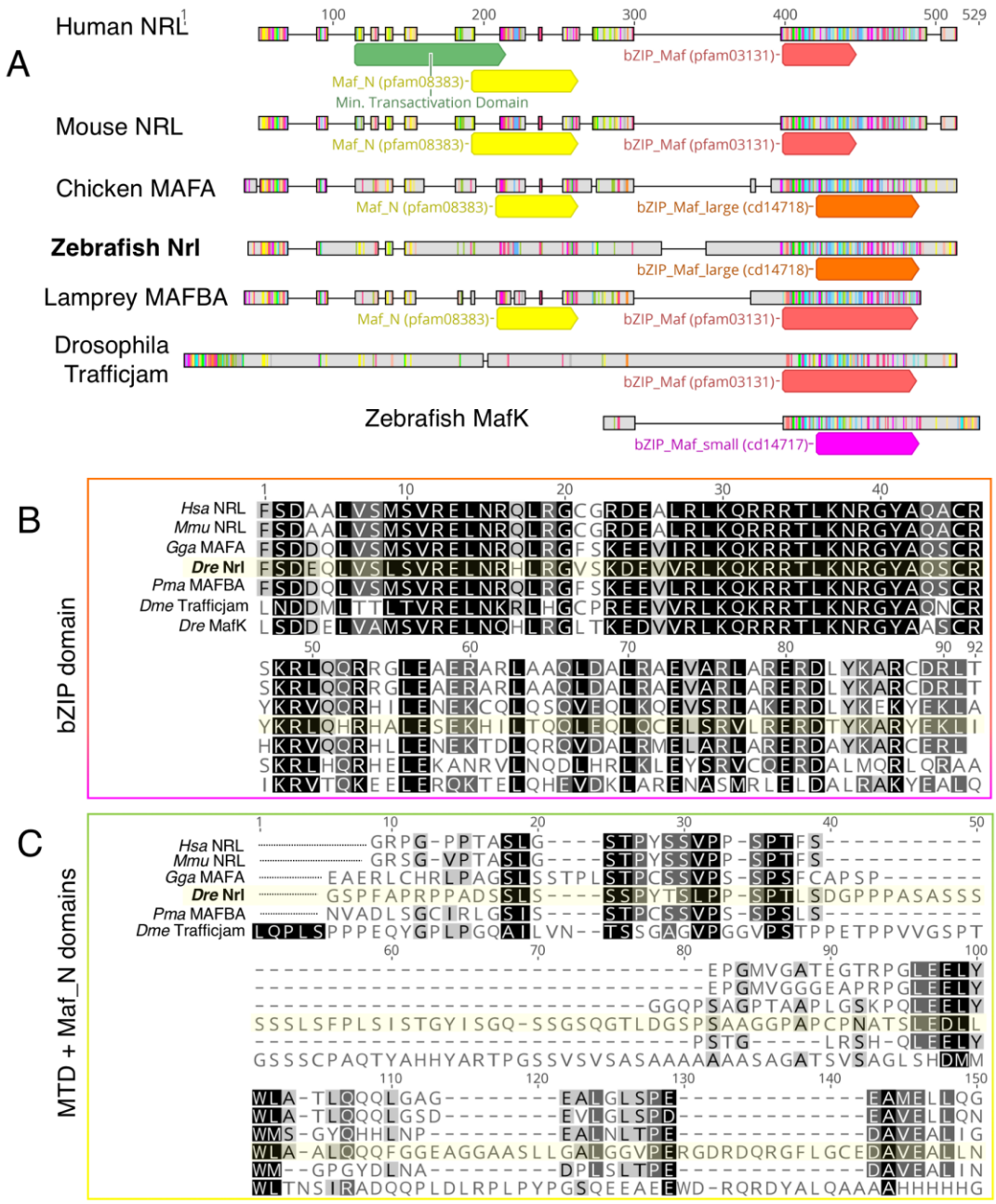

Figure 4.S1: Domain conservation of Nrl and homologs.

(**A**) ClustalW alignment of peptide sequences for human NRL (NP_006168), mouse Nrl (NP_001258846), chicken MAFA (NP_990356), zebrafish Nrl (NP_001035421), lamprey MAFBA (GENSCAN00000012317), *Drosophila* Trafficjam (NP_609969.2), and zebrafish MafK (NP_001002044.2). Zebrafish Nrl has an overall (A) conservation of 32% identity with human NRL, but 63% at the bZIP domain (**B**). Zebrafish Nrl also has the conserved elements of human MTD and Maf_N domains (**C**), split between

stretches of non-conserved or novel sequence, resulting in a low percent identity of this region relative to humans (25.2%). See Fig. 4.S2 for full table of percent identity conservation values. Domain accession numbers were retrieved through NCBI Conserved Domain search, while the Minimal Transactivation Domain of human NRL was experimentally determined first in Friedman et al., 2004. Abbreviations: *Hsa*, *Mmu*, *Gga*, *Dre*, *Pma*, *Dme* are *Homo sapiens*, *Mus musculus*, *Gallus gallus*, *Danio rerio*, *Petromyzon marinus*, and *Drosophila melanogaster*. In (**B**) and (**C**), grayscale shade indicates similarity under BLOSUM62 substitution matrix with a threshold of 1; black, dark gray, light gray, and white denote 100%, 80-99%, 60-79%, and ≤59% similarity scores, respectively.

		Human NRL	Mouse NRL	Chicken MAFA	**Zebrafish Nrl**	Lamprey Mafba	Drosophila traffic jam	Zebrafish mafk
Full Alignment	Human NRL		89.5	42.0	**32.1**	46.5	16.0	33.8
	Mouse NRL	89.5		41.3	**30.6**	46.5	15.4	33.1
	Chicken MAFA	42.0	41.3		**29.8**	57.7	17.6	38.7
	Zebrafish Nrl	**32.1**	**30.6**	**29.8**		**30.7**	**18.9**	**25.2**
	Lamprey Mafba	46.5	46.5	57.7	**30.7**		17.0	42.2
	Drosophila traffic jam	16.0	15.4	17.6	**18.9**	17.0		19.1
	Zebrafish mafk	33.8	33.1	38.7	**25.2**	42.2	19.1	
bZIP Domain only	Human NRL		100	64.1	**63.0**	73.6	51.1	48.9
	Mouse NRL	100		64.1	**63.0**	73.6	51.1	48.9
	Chicken MAFA	64.1	64.1		**72.8**	80.2	52.2	57.6
	Zebrafish Nrl	**63.0**	**63.0**	**72.8**		**71.4**	**54.3**	**52.2**
	Lamprey Mafba	73.6	73.6	80.2	**71.4**		52.7	61.5
	Drosophila traffic jam	51.1	51.1	52.2	**54.3**	52.7		46.7
	Zebrafish mafk	48.9	48.9	57.6	**52.2**	61.5	46.7	
MTD+Maf Domain only	Human NRL		83.3	41.2	**25.2**	37.8	9.4	N/A
	Mouse NRL	83.3		36.5	**23.0**	39.2	6.5	N/A
	Chicken MAFA	41.2	36.5		**21.8**	50.6	10.4	N/A
	Zebrafish Nrl	**25.2**	**23.0**	**21.8**		**18.9**	**18.2**	N/A
	Lamprey Mafba	37.8	39.2	50.6	**18.8**		7.7	N/A
	Drosophila traffic jam	9.4	6.5	10.4	**18.2**	7.7		N/A
	Zebrafish mafk	N/A	N/A	N/A	N/A	N/A	N/A	

Figure 4.S2: Percent identity conservation of Nrl and homologs.

Alignment of zebrafish Nrl to its closest homologs in human, mouse, chicken, or lamprey demonstrates low percent identity overall, but with higher identity at the two major protein domains illustrated. Domain accession numbers were retrieved through NCBI Conserved Domain search, while the Minimal Transactivation Domain of human NRL was experimentally determined first in Friedman et al., 2004. All values given are percent identity.

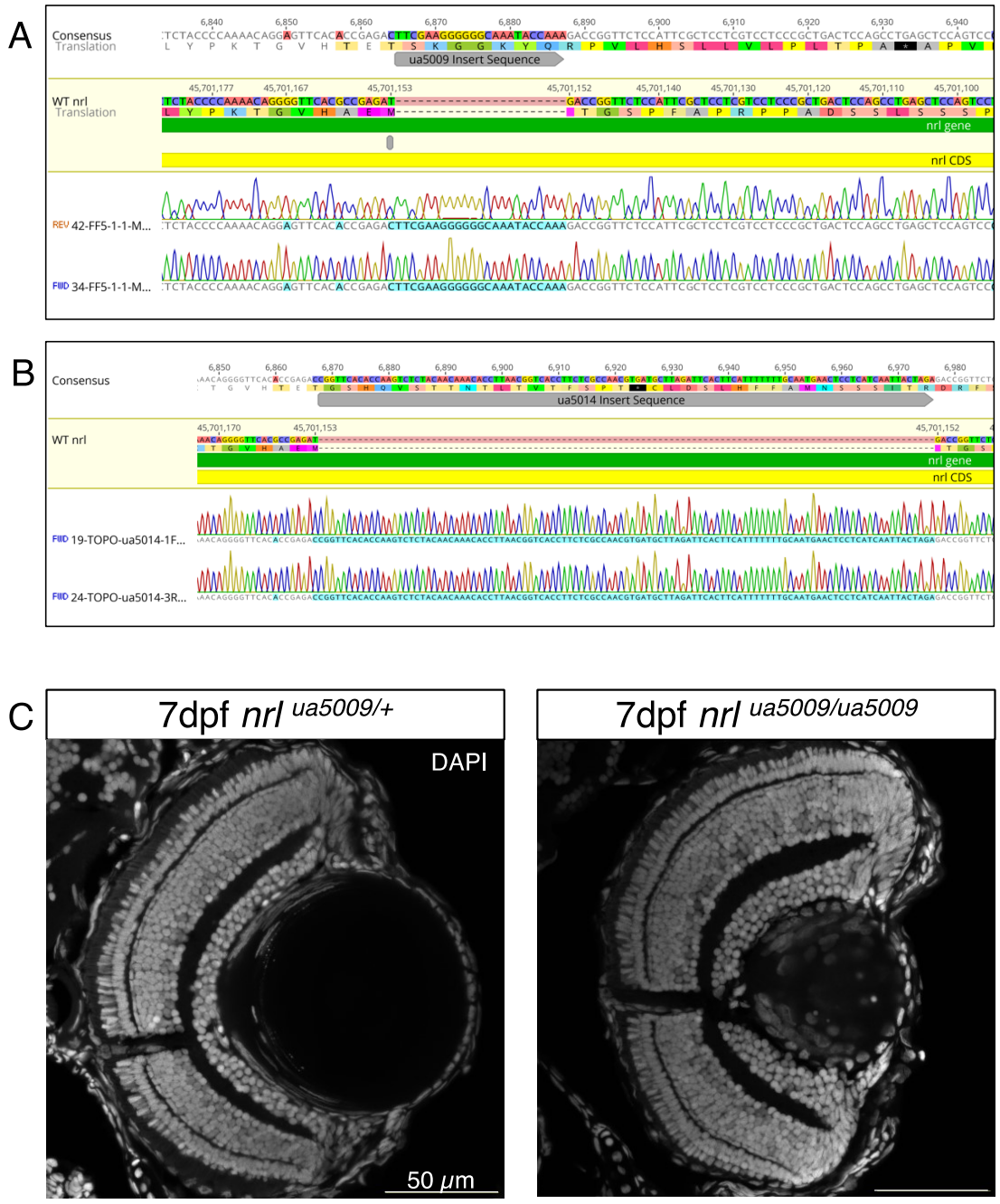

Figure 4.S3: The nature of the two *nrl* lesions ua5009 and ua5014, and the overtly normal retinal histology of larval mutants.

This data complements Figure 4.1A. (**A**) Chromatogram from Sanger sequencing of the ua5009 nrl lesion, which induced insertion of 23 bp of apparently random sequence.

BLASTing this insert results in a top result of genomic sequence from *Candida tropicalis* with and e-value of 1.7 and the top hits in the zebrafish genome map to Chromosomes 2, 13, and 17 with equal identity and e-value of 6.6, but not to Chromosome 23 or 20, to which zebrafish *nrl* has been mapped (Chr 20 in current genome assembly GRCz11, Chr 23 in previous genome assembly GRCz10). Mutants used for analysis in this publication, bearing the ua5009 lesion, were outcrossed twice to wildtype animals to remove background lesions, and then in-crossed to retrieve homozygous mutants. (**B**) Chromatogram from Sanger sequencing of the ua5014 lesion, which induced insertion of 109 bp of sequence that matches more than 90% of a region of intron 4 of *E3 UMF1-protein ligase1* (*ufl1*). Animals bearing ua5014 were outcrossed twice to wildtype animals to remove background lesions prior to in-crossing to recover homozygotes, but were not used to generate data for this paper. Homozygotes do not have rods at 4dpf, and show lens defects (data not shown), similar to ua5009 homozygotes in Fig. 4.1**B** and Fig. 4.S7**B**. (**C**) Frozen sections stained with DAPI nuclear stain, of sibling and *nrl* mutant 7 day old larvae, demonstrating overt wildtype-like retinal morphology of the mutants, aside from the lens.

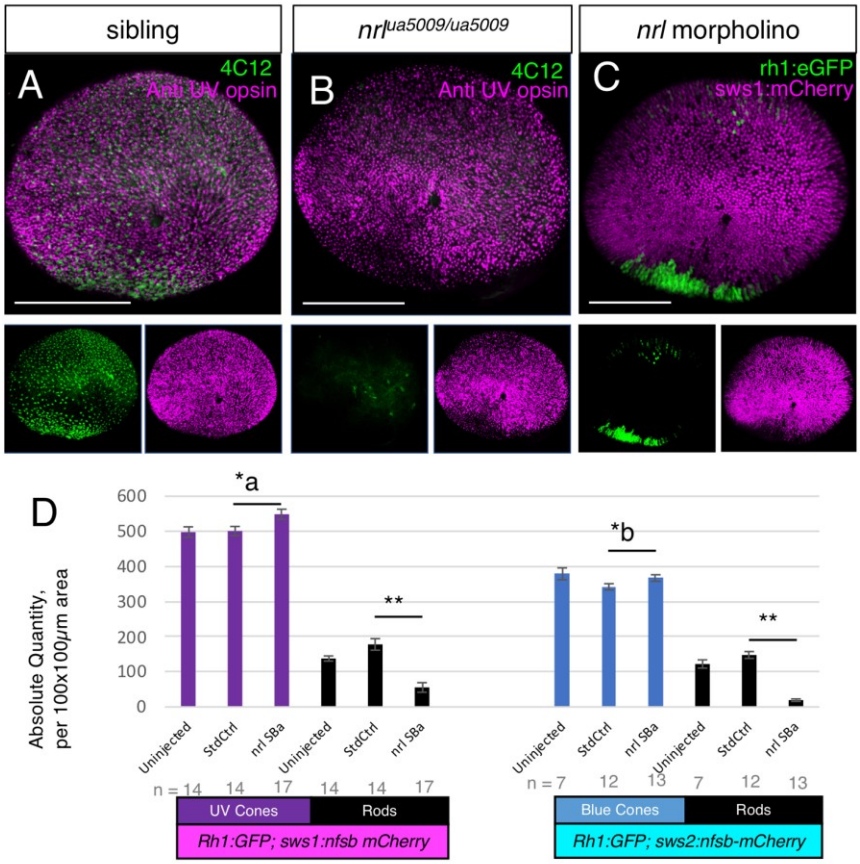

Figure 4.S4: Reduction of rod abundance by *nrl*-targeted morpholino phenocopies *nrl* mutation.

(**A-C**) mounted retinas from 4dpf zebrafish; (**A, B**) green is 4C12 rod immunolabeling, while magenta is 10C9.1 UV cone immunolabeling; in C, rods express eGFP from rh1:eGFP and UV cones express nfsb-mCherry. (**A, B**) as in Fig. 4.2, *nrl* mutation blocks rod development. (**C**) 10ng of splice-blocking morpholino injected into *nrl*$^{+/+}$ zebrafish, targeting the first exon-intron boundary of nrl transcript, reduced the abundance of rod photoreceptors in the whole retina. (**D**) *nrl* splice-blocking morpholino, or standard control morpholino, was injected into *nrl*$^{+/+}$ zebrafish with the indicated fluorescent markers, and rods and UV cones or blue cones were quantified within a 100 x 100 μm box dorsal to the optic nerve head. Rod abundance was lower in *nrl* morphants relative to standard control-injected larvae, and a minor but significant increase in UV cones and blue cones was observed. * is $p < 0.05$ (*a = 0.041; *b=0.015), and ** is p <<< 0.01 by Mann-Whitney U. Scale bars are 100 μm.

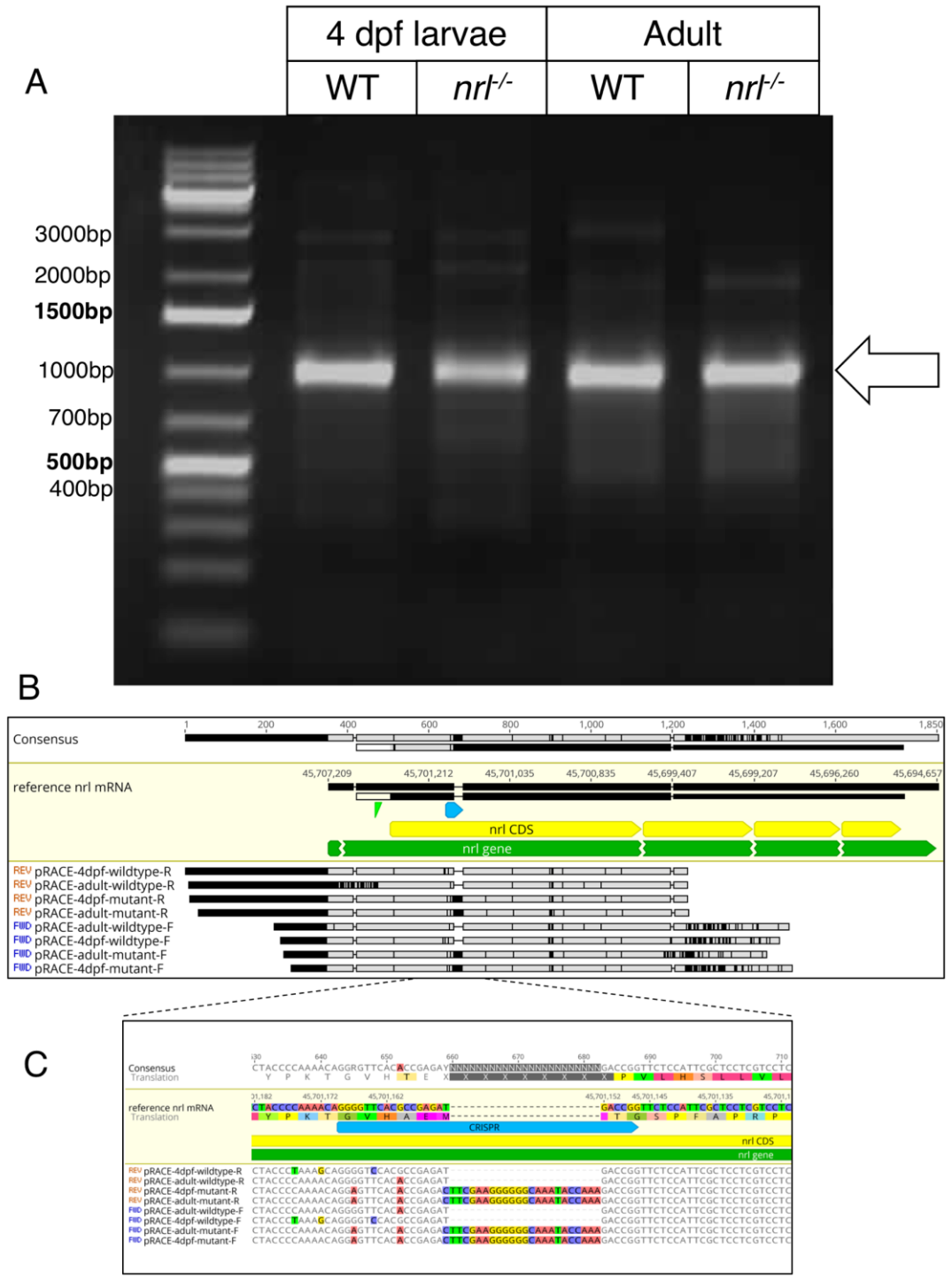

Figure 4.S5: 5' Rapid Amplification of cDNA Ends (RACE) reveals a single dominant transcript produced in wildtype and *nrl* mutants and larval and adult ages.

(**A**) 5’ RACE was performed from total RNAs extracted from whole larvae and adult neural retina, anchored in the second coding exon. A single dominant band was produced, which was cloned and sequenced. (**B**) Alignment of sequencing results from larvae and adults shows the presence of the ua5009 lesion in the first coding exon of zebrafish *nrl*. Moreover, the lesion in this transcript is continuous and in-frame with the next coding exon, suggesting that the transcript is not spliced differently from wildtype. (**C**) Zoom of (**B**), demonstrating that the sequence of the insert in the *nrl* allele ua5009 is present in *nrl* transcripts from *nrl* mutant animals of both larval and adult ages.

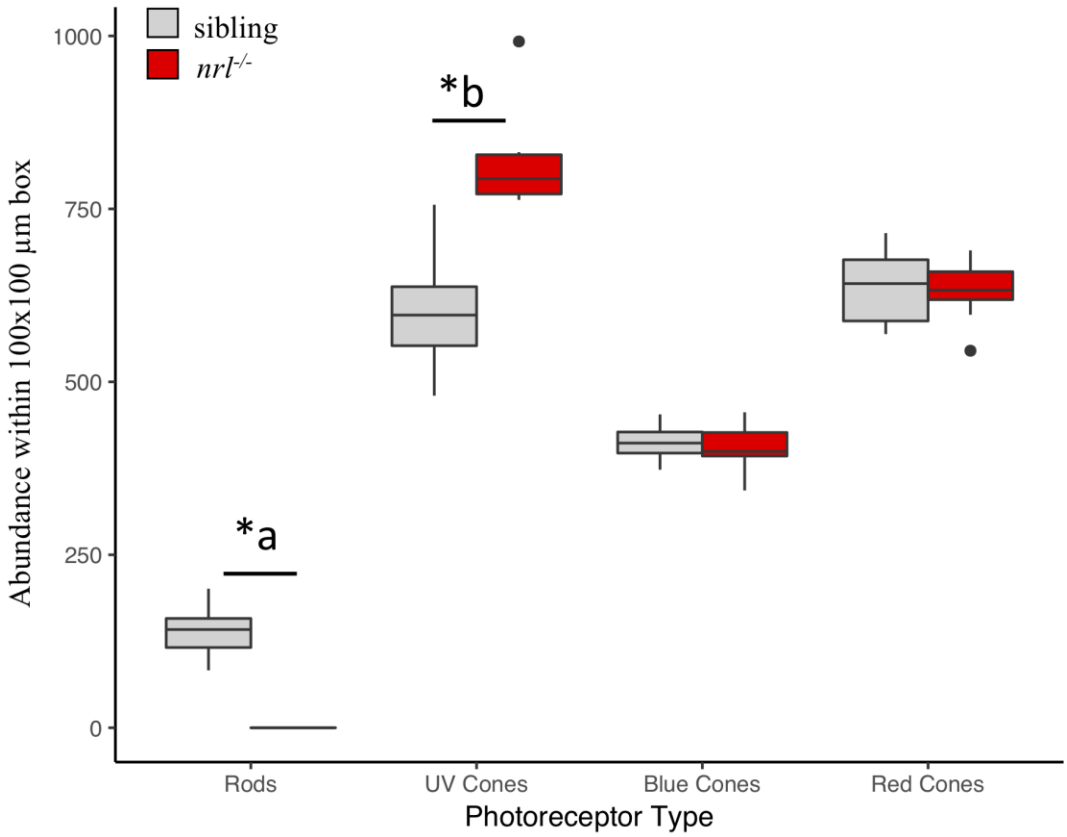

Figure 4.S6: *nrl* mutant larvae do not have rods, and instead have more UV cones. Counts of photoreceptor populations within a 100x100um box, positioned just dorsal to the optic nerve head, in 4dpf larvae, as revealed by antibody (rods, 4C12; UV cones, 10C9.1). UV cones are over-produced in nrl mutant zebrafish, per Mann-Whitney U test (*a: rods, U = 0, p = 2.36e-14; *b: UV cones, U = 112, p = 0.0001512). Blue cones and red counts were not differentially abundant between genotypes; blue cones were revealed by transgenic mCherry expression, red cones were stained with 1D4 antibody. Free floating dots are statistical outliers. Associated with Fig. 4.1**D**.

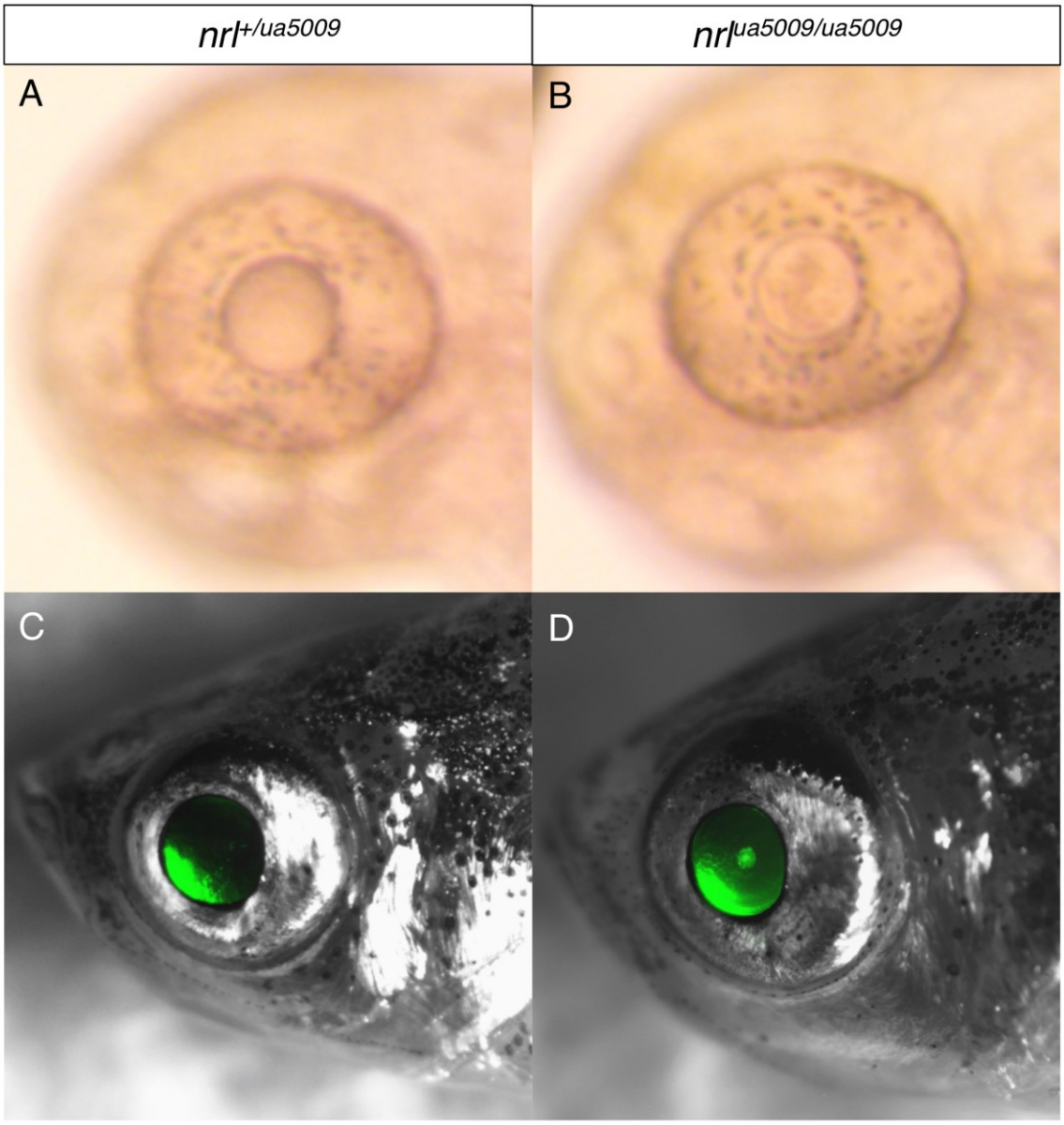

Figure 4.S7: Zebrafish *nrl* mutants have lens defects present in larvae and visible in adults.

(**A, B**) 3 day old larvae either heterozygous (**A**) or mutant (**B**) for *nrl* mutation. (**C, D**) 3 month old adult zebrafish, with lenses back-lit with fluorescence from rh1:GFP transgene, which drives GFP expression in rods.

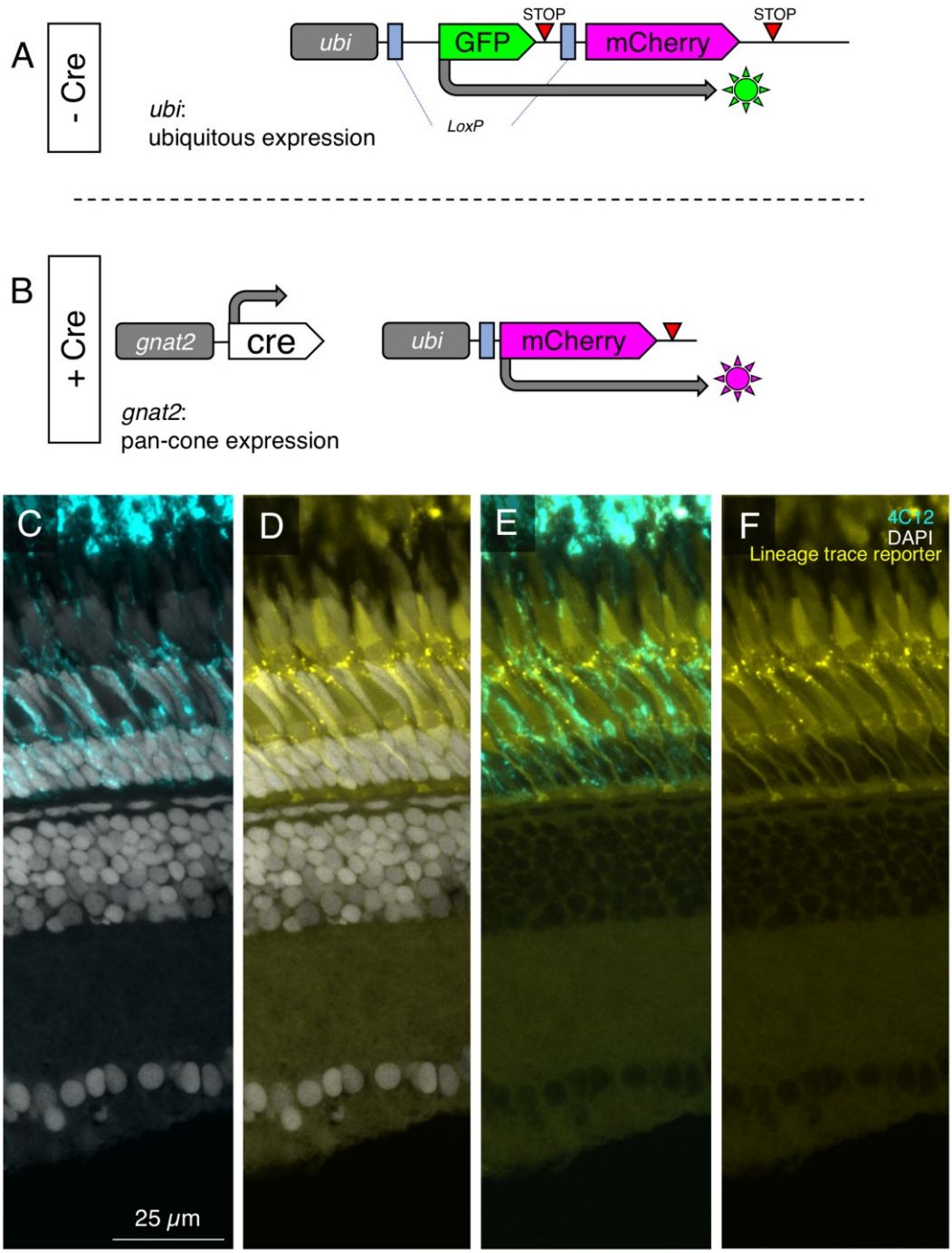

Figure 4.S8: Schematic of the ubi:Switch lox-mediated Cre reporter construct. In the absence of Cre recombinase (**A**), zebrafish bearing this construct ubiquitously express GFP (Mosimann et al., 2011; Solek et al., 2017). In the presence of Cre recombinase (**B**), recombination of the LoxP sites occur, and GFP is permanently lost. Cells begin to express mCherry fluorescent protein under the ubiquitin promoter. (**C-F**)

representative confocal micrograph of wildtype fish with the ubi:Switch construct combined with gnat2:cre transgene. In 7/7 animals examined, there was no rod with lineage tracing at any region between the ciliary marginal zone and the optic nerve head. Associated with Fig. 4.3.

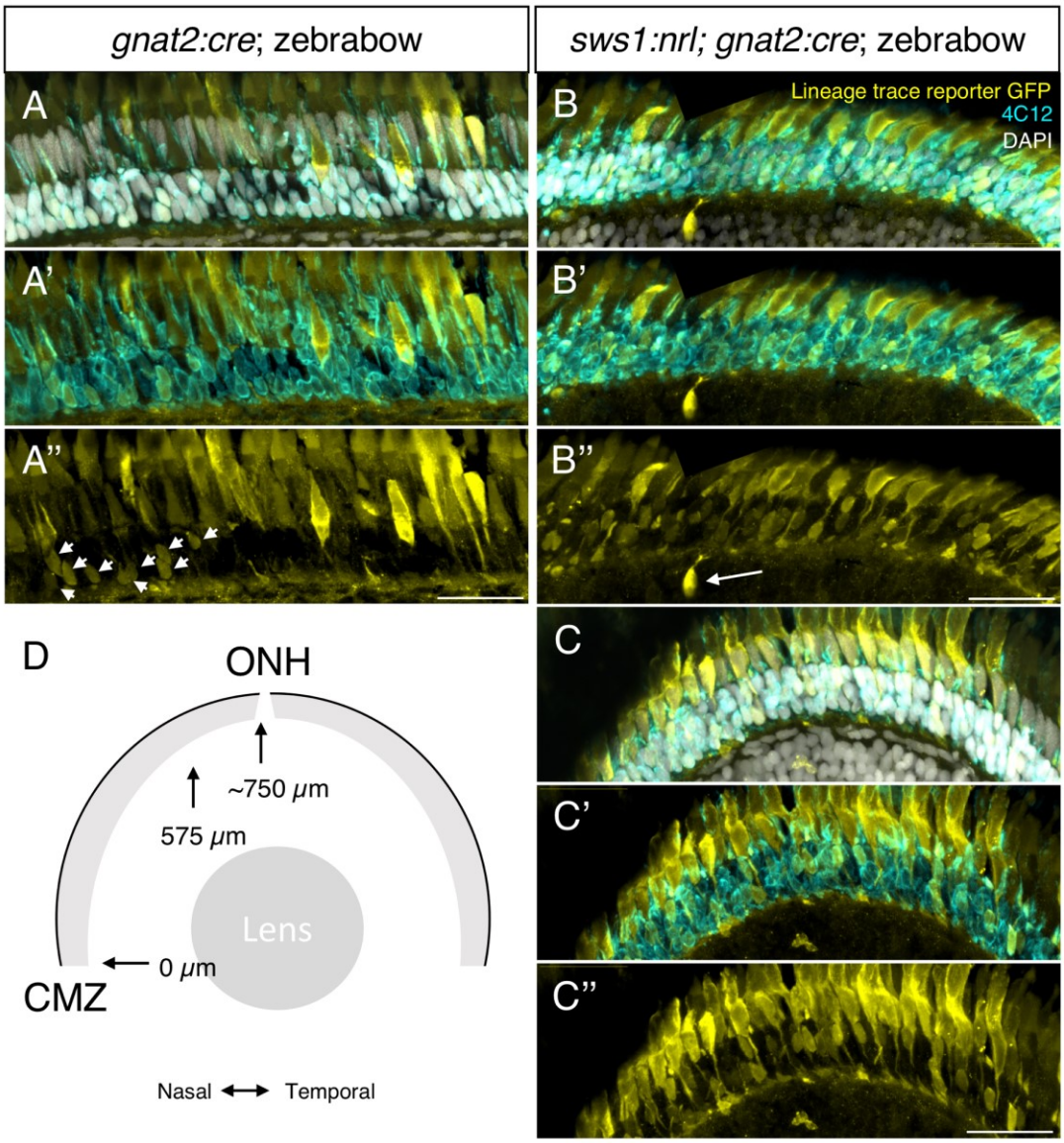

Figure 4.S9: Gnat2:Cre lineage tracing signal is evident in central retinal rods of otherwise wildtype adult zebrafish, but not in any larval rods.

(**A-A''**) A zebrafish with lineage tracing transgenes but no sws1:nrl had 5 clusters of rods that were labeled with lineage tracing construct toward the central retina, for a CMZ-to-ONH total of 27 rods. Shown: the largest cluster of this animal, with 9 lineage reporter-positive rods, at 575μm from the CMZ (arrowheads). (**B-B''**) A zebrafish with lineage tracing transgenes and also sws1:nrl, showing lineage reporter-positive rods at 575μm from the CMZ. Also shown: a lineage reporter-positive bipolar cell (long arrow).

There were a total of 3 bipolar cells labeled in this section, assessed between the CMZ and ONH. (**C-C’’**) The same section as B-B’’, at position 640μm from the CMZ. Scale bars are 25μm. (**D**) Schematic showing a cryosection of adult zebrafish retina, with distances relative to the CMZ plotted for reference. CMZ, ONH are ciliary marginal zone and optic nerve head. Associated with Fig. 4.3.

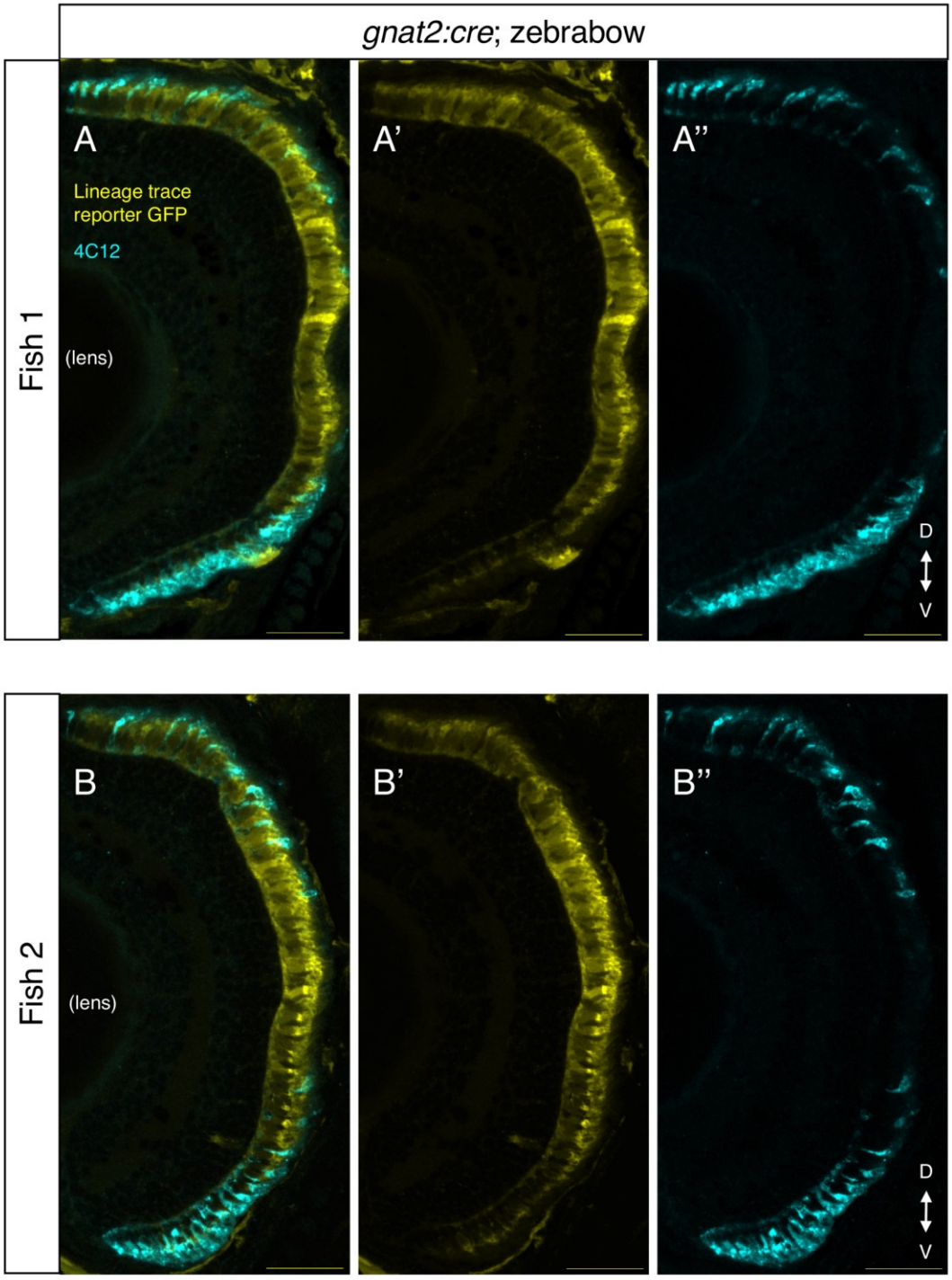

Figure 4.S10: Gnat2:Cre lineage tracing does not label any larval rods.
(**A-A'', B-B''**) Two representative sections of 6 retinas examined, from 5 dpf transgenic larvae. There was never any gnat2:cre lineage tracing in 358 manually-examined rods over 6 retinas. Scale bars are 25μm.

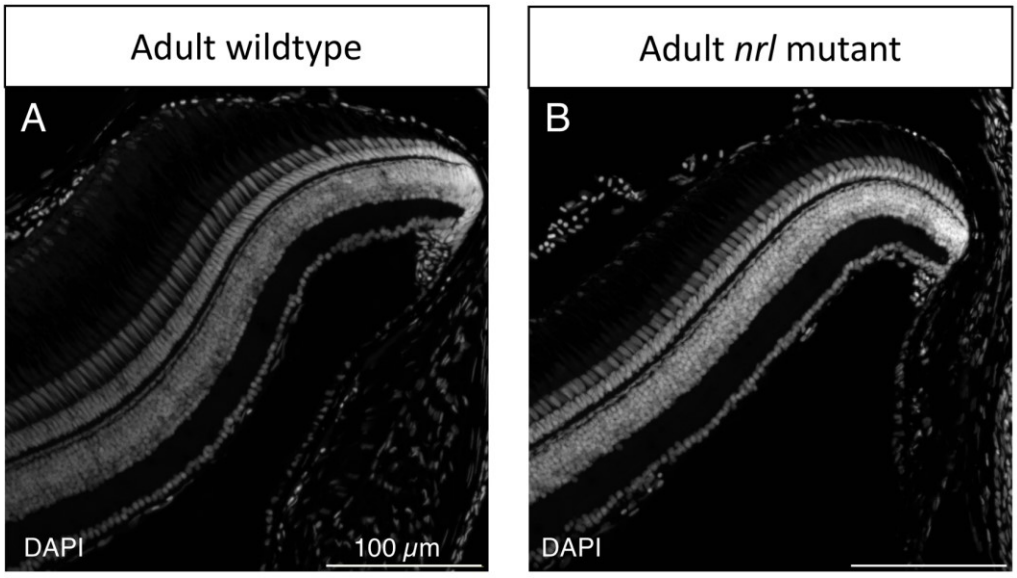

Figure 4.S11: Adult *nrl* mutant zebrafish have no gross morphological or lamination defects in the neural retina.

(**A**) Frozen section demonstrating a representative wildtype adult zebrafish retina cross-section, with nuclei stained with DAPI. (**B**) Frozen section demonstrating a representative *nrl* mutant adult zebrafish retina cross-section, demonstrating no gross morphological distortions in the normal layering of the retina, nor whorls or rosettes in the photoreceptor layer.

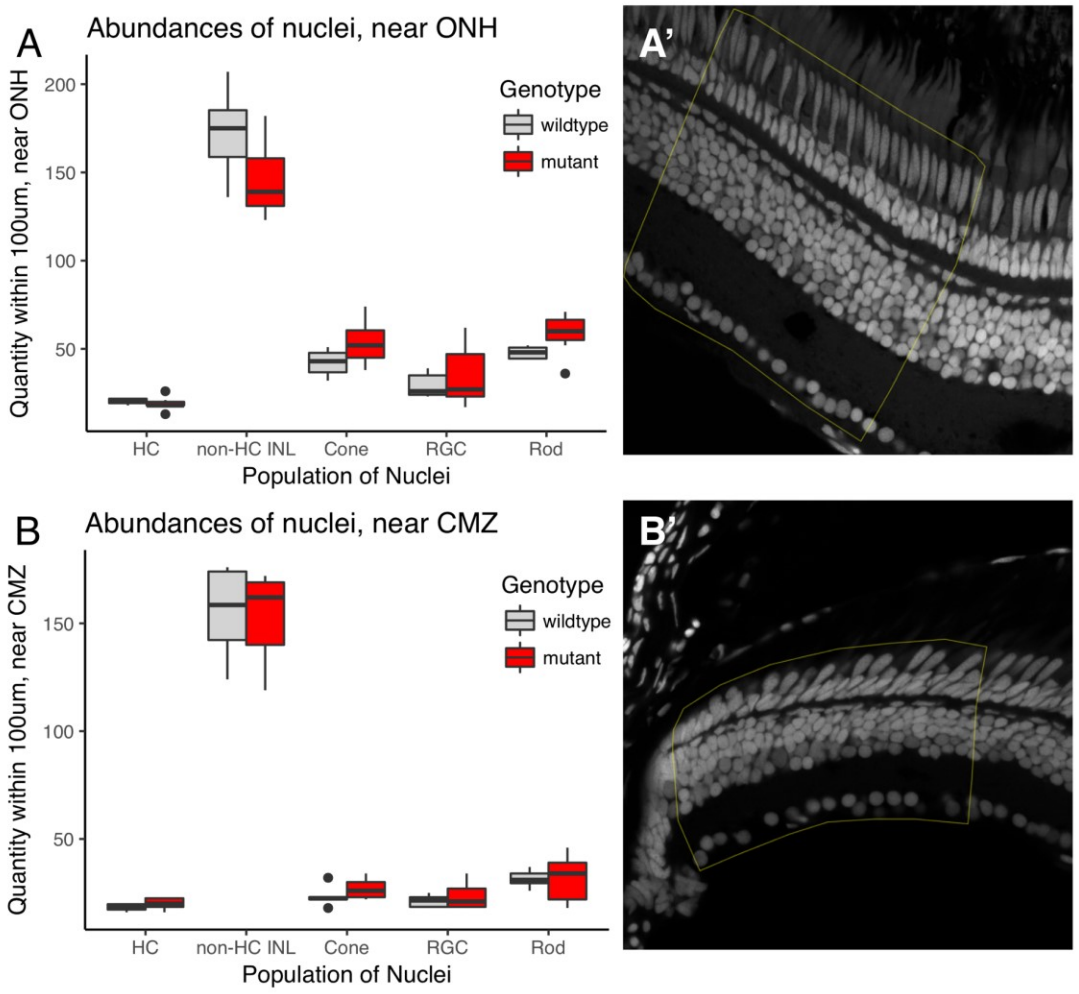

HC: horizontal cell nuclei
Non-HC INL: non-HC inner nuclear layer nuclei
Cone: cone nuclei (including UV nuclei)
RGC: retinal ganglion cell nuclei
Rod nuclei: non-UV cone nuclei in rod nuclear layer

W stat	Raw P-value	Cell Counted	Location
29.5	0.24783380	HC nuclei	CMZ
12.5	0.24449342	HC nuclei	Near ONH
17.0	0.61659056	INL nuclei	CMZ
8.0	0.07342657	INL nuclei	Near ONH
30.0	0.21690111	ObvC nuclei	CMZ
33.0	0.10139860	ObvC nuclei	Near ONH
24.0	0.71685536	RGC nuclei	CMZ
20.0	0.74490219	RGC nuclei	Near ONH
22.0	0.94297842	rod nuclei	CMZ
35.5	0.04490778	rod nuclei	Near ONH

Figure 4.S12: There are no overt changes in retinal neuron populations between adult *nrl* mutant zebrafish and adult wildtype zebrafish.

(**A, B**) Radial sections selected for analysis were 10μm thick cryosections, cut parallel to the nasal-temporal axis of the eye, transecting the optic nerve head. (**A**) Counts of various nuclei from a region of the retina delineated by measuring a continuous 100μm along the outer plexiform layer from a point not more than 50μm away from the optic nerve head (ONH), chosen to minimize retinal curve within the counting boundary. (**A'**) A representative image of a wildtype retina, near the ONH, depicting a counting boundary (**B**) Counts of various nuclei from a region of retina delineated by measuring 100μm along the outer plexiform layer from its start at the ciliary marginal zone (CMZ), and then drawing a box that takes retinal curve into consideration. Counts were made on the basis of a single 0.58 μm thick optical section, captured from a 10μm thick cryosection of adult wildtype or *nrl* mutant zebrafish. (**B'**) A representative image of a wildtype retina at the CMZ, depicting a counting boundary. Wilcoxon rank sum tests of each population of neurons by genotype reveal no significant differences after Bonferroni correction for multiple comparisons. n = 6 wildtype and 6 *nrl*$^{-/-}$ mutants. Free floating dots are statistical outliers.

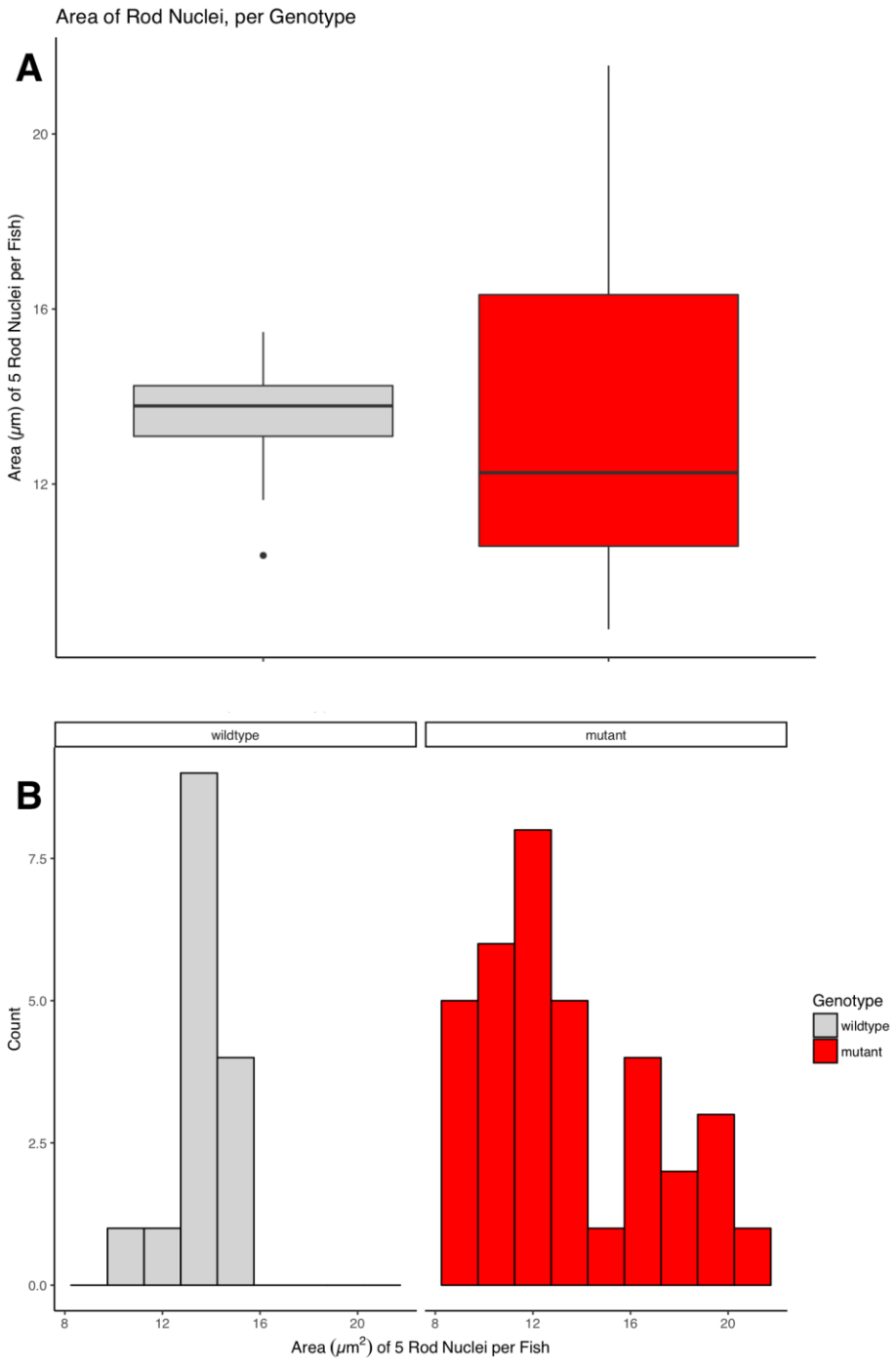

Figure 4.S13: *nrl* mutant rod nuclei are not overtly larger than wildtype rod nuclei. Radial sections selected for analysis were 10μm thick cryosections, cut parallel to the nasal-temporal axis of the eye, transecting the optic nerve head. The area of 5 nuclei per animal was quantified near the optic nerve head, and reported for 3 wildtype and 6 mutants. Mann-Whitney U rank sum test indicates no difference between genotypes (W

= 213.5, p-value = 0.2996) when examined as single populations per genotype (**A**), although the mutant data are bimodal and contain a larger subpopulation (**B**). Free floating dots are statistical outliers.

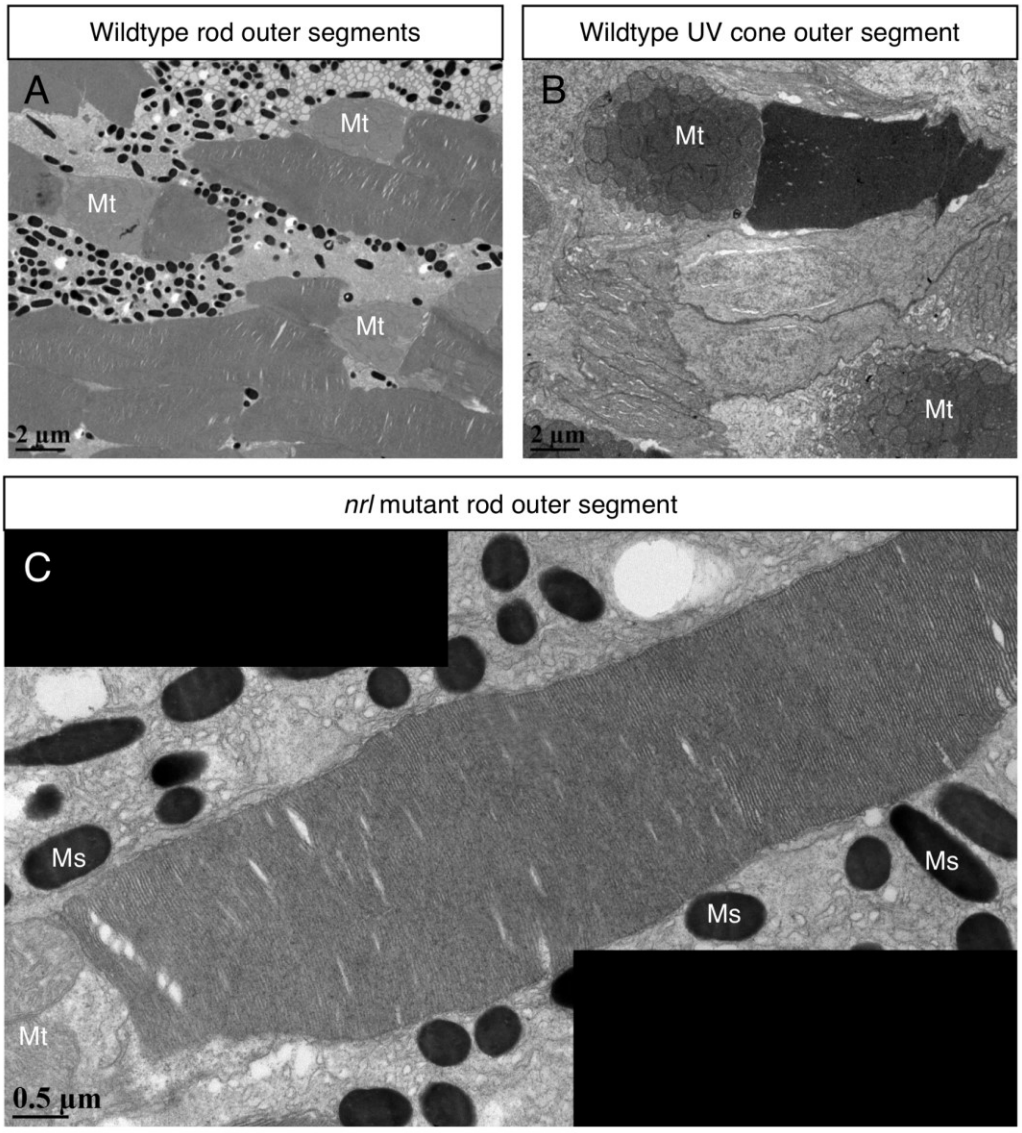

Figure 4.S14: The outer segments of rod-like photoreceptors in adult *nrl* mutant zebrafish are long and slender, similar to wildtype rod and not wildtype cone outer segments.

(**A, B**) Representative transmission electron microscopy micrographs of rod (**A**) and cone (**B**) Outer segments, showing that rod outer segments are long and slender, while cone outer segments are wider and shorter. (**C**) A representative rod-like outer segment from an adult nrl mutant zebrafish. Ms, Mt are melanosomes and mitochondria, respectively.

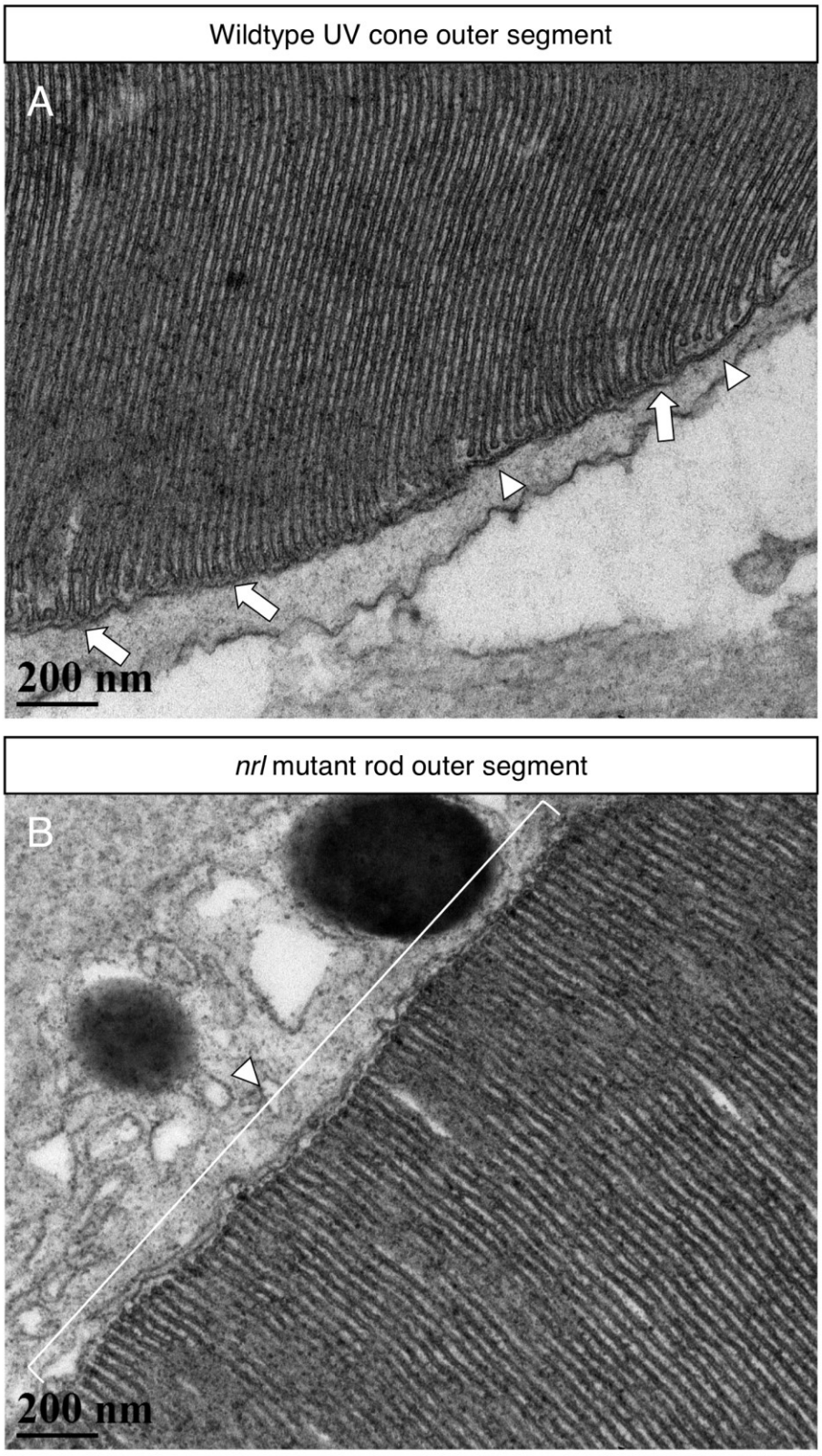
Wildtype UV cone outer segment
A
200 nm
nrl mutant rod outer segment
B
200 nm

Figure 4.S15: The *nrl* mutant rod outer segments do not detectably have cone-like membrane invaginations, nor are the internalized membrane discs in direct contact with the cell membrane.

(**A**) Transmission electron micrograph of a distal region of a representative adult wildtype UV cone outer segment. Arrows indicate points of contact between the cell membrane and the internal membrane structures. Arrowheads indicate internal membrane structures which do not contact the cell membrane. (**B**) Micrograph of a distal region of a representative adult *nrl* mutant rod-like outer segment. The rod-like outer segments did not show detectable membrane invaginations, or points of contact between internal membrane structures and the cell membrane.

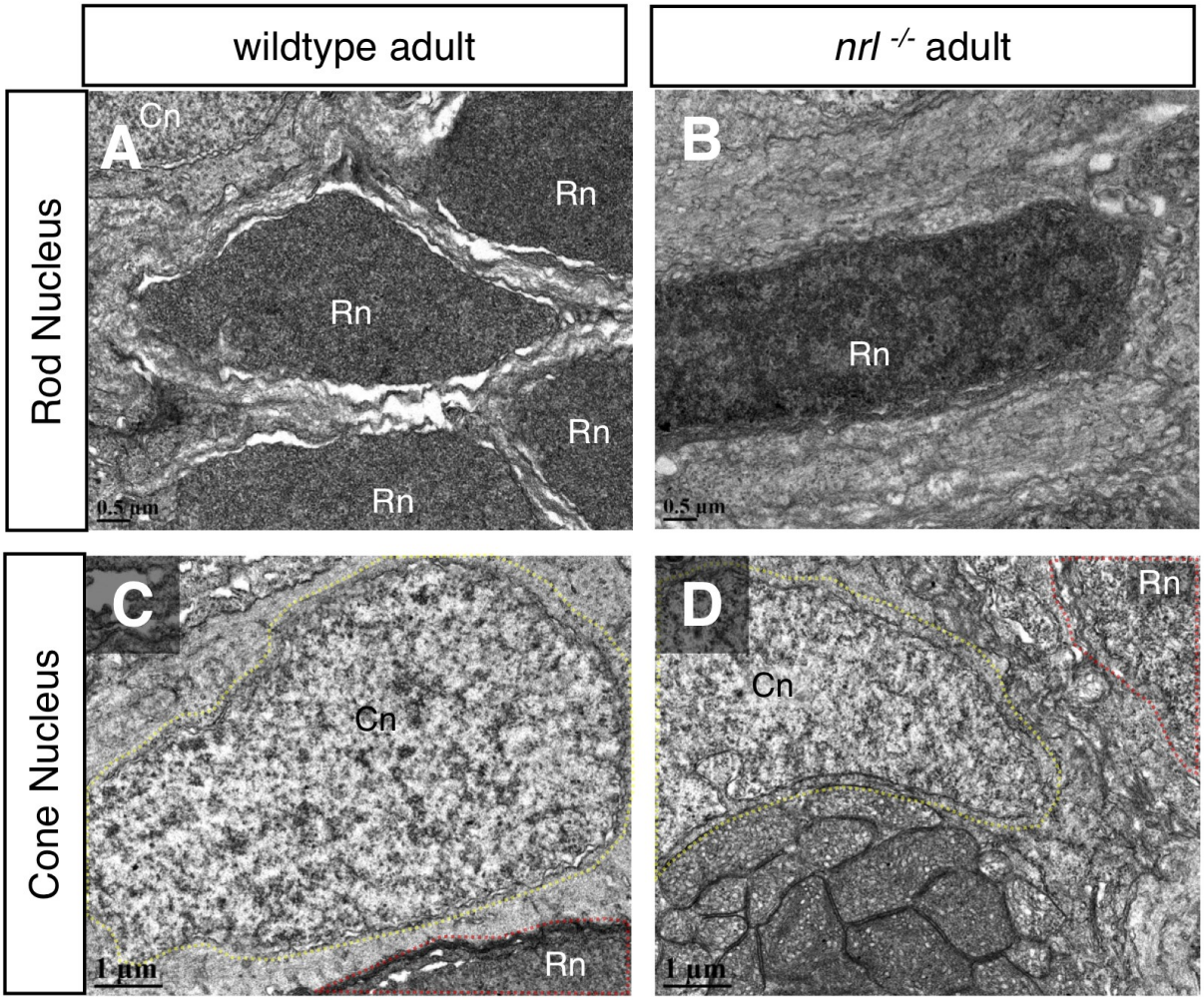

Figure 4.S16: The rods of adult *nrl* mutant zebrafish have a clumped, cone-like chromatin arrangement.

In (**A)**, a homogenous, electron-dense chromatin appearance was characteristic of wildtype rods (37/37 examined, two animals), whereas in (**B**), *nrl* mutant rods had a mottled chromatin appearance (20/26 examined, two animals). A blinded sort of nuclei textures mistook wildtype rods for cones 17.5% of the time (7/40 total wildtype rods assessed), while mutant rods were mistaken for cones 61.5% of the time (16/26 total mutant rods assessed). (**C, D**) Representative wildtype (**C**) and *nrl*$^{-/-}$ mutant (**D**) cone nuclei, showing similar mottled chromatin appearances (Cn, cone nucleus; Rn, rod nucleus).

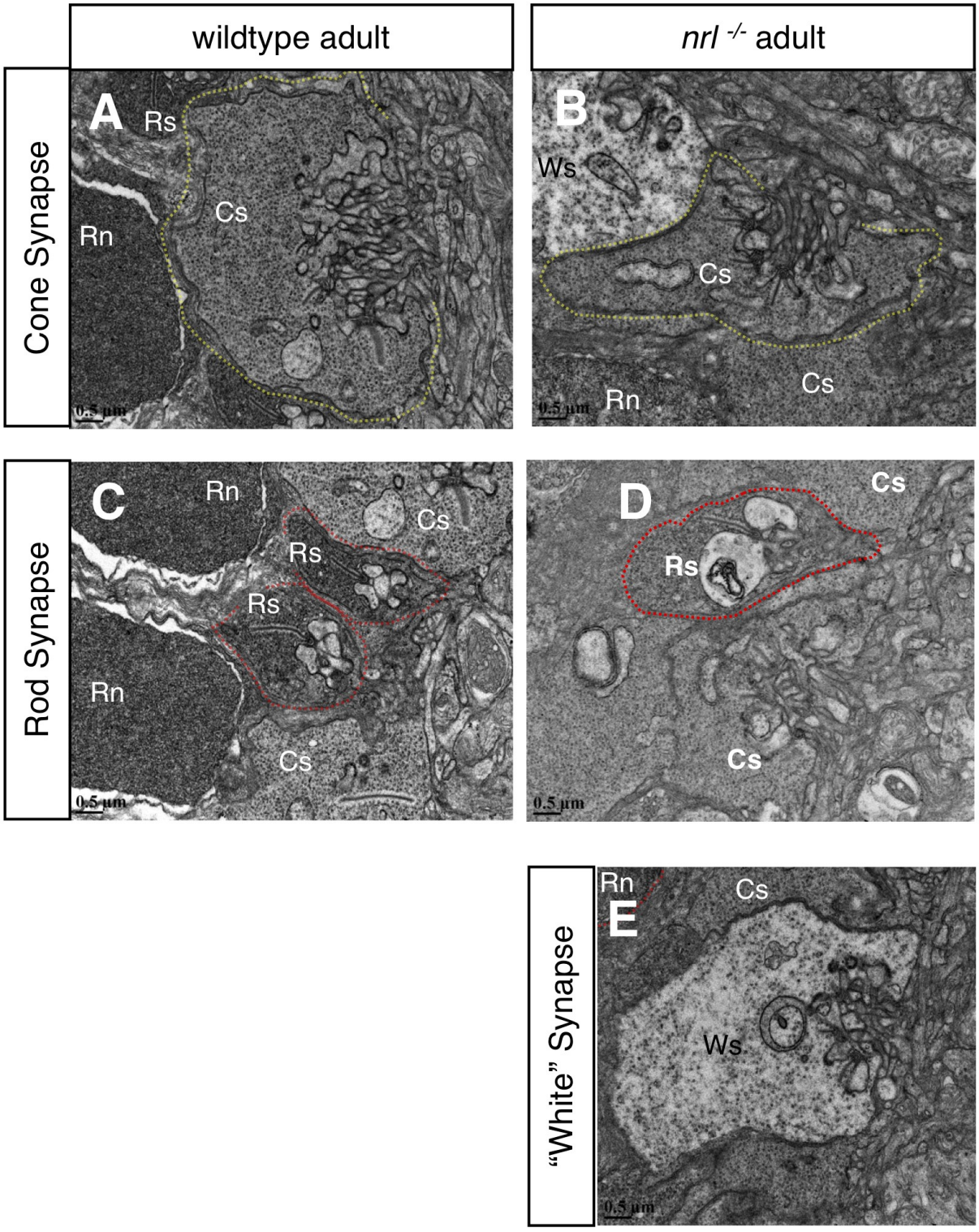

Figure 4.S17: Adult *nrl* mutant zebrafish rods have a dearth of wildtype-like rod synapses.

Representative wildtype (**A**) and *nrl*$^{-/-}$ mutant (**B**) cone synapses, showing typical electrolucency and numerous synaptic ribbons per synapse. (**C**) Representative rod synapses of a wildtype retina, showing sclerad-positioned, smaller, and electron-denser synapses relative to neighboring cone synapses. (**D**) Across two mutants examined, a single wildtype-like rod synapse was found, as defined by relative electron density and slightly sclerad position within the synaptic layer. (**E**) In 1 of 2 mutants examined, numerous large, extremely electrolucent “white” synapses were found interdigitated among cone synapses (characterized in Fig. 4.S18 and 4.S19). Cs, cone synapse; Rs, rod synapse; Ws, white synapse.

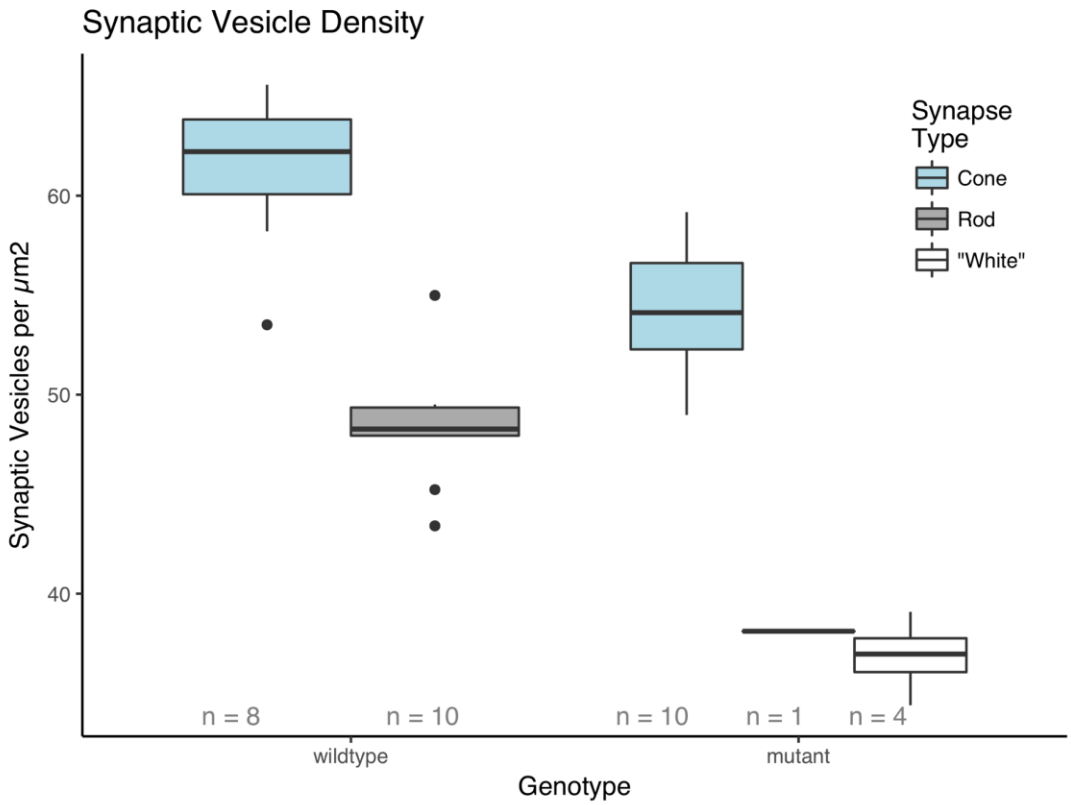

Figure 4.S18: *nrl* mutant adult zebrafish cone synapses have an intermediate synaptic vesicle density relative to wildtype cone and rod synapses, and mutant ”white” synapses and rod synapse have dramatically lower vesicle density. Transmission electron microscopy micrographs of synapses were used to find the total number of synaptic vesicles per section of synapse, then normalized by the area of synapse scanned. Wildtype cone and rod synapses had different synaptic vesicle densities (SVD) (Mann-Whitney U, W = 79, p = 9.141e-5), mutant cone and wildtype cone synapses had different SVD (W = 72, p = 0.003062), mutant cone and wildtype rod synapses had different SVD (W = 9, p = 0.00105), and mutant “white” synapses and wildtype rod synapses had different SVD (W = 40, p = 0.001998). Free floating dots are statistical outliers.

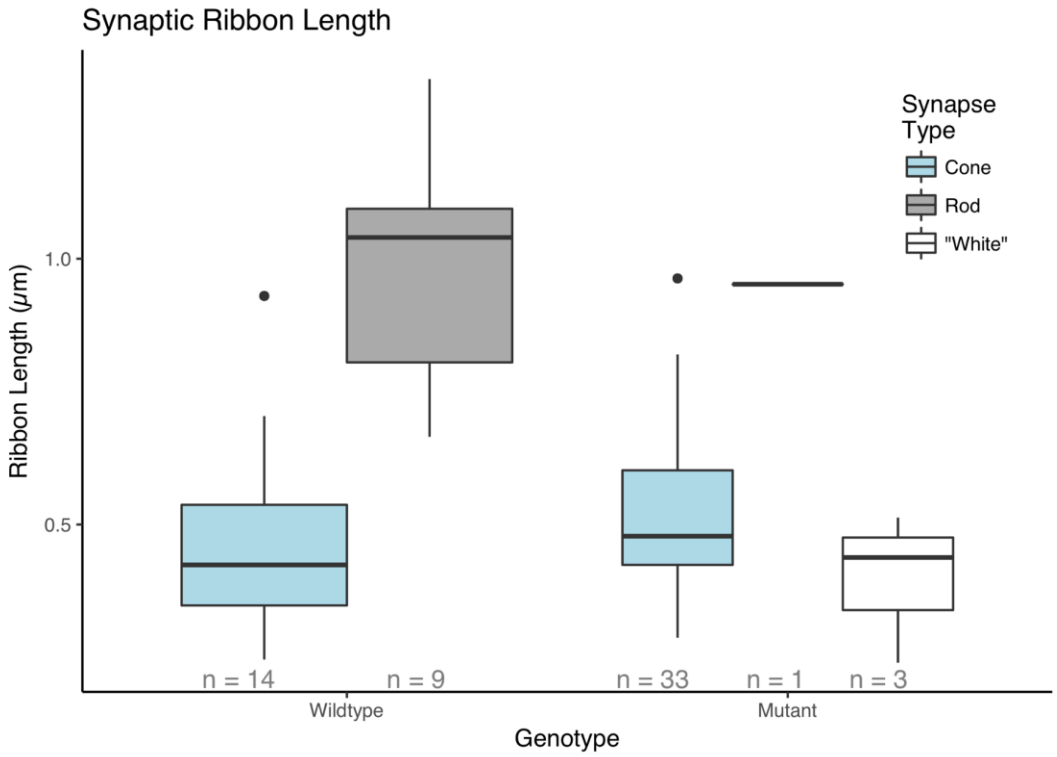

Figure 4.S19: Synaptic ribbons of wildtype cones are the same length as of mutant cones, and ”white synapse” synaptic ribbons are cone-like.
Comparison of lengths of synaptic ribbons in cone, rod, and “white” synapses of two animals per genotype genotypes were compared by Mann-Whitney U rank sum. Wildtype rod ribbons are longer than wildtype cone ribbons (W = 5, p = 4.65e-05). Wildtype and mutant cone ribbons were not different (W = 170.5, p = 0.1593), wildtype cone and mutant “white” synapse ribbons were not different (W = 24, p = 0.7676), and mutant cone and mutant “white” synapse ribbons were not different (W = 71.5, p = 0.2079). Free floating dots are statistical outliers.

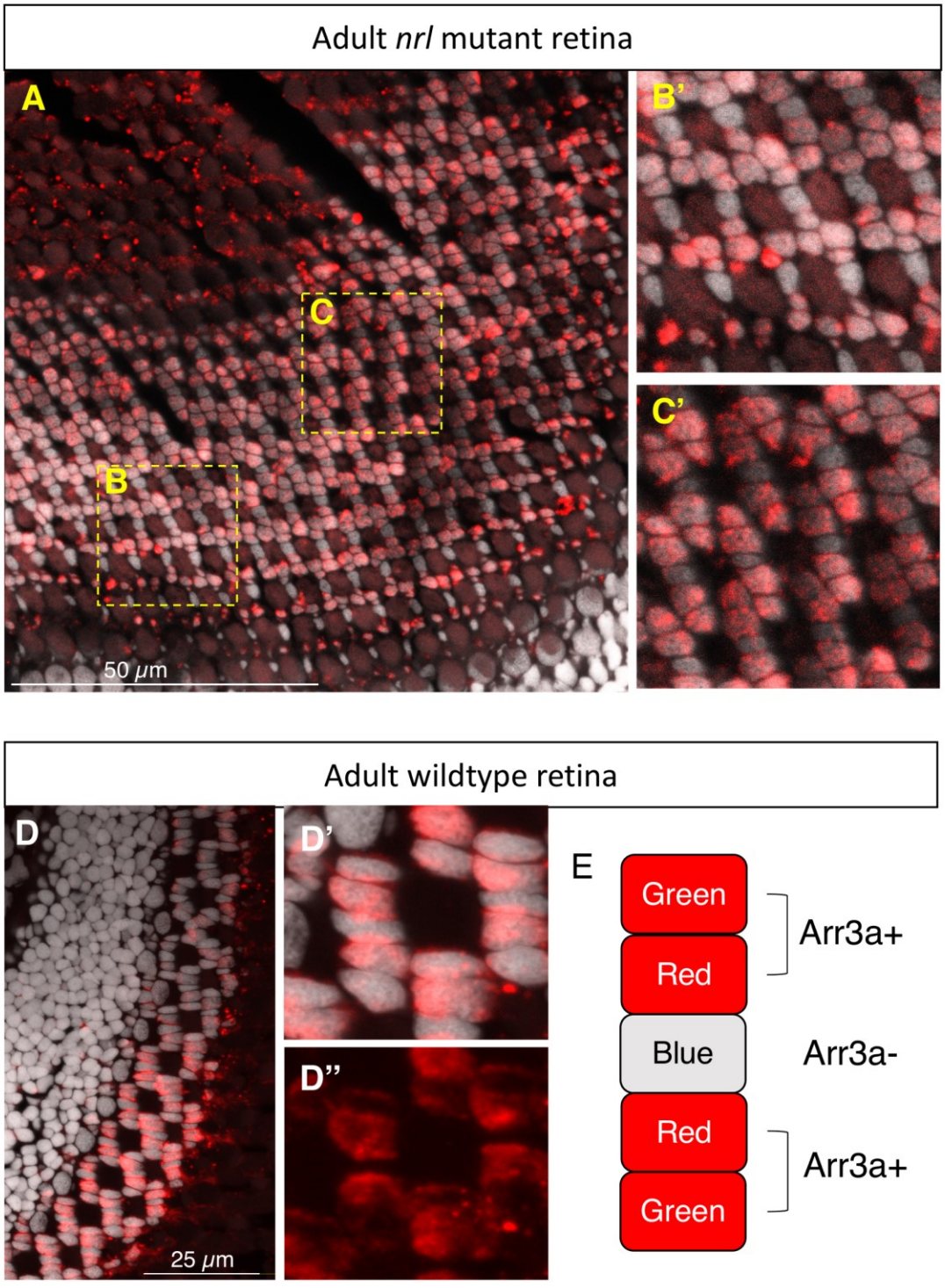

Figure 4.S20: Adult *nrl* mutant zebrafish cone pentamers begin and end in pairs of Arr3a+ cells.

(**A**) Frozen section of an adult *nrl* mutant zebrafish, sectioned tangentially to the photoreceptor layer, revealing the pentameric arrangement of the cone nuclei. Nuclei

stained in DAPI, double cones stained by anti-Arr3a (zpr-1). (**B, C**) Insets of (**A**), selected to demonstrate the staining pattern of anti-Arr3a on the pentamer. (**D**) Representative wildtype adult retina, showing the staining pattern of anti-Arr3a. (**E**) Schematic of the cone subtype make up of the wildtype retina, indicating the identities of the paired Arr3a immunopositive cones in wildtype retinas. The gamma and min/max values of the Arr3a (red) channel were manually adjusted to improve contrast, and to make Arr3a+ cells more distinguishable from Arr3a- cells. Manipulations were performed on the entire image.

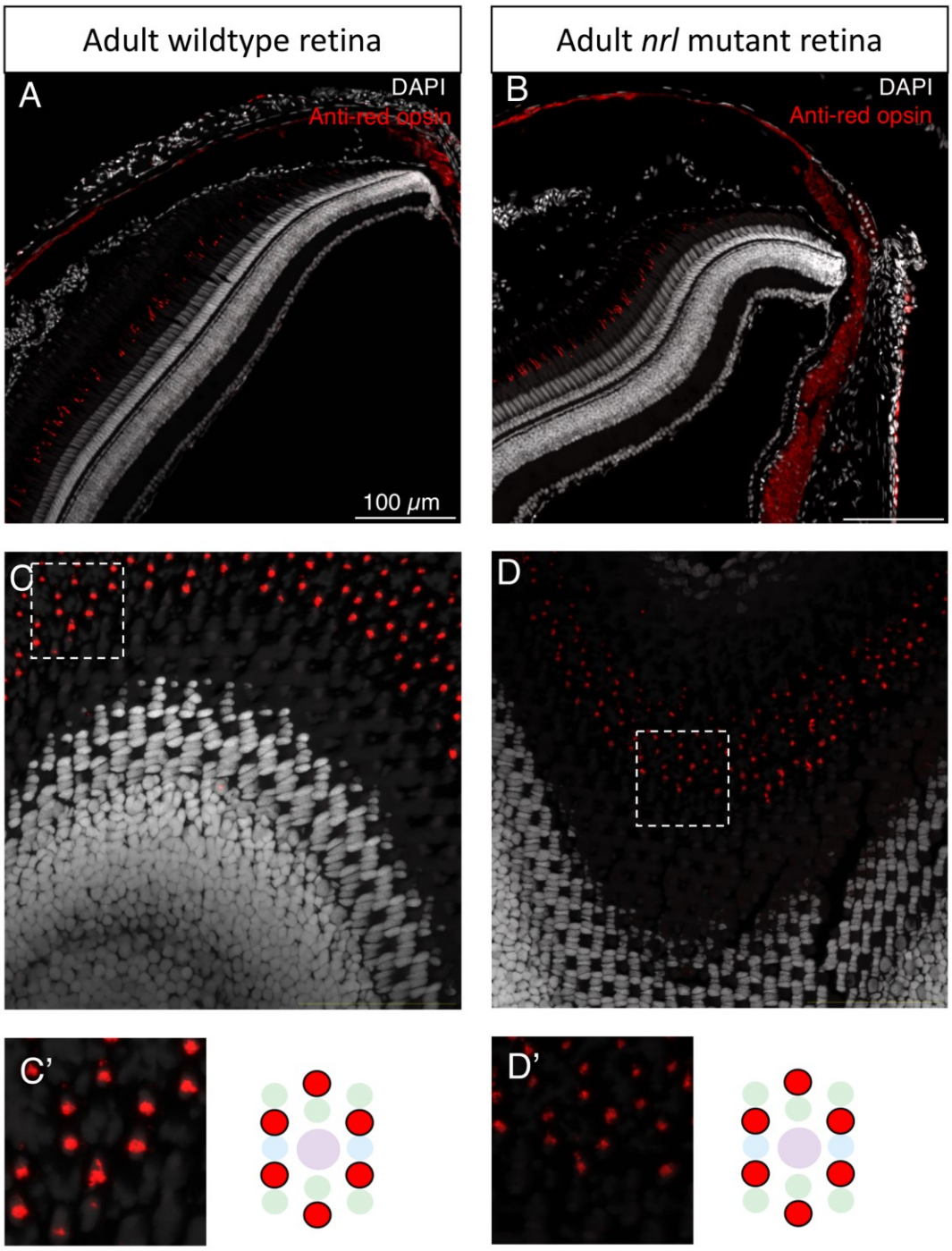

Figure 4.S21: Adult *nrl* mutant zebrafish have normal distributions and proportions of red cone opsin-expressing photoreceptors.

(**A-D**) Frozen sections of adult wildtype (**A, C**) and *nrl* mutant (**B, D**) retinas, with nuclei stained with DAPI and red cone opsin stained with 1D4 antibody. Quantification of red cones along a representative stretch of 100 μm of retina in 3 wildtype and 4 mutants (**A,**

B) showed no difference in red cone abundances (wildtype mean 20 red cones, standard deviation 3; mutant mean 17.25, standard deviation 2.5, Mann-Whitney U p-value = 0.2801). Examination of the red cone mosaic in wildtype (**C**) and mutant (**D**) shows a standard arrangement of red cones in *nrl* adult mutants.

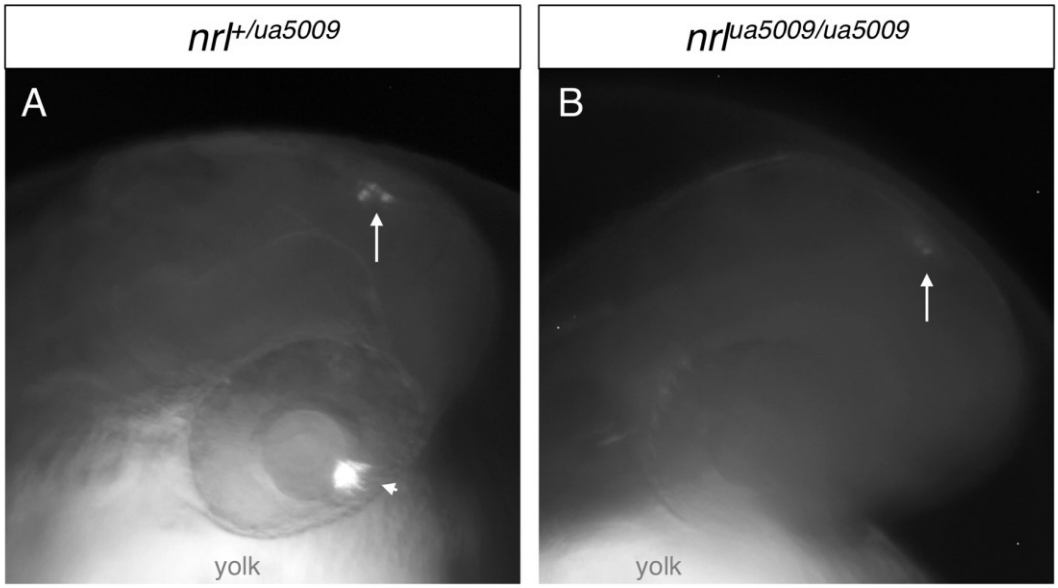

Figure 4.S22: *nrl* mutant larvae show *rh1:eGFP* expression in the pineal gland at 2dpf, similarly to sibling.

Fluorescent stereomicroscopy image of 2 day old zebrafish larvae, (**A**) sibling, or (**B**) *nrl* mutant, bearing *rh1:eGFP*. While the *rh1:eGFP* expression is weaker in the *nrl* mutant, it is nevertheless present briefly (not visible 3dpf or later), and sorting larvae with a chance to inherit *rh1:eGFP* at Mendelian ratios of inheritance yields adult animals with *rh1:eGFP* expression. Arrows: eGFP expression from *rh1:eGFP* in the pineal gland. Arrowhead: eGFP expression from *rh1:eGFP* in the nascent ventral patch of rod photoreceptors. Note that the yolk shows in these images as autofluorescence in the eGFP channel.

A

Peptide Grouping	Ensembl peptide name :
MAFB group	ENSDARP00000018087.5
	ENSDARP00000099244.2
MAFA group	ENSDARP00000064832_4
NRL group	ENSDARP00000132985.1
c-MAF group	ENSDARP000000101942.3
	ENSDARP00000108952.2

B

Zfin gene name and ID:	Mammalian homolog gene name	Webpage link:	Larval gene expression assessment:	Comment:
mafba **ZFIN ID: ZDB-GENE-980526-515**	*MafB*	https://zfin.org/ZDB-GENE-980526-515	Rhomomeres[1], lens[2],	No Thisse expression data. Knockout generated (Koltowska2015)
mafbb **ZFIN ID: ZDB-GENE-010605-4**	*MafB*	https://zfin.org/ZDB-GENE-010605-4	Possibly lens, mostly somites[3]. Primitive myeloid blood cells (gene named *krml2*)[4]	No data from later developing embryos (which have eyes with photoreceptors)
mafa **ZFIN ID: ZDB-GENE-010605-2**	*C-Maf* (not *MafA*)	https://zfin.org/ZDB-GENE-010605-2	Lens[2]	Aka. C-maf (one of two paralogs; see mafb for other paralog)
mafaa **ZFIN ID: ZDB-GENE-010605-3**	*MafA*	https://zfin.org/ZDB-GENE-010605-3	Trunk[3]	This is the homolog of chicken MAFA
mafb **ZFIN ID: ZDB-GENE-141211-38**	*C-Maf* (not MafB)	https://zfin.org/ZDB-GENE-141211-38	Expression unknown	Aka. C-maf (one of two paralogs; see mafa for other paralog)

Figure 4.S23: A list of the *maf* genes considered in this study

(**A**) Summary of the zebrafish long Maf peptides with the reference peptide sequence used to generate the Maf phylogeny of Figure 3.7B. These peptide names (ENS = ensembl; DAR = **Da**nio **r**erio; P = peptide) are the names from a peptide database hosted by Ensembl. (**B**) To identify possible *maf* genes which may plausibly be able to rescue *nrl* loss of function to produce adult *nrl* mutant rods (see Fig. 4.4), an overview of the expression information for all identified zebrafish long *mafs* was constructed. [1](Wada et al., 2005), [2](Nakayama et al., 2008) , [3](Thisse and Thisse, 2004), [4](Gomez et al., 2009).

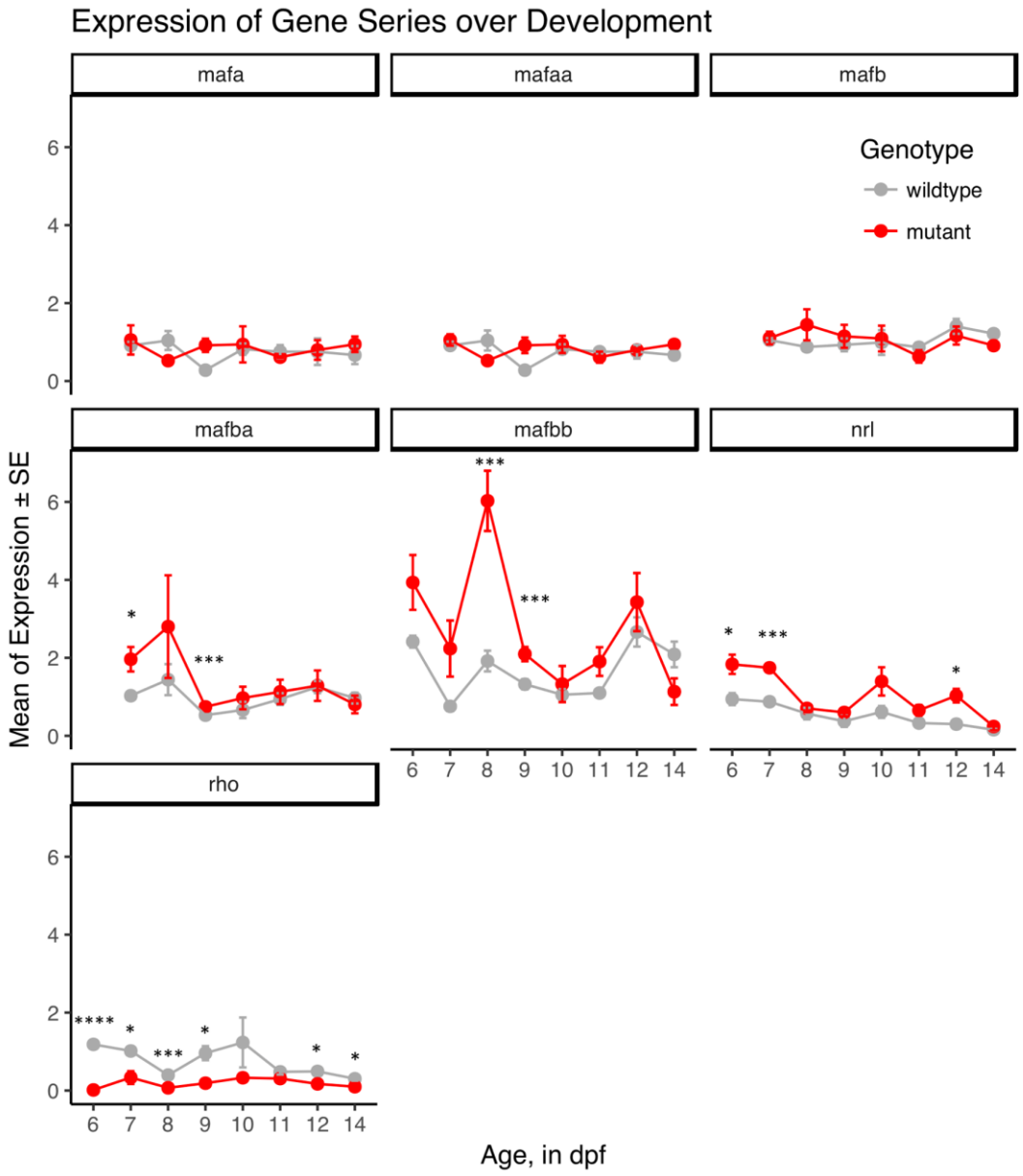

Figure 4.S24: Larval *nrl* mutant zebrafish show dynamic changes in *mafaa* and *mafbb* expression over developmental time.

Total RNA from whole animals was extracted from 5 larvae per biological replicate, with n = 3 replicates, per time point. Data are presented without normalization. p-values: * $p < 0.05$, *** $p < 0.01$, **** $p < 0.001$.

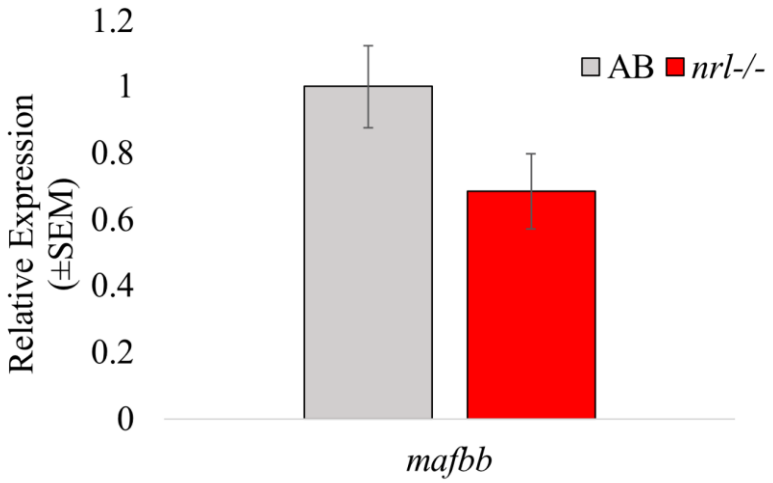

Figure 4.S25: *mafbb* transcript abundance was not significantly different from wildtype in adult *nrl* mutant zebrafish retina.

Neural retina was isolated from dark-adapted zebrafish eyes, and qPCR was performed on cDNAs from extracted total RNA. By Mann-Whitney U test, there was no significant difference in *mafbb* transcript abundance between wildtype and mutant retinas, n = 5 per genotype, p = 0.1681.

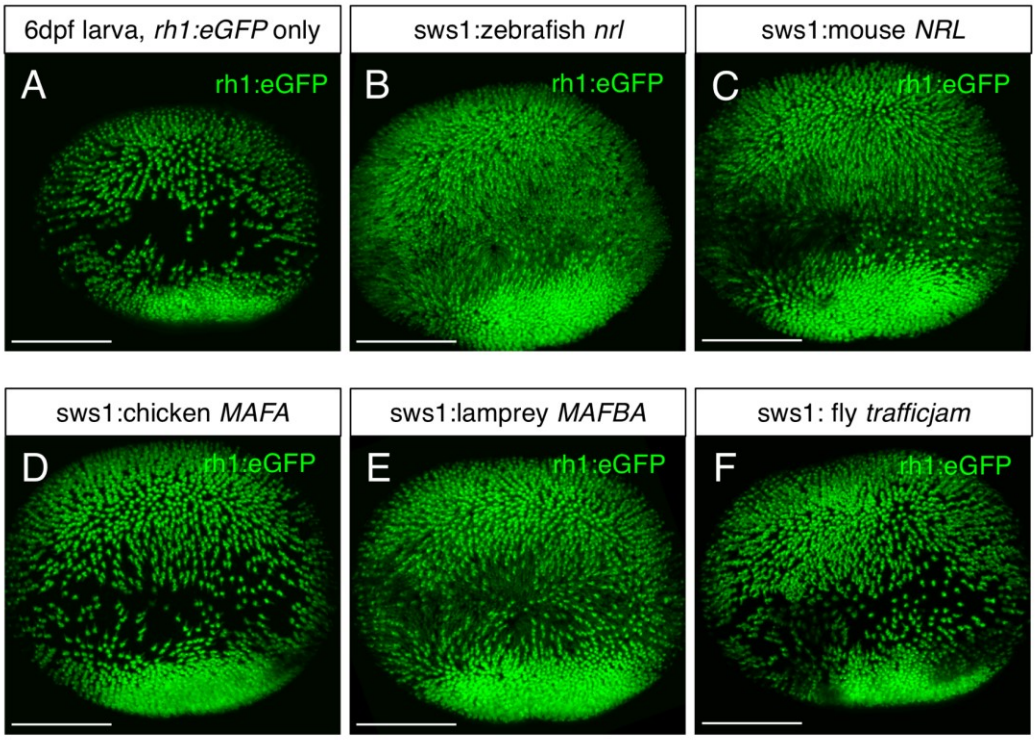

Figure 4.S26: Expression of the rh1:eGFP reporter construct can be activated in UV cones by various *nrl* homologs, but not by chicken *MAFA* or *Drosophila trafficjam*.

(**A-F**) 6 day old zebrafish larvae ectopically expressing the indicated *nrl* homolog in UV cones using *sws1* promoter sequences, as well as eGFP under control of the *rh1* promotor sequences. eGFP signal is apparent in UV cones of animals expressing zebrafish (**B**), mouse (**C**), and lamprey (**E**) *nrl* homologs, but not chicken (**D**) or *Drosophila* (**F**) homologs. Scale bars are 100 μm.

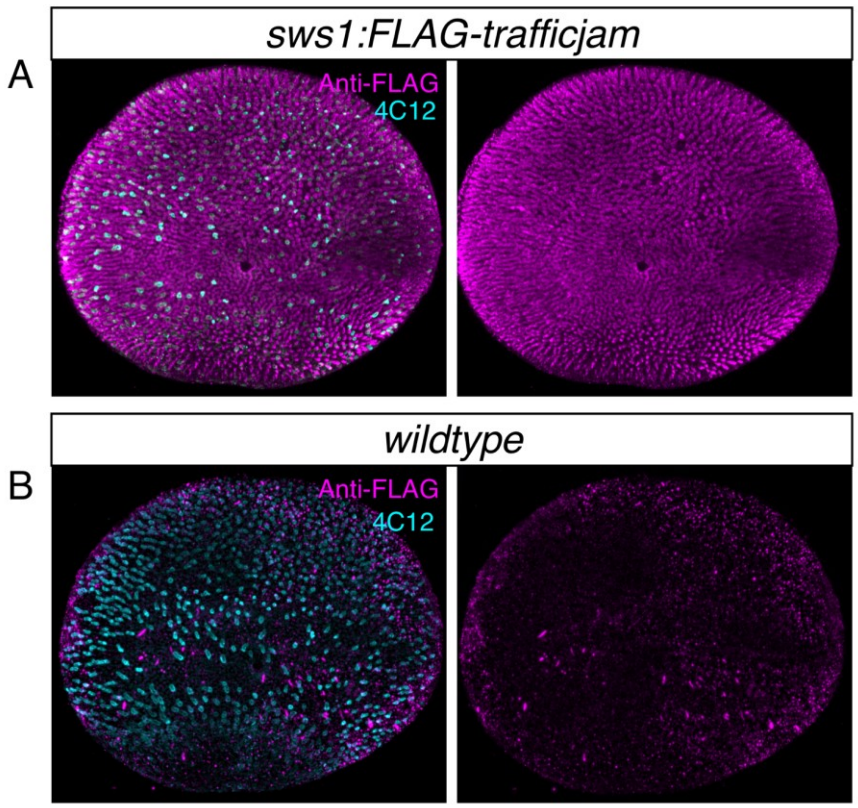

Figure 4.S27: Trafficjam protein is abundantly expressed in zebrafish UV cones via the transgene *sws1:FLAG-trafficjam,* at 6 days post fertilization.

(**A**) Transgenic and (**B**) non-transgenic sibling larvae, stained with 4C12 (rod-specific) and anti-FLAG tag.

Peptide	Reference Sequence Used	Modifications	Transgene identifier
Zebrafish Nrl	(NCBI) NP_001035421.1	Zebrafish codon-optimized Silent mutations	ua3172
Mouse NRL	(NCBI) NM_001136074.2	3xFLAG tag (N-terminal) Zebrafish codon-optimized Silent mutations	ua3174
Chicken MAFA	(NCBI) NM_205025.1	As above	ua3176
Lamprey MAFBA	Peptide ENSPMAP00000004970 in ftp://ftp.ensembl.org/pub/release-83/fasta/petromyzon_marinus/pep/ as published in Table S1, (Kim et al., 2016b)	As above	ua3175
Drosophila Trafficjam	(NCBI) NM_001273653.1	As above	ua3179
Zebrafish Mafk	(NCBI) BC096990.1	3xHA tag (N-terminal) Zebrafish codon-optimized Silent mutations	No stable insertion isolated

Table 4.1 List of reference sequences used for cloning *nrl* homologs and crafting transgenic tools.

All raw coding sequences were modified from their natural reported state due to nucleotide composition requirements from IDT, the company used to generate full-

length cDNAs with Gateway-compatible attB sites (“gBlock Gene Fragments”). Optimizing for zebrafish codon usage addressed most nucleotide composition requirements, but additional silent mutations in the wobble position of numerous codons was necessary before the fragments could be synthesized. The predicted peptides in all cases are wildtype sequences, with FLAG or HA tags where indicated.

4.6 Materials and Methods

4.6.1 Peptide alignment

Peptides listed in Table 4.1 were aligned via ClustalW in Geneious version R9.1.7 (Biomatters Ltd., Auckland, New Zealand) using a BLOSUM cost matrix (gap cost 10, gap extend cost 0.1), and distances computed as percent identity were recorded as "full alignment" on Fig. 4.S2.

For bZIP domain alignment, all peptides were first submitted to NCBI Conserved Domain Search utility (https://www.ncbi.nlm.nih.gov/Structure/cdd/wrpsb.cgi) with default settings; the resulting calls (pfam03131 bZIP_Maf, in Drosophila Trafficjam, lamprey MAFBA, mouse NRL, and human NRL; cd14718 bZIP_Maf_large in zebrafish Nrl and chicken MAFA, and cd1417 bZIP_Maf_small in zebrafish Mafk) were aligned for the full peptides. Within the full-peptide alignment, the Drosophila Trafficjam bZIP domain was the longest contiguous annotated sequence in the alignment, so all residues per peptide in a column mapped to that region (see Fig. 4.S1A) were extracted individually and re-aligned with the same parameters as the full peptide alignment (above).

For MafN+Minimal Transactivation Domain, after full peptide alignment, all residues per peptide that mapped to within the human NRL annotated Minimal Transactivation Domain (Friedman et al., 2004), and to the end of the pfam08380 Maf_N domain as annotated to the human NRL, were separately extracted and re-aligned with the same parameters as above, omitting zebrafish MafK.

4.6.2 Construct cloning

For the creation of expression plasmids featuring zebrafish and mouse *nrl*, chicken *MAFA*, lamprey *MAFBA*, *Drosophila trafficjam*, and zebrafish *mafk*, the peptide sequences listed in (Table 4.1) were imported into Geneious version R9.1.7, and there appended with attB1 and attB2r flanking sequences. A Kozak sequence was encoded, and then a 3xFLAG or 3xHA tag, where indicated, was added to the 5' end of the gene

in place of the endogenous starting methionine, and the full sequence was ordered as a gBlock Gene Fragment from IDT Integrated DNA Technologies (Coralville, Iowa). Where applicable, (indicated in Table 4.1), silent mutations were engineered into the CDS of the various peptides in order to optimize for zebrafish codon bias and to circumvent nucleotide composition/complexity requirements; in all cases, the predicted peptide produced is wholly wildtype aside from the relevant N-terminal tag. Received gBlocks were then processed for Multisite Gateway Cloning using the zebrafish Tol2Kit reagents (Kwan et al., 2007) and Gateway system (Life Technologies), and were ultimately recombined with regulatory sequences of p5E-sws1 (Takechi et al., 2003) and a p3E-polyA sequence into an expression vector. The expression vector backbone pDestTol2CG2 has a cmlc:eGFP reporter that drives eGFP expression in the heart muscle cells, to aid in identifying transgenic fish.

For the creation of Cre recombinase expression constructs, the CDS of Cre recombinase was ordered with flanking attB sites from IDT as a gBlock, and cloned as above in front of p5E-sws1 and p5E-gnat2 promoter plasmids using Tol2kit and Gateway reagents. We never recovered a recombinase-active stable sws1:cre insert. The p5E-gnat2 promoting sequence gateway element (STAR methods) was a kind gift from Dr. Rachel Wong of the University of Washington, USA.

For *nrl* riboprobe production, an amplicon corresponding to the first 972nt of *nrl* mRNA was amplified from whole retina cDNA library, with 5' *HindIII* and 3' *KpnI* restriction enzyme site extensions. Digestion was with FastDigest enzymes (ThermoFisher). Double-digested fragment was ligated to pCS2+ plasmid backbone digested with the same enzymes. The resulting plasmid sequence was confirmed by direct sequencing. Plasmid was prepared for T3 (anti-sense) or T7 (sense) *in vitro* transcription by *NotI* digestion to linearize the plasmid. Riboprobes were produced with T7 or T3 RNA polymerase (Roche), and specific yield of riboprobe was confirmed by gel electrophoresis.

4.6.3 Morpholino and Plasmid injection

Morpholino: single cell embryos bearing rh1:eGFP and either sws1:nfsb-mCherry or sws2:nfsb-mCherry were injected with 10ng of standard control (CCT CTT ACC TCA GTT ACA ATT TAT A) or nrl splice-blocking morpholino (ACG TGT CAG ATC ATA CCT GTG AAG T) (Genetools, LLC, Philomath, Oregon), delivered to the yolk as a 5nL bolus. Morpholinos were first suspended in water and then diluted into 0.1M potassium chloride with 0.1% phenol red added to assess injection success. Morphants were reared to 4dpf, euthanized, and then processed for retinal mounting and imaged. Plasmid: Injection mixtures were prepared by diluting 750ng plasmid construct and 250ng Tol2 mRNA into 0.1M potassium chloride with 0.1% phenol red to a total volume of 10 µL. 5-10nL were delivered to the yolk of the single cell embryo. Injected animals were raised to 2 dpf, and then inspected for eGFP-expressing heart cells, the marker of stable integration of pDestTol2CG2 backbone plasmids. Larvae with GFP-expressing heart cells were reared to adulthood, and germline transmissible transgenes sought in the next generation.

4.6.4 CRISPR mutagenesis

nrl^{ua5014} was established using a mixture of three guide RNAs targeting the first coding exon of zebrafish nrl, before the start of the aligned Minimal Transactivation Domain as identified in humans (Friedman et al., 2004), designed in Geneious R9.1.7 and synthesized per Gagnon and colleagues (Gagnon et al., 2014), but using mMessageMachine SP6 kit (Invitrogen). The guide RNAs were mixed with protein Cas9 (NEB), allowed 5 minutes at 37ºC to assemble into ribonucleoprotein complexes, and the mixture was microinjected into the cell of zebrafish embryos at the 1 cell-stage. Injected animals bore the rh1:eGFP transgene. Animals at 2dpf were sacrificed for high-resolution meltcurve (HRM) analysis of *nrl* cutting (STAR methods for primers; methods as previously described (Fleisch et al., 2013; Pillay et al., 2013). Despite numerous nrl variants detected in injected animals, rh1:eGFP positive cells did not obviously become scarcer in injected larvae, and detecting germline transmitted nrl mutations proved

inefficient. The *nrl*^{ua5014} allele was eventually recovered from this mutagenesis experiment.

For *nrl*^{ua5009}, the 5'-most guide RNA used above, and a second guide RNA targeting eGFP (CR.GFP.GA5'.break, STAR methods) were mixed together and allowed to complex with protein Cas9. This mixture was microinjected into the cell of 1 cell-stage zebrafish embryos, bearing the ubi:eGFP transgene (STAR Methods), which promotes eGFP expression in all cells. At 2dpf, a subset of animals with disrupted eGFP were checked for nrl mutation, and the remainder of eGFP-disrupted fish were reared to adulthood and visually screened for germline transmission of mutant eGFP (carriers had no eGFP fluorescence, but the transgene bears a cardiac-expressed RFP marker cassette (Fraser et al., 2013)). Fish with germline CRISPR editing were then checked for germline-transmitted nrl mutation, the *nrl*^{ua5009} allele was recovered, and ubi:eGFP^{mutant} was bred out in subsequent generations.

For *mafbb*, which like all other non-nrl zebrafish long *maf*s exists in the genome as a single coding exon, two guide RNAs (STAR methods) were designed to have minimal predicted cutting efficiency on other *maf* loci in Geneious R9.1.7. These were mixed, allowed to complex with protein Cas9, and injected into the cell of 1 cell-stage *nrl*^{ua5009} homozygous mutant embryos bearing the rh1:eGFP transgene. Injected adults were screened as adults for regions rod-free retina, predicted to be *mafbb*$^{-/-}$*; nrl*$^{-/-}$ mosaic cells, using eGFP as a marker for rods, but we did not recover any phenotypes of note (data not shown).

4.6.5 Genotyping RFLP for *nrl*^{ua5009} and *nrl*^{ua5014}

The *nrl*^{ua5009} allele introduces a *TaqI* restriction enzyme cut site. To genotype, PCR amplification of 675bp of *nrl* sequence, using primers listed in STAR Methods table, was performed from genomic DNA extracted from finclips of larval or adult tail fin biopsies (Meeker et al., 2007). PCR parameters: 96ºC 2min, 35x [56ºC 15s, 72ºC 1min, 96ºC 15s], 72ºC 5 minutes. PCR product was digested with *TaqI* restriction enzyme (STAR Methods) for 30min at 65ºC, then results of digestion were analyzed by gel electrophoresis; the *nrl*^{ua5009} allele is cloven into two products.

The *nrl*^{ua5014} allele is not cut by *TaqI*, but the 109bp insert causes the mutant PCR product to be visibly shifted away from wildtype amplicons by gel electrophoresis, when run on 3% agarose gel at the slowest possible setting for an hour, and then a faster setting until the bands are resolvable.

4.6.6 Wholemount immunostaining

Larvae were anaesthetized before fixation with 4% paraformaldehyde in 0.1M phosphate buffer with 5% sucrose pH 7.4; fixation was at room temperature for at least two hours, or overnight at 4ºC. Fixed larvae were washed from PFA with phosphate buffered saline pH 7.4 with 0.1% Tween20 ("PBSTw"), then prepared for immunohistochemistry. Fish were washed in pure water 5 minutes, -20ºC acetone for 7 minutes, rinsed out of acetone with PBSTw + 1.0% DMSO, and then blocked for at least 30 minutes in 10% normal goat serum (ThermoFisher) in PBSTw. Blocking solution was drained away, and primary antibody was applied. Antibody incubations were mixed 1:100 for primary, and 1:1000 for secondary antibodies, and incubated at 4ºC at least overnight. Larvae were washed from antibody over 2x5min and then 2x1hr washes in PBSTw, and then transferred to 70% glycerol in PBSTw until equilibrated. The retinas of equilibrated larvae were then prepared for mounting.

4.6.7 Wholemount larval retinal dissections

For mounting whole retinas, glycerol-equilibrated larvae were relieved of their lenses using electrically-sharpened tungsten wire needles, as previously described (Conrad et al., 1993). After de-lensing, the corneal and scleral tissues covering the retina were cut and folded back, and the retina removed from the socket with the tungsten needles using a scooping manoeuvre. The retinas were then positioned vitreal-side down upon slides, and cover slips positioned upon the scleral side. Excess 70% glycerol was added as a mounting medium, and the slides were then imaged as below.

4.6.8 Cryosectioning and immunocytochemistry

Larvae were sacrificed and fixed as for wholemount immunostaining. After PFA was washed away, the fixed larvae were subjected to a graded series of sucrose washes, from 5% to 20% sucrose in 0.1M phosphate buffer, and cryoprotected overnight in the final 20% sucrose stage. After, the fixed larvae were transferred to a 2:1 mixture of 20% sucrose buffer : OCT cryosection fluid (TissueTek) for one hour, then transferred to a final 1:1 mixture of the same. After equilibrating to this new buffer, fixed larvae were embedded into plastic molds, frozen at -80ºC for at least two hours, and then sectioned at 10 um thickness. Cut sections were allowed to air dry 30 minutes before storage at -80ºC at least overnight. Retrieved sections were warmed to room temperature over 20 minutes, then washed 3x5min in PBS + 0.1% Tween20 (“PBSTw”) to remove sectioning media residue. Sections were then blocked and stained as for wholemount immunohistochemistry (above), then covered with 70% glycerol in PBSTw as a mounting medium, mounted under a coverslip, and imaged as previously described (Michèle G. DuVal et al., 2014; Kim et al., 2016b).

4.6.9 Custom antibody commissioned for zebrafish Nrl

A custom polyclonal antibody against the C-terminal 112 amino acids of zebrafish Nrl, targeting the entire conserved bZIP domain, was commissioned from Genscript (Piscataway, NJ, USA) in a rabbit host (order ID: 788179-1, lot number A516020016). We were unable to demonstrate specific binding in Western blots or by immunofluorescent imaging of larval and adult retinal sections, both mutant and wildtype (data not shown).

4.6.10 In situ hybridization

In situ hybridization on frozen sections was performed as previously described (Barthel and Raymond, 1993). Briefly, frozen sections were thawed and rehydrated, then immediately re-fixed in 4% PFA to help tissue adhere to slides. Sectioned tissue was digested briefly with proteinase K and then re-fixed with 4% PFA. Sections were then

acetylated with a mixture of triethanolamine and acetic anhydride as previously described, then dehydrated in a graded ethanol series with diluted 2x sodium citrate buffer as previously described. Probes were then pre-hybridized in Hauptmann's buffer, then hybridized at 70ºC to 1µg/mL DIG-labeled riboprobe overnight. Probe was washed off in a graded series of sodium citrate buffer diluted in maleate buffer as previously described. Sections were blocked and then incubated with anti-DIG-conjugated alkaline phosphatase antibody (Roche) at 1:5000 dilution overnight. Alkaline phosphatase chromogen reaction was performed as previously described, terminated with excess alkaline phosphate buffer and subsequent fixation with 4% PFA. Sections were mounted with glycerol. Developed sections were imaged on an Axioscope A.1 microscope (Carl Zeiss MicroImaging, Oberkochen) with 12 bit MacroFIRE camera (Optronics, Goleta, CA, USA).

4.6.11 Confocal and stereomicroscopy

Confocal microscopy was performed with an LSM 700 confocal microscope mounted on a Zeiss Axio observer, located at the Centre for Prion and Protein Folding Diseases, University of Alberta. Images were acquired with ZEN 2010 (v6.0, Carl Zeiss AG, Oberkochen, Germany). Micrographs were taken using 63x oil immersion (numerical aperture of 1.4) and 20x objectives (numerical aperture of 0.8). Images acquired with the confocal microscope were captured with gain adjusted to avoid any empty or saturated pixels, and after acquisition, image minima, maxima, and gamma were adjusted in Fiji (ImageJ, Version 2.0.0-rc-54/1.51h, NIH, Bethesda, MD, USA) to improve contrast. Stereoscopy images were taken as previously described (Duval et al., 2013) using brightfield and fluorescent channels in separate photos. Where relevant (e.g. Fig. 4.S7, 4.S22), brightfield images were converted to grayscale and merged in Fiji with fluorescent channel images to improve GFP visibility.

4.6.12 Transmission Electron Microscopy

Whole larvae, or whole adult eyes with the lenses removed, were fixed overnight at 4ºC. Fixative was 2.5% glutaraldehyde, 2% paraformaldehyde in 0.1M phosphate buffer PH

7.4. Fixative was washed out of the samples, which were then subjected to a graded series of ethanol washes, and then infiltrated with resin and embedded. Samples were then sectioned on a Richert-Jung Ultracut E Ultramicrotome to sections of 70-90 nm thickness. Gridded sections were then stained with uranyl acetate and lead citrate, and imaged at 80 kV on a FEI COMPANY transmission electron microscope, model Morgagni 268 (FEI company, Hillsboro, Oregon). Images acquired with a Gatan Orius CCD camera using Gatan DigitalMicrograph image acquisition software, version 1.81.78 (Gatan, Inc., Pleasanton, CA).

4.6.13 Wholemount larvae photoreceptor quantification

In larval whole mounted eyes, the dorsal-ventral axis is readily apparent while imaging. After confocal imaging, using Fiji image analysis software a 100x100 µm boundary was positioned just dorsal to and centered above the optic nerve head of the retina. Within the delineated box, the *Process>Smooth* function of Fiji tamed wild background pixels, and then the *Process>Find Maxima* function was used to efficiently count fluorescently labeled photoreceptors.

4.6.14 Quantification of adult nuclei in histological sections

To compare the relative abundance of retinal nuclei between adult wildtype and *nrl*$^{-/-}$ mutant zebrafish, a counting region of interest (ROI) boundary was first established, consisting of 100µm measured along the outer plexiform layer in the indicated region (Fig. S12). From this, an ROI boundary was drawn to encapsulate all the nuclei within this stretch, taking into account the bends in the retinal tissue. All nuclei were hand-counted except for the non-HC INL nuclei, which were counted as for wholemount larval photoreceptors (above).
To compare the relative area of rod photoreceptors, within each ROI the 5 largest rod photoreceptor nuclei were selected and measured in Fiji.

4.6.15 Ultrastructural synapse and chromatin appearance quantification

For all quantification and analysis, transmission electron micrographs of synapses and nuclei were imported into Fiji, and analysed as described.

To quantify synaptic vesicle density: A region of interest (ROI) boundary was drawn around a photoreceptor synapse that excluded bipolar and horizontal cell processes. The interior of the ROI was then processed in the following way in Fiji: First, *Process>Subtract Background*, rolling ball radius = 5.0 pixels, “light background”. Next, background pixel noise was suppressed using *Process>Filter>Median*, radius = 1.0 pixel. The image was then thresholded with *Image>Adjust>Threshold*, auto. Finally, *Analyze>Analyze Particles* was used to count particles, with minimum and maximum particle radius set to 0.001 and 0.005µm (based on previous calibration). The area of the total ROI was recorded as the area of the synapse.

To measure synaptic ribbon length: In selecting ribbons to measure, only ribbons with a clear synaptic ribbon “head” were measured; numerous synapses with oblique cut angles showed shadows of synapse ribbons slightly out of plane with the image, and the lengths of these shadows varied considerably (data not shown). Thus, only synaptic ribbons cut *en face* were measured; for example, Fig. 6E shows two ribbons that were measured within the ROI, and a third “shadow” that was not measured; Fig. 6F shows three. The segmented line tool of Fiji was used to trace the length of each ribbon, calibrated to the scale bar in each micrograph.

For blinded sorting of chromatin appearance of wildtype and *nrl*$^{-/-}$ rods: 200x200 pixel boxes were extracted from a representative location from within each nucleus, in order to avoid the nuclear morphology or surrounding structures giving the blinded sorter context clues. Next, *Process>Subtract Background* (50 pixels, light background) was performed in order to neutralize the tint of the nucleus, as mutant rod nuclei were routinely darker (similar to wildtype rods; see Fig. 4.S16A,B), and the intended assay was to sort by chromatin texture alone. Files were coded, and the sorter was given a known (wildtype) cone sample and a known (wildtype) rod sample, then instructed to sort the remaining sample images to group with one or the other.

4.6.16 Statistical Analysis

Statistical analyses and plot generation for larval photoreceptor abundances, synaptic vesicle density and ribbon length, relative abundances of nuclei in retinal sections, and rod nuclear sizes were performed in R (version 3.4.1, R Foundation for Statistical Computing, Vienna, Austria).
All qRT-PCR data is presented as mean ± Standard Error of Mean (SEM) and is standardized to wild type (AB strain) abundances, except in Fig. 4.S24 where relative expression is not standardized. To analyze differences in mean expression between wild type and mutant larvae and retinal tissue, a Mann-Whitney Test was performed using GraphPad Prism (Version 7.02 for Windows, GraphPad Software, La Jolla California USA, www.graphpad.com). Statistical significances are denoted in each respective figure legend.

4.6.17 RNA Isolation and Quantitative real time polymerase chain reaction (qRT-PCR)

Pooled samples of n=10 whole larval zebrafish aged 4-14 days post fertilization (dpf) were collected between 5:30 PM and 6:30 PM Mountain Standard Time (MST) and stored in RNAlater (Ambion) at 4°C until extraction. Total RNA was isolated from each sample using the RNeasy Mini Kit (Qiagen) according to the manufacturer's instructions. Samples were homogenized in 600 µl of Buffer RLT (Qiagen) containing 1% of β-mercaptoethanol (Sigma) with a rotor stator homogenizer (VMR) and put through an “on column” DNAse digestion using DNAse I (Qiagen). RNA concentration was determined by a Nanodrop spectrophotometer (GE Healthcare 28 9244-02) and Agilent 2100 Bioanalyzer (Agilent RNA 6000 NanoChip). For each sample, 500 ng of total RNA was reverse transcribed using qScript cDNA Supermix (Quanta Biosciences) as per the manufacturer’s instructions. cDNA was diluted 1:10 in Nuclease-free H_2O (Ambion) and stored at -20°C until use. Primers were designed using the Primer 3 algorithm in Geneious R.9.1.7(Kearse et al., 2012)) to amplify cDNA products. All primers were validated using a standard serial dilution to determine efficiency under MIQE guidelines (Bustin et al., 2009). Dissociation curves were analyzed in 7500 Software v1.4.1

(Applied Biosystems, 2011) and only single products were detected. *Rpl13a* (for larvae) and *β-actin* (for adult) were used as endogenous control genes for normalization (Fleisch et al., 2013; Tang et al., 2007). Primer sequences can be found in STAR Methods. Each qRT-PCR reaction consisted of 2.5 µL of 3.2 µM primer solution, 5 µL of 2x (*Dynamite*) qPCR MasterMix (MBSU, University of Alberta) and 2.5 µL of cDNA in a 10 µL reaction volume. Technical replicates were performed in triplicate. Biological sample sizes (n>3) are stated for each experiment in respective figure legends. RT-qPCR reactions were run on 7500 Fast Mode (pre-incubation 95°C, 2:00 min; 2 step amplification 95 °C 15s, 60 °C 1:00 min; 40 cycles; dissociation 95°C 15s, 60°C 20s, 95°C 15s, 60°C 15s) using the 7500 Fast Real-Time PCR System (Applied Biosystems). RNA Collection, cDNA synthesis and RT-qPCR on adult retina was performed like larval experiments except the following: *1)* Neural retinae were dissected from adult zebrafish dark adapted for 12 hours between 5:30 PM and 6:30 PM Mountain Standard Time (MST). *2)* Total RNA was isolated from one retina using RNeasy Lipid/Tissue Mini Kit (Qiagen) according to the manufacturer's instructions. Samples were homogenized in 700 µL of Qiazol (Qiagen). *3)* For each sample, 100ng of total RNA was reverse transcribed using qScript cDNA Supermix (Quanta Biosciences) as per manufacturer's instructions.

4.6.18 STAR Methods

Table 4.2: STAR Methods "KEY RESOURCES TABLE"

REAGENT or RESOURCE	SOURCE	IDENTIFIER
Antibodies		
Rat anti-trout UV cone opsin; 10C9.1	(Michèle G. DuVal et al., 2014)	10C9.1; ZFIN ID: ZDB-ATB-140728-2
Mouse anti-bovine rhodopsin; 4C12	(Morris et al., 2005)	4C12; ZFIN ID: ZDB-ATB-090506-2
Rabbit anti-GFP	Invitrogen	Cat#A11122
Rabbit anti-FLAG tag	ThermoFisher	Cat#PA1-984B

Rabbit anti-mouse Nrl	(Kim et al., 2012)	N/A
Rabbit ant-mouse phospho-S50-Nrl	(Kim et al., 2012)	N/A
Goat anti-human NRL	Santa Cruz	Cat#sc-10791 (discontinued)
Rabbit Genscript: anti zebrafish NRL	Genscript	N/A
Rabbit anti-HA tag	Abcam	Cat#ab137838
Mouse anti-Arr3a; zpr-1	ZIRC	Cat# Zpr-1 ZFin ID: ZDB-ATB-081002-43
Alexa Fluor 647 donkey anti-rat	Invitrogen	Cat#A21472
Alexa Fluor 647 donkey anti-mouse	Invitrogen	Cat#A31571
Alexa Fluor 555 donkey anti-mouse	Invitrogen	Cat#A31570
Alexa Fluor 488 donkey anti-mouse	Invitrogen	Cat#A21202
Biological Samples		
Gateway-compatible middle element donor (empty) vector: pDONR221	Tol2Kit; http://tol2kit.genetics.utah.edu/index.php/Main_Page	pDONR221
Multi-site gateway-compatible destination (empty) vector: pDestTol2CG2	Tol2Kit; http://tol2kit.genetics.utah.edu/index.php/PDestTol2CG2	pDestTol2CG2
Gateway-compatible middle element (“pME”) nfsb-mCherry	(Davison et al., 2007)	N/A
Gateway-compatible 5’ element (“p5E”) ubi:loxP-eGFP-loxP	Addgene; (Mosimann et al., 2011)	Addgene#27322

Gateway-compatible 3' element (polyadenylation signal) vector: p3E-polyA	Tol2Kit; http://tol2kit.genetics.utah.edu/index.php/P3E-polyA	P3E-polyA
Gateway-compatible 5' element (*sws1* regulatory sequences) vector: p5E-sws1	(Takechi et al., 2003)	P5E-sws1
Gateway-compatible 5' element (*gnat2* regulatory sequences) vector: p5E-gnat2	(Suzuki et al., 2013)	P5E-gnat2

Chemicals, Peptides, and Recombinant Proteins		
EnGen *S. pyogenes* protein Cas9	New England Biolabs (NEB)	Cat#M0646M
Fast digest TaqI restriction enzyme	ThermoFisher	Cat#FD0674
Fast digest KpnI restriction enzyme	ThermoFisher	Cat#FD0524
Fast digest HindIII restriction enzyme	ThermoFisher	Cat#FD0505
Fast digest NotI restriction enzyme	ThermoFisher	Cat#FD0596
RNase-Free DNase I Set	Qiagen	Cat#79254
2x (*Dynamite*) qPCR MasterMix	Molecular Biology Service Unit (MBSU), University of Alberta	N/A
qScript cDNA SuperMix	Quanta Biosciences	Cat#95048-100
RNAlater RNA Stabilization Solution	Ambion	Cat#AM7020
β-mercaptoethanol	Sigma	Cat#M3148
Nuclease-free H2O	Ambion	Cat#4387936
Critical Commercial Assays		
RNeasy Mini Kit	Qiagen	Cat#74104
RNeasy Lipid Tissue Mini Kit	Qiagen	Cat#74804

DAPI (4',6-diamidino-2-phenylindole) nuclear stain	ThermoFisher	Cat#D1306
TissueTek OCT Compound	Cedar Lane	Cat#62550-12
T7 RNA polymerase	Roche	10881775001
T3 RNA polymerase	Roche	11031171001
Goat blood serum for immunohisto- or cytochemistry	ThermoFisher	Cat#16210064

Experimental Models: Organisms/Strains		
Zebrafish: tg[ubi:lox-GFP-lox-nfsb-mCherry; cmlc:RFP]ua3140: ua3140	This paper	N/A
Zebrafish: tg[sws1:nfsb-mCherry]q28tg : sws1:nfsb-mCh	Yoshimatsu et al. 2016 (Yoshimatsu et al., 2016)	ZDB-ALT-160425-1
Zebrafish: tg[sws2:nfsb-mCherry]q30tg : sws2:nfsb-mCh	D'Orazi et al., 2016 (D'Orazi et al., 2016)	ZDB-ALT-160425-3
Zebrafish: tg[rh1:GFP]kj2 : rh1:GFP	Hamaoka et al, 2002. (Hamaoka et al., 2002)	ZDB-ALT-060830-4
Zebrafish: Tg(sws1:GFP)^{kj9} : sws1:GFP	Takechi, Hamaoka, and Kawamura, 2003. (Takechi et al., 2003)	ZDB-ALT-080227-1
Zebrafish: tg[sws1:zebrafish nr]ua3162 : sws1:nrl	This paper	N/A
Zebrafish: tg[gnat2:cre]ua3162 : gnat2:cre	This paper	N/A

Zebrafish: Tg(ubb:lox2272-loxP-RFP-lox2272-CFP-loxP-YFP)a131 : zebrabow	Pan et al., 2013 (Pan et al., 2013)	ZDB-ALT-130816-2
Zebrafish: tg[sws1:FLAG-mouseNRL]ua3174 : sws1:mouseNRL	This paper	N/A
Zebrafish: tg[sws1:FLAG-chickenMAFA]ua3175 : sws1:chickenMAFA:	This paper	N/A
Zebrafish: sws1:lampreyMAFBA: tg[sws1:FLAG-lampreyMAFBA]ua3176	This paper	N/A
Zebrafish: sws1:trafficjam: tg[sws1:FLAG-DrosophilaTrafficJam]ua3179	This paper	N/A
Oligonucleotides		
Primer: nrl genotyping Forward TGAACAACAGCTTCCAGCGAT	This paper	20160516.NCBI.nrl.E1F
Primer: nrl genotyping Reverse AGCTGTAAAACTTTGCATTCACG	This paper	20160516.NCBI.nrl.E1R
Primer: nrl High Resolution Meltcurve analysis Forward GTAAAGCCTGACACCCCTCC	This paper	N/A
Primer: nrl HRM Reverse CTGGAGCTCAGGCTGGAGT	This paper	N/A
Primer: nrl qPCR Forward AGCCTTCGCATCCCAACA	This paper	N/A
Primer: nrl qPCR Reverse CAGTGTCCGTTCAAGTGTGTCA	This paper	N/A
Primer: nr2e3 qPCR Forward CAACTGCCCTCTGCTGTCTCT	This paper	N/A
Primer: nr2e3 qPCR Reverse CTTGCAGAACCCTCACATCTGA	This paper	N/A

Primer: crx qPCR Forward TCTCCTTACTTCAGCGGATTGG	This paper	N/A
Primer: crx qPCR Reverse CGCCTCCACTTGCTGACA	This paper	N/A
Primer: rorb qPCR Forward CGTGGTTAATGGAGCCTAGAAAA	This paper	N/A
Primer: rorb qPCR Reverse AGCGCATCCTCGTCCAGAT	This paper	N/A
Primer: rhodopsin qPCR Forward CCCTGCCCGCCTTCTT	This paper	N/A
Primer: rhodopsin qPCR Reverse CGGAACTGCTTGTTCATGCA	This paper	N/A
Primer: sws1 qPCR Forward TCCTCCCGCAGCACATTTAC	This paper	N/A
Primer: sws1 qPCR Reverse AAAGTTACGGGATTTGAACAATCAG	This paper	N/A
Primer: tbx2b qPCR Forward TCAACACATGCTTGCCTCTCA	This paper	N/A
Primer: tbx2b qPCR Reverse CTGCCGCGGCCATGTA	This paper	N/A
Primer: mafa qPCR Forward CGAGGAGTCACCAAAGTGTTA	This paper	N/A
Primer: mafa qPCR Reverse ATCCGTGGCACAGTCTATTG	This paper	N/A
Primer: mafaa qPCR Forward TGAACTGAGGTTGAGGGGACTTG	This paper	N/A
Primer: mafaa qPCR Reverse ATGTCCCGCATGCAGGATTG	This paper	N/A
Primer: mafb qPCR Forward CGACGCGTACAAGGAGAAATA	This paper	N/A

Primer: mafb qPCR Reverse AAGAAGTGGCGAGCAGAAA	This paper	N/A
Primer: mafba qPCR Forward GAGAGACGCCTACAAACTCAAA	This paper	N/A
Primer: mafba qPCR Reverse ACACGCACTCACATGAAGAA	This paper	N/A
Primer: mafbb qPCR Forward TTGATCGAAACATCAGCAGAAATC	This paper	N/A
Primer: mafbb qPCR Reverse TCATGTCAAAGTCACCGTAGTC	This paper	N/A
Primer: B-actin qPCR Forward CGGACAGGTCATCACCATTG	(Fleisch et al., 2013)	N/A
Primer: B-actin qPCR Reverse GATGTCGACGTCACACTTCA	(Fleisch et al., 2013)	N/A
Primer: rpl13a qPCR Forward CGCCACACTGGAGGAGAAGA	This paper	N/A
Primer: rpl13a qPCR Reverse CTGCTTAGTCAGCTTCATCTCAACTT	This paper	N/A
Primer: nrl in situ probe template amplicon Forward (adds HindII digest site for plasmid insertion to pCS2+) AAGCTTCGTGCGCCTTGAAAACTGAA	This paper	'160711.NCBI.ISHnrl.F
Primer: nrl in situ probe template amplicon Reverse (adds KpnI digest site for plasmid insertion to pCS2+) GGTACCGACCACCTCGTCTTTGCTGA	This paper	'160711.NCBI.ISHnrl.R
Primer: ua3162 genotyping Forward GTCACTTCACAGTTCCCGGT	This paper	20170712.ua3162.F1

Primer: ua3162 genotyping Reverse TCTTCAGCGTCCGTCGTTTC	This paper	20170712.ua3162.R2
Oligonucleotide: nrl-specific gRNA template component1 ATTTAGGTGACACTATAGGGGTTCACGCCGAGATGACGTTTTAGAGCTAGAAATAGCAAG	This paper	20160126.nrl.Exon1.1
Oligonucleotide: nrl-specific gRNA template component2 ATTTAGGTGACACTATAGGGAGGTCCGTCACTCAGCGGTTTTAGAGCTAGAAATAGCAAG	This paper	20160126.nrl.Exon1.2
Oligonucleotide: nrl-specific gRNA template component3 ATTTAGGTGACACTATAGCTGGACGGGAGCCCTTCTGGTTTTAGAGCTAGAAATAGCAAG	This paper	20160126.nrl.Exon1.3
Oligonucleotide: gfp-specific gRNA template component ATTTAGGTGACACTATAGACCAGGATGGGCACCACCCGTTTTAGAGCTAGAAATAGCAAG	This paper	CR.GFP.GA5'.break
Oligonucleotide: first mafbb-specific gRNA template component ATTTAGGTGACACTATAGCTCGGGCTGAAGCTCGGCGGTTTTAGAGCTAGAAATAGCAAG	This paper	CR.mafbb.no25
Oligonucleotide: second mafbb-specific gRNA template component ATTTAGGTGACACTATATATCGTCCTTGCTCATCCCGGTTTTAGAGCTAGAAATAGCAAG	This paper	CR.mafbb.no2

Oligonucleotide: constant gRNA template component AAAAGCACCGACTCGGTGCCACTTTTTCAAGTTGATAACGGACTAGCCTTATTTTAACTTGCTATTTCTAGCTCTAAAAC	Gagnon et al., 2014 (Gagnon et al., 2014)	Constant oligonucleotide
Morpholino: nrl splice-blocking ACGTGTCAGATCATACCTGTGAAGT	This paper	N/A
Primer: to detect nrl splice-blocked transcripts Forward ATGCCACCTCTCTGGAGGAT	This paper	20161110.nrl.Int1.RetF
Primer: to detect nrl splice-blocked transcripts Reverse TCTGACGGCTTGTTCAGGAC	This paper	20161110.nrl.Int1.RetR
Morpholino: standard control morpholino CCT CTT ACC TCA GTT ACA ATT TAT A	Gene Tools, LLC (Philomath, OR)	Standard Control morpholino
Recombinant DNA		
Plasmid: multisite Gateway-compatible middle element (“pME”): zebrafish nrl CDS	This paper	N/A
Plasmid: pME zebrafish codon-optimized cre recombinase	This paper	N/A
Plasmid: pME zebrafish codon-optimized mouse NRL CDS with 3x N-terminal FLAG tag	This paper	N/A
Plasmid: pME zebrafish codon-optimized chicken MAFA CDS with 3x N-terminal FLAG tag	This paper	N/A
Plasmid: pME zebrafish codon-optimized lamprey MAFBA CDS with 3x N-terminal FLAG tag	This paper	N/A

Plasmid: pME zebrafish codon-optimized Drosophila trafficjam CDS with 3x N-terminal FLAG tag	This paper	N/A
Plasmid: pME zebrafish mafk CDS with 3x N-terminal HA tag	This paper	N/A
Plasmid: Tol2kit-style transgenic insert vector: pDestTol2CG2(gnat2:cre.pA)	This paper	N/A
Software and Algorithms		
ZEN 2010 (version 6.0)	Carl Zeiss AG (Oberkochen, Germany)	https://www.zeiss.com/microscopy/int/downloads/zen.html
Gatan DigitalMicrograph, version 1.81.78	Gatan Inc. (Pleasanton, CA)	http://www.gatan.com/products/tem-analysis/gatan-microscopy-suite-software
Geneious R9.1.7	(Kearse et al., 2012)	https://www.geneious.com
Fiji (NIH)	(Schindelin et al., 2012)	http://imagej.net/Fiji
R (version 3.4.1.)	(R Core Team, 2017)	https://www.r-project.org
GraphPad Prism 7.02	GraphPad Software (La Jolla, CA)	https://www.graphpad.com/scientific-software/prism/

Applied Biosystems 7500 Software v1.4.1	Applied Biosystems, Thermofisher	https://www.thermofisher.com/ca/en/home/brands/applied-biosystems.html
Agilent 2100 Bioanalyzer 2100 Expert	Agilent Technologies, (Santa Clara, CA)	https://www.genomics.agilent.com/en/home.jsp

CHAPTER 5:

CONCLUSIONS, GENERAL DISCUSSION, AND FUTURE DIRECTIONS

5.1 Overview of Chapter 5

In this final chapter, I first provide a summary of the results of the preceding data Chapters 2-4 (Section 5.2).

In the second section of this Chapter, I discuss some hypotheses I have generated in consideration of data from Chapters 2-4, combined with recent information published after Chapters 2 or 3. These hypotheses should be interpreted as providing a hypothesis-based framework for future investigations, and were formed in the interpretation of all the literature I am aware of, but are not exhaustive reviews of each subject.

In the third section of this Chapter, I consider the evolutionary implications of my work from Chapter 4, and provide outlines for experiments which would enable more robust comparative molecular biological study of tetrachromat photoreceptor development. I discuss the biological significance, and possible natural examples, of my finding that zebrafish do not require *nrl* for rod specification in adults. I then provide an experiment whereby this can be tested in other tetrachromats without needing the species-specific robust genetic tools I developed in Chapter 4. I also discuss the implications of my finding in Chapter 4 that lamprey *MAFBA* can promote the rod phenotype in zebrafish, and outline the necessary next steps to establishing a role for *MAFBA* in lamprey rod development.

Finally, I conclude this chapter with a brief discussion of the necessary next steps to make progress on understanding tetrachromat photoreceptors specification, continuing to use zebrafish as a primary model organism.

5.2 Summary of Results

The specification of mammalian rod photoreceptors has been well studied, and numerous factors have been identified in the specification of the two phenotypes of mammalian cones, although the specification pathway is less well understood. However, most vertebrate lineages have four cone subtypes. Very little is known about the specification of cones and rods in the tetrachromat eye. The scope of my thesis was

to understand photoreceptor differentiation in tetrachromats, using zebrafish as a model.

In Chapter 2, my colleagues and I demonstrated that a previously identified modulator of zebrafish cone and rod abundance, *tbx2b*, was subtly affected by the genetic status of *gdf6a*, implying that the two factors interacted somehow to regulate UV cone and rod abundance. We also showed that *gdf6a* mutant zebrafish had reduced abundance of blue cones, but not of other cone subtypes. This indicated a role for *gdf6a* in blue cone abundance modulation.

In Chapter 3, my colleagues demonstrated that the rod-dominated retinas of mice augmented their rod population by recruiting cells to the rod fate, which were previously en route to becoming S cones. My colleagues and I engineered, and I then deployed and characterized novel lineage tracing technology in zebrafish using two different markers for cone phenotype, and found no corresponding evidence that zebrafish larvae ever convert cones to produce rods. I then proposed that this difference between zebrafish and mouse, which was not practically possible to test in other organisms, might extend to a mammalian-specific adaptation to an ancient evolutionary bottleneck which would have strongly favoured such an innovation. My colleagues and I then hypothesized that the role of *Nrl* in mammalian rod specification may have evolved in concert with the mammal-specific rod adaptation we found. This predicted that non-mammalian rod development may have different requirements for *nrl*.

In Chapter 4, I examined the role of *nrl* in zebrafish rod development, and demonstrated its conserved requirement in larval zebrafish rod development, but that adult zebrafish do not require *nrl* to produce overtly normal rods. I developed and deployed novel lineage tracing technology to demonstrate that *nrl* was sufficient to induce a rod-like phenotype in UV cones which lasted into adulthood. This suggested that before the split of mammals from other vertebrate lineages, *nrl* was an important component to normal rod development and was sufficient to promote the rod phenotype when expressed in committed cones; this is consistent with a major proposal in Chapter 3. Finally, in Chapter 4, I also demonstrated that various vertebrate *nrl* orthologs, crucially that of lamprey, were capable of promoting the rod phenotype in zebrafish

cones. This suggested that lamprey may use their *nrl* homolog in rod development, which has implications for investigations of the evolutionary origins of rods and cones.

5.3 Genetic hypotheses aimed at uncovering the mechanisms behind *tbx2b*, *gdf6a*, and *nrl* zebrafish mutant phenotypes

Recent publications have stimulated new considerations of the role of *tbx2b*, *gdf6a*, and *nrl* in photoreceptor specification. In the following section, I propose novel hypotheses based on the findings my colleagues and I generated, together with new information that came to light where relevant. Several of these hypotheses are not mutually exclusive, and are proposed to provide a framework for future investigations of the genetic mechanisms for photoreceptor specification.

I first outline hypotheses which aim to address the mechanism of *tbx2b* in regulating rod and UV cone abundances in zebrafish. At present, we know only that loss of *tbx2b* causes larval zebrafish to have very few or no UV cones, and an increased abundance of rods (Alvarez-Delfin et al., 2009; Michèle G. DuVal et al., 2014; Saade et al., 2013; Sotolongo-Lopez et al., 2016), and this has been interpreted as a fate switch of UV cone progenitors to rods (Alvarez-Delfin et al., 2009; Cepko, 2015; Musser and Arendt, 2017). We also know that *tbx2b* mutant adult zebrafish do produce UV cones, but that these are apparently lost from the photoreceptor mosaic and become undetectable with previously published methods (Raymond et al., 2014). This could be due to UV cone death, or to conversion to a rod-like phenotype. In Chapter 2, my colleagues and I found that whatever role *tbx2b* plays in regulating photoreceptor diversity, it is dependent in some way on the normal activity of *gdf6a*. While we didn't find evidence that *tbx2b* was expressed in the UV cones of zebrafish, another group recently found UV cone-enriched expression in developing chick retina (Enright et al., 2015a). To guide future examination of the role in *tbx2b* in regulating photoreceptor diversity in zebrafish, I propose the following three hypotheses (H):

1) Tbx2b H1: *tbx2b* is directly and continually used by UV cones to repress the rod phenotype;
2) Tbx2b H2: *tbx2b* regulates larval photoreceptor type by influencing the timing of their exit from the cell cycle;
3) Tbx2b H3: Notch signaling and *tbx2b* antagonize each other to regulate at least UV cone precursor differentiation.

Evidence for, and predictions made by these hypotheses are then provided.

Second, I outline hypotheses which aim to explain the possible ways in which *gdf6a* might modulate blue cone abundance. The expression of *gdf6a* in developing zebrafish eyes occurs early in eye field patterning (French et al., 2009; Gosse and Baier, 2009), and lingers later in a tiny patch of dorsal retina above the lens during time periods when retinal cells differentiate (Valdivia et al., 2016). Thus, the documented expression period of *gdf6a* suggests it affects the abundance of blue cones by modulating some earlier developmental process. One candidate time point is the split between horizontal cell and cone lineages, which is presently not well studied. I outline four hypotheses which aim to uncover a possible role for *gdf6a* in regulating cone/horizontal retinal progenitor cell abundances:

1) Gdf6a H1: *gdf6a* regulates blue cone abundance during the stage where cone and horizontal cell lineages have not diverged;
2) Gdf6a H2: *gdf6a* regulates blue cone abundance at a time point where retinal progenitor cells with blue cone potential have differentiated from other cone-potential retinal progenitor cells, but before horizontal lineage has diverged;
3) Gdf6a H3: *gdf6a* regulates blue cone abundance after blue cone precursors split from horizontal cell precursors and from all other cone potentials;
4) Gdf6a H4: There is a single class of RPC[cone/HC], which can become RPC[cone] and RPC[HC] before terminal divisions; and after the cone-only specification occurs, *gdf6a* modulates the blue fate.

Evidence for, and predictions made by these hypotheses are then provided.

Finally, I outline three hypotheses designed to elucidate three unexpected findings from the qPCR data in Chapter 4. My colleagues and I show that *nrl* mutant larval zebrafish show decreased *crx* transcript abundance, and that both larval and adult *nrl* mutants have increased *nrl* transcript abundance. The three hypotheses I propose are:

1) Nrl H1: Nrl binds to and stimulates the *crx* promoter in zebrafish larvae;
2) Nrl H2: Zebrafish Nrl induces the expression of regulatory ncRNAs, which repress *nrl* activity;
3) Nrl H3: Nrl binds to and reduces expression of its own promoter.

Evidence for, and predictions made by these hypotheses are then provided.

In the following sections, I propose modulating gene activity with a variety of tools at timepoints that match the generation of rods and cones, or their progenitors. The birthdates of the relevant cells for zebrafish, as well as for other model organisms, are tabulated in Chapter 1, in Table 1.1. However, I note here again a difference between tetrapod and fish cell type birth order, which may cause confusion in a reader familiar with tetrapod birth order literature. In brief, tetrapods produce ganglion cells, horizontal cells, and cones in Phase1 (Table 1.1), and rods, bipolar cells, and Müller glia in Phase2. Amacrine cells are produced in Phase1, Phase2, or interphase, in various species (Table 1.1) (Dowling, 2012; Wong, 2006). In model fish species, the development of the retina is so rapid that the two phases are difficult to distinguish. **However, it appears that for non-tetrapods like zebrafish, Phase1 and Phase2 are swapped**. Retinal ganglion cells are still produced first, but the next cell types borne appear to be rods/bipolar cells and Müller glia (tetrapod Phase2), followed by cone and horizontal cells (tetrapod Phase1) (Table 1.1).

For the purposes of the following proposed experiments in zebrafish, the timing of inducible genetic constructs should be guided by the following observations. First, the onset of retinal ganglion cells leaving the cell cycle occurs at 28hpf (Das et al., 2003; Nawrocki, 1985). The double cones, which include the red cones, are born approximately 48hpf (Larison and Bremiller, 1990), and the red cones express opsin first among the cones, between 53 and 73hpf (Raymond et al., 1995). A small cluster of

rods, usually fewer than ten, detectably express rhodopsin by 50hpf in the ventral retina, but the timing of their birth is not currently known. Rhodopsin expression by the rest of the rods is first detectable around 60hpf (Raymond et al., 1995), and it is not clear when either of these groups of rods are born, or if they are born together but one post-mitotic group simply delays opsin expression.

5.3.1 Tbx2b

The chief photoreceptor phenotype in zebrafish *tbx2b* mutants is a paucity of UV cones and over-abundance of rods. This has been interpreted as a shift in fate from UV cones to rods. However, aside from the discovery shown in Chapter 2 that *gdf6a* influences the *tbx2b* phenotype, nothing is known about the mechanisms by which *tbx2b* might control photoreceptor diversity in zebrafish. These three hypotheses and associated predictions may help to guide further investigations into this.

5.3.1.1 Tbx2b H1: tbx2b is directly and continually used by UV cones to repress the rod phenotype

Available evidence that supports this hypothesis:

1. Chicken *TBX2* expression is enriched in violet cones (homologs of fish UV cones) at hatching-equivalent age (Enright et al., 2015a).
2. Adult zebrafish *tbx2b* null mutants produce UV cones initially, and are detectable in the youngest cells of the ever-growing edges of the retina, but appear to drop out of the aging cone mosaic (Raymond et al., 2014). TUNEL staining was used to look for evidence of cell death, but none was found. In Chapter 4, I show that zebrafish UV cones can be induced to assume a rod phenotype which is not easily distinguished from natural rods, using ectopic *nrl* expression. Together, this indicates that UV cones have the potential to slip into the rod phenotype in adult animals
3. In mouse heart development, the role of Tbx2 in modulating transcription is primarily repressive (Kokubo et al., 2007; Rutenberg et al., 2006).

4. In zebrafish pineal/parapineal development, *tbx2b* may repress Nr2e3-mediated repression of the parapineal fate (Khuansuwan et al., 2016).

Available evidence that does not support this hypothesis:

1. Chicken *TBX2* expression appears to subside in post-hatch photoreceptors (7 and 13 days post-hatch) (Enright et al., 2015a).
2. We did not detect *tbx2b* expression in larval photoreceptors at 3dpf, when there are UV opsin-expressing cells. Instead, we found expression concentrated in the INL (Chapter 2). However, a subsequent publication from work in the chicken shows that *TBX2* is robustly expressed in the INL and only weakly expressed in nascent UV cones (Enright et al., 2015a). Due to the nature of wholemount *in situ* hybridization, our method would not have made faint UV cone expression obvious.

This hypothesis makes 4 key predictions which can be tested.

1. **In larvae, Tbx2b should repress promoters of factors with pro-rod phenotype activities like *nrl* and *nr2e3***. To test this, an antibody against Tbx2b can be raised, or tagged *tbx2b* can be ectopically expressed under *crx* promoter (active in all nascent and mature photoreceptors), followed by either ChIP-seq to determine all promoters possibly occupied by Tbx2b, or ChIP and querying candidate genes such as *nrl* and *nr2e3*. Tbx2b should be found to occupy rod genes and not cone genes if it is primarily repressive. The repressive/stimulatory activity of Tbx2b promoter occupancy should then be characterized *in vitro* with luciferase reporter assays. Tagged Tbx2b pulldown with subsequent analysis by mass spectrometry can be used to identify binding partners. Crx is a candidate binding partner, as it facilitates transcriptional regulation in all photoreceptors of the mouse and dimerizes with numerous binding partners.
2. **In larvae, *tbx2b* expression in rods should interrupt or block the rod phenotype**. To test this, a tagged *tbx2b* should be expressed in rods using the well-characterized *rh1* promoter, which promotes reporter expression in rods, or using the *crx*-promoted construct described above. The criteria of *tbx2b*-

mediated loss of rod phenotype would include reduction/abolition of *nrl*, *nr2e3*, rod opsin, or 4C12 antigen expression, and the loss of rod morphology, as examined in Chapter 4.

3. **In larvae, *tbx2b* expression in rods should lead to assumption of UV cone phenotype**. I demonstrated that larvae without functional nrl have no rods, and instead have extra UV cone-phenotype photoreceptors. If *tbx2b* represses rod phenotype, the cell should default into a UV cone-like phenotype, consistent with my data on larval *nrl* knockouts in Chapter 4. This would be detectable by onset of UV opsin expression, directly stained for by anti-UV opsin antibody. Assumption of UV cone morphology could be assayed for in the same manner I used in Chapter 4.
4. **In adult *tbx2b* mutants, lineage-tracing of nascent UV cones generated at the retinal periphery should reveal conversion to a rod-like phenotype**. I have already developed gnat2:cre lineage tracing tools, and shown that it can trace UV cones that adopt rod phenotype (Chapter 4).

5.3.1.2 Tbx2b H2: Zebrafish tbx2b regulates larval photoreceptor type during their exit from the cell cycle

Available evidence that supports this hypothesis:

1. *tbx2b* is expressed in retinal progenitor cells during timepoints which correspond to the exit from cell cycle of all major retinal neurons in zebrafish (Gosse and Baier, 2009; Gross and Dowling, 2005).
2. In Chapter 2, my colleagues and I did not detect obvious sign of UV cones expressing *tbx2b* at 3dpf, the youngest time we have observed UV opsin expression (and thus, the youngest time we have been able to discriminate UV cones).
3. Chicken *TBX2* is not enduringly expressed in 7 and 13 days post-hatch retinas (Enright et al., 2015a). Thus, in the sole other tetrachromat model with any information on *TBX2/tbx2b* in photoreceptor development beyond zebrafish, it seems like *TBX2* has a transient role, if any. This may be conserved in zebrafish.

4. In at least 3 fish species including the zebrafish, cones probably leave the cell cycle later than rods (Hollyfield, 1972; Nawrocki, 1985; Sharma and Ungar, 1980), Loss of *tbx2b* activity could feasibly cause cycling progenitors, otherwise fated to become cones, to prematurely exit the cell cycle precociously and to develop as rods, consistent with the current consensus understanding of *tbx2b* mutant phenotype.

This hypothesis makes two key predictions:

1. **Ectopic expression of *tbx2b* in retinal precursor cells during the phase of cell cycle exit of rods should increase UV abundance at the expense of rods**. Heatshock or optogenetic inducible expression of ectopic tagged *tbx2b* can be used to modulate *tbx2b* expression with temporal control.
2. **Conditional retina-wide loss of *tbx2b* during or before the phase of cell cycle exit of rods should cause progenitor cells with UV cone potential to exit the cell cycle yielding more rods and fewer UV cones, phenocopying *tbx2b* loss of function allele**. Conditional loss of *tbx2b* during or shortly before the normal point of cycle exit for cones should not phenocopy *tbx2b* mutation. A floxed allele of *tbx2b* could feasibly be engineered, and hsp70:cre could be used to excise it with temporal control.

5.3.1.3 Tbx2b H3: Notch signaling and tbx2b antagonize each other to regulate UV cone precursor differentiation during the period of cone exit from the cell cycle.

Available evidence which makes this hypothesis plausible:

1. In mouse, loss of *Dll1*, a Notch ligand, causes excess cell production of all types of tetrapod early differentiating cells (RGC, HC, cone, AC) (Rocha et al., 2009).
2. In mouse, bipotent retinal progenitor cells, which can produce horizontal cells or cones, use Foxn4 to induce expression of *Dll4*, which induces Notch signaling to antagonize photoreceptor production (Luo et al., 2012).

3. In mouse models of cardiac patterning, Notch downstream regulators Hey1 and Hey2 repress expression of *Bmp2*, which is required for *Tbx2* expression (Rutenberg et al., 2006). Tbx2 inhibits expression of *Hey2* strongly and *Hey1* weakly. Ectopic expression of *Hey1* strongly decreases *Bmp2* and *Tbx2* expression (Kokubo et al., 2007), and ectopic expression of *Hey2* does not allow the structure to be formed where *Bmp2* and *Tbx2* would be expressed. Thus, in non-retinal mouse tissues, Notch signaling and *Tbx2* antagonize each other, and Bmp signaling mediates Notch effects on *Tbx2*. These interactions may be conserved in zebrafish; the zebrafish *hey2* mutant shows over-expression of *bmp4* (Rutenberg et al., 2006) in heart tissue, as in mouse, although it is not yet known if this then regulates *tbx2a/b* activity. However, *tbx2a/b* are required for proper heart chamber development in zebrafish (Sedletcaia and Evans, 2011). Thus, in zebrafish there is a scenario where Notch regulates BMP signaling in a tissue known to depend on proper *tbx2a/b* gene function. In the conserved pathway in the mouse, this activity of Notch is ultimately antagonistic to *tbx2b* expression.
4. In Chapter 2, my colleagues and I showed that *tbx2b* mutant phenotype can be evoked in *tbx2b* heterozygotes (haploinsufficiency) when *gdf6a* (a BMP ligand) is homozygous mutant. Thus, a photoreceptor-relevant *tbx2b* phenotype is affected by BMP signaling.

This hypothesis makes two key predictions:

1. **Ectopic *tbx2b* expression during or before normal cone exit from the cell cycle in zebrafish should decrease expression of Notch downstream factors in the retina**. Heatshock or optogenetic induction of tagged-*tbx2b* expression should reduce transcript abundance of Notch-stimulated genes.
2. **Ectopic Notch signaling should reduce *tbx2b* and *bmp2/4* expression**. Heatshock induction of the constitutively active Notch intracellular domain, NICD, should lower *tbx2b* transcript abundance.

5.3.2 Gdf6a

In Chapter 2, my colleagues and I identified a specific deficit in blue cone abundance in *gdf6a* mutants, relative to rods and UV cones. At the time, resources were not in place to assess red and green cone abundances for similar deficits. In total, we showed that *gdf6a* modulates blue cone abundance and affects UV cone abundance when *tbx2b* expression is partially impaired. However, *gdf6a* is not expressed in photoreceptors in maturing photoreceptors at 3dpf (Valdivia et al., 2016), a time when zebrafish cones begin to express cone opsins (Raymond and Barthel, 2004). For *gdf6a* to be modulating cone abundance, such a role likely occurs earlier in the photoreceptor lineage specification, perhaps at the point where cone-fated cells split form horizontal cell-fated precursors.

There is evidence that horizontal cells and cones share a progenitor even up to their terminal mitosis, detailed in the next paragraph. However, the lineages of cones and horizontal cells may also separate earlier than at the terminal mitosis: cones can certainly be generated in homotypic pairs from a terminal mitosis (Suzuki et al., 2013), and it is likely that horizontal cells can, too (Rompani and Cepko, 2008). It is not currently known which of these two terminal mitosis scenarios predominates in cone production. In the first scenario (Fig. 5.2.1), I identify 3 possible opportunities for gdf6a action to regulate blue cone abundance, and propose experimental predictions to discriminate between them (Gdf6a H1-3). In the second scenario (Fig. 5.2.2), the developmental knowledge of early cone production does not yet give adequate resolution for me to suggest testable hypotheses, but the predictions of Gdf6a H3 cannot be discriminated from those by this second scenario, so I detail it in Gdf6a H4.

Gdf6a Hypotheses 1-3: Bipotent retinal progenitor cells competent to become cones or horizontal cells, shorthand RPC[cone:HC], exist in multiple subtypes, of paired HC and cone subtypes, one of which is regulated by *gdf6a* (Figure 5.2.1).

Available evidence which supports all of Gdf6a H1, Gdf6a H2, and Gdf6a H3 (listed below):

1. There are at least three types of horizontal cells in the zebrafish retina, which connect solely with cones, and another type which connects solely with rods (Song et al., 2008), and these can be labeled with ptf1a:eGFP (Suzuki et al., 2013) and with cx55.5:eGFP transgenes (Godinho et al., 2007).
2. Cones and horizontal cells appear to share a common progenitor cell, which can clonally produce pairs of HC, pairs of cones, or critically, pairs of 1 HC and 1 cone (Emerson et al., 2013; Suzuki et al., 2013).
3. Of the 3 types of cone horizontal cells in the chicken, H2 was not found to be produced in clones where another horizontal cell of any type was generated; it is likely a non-horizontal cell was generated for each H2 born (Rompani and Cepko, 2008).
4. When zebrafish cones are born in pairs, they are of one type, not of mixed type (Suzuki et al., 2013); there is probably not a terminal progenitor cell with blue cone and another cone type bipotency.

5.3.2.1 Gdf6a H1: Gdf6a regulates blue cone abundance during the stage where cone and horizontal cell lineages have not diverged.

Available evidence which supports Gdf6a H1 specifically:

1. My colleagues and I showed in Chapter2 that *gdf6a* is genetically upstream of *tbx2b*. We do not know when *tbx2b* is active in specifying photoreceptors, but *trβ2* expression under *crx* promoter, active just after terminal mitosis, is capable of dictating red versus UV cone subtype (Suzuki et al., 2013). Thus, *gdf6a* activity may be upstream of both *tbx2b* and *trβ2* regulatory timepoints.
2. We did not assess red or green cone abundance in Chapter 2.

This hypothesis makes two key predictions:

1. **In *gdf6a* mutant zebrafish, the abundance of one or more horizontal cell subtypes should also be decreased, concordant with blue cone decrease**. This can be tested by using *gdf6a* mutant zebrafish that express GFP under control of *ptf1a* promoter, which labels all horizontal cells and progenitors, and

evaluating the morphologies of H1/2 horizontal cells (two morphologically indistinguishable types) and H3 cells. Distinguishing between H1 and H2 subtypes can be done by electrophysiology or by connectivity; H1 cell types hyperpolarize in response to red light, and H2 depolarize in response to red light (Li et al., 2009). In wildtype zebrafish, H1 cells contact red, green, and blue cones; H2 contact green, blue, and UV cones; and H3 contact UV and blue cones. Thus, even with decreased blue cone abundance, H1 and H2 subtypes may possibly be discriminated on the basis of whether a cell of interest makes contact with red (H1) or with UV (H2) cones (Li et al., 2009). Rod HC connect only to rod synapses. Careful morphological and electrophysiological characterization of the horizontal cells in *gdf6a* mutants can thus directly test the prediction that *gdf6a* mutation affects the proportions of progenitor cells which are bipotent for cone and horizontal subtypes. This would also be the first indication that cone subtypes are developmentally bundled with horizontal cell subtypes, which would be pretty neat. If no changes in horizontal cell population total numbers or subtype abundances are observed, *gdf6a* most likely does not regulate cone abundances at this point, where precursors are shared with horizontal cells.

2. **Modulating *gdf6a* will affect red cone abundance**. Homozygous *gdf6a* mutants should be assessed for red cone abundance changes; as for blue cones, reductions in *gdf6a* activity should reduce abundance of these cones. There might not be a strong change, as my colleagues and I showed there was no change in UV cone abundance relative to rods in *gdf6a* mutants (Chapter 2, Fig 2.4A). In that case, careful modulation of *trβ2* should also be done using an inducible dominant negative *trβ2* construct, to attenuate levels of *trβ2*. In Chapter 2, my colleagues and I demonstrated haploinsufficiency for *tbx2b* when *gdf6a* was homozygous mutant; this may be the case for *trβ2*, as well. *Gdf6a* can be ectopically expressed similarly to the experiments outlined for *tbx2b* above; additionally, a recent hypermorph allele of human *GDF6* was characterized *in vitro* (Wang et al., 2016); it appeared to be less sensitive to BMP inhibitor Noggin, and to stimulate signalling more strongly than wildtype GDF6; genome

editing of the zebrafish *gdf6a* could be performed to create a hypermorphic allele. Hypermorph activity would need to be demonstrated. Modulation of *gdf6a* activity can also be done by expressing *gdf6a* as an ectopic gain of function, or its downstream antagonist *smad7*, transgenically under *rx3* promoter, which has previously been used to control levels of *gdf6a* in the retina (French et al., 2009). If *gdf6a* modulation is not found to modulate the abundances of red and green cones, it likely does not regulate blue cone abundance at the developmental timepoint where blue cones are not yet segregated into their own lineage. Note: green cones should also be assessed, but we currently do not know anything about the developmental lineage of green cones, including their developmental relationship to other cone subtypes. They should be included in the experiment to generate novel data, but are not considered in this prediction.

5.3.2.2 Gdf6a H2: Gdf6a regulates blue cone abundance at a time point where retinal progenitor cells with blue cone potential have differentiated from other cone-potential retinal progenitor cells, but before horizontal lineage has diverged.

Evidence supporting Gdf6a H2:

1. Zebrafish cones are produced as homotypic pairs when the terminal mitosis yields to cones (Suzuki et al., 2013). However, horizontal cells are at least occasionally one daughter of a terminal mitosis which also yields a cone (Suzuki et al., 2013). Thus, retinal progenitor cells with horizontal and cone potential may be segregated into cone subtype/horizontal cell lineages before the terminal mitosis.

This hypothesis makes two key predictions:

1. **In *gdf6a* mutant zebrafish, the abundance of one or more horizontal cell subtypes should also be decreased, concordant with blue cone decrease**. This can be assessed as for Gdf6a H1.

2. **Modulating *gdf6a* will <u>not</u> affect red cone abundance**. This can be assessed as for Gdf6a H1.

5.3.2.3 Gdf6a H3: Gdf6a regulates blue cone abundance after blue cone precursors split from horizontal cell precursors and from all other cone potentials.

This hypothesis makes two key predictions:

1. **Modulation *gdf6a* should <u>not</u> affect horizontal cell abundance**. This can be assessed as for AH5.1
2. **Modulating *gdf6a* should <u>not</u> affect red cone abundance**. This can be assessed as for HA5.1.

5.3.2.4 Gdf6a H4: There is a single class of RPC[cone/HC], which can become RPC[cone] and RPC[HC] before terminal divisions; and <u>after</u> the cone-only specification occurs, gdf6a modulates the blue fate.

Available evidence which supports this hypothesis:

1. In a study of chicken horizontal cone genesis, most horizontal cells in chicken are produced as homotypic clones when examined in small or paired clones, larger clones showed equal proportions of mixed horizontal cell types (H1 and H3) and cones were not reported (Rompani and Cepko, 2008). H2 cells were not found to be generated in pairs with any other horizontal cell. It is possible H1 and H3 cells, generated in homotypic pairs, have a shared bipotential precursor cell whose granddaughters can be pairs of either H1 or H3. Thus, there is possible there is a horizontal cell precursor which does not have a cone lineage possibility; in other words, the retina progenitor cells with bipotential HC or cone lineage possibilities could feasibly become restricted to one fate before undergoing a terminal mitosis.

Available evidence which is not in support of this hypothesis:

1. It is clearly possible for a terminal mitosis to produce a pair of daughter in which one is a horizontal cell and one is a cone (Emerson et al., 2013; Suzuki et al., 2013).

This hypothesis makes one key prediction:

1. **Modulating *gdf6a* should not affect horizontal cell abundance**. Horizontal cell characterization can be performed in *gdf6a* homozygous mutants as outlined in AH2.

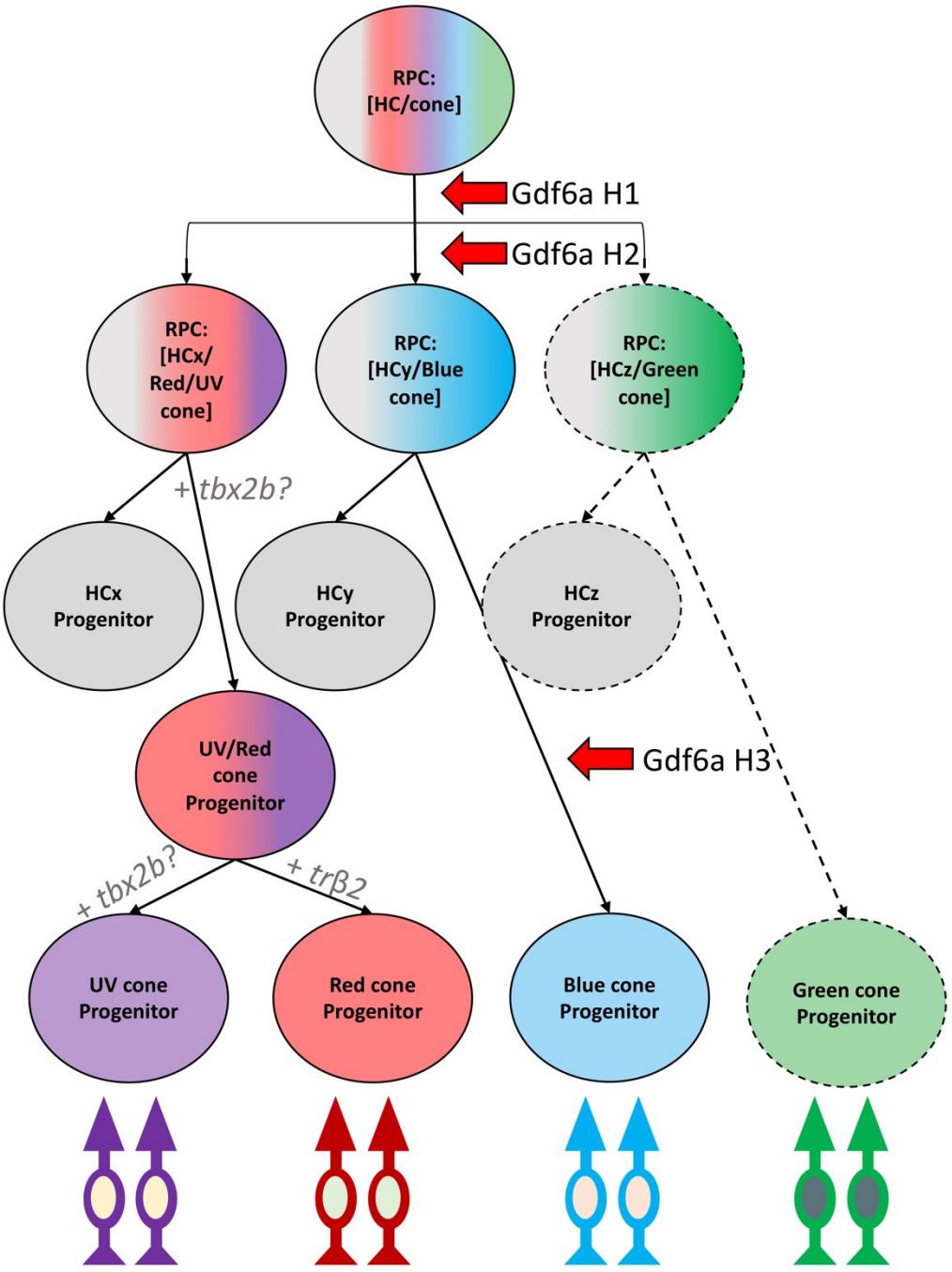

Figure 5.2.1: Summary of Gdf6a Hypotheses1-3.

Each alternative hypothesis posits that the role of *gdf6a* in regulating blue cone abundance occurs at different time points in the generation of blue cones.

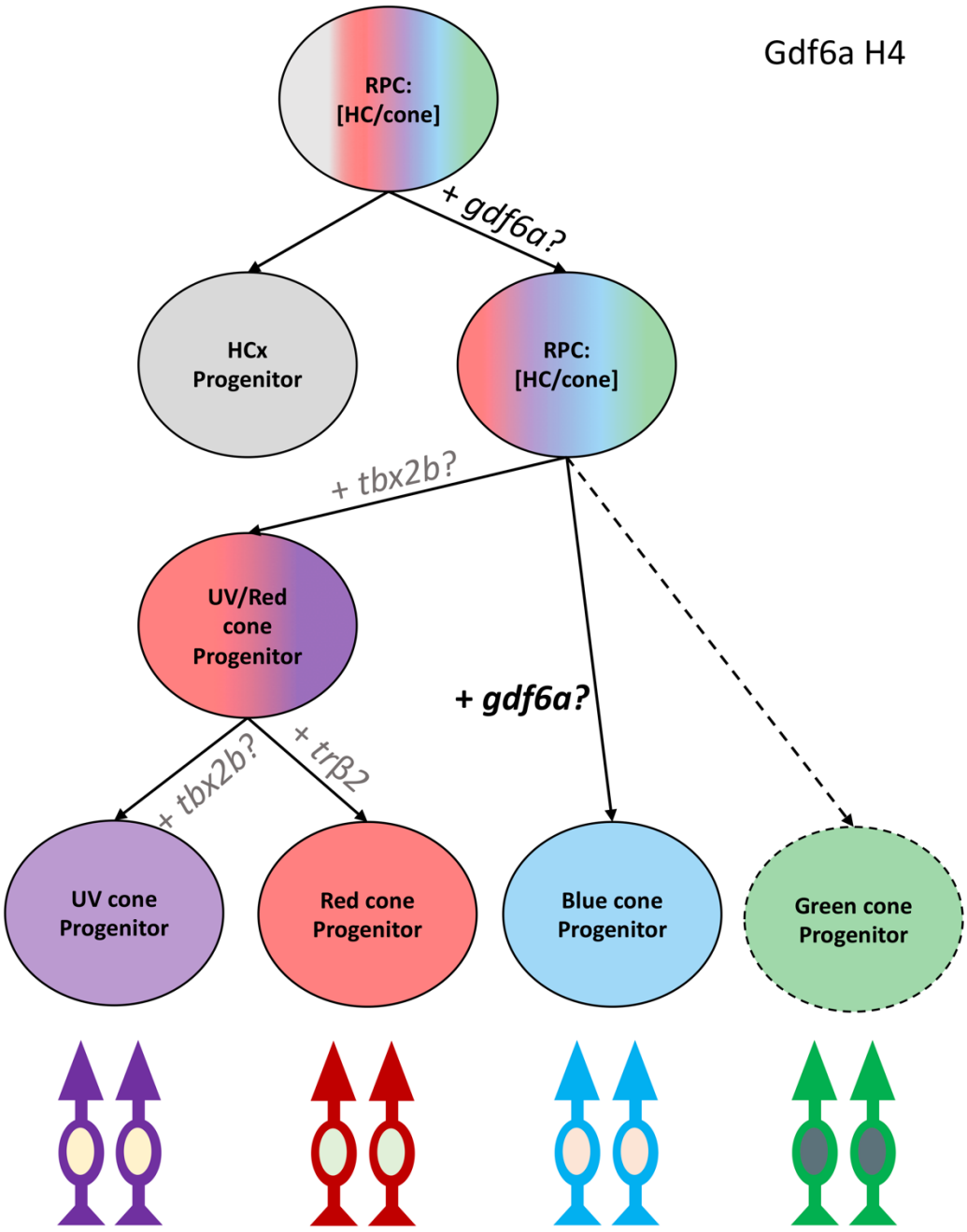

Figure 5.2.2: Summary of Gdf6a Hypothesis4.

This hypothesis requires that cone progenitor cells separate from horizontal progenitor cells before the cone subtypes begin to specify. *gdf6a* can exert its influence on blue cone abundances at the indicated positions in the specification schematic.

5.3.3 Nrl

In Chapter 4, my colleagues and I showed surprising changes in the transcript abundances of *nrl* and *crx* of larval and adult *nrl* mutant zebrafish. Nrl has not been demonstrated to regulate *Crx* expression in the mouse, but is certainly downstream of and directly activated by it (Montana et al., 2011). In the zebrafish larval *nrl* mutant, we found that the *crx* transcript was less abundant, even though the animals possessed abundant (cone) photoreceptors. We also found that *nrl* transcript abundance was increased in both larvae and adult mutants, which has also not been demonstrated in the mouse model. In the following section, I propose three mechanism-oriented hypotheses to explain these two unexpected findings, which may help identify novel layers of regulation in photoreceptor specification even in mammals. These hypotheses are:

1. Nrl H1: Nrl binds to and stimulates *crx* promoter in larval zebrafish;
2. Nrl H2: Zebrafish Nrl induces the expression of regulatory ncRNAs, which repress *nrl* activity;
3. Nrl H3: Zebrafish Nrl binds to and reduces expression of its own promoter.

For each instance, I review available evidence for each hypothesis, and provide experimentally-testable predictions.

5.3.3.1 Nrl H1: nrl binds to and stimulates crx promoter in larval zebrafish.

Available evidence which supports this hypothesis:

1. In Chapter 4, my colleagues and I show that *nrl* mutant zebrafish have decreased *crx* transcript abundance.
2. Mouse *Nrl* expression is stimulated by Crx activity (Montana et al., 2011) and by Rorβ activity (Fu et al., 2014). Nrl feeds back positively upon *Rorβ* (Fu et al., 2014), and it is therefore plausible it could engage in a positive feedback loop with *Crx* as well.

This hypothesis makes two key predictions:

1. **Nrl protein binds to *crx* regulatory regions in larvae**. ChIP seq, to assess all points of binding in the genome by zebrafish Nrl, or ChIP and querying for candidate gene sequences should reveal whether tagged zebrafish Nrl occupies *crx* regulatory sites. This can be tested using tagged *nrl* expressed in rods using *rh1* promoter, in order to simulate endogenous *nrl* ChIP as closely as possible without developing a novel zebrafish *nrl* antibody. Conservation of local non-coding sequences around the *crx* locus among fishes with sequenced genomes can be used to identified candidate sequences to pull down with ChIP. Alternatively, ATAC-seq can be used to identify regions of open chromatin within the genomes of zebrafish rods, which can then be used as candidate sequences for ChIP.
2. **Nrl protein occupancy at *crx* regulatory regions is stimulatory**. This can be tested *in vitro* by luciferase reporter assay. Because Crx may induce *nrl* expression in zebrafish as in mouse, Nrl stimulation of *crx* promoter-driven luciferase should be compared with and without Crx, to assess if Crx participates in this feedback loop.

5.3.3.2 Nrl H2: Zebrafish nrl induces the expression of regulatory ncRNAs, which repress nrl activity

Available evidence which supports this hypothesis:

1. In *Drosophila*, the *nrl* homolog *trafficjam* transcript 3'UTR is the source of 351 individual piRNAs, and Trafficjam directly upregulates the expression of *piwi*. Piwi which binds to piRNAs to reduce retrotransposon activity in the germline (Saito et al., 2009). The *trafficjam* transcript is itself a target of piRNA-mediated silencing (Saito et al., 2009).
2. Recent work by Sreekanth et al. showed that the mouse *Nrl* transcript 3'UTR is a target of miR-143/145 microRNAs *in vitro* (Sreekanth et al., 2017), and the transcript abundance of this microRNA cluster is lowest during peak rod generation (P0 mice), and higher in earlier and later ages. Electroporation of

eyes to introduce ectopic miR-143/145, followed by *in vitro* explant culture, was associated with decreases in *Nrl* and rod opsin transcript levels. Finally, *Nrl* was able to bind and stimulate the *miR 143/145* promoters in luciferase assays, and to bind specifically to the promoter sequence in EMSA assay. Thus, mouse Nrl could feasibly engage in a microRNA-mediated negative feedback loop, and this may be conserved in the zebrafish

3. Mouse Nrl putatively binds to the promoters of up to 6% of known long non-coding RNAs and antisense RNAs yet identified in the mouse genome, and may regulate about 174 antisense RNAs (defined as transcribed from the antisense strand of a gene) (Zelinger et al., 2017). None of these were reported to interact with *Nrl* transcript.
4. *trafficjam* coding DNA sequence (CDS) comprises 48% of its transcript, while its 3'UTR comprises 38% of its transcript, and is 1335nt long (transcript NM_001273633.1, accessed from NCBI Gene 2 March 2018). Mouse *Nrl* CDS is 28% of its total transcript length, while the 3'UTR comprises 63.5% of the total transcript length and is 1577nt long (NM_001136074.2, NCBI Gene, accessed 2 March 2018). These two 3'UTRs share 47% nucleotide identity; it is feasible that mouse *Nrl* 3'UTR may be the source of unidentified sense-encoded small RNAs. This would not have been discovered in the recent characterization of the *Nrl* noncoding transcriptome, as novel non-coding RNAs were limited to anti-sense RNAs and intergenic RNAs (Zelinger et al., 2017), and the authors set a size threshold for new RNA discovery to be 201nt or longer; piRNA are between 26 and 31nt in length (Luo and Lu, 2017; Robine et al., 2009).

Available evidence which does not support this hypothesis:

1. The zebrafish *nrl* transcript is 1480nt long, and the CDS comprises 83.7% of it, while the 3'UTR is only 89nt long, representing 6.7% of the total transcript (NM_001040331.1, NCBI Gene, accessed 2 March 2018). Thus, zebrafish *nrl* transcript does not have a large 3'UTR, and is certainly not highly conserved with mouse and *Drosophila* homolog 3'UTR.

This hypothesis makes 2 key predictions:

1. **Zebrafish Nrl binds to and activates noncoding RNA promoters**. A zebrafish tagged-Nrl ChIPseq should show binding of Nrl to the putative promoters of noncoding RNA genes, and *in vitro* assays of promoter simulation (e.g. luciferase assay) should indicate that zebrafish Nrl stimulates candidate noncoding RNAs.
2. **Zebrafish *nrl* 3'UTR contains sequences required to lower transcript abundance *in vivo***. *nrl* 3'UTR is only 89nt long, and miRNA and piRNA each bind a maximum of about 10 nucleotides with perfect complementarity to their target mRNA (Gorski et al., 2017; Luo and Lu, 2017). The binding sites of these small RNAs can be identified by mutating 10 nucleotides at a time throughout the length of the *nrl* 3'UTR, and then appending that 3'UTR to a reporter gene like eGFP, expressed in rods under a safe harbor insert locus. If *nrl* 3' UTR has sequences bound to and repressed by small RNAs, then eGFP expression should be increased when the small RNA binding sites are mutated. Alternatively, a "sponge construct" could be generated (Bak and Mikkelsen, 2014; Ebert and Sharp, 2010; Kluiver et al., 2012), consisting of tens of copies of zebrafish *nrl* 3'UTR concatemerized into a single transcript, and expressed under a high-production promoter like the rod opsin promoter. In the background of *nrl* wildtype animals, which my colleagues and I show have lower *nrl* transcript abundance relative to mutants, this sponge construct should relieve suppression of *nrl* transcript abundance. This should manifest as *nrl* transcript abundance being more abundant in *nrl* wildtype animals.

5.3.3.3 Nrl H3: Zebrafish Nrl binds to and reduces expression of its own promoter

Available evidence to support this:

1. In Chapter 4, my colleagues and I show that *nrl* transcript abundance is higher in mutants than in wildtype animals, suggesting that *nrl* participates in or induces its own negative regulation.

2. Mouse *Nrl* has numerous binding sites for Crx, predominantly arranged in three clusters of binding sites upstream of each of the first two exons and within the third intron (Montana et al., 2011). Crx dimerizes with Nrl to co-regulate the expression of numerous genes (White et al., 2016). Thus, it is feasible that mouse Nrl binds with Crx at some of these binding sites.
3. While Nrl is most associated with stimulatory activity at gene promoters, notably for rod genes, it is present at cone gene promoters too, where it presumably aids in repressing transcription (Hao et al., 2012).

Available evidence which does not support this:

1. *Nrl* transcript is undetectable in the widely-used *Nrl* mutant mouse (Mears et al., 2001). However, the homologous recombination cassette used to delete the mouse *Nrl* gene removed the entire gene, and much of the 5' and 3' UTR. Thus, there is no longer a gene to transcribe, nor regulatory regions to promote it. Thus, the method of mutation would obscure any change in *Nrl* transcript abundance caused by loss of Nrl-mediated regulation
2. Recently, retrovirally-introduced CRISPR was used to mutate *Nrl* in in mature mice, with the goal of demonstrating proof of principle that loss of *Nrl* could prevent some forms of retinal degeneration in humans (Yu et al., 2017). The CRISPR reagent targeted the first protein-coding exon in the gene, and presumably did not affect intronic regions. The study showed robust evidence of loss of rod gene expression in CRISPR-infected mice, consistent with loss of *Nrl* function, but *Nrl* transcript was slightly less abundant, unlike what my colleagues and I showed in the zebrafish. This may suggest a difference in regulation for mouse *Nrl* versus fish *nrl*.

This hypothesis makes two key predictions:

1. **Zebrafish Nrl binds to *nrl* regulatory sequences**. This can be tested by using tagged Nrl in a ChIP experiment to assess if it binds to candidate *nrl* regulatory regions, with a complementary EMSA experiment to assess binding site specificity

2. **Zebrafish *nrl* promoter activity is reduced in the presence of Nrl protein**. This can be assessed *in vitro* using luciferase reporter assays. Combinations of Crx and Nr2e3 should also be assessed, as these are primary co-factors for Nrl-mediated transcriptional regulation in the mouse. This can be assessed *in vivo* by cloning *nrl* regulatory regions which recapitulate *nrl* expression, driving a fluorescent protein instead. A single insert with consistent expression should show different fluorescence levels in wildtype and *nrl* mutant backgrounds. In parallel, similar constructs with manipulated copy number of Nrl binding sites should test whether Nrl binding site manipulation modulates fluorescence output in the wildtype or nrl mutant backgrounds. These numerous constructs should be inserted into a genomic safe harbor locus to minimize expression variation due to random insert location effects. Safe harbor loci have been described using lentiviral tools (Torres et al., 2014), but in zebrafish this could feasibly be accomplished by random genomic insertion of a construct with a single loxP site upstream of a eGFP reporter lacking any promoter. After screening to identify a recombination-accessible insert, these safe harbor fish could be injected with an integration-defective plasmid containing a single loxP site upstream of a desired promoter, together with Cre recombinase mRNA, to “flip in” the promoter and then allow production of eGFP under the new regulatory sequences.

5.4 Evolutionary implications

5.4.1 Evidence for two rod programs in vertebrates

In Chapter 4, I demonstrated a conserved requirement for *nrl* in zebrafish larval rods, but that adult zebrafish can generate rods without *nrl*. The rods produced in the adult zebrafish did not appear to come at the expense of another cell type, as all retinal layers had wildtype-like proportions of cell nuclei in older and younger regions of retina, and four classes of cone photoreceptor could be distinguished on the basis of morphology, histology, immunoreactivity, and opsin expression. Only a single *nrl* transcript was found in adult retinal total RNA, which contained the *nrl* lesion, indicating that the *nrl* mutants did not splice out or otherwise repair the lesion to yield a *nrl* transcript capable of

producing functional protein. Moreover, my colleagues and I did detect a molecular phenotype, as *nr2e3* transcript abundance was significantly less abundant in mutants versus wildtype, while *nrl* transcript itself was significantly more abundant. There was also an ultrastructural phenotype: similar to *nrl* mutant mice, the *nrl* mutant rod nuclei in zebrafish had cone-like chromatin arrangement. The mutant rods also appeared to have cone-like synapses. However, despite these differences in *nrl* mutants, the animals expressed rod opsin and 4C12 antigen, made rod-like outer segments, and did not express UV cone opsin in rods. This indicates that the *nrl*-mediated rod specification pathway was impaired in these mutants, but that it isn't required for the production of most of the rod phenotype in adult zebrafish.

One possible confound to this would be a cryptic *nrl* paralog, termed here for simplicity as ***nrlb***. Previous work evaluating the *maf* family member phylogeny of frogs and fish found a single Maf family member to be the ortholog of mammalian Nrl (Coolen et al., 2005). In Chapter 3, I show a phylogeny produced by my colleague, which features 15 mammals and 15 non-mammal vertebrates and demonstrates with access to newer genomic information that zebrafish have a single Maf peptide which clades with mammalian Nrl. That *maf* is the same *nrl* as previously identified, and is the one I studied in Chapter 4. An *nrlb* may still exist which has eluded detection, or another *maf* may be expressed in the adult rods which may rescue loss of *nrl*. This can be definitively addressed with new massively parallel sequencing technologies. A recent study published comparative rod transcriptomes from larval and adult wildtype zebrafish (Sun et al., 2018), but that study used bulk RNAseq, and the input was flow-sorted rods from rh1:eGFP transgenic retinas. As discussed in Chapter 3, it is impossible to flow sort to perfect purity. Furthermore, in the chicken, *MAFA* appears to be expressed in rods and *MAFB* may be expressed in green cones, both of which may have regulatory or specifying roles governing the photoreceptor phenotypes (Enright et al., 2015a). *MAFB* was also abundantly expressed in bipolar cells in the chicken. Off-target cells present in a bulk RNAseq will confound attempts to find rare or unexpected transcripts expressed in mutant rods. In order to attempt to test the prediction that no putative *nrlb* is expressed in rods, a method must be used that allows for perfect purity of input, balanced with the ability to detect extremely rare transcripts.

The ability to sequence the transcriptomes of **single cells**, and to take data from dozens of cells to create an essentially complete profile of what constitutes normal transcription for that cell type, will be key to addressing this, and guides to budget-friendly experimental design exist (Baran-Gale et al., 2017). A recent analysis of 15 currently used single cell RNAseq protocols revealed that an accurate description of the relative abundance of detected molecules can be expected to saturate at 250 000 reads per cell (Svensson et al., 2017). Saturation of the ability to detect rare transcripts begins at 1 million reads per cell, with a 1-fold gain in sensitivity when increased to 4.5 million reads per cell, after which point no appreciable gain in sensitivity was found. At 1 million reads, spiked-in transcripts with a known concentration of less than 10 molecules per cell were reliably detected. Thus, assuming the expression of cryptic *nrlb* is at or above 10 transcripts per cell, single cell sequencing should provide a definitive answer to what transcripts may be at work in *nrl* mutant rods, which putatively promote the rod phenotype. An experimental design might involve dissociating retinas of mutant and wildtype animals, manually selecting two rh1:eGFP+ rods from each of five animals per genotype, to a total of 20 cells. These would then be processed for single cell RNAseq at a read depth of 1 million reads, for an experiment-total of 20 million reads. Any *nrlb* candidate identified in this method can then be targeted for traditional genetic analysis to assess if it plays a role in rescuing *nrl* loss of function in adult animals, or indeed if it plays a dominant role in specifying rods in adult zebrafish.

Accepting, at least for a moment, my tentative conclusion that the production of rods in zebrafish adult *nrl* mutants represents a biologically meaningful separate rod specification program, we can then consider that there is an *nrl*-dependent Program1 used for rod specification in larval zebrafish and mammals, and an *nrl*-independent Program2 used at least in zebrafish adults. Is there evidence for this program in other species? Work in cod, chicken, and lamprey is suggestive.

Recently, **Atlantic cod** were demonstrated to produce rods only during and after metamorphosis, when the animals progress from larvae to juveniles (Valen et al., 2016). Prior to this, larvae have pure cone retinas. They used bulk RNAseq analysis at multiple time points during larval, pre-metamorphic, and metamorphic stages, which include the onset of and peak rod generation times. Interestingly, *nrl* was expressed in larvae. I

showed in Chapter 4 that zebrafish *nrl* mutant larvae have defects in the structures of their lenses, and *maf* genes have previously been implicated in lens fibre differentiation (Reza and Yasuda, 2004). Possibly the larval cod used *nrl* during lens development, as this expression was transient and only apparent in a single RNAseq time point. During onset of and peak rod generation in older animals, *nrl* relative abundance was actually *decreased* relative to other timepoints. This tentatively hints that one might ask whether cod may also use Program2 to specify rods.

Chickens (and most/all birds) have typical vertebrate rods, but appear to lack an *NRL* gene, and *MAFA* has been proposed to be the gene used to specify them. *MAFA* is expressed in rods and not in cones during photoreceptor maturation (Ochi et al., 2004), and its expression in developing photoreceptors was recently shown to be enriched in rhodopsin reporter transgene-expressing cells, presumably rods (Enright et al., 2015a). In Chapter 3, the phylogeny generated by my colleague shows that three bird species lack an MAF peptide which can clade with Nrl, and instead have representatives of the three other major Maf members (MAFA, MAFB, and c/v-MAF). However, there is no evidence in chickens indicating a requirement for/sufficiency of *MAFA* to direct avian rod development. Moreover, *nrl* is expressed in adult zebrafish rods (Sun et al., 2018), but in Chapter 4 I show that adult zebrafish do not require *nrl* to produce rod-like photoreceptors. This demonstrates that detecting expression of an *nrl*-like gene in a cell type cannot be used to conclude it is necessary for the production/maintenance of that cell type. In Chapter 4, I show that *nrl* mutant rods have ultrastructural cone-like nuclei, and likely have cone-like synapses. This suggests that *nrl* has a role in maintaining (and/or differentiating) adult zebrafish rods (Program2), but it isn't required for specification. Program2 may well be how chicken rods are specified. To align observations from zebrafish and birds: in zebrafish, *nrl* is not required to specify zebrafish rods, but the rods have some cone-like phenotypes, such as cone-like chromatin appearance, which mouse Nrl knockout photoreceptors also show. In at least one bird, the European buzzard *Buteo buteo* (El-Beltagy, 2015), transmission electron micrographs show nuclear chromatin appearance similar to what I found in zebrafish cones and *nrl* mutant rods (Chapter 4). Thus, zebrafish *nrl* mutant rods have cone-like mottled chromatin appearance; birds appear to lack *NRL*, and have rods with chromatin

appearance reminiscent of zebrafish cones (and bird cones). This constellation of observations suggests it possible that mammals use Program1 exclusively, birds use Program2 exclusively, and fish use Programs1 and 2 differentially over development; direct genetic analysis of rod development of birds is needed to test this. A role for *MAFA* in specifying bird rods should be tested for; moreover, a similarly high-resolution examination as described above should be carried out for bird rods, to definitively rule out the possibility that an as-yet undetected avian *NRL* exists and is expressed in the retina.

Lamprey are a good final test case to explore naturally-occurring Program1 and Program2 rod generation. Extensive previous examinations of at least five species of lamprey have demonstrated that they achieve rod-like physiology (Asteriti et al., 2015; Collin et al., 2004; Govardovskii and Lychakov, 1984; Morshedian and Fain, 2017, 2015; Teranishi et al., 1982) with cone-like morphology (Collin et al., 2004, 1999; Shaun P Collin et al., 2003; Collin and Potter, 2000; Dickson and Graves, 1979; Lamb et al., 2016). This morphology includes cone-like synaptic termini and outer segments in several species (Collin et al., 1999; Collin and Potter, 2000; Dickson and Graves, 1979). In examining published transmission electron micrographs of sections fortuitously angled to include high-resolution images of the nuclei for *Geotria australis* (which have 5 photoreceptor types) and *Petromyzon marinus* (which have 1 cone-like and 1 rod-like photoreceptor, and whose *MAFBA* was analyzed in Chapters 3 and 4), it appears that lamprey rod-like cells have cone-like chromatin arrangements (Collin et al., 1999; Dickson and Graves, 1979). A published genome exists only for the sea lamprey *P. marinus* (Smith et al., 2018), which definitively has a rod-like and a cone-like cell by physiological definitions (Morshedian and Fain, 2017, 2015). It also has *LWS* opsin (homologous to zebrafish red cone opsin) and an *RH1* opsin (homologous to zebrafish rod opsin), and pseudogenes for *SWS1* and *SWS2* have been identified (Wayne L. Davies et al., 2009). However, as demonstrated in the Maf phylogeny constructed by my colleague in Chapter 3, lamprey appear to have only a single MAF gene family member (Kim et al., 2016b), which clades with vertebrate Mafb. In chicken, *MAFB* is expressed in green cones and in bipolar cells. *MAFA* is expressed in rods, but also in a subset of INL cells which may be amacrine or bipolar cells. *MAFA* is also knows as *L-*

MAF, in reference to its expression in the developing lens (Ochi et al., 2004; Yoshida and Yasuda, 2002). Lamprey have vertebrate-like lenses; it is possible that the single *MAF* detected so far in the lamprey genome has non-photoreceptor functions. It is possible that it is not endogenously used to specify photoreceptors, although my experiments in Chapter 4 demonstrated it has the capacity to do so. The similarities to bird rods, with cone-like nuclei and no identified *NRL*, and to zebrafish *nrl* mutant adult rods, which like the lamprey have cone-like nuclei and synapses, suggest that lamprey may use Program2 for rod specification (The implications of this for appreciating evolution of the duplex retina are addressed in the section below). A high resolution analysis of lamprey rod transcriptome should be carried out, to assess if cryptic *MAF* paralogs are expressed which have eluded detection so far. This experiment would also be useful for addressing questions of evolutionary homology to jawed vertebrate rods, which I describe in more detail in the next section.

If a rod specification Program2 truly exists in some or many vertebrates, characterizing it may well be informative to our understanding of photoreceptor specification in mammals, despite our apparent lack of Program2. Part of the promise of building an understanding of tetrachromat cone specification, including of *sws2* and *rh2*-expressing cones which mammals have lost, is that elements of the ancestral genetic program may still be used in mammalian retinal development. A tantalizing example of this is zebrafish *six7* and mammalian *Six3*. Zebrafish *six7* is a homolog of mammalian *Six3*, and as described in Section 1.2 of Chapter1, appears to have some role in the generation of rods and green cones. Mammals do not have the ancestral green cone subtype. However, both the ancestral green cone and mammalian rods express RH-related opsins (Rh1 for rods, Rh2 for green cones). In mouse, Six3 has some capacity to stimulate rod opsin expression, and can enhance the capacity of Nrl and Crx to stimulate rod opsin expression *in vitro* (Manavathi et al., 2007). If we can identify the components of Program2 in the zebrafish, we can look for it in various vertebrates, but especially in mammals, where it may play an unappreciated role in photoreceptor development or maintenance.

5.4.2 Rod/Cone evolution and emergence of the duplex retina

5.4.2.1 Cell type homology theory

As will be discussed in the next section, it is not clear whether lamprey rod-like photoreceptors are actually *homologous* to jawed vertebrate rod photoreceptors. In this subsection, I will briefly review the current standards for considering cell type evolution, and introduce the concept of *cell type homology*, and the related concepts of *sister cell types* and *cell phenotypic convergence*. These terms will be used to frame the discussion of lamprey rod homology in the next section.

The concept of cell type homology has been extensively explored in comparative molecular biology literature (Arendt, 2008, 2003, Arendt et al., 2016, 2009), and three definitions have emerged, which are key to understanding questions of rod homology. First, a given cell type found in two different organisms is considered *homologous* if the last common ancestor between those organisms can be demonstrated to have had a single cell type from which both extant cell types were derived (Arendt et al., 2016). Second, two cell types *within an organism* are considered sister cell types if they can be demonstrated to have diversified out of a single cell type in an ancestor (Arendt et al., 2016). Third, two cells with similar phenotype but which were derived separately in compared lineages are considered to show *cell phenotypic convergence*; they are convergently evolved cell types (Arendt et al., 2016).

An example of cell type homology is human M cones and mouse M cones; there is no current evidence to suggest any scenario but that both organisms produce M cones because the last common ancestor did. An example of sister cell types would be human M and L cones (green- and red-sensitive cones); the primate lineage that includes humans duplicated M opsin and then red-shifted it to generate a new L opsin (Jacobs, 2013, 1996). Over time, L opsin-expressing cones have apparently come to adopt a new phenotype that can be distinguished somehow from M opsin-expressing cones by retinal wiring processes. We recognize these cones as M and L cones, and they are sister cell types which were derived from an ancestral M cone, which was homologous to mouse M cones. This scenario can also demonstrate cell phenotypic convergence: the human M cone (slightly more sensitive to green light than the L cone) is not directly homologous to the zebrafish green cone. Instead, the human M cone

convergently evolved to fulfill a similar role as the ancestral (and lost) vertebrate green cone.

An experimental framework was recently put forward to resolve situations of disputed cell type homology (Arendt et al., 2016). This method relies on previously-established criteria for demonstrating peptide orthology, and integrates this information with genetic information that demonstrates how a given cell type is specified. Putative homology between two cell types can be tested by looking for the following evidence: both cells should rely on a similar minimal combination or complex of orthologous transcription factors to specify the cell type from other possible cell types in its developmental lineage. Thus, the proposed standard is to demonstrate that orthologous genes in both organisms similarly interact with other orthologs to regulate the cell phenotype.

When it comes to the origin of rods and cones in vertebrate retinas, there is a lack of diversity in basally-branching species we can access as informative outgroups for comparative assessment. The sister group to the vertebrates is the non-vertebrate chordates, which include the tunicates and the cephalochordates. Neither tunicates nor cephalochordates have vertebrate-like eyes, nor retinas, and their photoreceptive cells are not yet sufficiently characterized to enable comparisons to vertebrate rods and cones. The most basal vertebrates are the jawless fish, lamprey and hagfish. Hagfish retina has been very difficult to interpret, as there are numerous structural differences between their eyes and retinas compared to the eyes and retinas of jawed vertebrates, no genome has been published, and it is difficult to even propose candidate cells for homologous relationships to the other agnathan vertebrates, at this time. Lamprey on the other hand have clearly jawed vertebrate-like camera-style eyes with conservation of retinal morphology and overt cell phenotypes (Lamb, 2013; Lamb et al., 2009). At least one lamprey species has 5 photoreceptor opsins which each seem to have clear orthologs to each of jawed vertebrate *Sws1*, *Sws2*, *Rh2*, *Lws*, and *Rh1* (UV, blue, green, red, and rod opsins) (Shaun P. Collin et al., 2003; Pisani et al., 2006). Moreover, other lamprey species have reduced opsin diversity (Wayne L. Davies et al., 2009) but a better characterized rod-like physiology (Morshedian and Fain, 2017, 2015). It is tempting to speculate that lamprey rods are homologous to jawed vertebrate rods,

which implies that the ancestor of jawless and jawed vertebrates had rods. In the next section, I detail why this scenario is still in debate. Finally, I discuss how work I did in Chapter 4 uses the framework of molecular homology detailed above to add a piece of evidence favouring the scenario where lamprey rods are indeed homologous to jawed vertebrate rods.

5.4.2.2 Support for lamprey rod homology

At least two scenarios exist to explain lamprey rod origins: first, the common ancestor between lamprey and the jawed vertebrates had 1 rod and 4 cone subtypes, and both lineages retained them. Second, the common ancestor had five photoreceptor types, and both lineages independently adapted one to mediate vision in dim light (ie, to become rod-like). At least one species of lamprey has 5 photoreceptor subtypes (Shaun P. Collin et al., 2003; Pisani et al., 2006), and these express clear orthologs of SWS1, SWS2, RH2, LWS, and RH1 opsins (UV, blue, green, red, and rod opsins, in jawed vertebrates). Many lamprey have photoreceptor cells with a rod-like physiology, including the ability to report absorption of single photons of light (Asteriti et al., 2015; Morshedian and Fain, 2015), and the disposition to saturate at daylight levels of illumination (Morshedian and Fain, 2017), which are hallmarks of rods, and not of cones. This argues for homology, although this cannot be conclusive, as rhabdomeric photoreceptors can also detect single photons of light (Fain et al., 2010), and rods are ciliary photoreceptors with deeply different phototransduction machinery (reviewed in Chapter 1). Sea Lamprey rod-like photoreceptors have cone-like outer segments, nuclei, and synapses (Dickson and Graves, 1979), suggesting that the physiology of rods is not absolutely dependent on vertebrate-style rod-like ultrastructure. A major piece of evidence that lamprey rods may not be homologous to jawed vertebrate rods is in their phototransduction machinery, elements of which are derived from gene duplications. The common ancestor of all vertebrates underwent two rounds of genome duplication (Kuraku et al., 2009), meaning that for a brief time, all genes existed in 4 copies. Many of these have been retained; for example, there is a cone-specific transducin alpha (*Gnat2*), and a rod-specific transducin alpha (*Gnat1*), reviewed in Chapter 1. In jawed vertebrates, there is no known *Gnat3* or *Gnat4* that derived from the

2 rounds of genome duplication. Lamprey however appear to have retained a different subset of many paralogs from the two rounds of genome duplication (Kuraku, 2013), including of the phototransduction machinery paralogs (Lamb et al., 2009; Muradov et al., 2008, 2007), reviewed in Chapter 1. Corroborating the possibility that lamprey may have independently evolved rods, there are numerous examples of cones evolving a rod phenotype, as demonstrated by the several documented cases of cone-rod transmutations I describe in Chapter 1. Bluntly put, it simply may not be *difficult* to evolve rod physiology from cones. Cumulatively then, it is not clear if lamprey rods are truly homologous to jawed vertebrate rods. It is possible that the common ancestor of lamprey and jawed vertebrates had 5 cones, and each lineage independently solved the problem of dim light vision by evolving high sensitivity photoreceptors. This is the sort of scenario for which cell type homology theory was developed (Arendt et al., 2016), as discussed above in Section 5.4.2.1.

The framework for molecularly defining cell type homology relies on characterization of the essential molecular regulators of the phenotype of a cell, in other words the major cohort of transcription factors which enforce the candidate cell phenotype (Arendt et al., 2016). In mammalian rods, this would be at least Otx2/Crx, Nrl, Nr2e3, which together are capable of enforcing the rod phenotype at the expense of the cone phenotype (Ng et al., 2011). Thus, under this framework, if lamprey rods are truly homologous to jawed vertebrate rods, lamprey should use homologous genes to enforce the rod phenotype. However, such an in-depth characterization of the specification of a cell type is laborious; Chapter 4 represents the characterization of a single rod core regulatory complex member, zebrafish *nrl*, and zebrafish have all the advantages of a major model organism to enable such a genetic investigation (reviewed in Chapter 1). Querying the roles of the core regulatory complex of lamprey rods will require shortcuts.

In Chapter 4, I demonstrated that the sole sea lamprey *MAF* gene yet identified, *MAFBA*, is sufficient to induce two markers of the zebrafish larval rod phenotype in cones, apparently as well as mouse *Nrl* and zebrafish *nrl*, and better than chicken *MAFA*. The sole *Drosophila nrl* homolog *trafficjam*, which is known to regulate phenotype in rhabdomeric fly photoreceptors (Jukam et al., 2013), was unable to influence the rod/cone phenotype in zebrafish. This indicates that despite 500 million

years of distance between the jawed and jawless vertebrate lineages, lamprey have a *MAF* gene capable of launching elements of the rod program in a jawed animal. This is good support for a role for *MAFBA* in rod specification in lamprey, and is evidence for homology between lamprey and jawed vertebrate rods. However, additional markers of rod phenotype induction could be examined, including the onset of expression of rod-specific phototransduction paralogs, morphology, and physiology, which I did not do in Chapter 4. Critically, a possible rod-regulatory role for lamprey *MAFBA* will need to be validated at least by documenting the normal expression of *MAFBA* in lamprey retinas. This is because there are numerous possible roles for Maf genes in the retina; for example, chicken *MAFA* and *MAFB* are expressed in non-rod cells (Enright et al., 2015a; Yoshida and Yasuda, 2002), and the Mafs have a role in lens specification (Reza and Yasuda, 2004). It could be that lamprey *MAFBA* indeed has the capacity to bind zebrafish rod gene promoters, but it may not be expressed in photoreceptors at all. *In situ* hybridization analysis should be performed, to demonstrate where lamprey *MAFBA* is expressed. Finally, detailed analysis of the recently published genome (Smith et al., 2018), combined with a high resolution characterization of retinal photoreceptors as outlined above, should be carried out to assess if lamprey have other *MAF* genes, or other *MAF* genes with expression in rods.

5.5 Unresolved questions and future directions

The scope of my thesis was to understand the specification of tetrachromat visual photoreceptors. In Chapter 2, my colleagues and I were able to demonstrate that the role of *tbx2b* in specifying photoreceptors, whatever that may be, is sensitive to *gdf6a* mutation status, a genetic interaction which suggests these two genes act in a common pathway. In Chapter 3, I found a difference in zebrafish rod/cone development relative to the mouse, suggesting divergent mechanisms of producing similar photoreceptor phenotypes. In Chapter 4, I characterized the specification of rod photoreceptors by *nrl*, and found an *nrl* status-dependent fate interaction between rods and UV cones in larvae. This is reminiscent of the *tbx2b* mutant phenotype, which also

modulates UV cone and rod abundances. Future work should assess the genetic interaction between *nrl* and *tbx2b*. The zebrafish *six7* mutant also modulates larval rod abundance, as well as green cone abundance. It will be interesting to see what genetic interaction may exist between *six7* and *nrl*. Finally, *trβ2* has been shown to promote red cone at the expense of UV cone phenotype; *tbx2b* may promote the UV cone phenotype at the expense of the rod phenotype, and *nrl* appears to promote the rod phenotype at the expense of the UV cone phenotype. The possibility of a genetic interaction between the three genes is tantalizing. In Chapter 4, I generated loss and gain of function tools for analysis of *nrl*; we have access to two mutant *tbx2b* alleles, and tools to modulate larval *trb2* activity have been demonstrated previously (Suzuki et al., 2013). However, those tools do not permit time-specific manipulation of trβ2 signaling, which an inducible dominant negative *trβ2* construct may allow. Finally, although numerous mutant *six7* alleles exist as stable zebrafish lines (Ogawa et al., 2015; Saade et al., 2013; Sotolongo-Lopez et al., 2016), the current embargo on zebrafish import into Canada means *six7* mutant fish will need to be derived *de novo*, possibly through CRISPR/Cas9-mediated targeted mutagenesis.

There are additional unknowns regarding the assumption and maintenance of the cone and rod phenotypes in tetrachromats. What genes positively activate the expression of the cone opsins? In the mouse, numerous transcription factors have been reported at the promoter of S cone opsin, including Sall3, Rorα, Crx, and Rorβ2 (de Melo et al., 2011; Fujieda et al., 2009; Srinivas et al., 2006). At least Trβ1 and Trβ2 can regulate M opsin expression (Applebury et al., 2007; Onishi et al., 2010). What controls *sws2* and *rh2* transcription in the zebrafish? In the chicken, *MAFA* and *MAFB* are expressed in or near photoreceptors during specification (Enright et al., 2015a), but expression of *MAFB* is not obviously long-term in the chicken, and the roles for these genes are currently only speculated upon. An experiment that would generate a wealth of novel hypotheses about the ongoing regulation of photoreceptor cell type phenotype would be a massively parallel sequencing analysis, similar to those described above in Section 5.4. In Chapter 4, I engineered a lineage-tracing construct that appear to label all non-rod photoreceptors. Using gnat2:cre to isolate cone photoreceptors, and high resolution single cell RNAseq, a definitive profile of cone photoreceptors can be

established and mined for differential expression between cone types. Rods can be assessed using rh1:eGFP in a similar experiment, or the data generated recently using bulk RNAseq from flow-sorted zebrafish rods (Sun et al., 2018), could be used as a comparison to the cone single cell RNAseq data. Experimentally, dissociation of the retina could be followed by fluorescence-activated cell sorting, or by manual retrieval of 100 dissociated cells. Morphology of dissociated cells can be directly assessed to attempt to get 25 of each cone subtype, or 100 cells can be collected, with the assumption of collecting 33 red, 33 green, 17 blue, and 17 UV cones, in keeping with the photoreceptor ratios in the adult retina (Allison et al., 2010). Sequencing depth should be 1 million reads per cell, as this has been proposed to represent saturation of transcript capture from single cells (Svensson et al., 2017). Unlike mouse (Applebury et al., 2000), zebrafish do not co-express the major classes of opsin within a single cone (Allison et al., 2010), so taking single cell transcriptomes and grouping them by which opsin is dominantly expressed will allow identification of the subtypes. Transcriptome alignments should then reveal differentially expressed factors that can generate hypotheses about cone type enforcement, which then inform hypotheses about cone type specification. Finally, this dataset can then be used as a comparator to study questions of homology for myriad other organisms with interesting visual adaptations, such as those described in Chapter 1.

REFERENCES

Abd-El-Barr, M.M., Pennesi, M.E., Saszik, S.M., Barrow, A.J., Lem, J., Bramblett, D.E., Paul, D.L., Frishman, L.J., Wu, S.M., 2009. Genetic Dissection of Rod and Cone Pathways in the Dark-Adapted Mouse Retina. J. Neurophysiol. 102, 1945–1955. https://doi.org/10.1152/jn.00142.2009

Acar, C., Mears, A.J., Yashar, B.M., Maheshwary, A.S., Andreasson, S., Baldi, A., Sieving, P.A., Iannaccone, A., Musarella, M.A., Jacobson, S.G., Swaroop, A., 2003. Mutation screening of patients with Leber Congenital Amaurosis or the enhanced S-Cone Syndrome reveals a lack of sequence variations in the NRL gene. Mol. Vis. 9, 14–7. https://doi.org/v9/a3 [pii]

Aït-Ali, N., Fridlich, R., Millet-Puel, G., Clérin, E., Delalande, F., Jaillard, C., Blond, F., Perrocheau, L., Reichman, S., Byrne, L.C., Olivier-Bandini, A., Bellalou, J., Moyse, E., Bouillaud, F., Nicol, X., Dalkara, D., Van Dorsselaer, A., Sahel, J.A., Léveillard, T., 2015. Rod-derived cone viability factor promotes cone survival by stimulating aerobic glycolysis. Cell 161, 817–832. https://doi.org/10.1016/j.cell.2015.03.023

Akalin, A., Kormaksson, M., Li, S., Garrett-Bakelman, F.E., Figueroa, M.E., Melnick, A., Mason, C.E., 2012. MethylKit: a comprehensive R package for the analysis of genome-wide DNA methylation profiles. Genome Biol. 13. https://doi.org/10.1186/gb-2012-13-10-R87

Akhmedov, N.B., Piriev, N.I., Chang, B., Rapoport, A.L., Hawes, N.L., Nishina, P.M., Nusinowitz, S., Heckenlively, J.R., Roderick, T.H., Kozak, C.A., Danciger, M., Davisson, M.T., Farber, D.B., 2000. A deletion in a photoreceptor-specific nuclear receptor mRNA causes retinal degeneration in the rd7 mouse. Proc. Natl. Acad. Sci. 97, 5551–5556. https://doi.org/10.1073/pnas.97.10.5551

Akimoto, M., Cheng, H., Zhu, D., Brzezinski, J.A., Khanna, R., Filippova, E., Oh, E.C.T., Jing, Y., Linares, J.-L., Brooks, M., Zareparsi, S., Mears, A.J., Hero, A., Glaser, T., Swaroop, A., 2006. Targeting of GFP to newborn rods by Nrl promoter and temporal expression profiling of flow-sorted photoreceptors. Proc. Natl. Acad. Sci. 103, 3890–3895. https://doi.org/10.1073/pnas.0508214103

Akimoto, M., Filippova, E., Gage, P.J., Zhu, X., Craft, C.M., Swaroop, A., 2004.

Transgenic Mice Expressing Cre-Recombinase Specifically in M- or S-Cone Photoreceptors. Investig. Ophthalmol. Vis. Sci. 45, 42–47. https://doi.org/10.1167/iovs.03-0804

Allison, W., 2004. Rainbow trout as a model of retinal photoreceptor death and regeneration. University of Victora.

Allison, W.T., Barthel, L.K., Skebo, K.M., Takechi, M., Kawamura, S., Raymond, P.A., 2010. Ontogeny of cone photoreceptor mosaics in zebrafish. J. Comp. Neurol. 518, 4182–4195. https://doi.org/10.1002/cne.22447

Allison, W.T., Dann, S.G., Veldhoen, K.M., Hawryshyn, C.W., 2006a. Degeneration and regeneration of ultraviolet cone photoreceptors during development in rainbow trout. J. Comp. Neurol. 499, 702–715. https://doi.org/10.1002/cne.21164

Allison, W.T., Dann, S.G., Vidar Helvik, J., Bradley, C., Moyer, H.D., Hawryshyn, C.W., 2003. Ontogeny of ultraviolet-sensitive cones in the retina of rainbow trout (Oncorhynchus mykiss). J. Comp. Neurol. 461, 294–306. https://doi.org/10.1002/cne.10682

Allison, W.T., Haimberger, T.J., Hawryshyn, C.W., Temple, S.E., 2004. Visual pigment composition in zebrafish : Evidence for a rhodopsin – porphyropsin interchange system *. Vis. Neurosci. 945–952.

Allison, W.T., Veldhoen, K.M., Hawryshyn, C.W., 2006b. Proteomic analysis of opsins and thyroid hormone-induced retinal development using isotope-coded affinity tags (ICAT) and mass spectrometry. Mol. Vis. 12, 655–72.

Altimus, C.M., Güler, A.D., Alam, N.M., Arman, A.C., Prusky, G.T., Sampath, A.P., Hattar, S., 2010. Rod photoreceptors drive circadian photoentrainment across a wide range of light intensities. Nat. Neurosci. 13, 1107–1112. https://doi.org/10.1038/nn.2617

Altschul, S.F., Madden, T.L., Schäffer, A.A., Zhang, J., Zhang, Z., Miller, W., Lipman, D.J., 1997. Gapped BLAST and PSI-BLAST: A new generation of protein database search programs. Nucleic Acids Res. 25, 3389–3402. https://doi.org/10.1093/nar/25.17.3389

Alvarez-Delfin, K., Morris, A.C., Snelson, C.D., Gamse, J.T., Gupta, T., Marlow, F.L., Mullins, M.C., Burgess, H.A., Granato, M., Fadool, J.M., 2009. Tbx2b is required for

ultraviolet photoreceptor cell specification during zebrafish retinal development. Proc. Natl. Acad. Sci. 106, 2023–2028. https://doi.org/10.1073/pnas.0809439106

Ancelin, K., Lange, U.C., Hajkova, P., Schneider, R., Bannister, A.J., Kouzarides, T., Surani, M.A., 2006. Blimp1 associates with Prmt5 and directs histone arginine methylation in mouse germ cells. Nat. Cell Biol. 8, 623–630. https://doi.org/10.1038/ncb1413

André, E., Gawlas, K., Becker-André, M., 1998. A novel isoform of the orphan nuclear receptor RORbeta is specifically expressed in pineal gland and retina. Gene 216, 277–283. https://doi.org/S0378111998003485 [pii]

Angueyra, J.M., Pulido, C., Malagón, G., Nasi, E., del Pilar Gomez, M., 2012. Melanopsin-expressing amphioxus photoreceptors transduce light via a phospholipase C signaling cascade. PLoS One 7, 1–9. https://doi.org/10.1371/journal.pone.0029813

Applebury, M.L., Antoch, M.P., Baxter, L.C., Chun, L.L., Falk, J.D., Farhangfar, F., Kage, K., Krzystolik, M.G., Lyass, L. a, Robbins, J.T., 2000. The murine cone photoreceptor: a single cone type expresses both S and M opsins with retinal spatial patterning. Neuron 27, 513–523. https://doi.org/10.1016/S0896-6273(00)00062-3

Applebury, M.L., Farhangfar, F., Glösmann, M., Hashimoto, K., Kage, K., Robbins, J.T., Shibusawa, N., Wondisford, F.E., Zhang, H., 2007. Transient expression of thyroid hormone nuclear receptor TRβ2 sets S opsin patterning during cone photoreceptor genesis. Dev. Dyn. 236, 1203–1212. https://doi.org/10.1002/dvdy.21155

Arendt, D., 2008. The evolution of cell types in animals: Emerging principles from molecular studies. Nat. Rev. Genet. 9, 868–882. https://doi.org/10.1038/nrg2416

Arendt, D., 2003. Evolution of eyes and photoreceptor cell types. Int. J. Dev. Biol. 47, 563–571. https://doi.org/10.1387/IJDB.14756332

Arendt, D., Hausen, H., Purschke, G., 2009. The “division of labour” model of eye evolution. Philos. Trans. R. Soc. B Biol. Sci. 364, 2809–2817. https://doi.org/10.1098/rstb.2009.0104

Arendt, D., Musser, J.M., Baker, C.V.H., Bergman, A., Cepko, C., Erwin, D.H., Pavlicev, M., Schlosser, G., Widder, S., Laubichler, M.D., Wagner, G.P., 2016. The origin

and evolution of cell types. Nat. Rev. Genet. 17, 744–757. https://doi.org/10.1038/nrg.2016.127

Arendt, D., Tessmar-Raible, K., Snyman, H., Dorresteijn, A.W., Wittbrodf, J., 2004. Ciliary photoreceptors with a vertebrate-type opsin in an invertebrate brain. Science (80-.). 306, 869–871. https://doi.org/10.1126/science.1099955

Asai-Coakwell, M., French, C.R., Berry, K.M., Ye, M., Koss, R., Somerville, M., Mueller, R., van Heyningen, V., Waskiewicz, A.J., Lehmann, O.J., 2007. GDF6, a novel locus for a spectrum of ocular developmental anomalies. Am. J. Hum. Genet. 80, 306–15. https://doi.org/10.1086/511280

Asai-Coakwell, M., French, C.R., Ye, M., Garcha, K., Bigot, K., Perera, A.G., Staehling-Hampton, K., Mema, S.C., Chanda, B., Mushegian, A., Bamforth, S., Doschak, M.R., Li, G., Dobbs, M.B., Giampietro, P.F., Brooks, B.P., Vijayalakshmi, P., Sauve, Y., Abitbol, M., Sundaresan, P., van Heyningen, V., Pourquie, O., Underhill, T.M., Waskiewicz, A.J., Lehmann, O.J., 2009. Incomplete penetrance and phenotypic variability characterize Gdf6-attributable oculo-skeletal phenotypes. Hum. Mol. Genet. 18, 1110–1121. https://doi.org/10.1093/hmg/ddp008

Asai-Coakwell, M., March, L., Dai, X.H., Duval, M., Lopez, I., French, C.R., Famulski, J., De baere, E., Francis, P.J., Sundaresan, P., Sauvé, Y., Koenekoop, R.K., Berry, F.B., Allison, W.T., Waskiewicz, A.J., Lehmann, O.J., 2013. Contribution of growth differentiation factor 6-dependent cell survival to early-onset retinal dystrophies. Hum. Mol. Genet. 22, 1432–1442. https://doi.org/10.1093/hmg/dds560

Asteriti, S., Gargini, C., Cangiano, L., 2014. Mouse rods signal through gap junctions with cones. Elife 2014, 1–21. https://doi.org/10.7554/eLife.01386.001

Asteriti, S., Grillner, S., Cangiano, L., 2015. A cambrian origin for vertebrate rods. Elife 4, 1–16. https://doi.org/10.7554/eLife.07166.001

Badea, T.C., Cahill, H., Ecker, J., Hattar, S., Nathans, J., 2009. Distinct Roles of Transcription Factors Brn3a and Brn3b in Controlling the Development, Morphology, and Function of Retinal Ganglion Cells. Neuron 61, 852–864. https://doi.org/10.1016/j.neuron.2009.01.020

Baden, T., Berens, P., Franke, K., Román Rosón, M., Bethge, M., Euler, T., 2016. The functional diversity of retinal ganglion cells in the mouse. Nature 529, 345–350.

https://doi.org/10.1038/nature16468

Bak, R.O., Mikkelsen, J.G., 2014. miRNA sponges: Soaking up miRNAs for regulation of gene expression. Wiley Interdiscip. Rev. RNA 5, 317–333. https://doi.org/10.1002/wrna.1213

Baran-Gale, J., Chandra, T., Kirschner, K., 2017. Experimental design for single-cell RNA sequencing. Brief. Funct. Genomics 1–7. https://doi.org/10.1093/bfgp/elx035

Barski, A., Cuddapah, S., Cui, K., Roh, T.Y., Schones, D.E., Wang, Z., Wei, G., Chepelev, I., Zhao, K., 2007. High-Resolution Profiling of Histone Methylations in the Human Genome. Cell 129, 823–837. https://doi.org/10.1016/j.cell.2007.05.009

Barthel, L.K., Raymond, P.A., 1993. Subcellular localization of α-tubulin and opsin mRNA in the goldfish retina using digoxigenin-labeled cRNA probes detected by alkaline phosphatase and HRP histochemistry. J. Neurosci. Methods 50, 145–152. https://doi.org/10.1016/0165-0270(93)90002-9

Bates, K.E., Sung, C.S., Robinow, S., 2010. The *unfulfilled* gene is required for the development of mushroom body neuropil in *Drosophila*. Neural Dev. 5, 4. https://doi.org/10.1186/1749-8104-5-4

Becker, T., Wullimann, M.F., Becker, C.G., Bernhardt, R.R., Schachner, M., 1997. Axonal regrowth after spinal cord transection in adult zebrafish. J. Comp. Neurol. 377, 577–595. https://doi.org/10.1002/(SICI)1096-9861(19970127)377:4<577::AID-CNE8>3.0.CO;2-#

Behesti, H., Papaioannou, V.E., Sowden, J.C., 2009. Loss of Tbx2 delays optic vesicle invagination leading to small optic cups. Dev. Biol. 333, 360–372. https://doi.org/10.1016/j.ydbio.2009.06.026

Bellingham, J., Chaurasia, S.S., Melyan, Z., Liu, C., Cameron, M.A., Tarttelin, E.E., Iuvone, P.M., Hankins, M.W., Tosini, G., Lucas, R.J., 2006. Evolution of melanopsin photoreceptors: Discovery and characterization of a new melanopsin in nonmammalian vertebrates. PLoS Biol. 4, 1334–1343. https://doi.org/10.1371/journal.pbio.0040254

Bernardos, R.L., Barthel, L.K., Meyers, J.R., Raymond, P.A., 2007. Late-Stage Neuronal Progenitors in the Retina Are Radial Muller Glia That Function as Retinal Stem Cells. J. Neurosci. 27, 7028–7040.

https://doi.org/10.1523/JNEUROSCI.1624-07.2007

Beuchle, D., Jaumouillé, E., Nagoshi, E., 2012. The nuclear receptor unfulfilled is required for free-running clocks in Drosophila pacemaker neurons. Curr. Biol. 22, 1221–1227. https://doi.org/10.1016/j.cub.2012.04.052

Bhattacharyya, N., Darren, B., Schott, R.K., Tropepe, V., Chang, B.S.W., 2017. Cone-like rhodopsin expressed in the all-cone retina of the colubrid pine snake as a potential adaptation to diurnality. J. Exp. Biol. 220, 2418–2425. https://doi.org/10.1242/jeb.156430

Bilican, B., Goding, C.R., 2006. Cell cycle regulation of the T-box transcription factor tbx2. Exp. Cell Res. 312, 2358–2366. https://doi.org/10.1016/j.yexcr.2006.03.033

Blixt, M.K.E., Hallböök, F., 2016. A regulatory sequence from theretinoid X receptor γ genedirects expression to horizontal cells and photoreceptors in the embryonic chicken retina. Mol. Vis. 22, 1405–1420.

Boije, H., Shirazi Fard, S., Edqvist, P.-H., Hallböök, F., 2016. Horizontal Cells, the Odd Ones Out in the Retina, Give Insights into Development and Disease. Front. Neuroanat. 10, 1–12. https://doi.org/10.3389/fnana.2016.00077

Borges, R., Johnson, W.E., O'Brien, S.J., Gomes, C., Heesy, C.P., Antunes, A., 2018. Adaptive genomic evolution of opsins reveals that early mammals flourished in nocturnal environments. BMC Genomics 1–12. https://doi.org/10.1186/s12864-017-4417-8

Braasch, I., Gehrke, A.R., Smith, J.J., Kawasaki, K., Manousaki, T., Pasquier, J., Amores, A., Desvignes, T., Batzel, P., Catchen, J., Berlin, A.M., Campbell, M.S., Barrell, D., Martin, K.J., Mulley, J.F., Ravi, V., Lee, A.P., Nakamura, T., Chalopin, D., Fan, S., Wcisel, D., Caestro, C., Sydes, J., Beaudry, F.E.G., Sun, Y., Hertel, J., Beam, M.J., Fasold, M., Ishiyama, M., Johnson, J., Kehr, S., Lara, M., Letaw, J.H., Litman, G.W., Litman, R.T., Mikami, M., Ota, T., Saha, N.R., Williams, L., Stadler, P.F., Wang, H., Taylor, J.S., Fontenot, Q., Ferrara, A., Searle, S.M.J., Aken, B., Yandell, M., Schneider, I., Yoder, J.A., Volff, J.N., Meyer, A., Amemiya, C.T., Venkatesh, B., Holland, P.W.H., Guiguen, Y., Bobe, J., Shubin, N.H., Di Palma, F., Alföldi, J., Lindblad-Toh, K., Postlethwait, J.H., 2016. The spotted gar genome illuminates vertebrate evolution and facilitates human-teleost comparisons. Nat.

Genet. 48, 427–437. https://doi.org/10.1038/ng.3526

Brightman, D.S., Razafsky, D., Potter, C., Hodzic, D., Chen, S., 2016. Nrl - Cre transgenic mouse mediates loxP recombination in developing rod photoreceptors. genesis 54, 129–135. https://doi.org/10.1002/dvg.22918

Brooks, M.J., Rajasimha, H.K., Swaroop, A., 2012. Retinal transcriptome profiling by directional next-generation sequencing using 100 ng of total RNA. Methods Mol. Biol. 884, 319–34. https://doi.org/10.1007/978-1-61779-848-1_23

Browman, Hawryshyn, 1994. RETINOIC ACID MODULATES RETINAL DEVELOPMENT IN THE JUVENILES OF A TELEOST FISH. J. Exp. Biol. 193, 191–207.

Brzezinski, J.A., Lamba, D.A., Reh, T.A., 2010. Blimp1 controls photoreceptor versus bipolar cell fate choice during retinal development. Development 137, 619–629. https://doi.org/10.1242/dev.043968

Burkhardt, D.A., 1994. Light adaptation and photopigment bleaching in cone photoreceptors in situ in the retina of the turtle. J. Neurosci. 14, 1091–105.

Bustin, S.A., Benes, V., Garson, J.A., Hellemans, J., Huggett, J., Kubista, M., Mueller, R., Nolan, T., Pfaffl, M.W., Shipley, G.L., Vandesompele, J., Wittwer, C.T., 2009. The MIQE guidelines: minimum information for publication of quantitative real-time PCR experiments. Clin. Chem. 55, 611–22. https://doi.org/10.1373/clinchem.2008.112797

Capella-Gutiérrez, S., Silla-Martínez, J.M., Gabaldón, T., 2009. trimAl: A tool for automated alignment trimming in large-scale phylogenetic analyses. Bioinformatics 25, 1972–1973. https://doi.org/10.1093/bioinformatics/btp348

Carter-Dawson, L.D., Lavail, M.M., 1979. Rods and cones in the mouse retina. I. Structural analysis using light and electron microscopy. J. Comp. Neurol. 188, 245–262. https://doi.org/10.1002/cne.901880204

Caruso, G., Bisegna, P., Shen, L., Andreucci, D., Hamm, H.E., DiBenedetto, E., 2006. Modeling the role of incisures in vertebrate phototransduction. Biophys. J. 91, 1192–212. https://doi.org/10.1529/biophysj.106.083618

Cepko, C.L., 2015. The Determination of Rod and Cone Photoreceptor Fate. Annu. Rev. Vis. Sci. 1, 211–234. https://doi.org/10.1146/annurev-vision-090814-121657

Chen, F., Figueroa, D.J., Marmorstein, A.D., Zhang, Q., Petrukhin, K., Caskey, C.T., Austin, C.P., 1999. Retina-specific nuclear receptor: A potential regulator of cellular retinaldehyde-binding protein expressed in retinal pigment epithelium and Müller glial cells. Proc. Natl. Acad. Sci. U. S. A. 96, 15149–54.

Chen, J., Rattner, A., Nathans, J., 2005. The rod photoreceptor-specific nuclear receptor Nr2e3 represses transcription of multiple cone-specific genes. J. Neurosci. 25, 118–29. https://doi.org/10.1523/JNEUROSCI.3571-04.2005

Chen, K., Durand, D., Farach-Colton, M., 2000. NOTUNG: A Program for Dating Gene Duplications and Optimizing Gene Family Trees. J. Comput. Biol. 7, 429–447. https://doi.org/10.1089/106652700750050871

Chen, S., Wang, Q.L., Nie, Z., Sun, H., Lennon, G., Copeland, N.G., Gilbert, D.J., Jenkins, N.A., Zack, D.J., 1997. Crx, a novel Otx-like paired-homeodomain protein, binds to and transactivates photoreceptor cell-specific genes. Neuron 19, 1017–1030. https://doi.org/10.1016/S0896-6273(00)80394-3

Cheng, H., Aleman, T.S., Cideciyan, A. V., Khanna, R., Jacobson, S.G., Swaroop, A., 2006. In vivo function of the orphan nuclear receptor NR2E3 in establishing photoreceptor identity during mammalian retinal development. Hum. Mol. Genet. 15, 2588–2602. https://doi.org/10.1093/hmg/ddl185

Cheng, H., Khan, N.W., Roger, J.E., Swaroop, A., 2011. Excess cones in the retinal degeneration rd7 mouse, caused by the loss of function of orphan nuclear receptor Nr2e3, originate from early-born photoreceptor precursors. Hum. Mol. Genet. 20, 4102–4115. https://doi.org/10.1093/hmg/ddr334

Cheng, H., Khanna, H., Oh, E.C.T., Hicks, D., Mitton, K.P., Swaroop, A., 2004. Photoreceptor-specific nuclear receptor NR2E3 functions as a transcriptional activator in rod photoreceptors. Hum. Mol. Genet. 13, 1563–1575. https://doi.org/10.1093/hmg/ddh173

Chi, N.C., Shaw, R.M., De Val, S., Kang, G., Jan, L.Y., Black, B.L., Stainier, D.Y.R., 2008. Foxn4 directly regulates tbx2b expression and atrioventricular canal formation. Genes Dev. 22, 734–9. https://doi.org/10.1101/gad.1629408

Chow, L., Levine, E.M., Reh, T. a, 1998. The nuclear receptor transcription factor, retinoid-related orphan receptor beta, regulates retinal progenitor proliferation.

Mech. Dev. 77, 149–64. https://doi.org/S092547739800135X [pii]

Clanton, J.A., Hope, K.D., Gamse, J.T., 2013. Fgf signaling governs cell fate in the zebrafish pineal complex. Development 140, 323–32. https://doi.org/10.1242/dev.083709

Collin, S.P., 2009. Early evolution of vertebrate photoreception: lessons from lampreys and lungfishes. Integr. Zool. 4, 87–98. https://doi.org/10.1111/j.1749-4877.2008.00138.x

Collin, S.P., Hart, N.S., Shand, J., Potter, I.C., 2003. Morphology and spectral absorption characteristics of retinal photoreceptors in the southern hemisphere lamprey (Geotria australis). Vis. Neurosci. 20, 119–130. https://doi.org/10.1017/S0952523803202030

Collin, S.P., Hart, N.S., Wallace, K.M., Shand, J., Potter, I.C., 2004. Vision in the southern hemisphere lamprey Mordacia mordax: Spatial distribution, spectral absorption characteristics, and optical sensitivity of a single class of retinal photoreceptor. Vis. Neurosci. 21, 765–773. https://doi.org/10.1017/S0952523804215103

Collin, S.P., Knight, M.A., Davies, W.L., Potter, I.C., Hunt, D.M., Trezise, A.E.O., 2003. Ancient colour vision: Multiple opsin genes in the ancestral vertebrates. Curr. Biol. https://doi.org/10.1016/j.cub.2003.10.044

Collin, S.P., Potter, I.C., 2000. The ocular morphology of the southern hemisphere lamprey Mordacia mordax Richardson with special reference to a single class of photoreceptor and a retinal tapetum. Brain. Behav. Evol. 55, 120–138. https://doi.org/6647

Collin, S.P., Potter, I.C., Braekevelt, C.R., 1999. The Ocular Morphology of the Southern Hemisphere Lamprey Geotria australis Gray, with Special Reference to Optical Specialisations and the Characterisation and Phylogeny of Photoreceptor Types. Brain. Behav. Evol. 54, 96–118. https://doi.org/10.1159/000006616

Collin, S.P., Trezise, A.E., 2004. The origins of colour vision in vertebrates. Clin. Exp. Optom. https://doi.org/10.1111/j.1444-0938.2004.tb05051.x

Conrad, G.W., Bee, J.A., Roche, S.M., Teillet, M.A., 1993. Fabrication of microscalpels by electrolysis of tungsten wire in a meniscus. J. Neurosci. Methods 50, 123–127.

https://doi.org/10.1016/0165-0270(93)90062-V

Contín, M.A., Verra, D.M., Salvador, G., Ilincheta, M., Giusto, N.M., Guido, M.E., 2010. Light activation of the phosphoinositide cycle in intrinsically photosensitive chicken retinal ganglion cells. Investig. Ophthalmol. Vis. Sci. 51, 5491–5498. https://doi.org/10.1167/iovs.10-5643

Coolen, M., Sii-Felice, K., Bronchain, O., Mazabraud, A., Bourrat, F., Rétaux, S., Felder-Schmittbuhl, M.P., Mazan, S., Plouhinec, J.L., 2005. Phylogenomic analysis and expression patterns of large Maf genes in Xenopus tropicalis provide new insights into the functional evolution of the gene family in osteichthyans. Dev. Genes Evol. 215, 327–339. https://doi.org/10.1007/s00427-005-0476-y

Corbo, J.C., Cepko, C.L., 2005. A hybrid photoreceptor expressing both rod and cone genes in a mouse model of enhanced S-cone syndrome. PLoS Genet. 1, 0140–0153. https://doi.org/10.1371/journal.pgen.0010011

Corbo, J.C., Lawrence, K.A., Karlstetter, M., Res, G., Corbo, J.C., Lawrence, K.A., Karlstetter, M., Myers, C.A., Abdelaziz, M., Dirkes, W., Weigelt, K., Seifert, M., Benes, V., Fritsche, L.G., Weber, B.H.F., Langmann, T., 2010. CRX ChIP-seq reveals the cis -regulatory architecture of mouse photoreceptors CRX ChIP-seq reveals the cis -regulatory architecture of mouse photoreceptors 1512–1525. https://doi.org/10.1101/gr.109405.110

Curcio, C.A., Allen, K.A., Sloan, K.R., Lerea, C.L., Hurley, J.B., Klock, I.B., Milam, A.H., 1991. Distribution and morphology of human cone photoreceptors stained with anti-blue opsin. J. Comp. Neurol. 312, 610–624. https://doi.org/10.1002/cne.903120411

D'Orazi, F.D., Zhao, X.F., Wong, R.O., Yoshimatsu, T., 2016. Mismatch of Synaptic Patterns between Neurons Produced in Regeneration and during Development of the Vertebrate Retina. Curr. Biol. 26, 2268–2279. https://doi.org/10.1016/j.cub.2016.06.063

Daniele, L.L., Lillo, C., Lyubarsky, A.L., Nikonov, S.S., Philp, N., Mears, A.J., Swaroop, A., Williams, D.S., Pugh, E.N., 2005. Cone-like morphological, molecular, and electrophysiological features of the photoreceptors of the Nrl knockout mouse. Investig. Ophthalmol. Vis. Sci. 46, 2156–2167. https://doi.org/10.1167/iovs.04-1427

Das, T., Payer, B., Cayouette, M., Harris, W.A., 2003. In vivo time-lapse imaging of cell

divisions during neurogenesis in the developing zebrafish retina. Neuron 37, 597–609. https://doi.org/10.1016/S0896-6273(03)00066-7

Davies, W.I.L., Collin, S.P., Hunt, D.M., 2012. Molecular ecology and adaptation of visual photopigments in craniates. Mol. Ecol. 21, 3121–3158. https://doi.org/10.1111/j.1365-294X.2012.05617.x

Davies, W.L., Carvalho, L.S., Cowing, J.A., Beazley, L.D., Hunt, D.M., Arrese, C.A., 2007. Visual pigments of the platypus: A novel route to mammalian colour vision. Curr. Biol. 17, 161–163. https://doi.org/10.1016/j.cub.2007.01.037

Davies, W.L., Collin, S.P., Hunt, D.M., 2009. Adaptive gene loss reflects differences in the visual ecology of basal vertebrates. Mol. Biol. Evol. 26, 1803–1809. https://doi.org/10.1093/molbev/msp089

Davies, W.L., Cowing, J.A., Bowmaker, J.K., Carvalho, L.S., Gower, D.J., Hunt, D.M., 2009. Shedding Light on Serpent Sight: The Visual Pigments of Henophidian Snakes. J. Neurosci. 29, 7519–7525. https://doi.org/10.1523/JNEUROSCI.0517-09.2009

Davison, J.M., Akitake, C.M., Goll, M.G., Rhee, J.M., Gosse, N., Baier, H., Halpern, M.E., Leach, S.D., Parsons, M.J., 2007. Transactivation from Gal4-VP16 transgenic insertions for tissue-specific cell labeling and ablation in zebrafish. Dev. Biol. 304, 811–824. https://doi.org/10.1016/j.ydbio.2007.01.033

de Busserolles, F., Cortesi, F., Helvik, J.V., Davies, W.I.L., Templin, R.M., Sullivan, R.K.P., Michell, C.T., Mountford, J.K., Collin, S.P., Irigoien, X., Kaartvedt, S., Marshall, J., 2017. Pushing the limits of photoreception in twilight conditions: The rod-like cone retina of the deep-sea pearlsides. Sci. Adv. 3, eaao4709. https://doi.org/10.1126/sciadv.aao4709

De Celis, J.F., Barrio, R., 2009. Regulation and function of Spalt proteins during animal development. Int. J. Dev. Biol. 53, 1385–1398. https://doi.org/10.1387/ijdb.072408jd

de Melo, J., Peng, G.-H., Chen, S., Blackshaw, S., 2011. The Spalt family transcription factor Sall3 regulates the development of cone photoreceptors and retinal horizontal interneurons. Development 138, 2325–2336. https://doi.org/10.1242/dev.061846

den Hollander, A.I., Biyanwila, J., Kovach, P., Bardakjian, T., Traboulsi, E.I., Ragge,

N.K., Schneider, A., Malicki, J., 2010. Genetic defects of GDF6 in the zebrafish out of sight mutant and in human eye developmental anomalies. BMC Genet. 11. https://doi.org/10.1186/1471-2156-11-102

Dickson, D.H., Graves, D.A., 1979. Fine structure of the lamprey photoreceptors and retinal pigment epithelium (Petromyzon marinus L.). Exp. Eye Res. 29, 45–60. https://doi.org/10.1016/0014-4835(79)90165-9

Distel, M., Wullimann, M.F., Koster, R.W., 2009. Optimized Gal4 genetics for permanent gene expression mapping in zebrafish. Proc. Natl. Acad. Sci. 106, 13365–13370. https://doi.org/10.1073/pnas.0903060106

Domingos, P.M., Brown, S., Barrio, R., Ratnakumar, K., Frankfort, B.J., Mardon, G., Steller, H., Mollereau, B., 2004a. Regulation of R7 and R8 differentiation by the spalt genes. Dev. Biol. 273, 121–133. https://doi.org/10.1016/j.ydbio.2004.05.026

Domingos, P.M., Mlodzik, M., Mendes, C.S., Brown, S., Steller, H., Mollereau, B., 2004b. Spalt transcription factors are required for R3/R4 specification and establishment of planar cell polarity in the Drosophila eye. Development 131, 5695–702. https://doi.org/10.1242/dev.01443

Dorsky, R.I., Chang, W.S., Rapaport, D.H., Harris, W.A., 1997. Regulation of neuronal diversity in the Xenopus retina by delta signalling. Nature 385, 67–70. https://doi.org/10.1038/385067a0

Dowling, J.E., 2012. The Retina: An Approachable Part of the Brain, Rev. Ed. ed. The Belknap Press of Harvard University Press, Cambridge, Massachusetts; London, England.

Drivenes, Ø., Seo, H.C., Fjose, A., 2000. Characterisation of the promoter region of the zebrafish six7 gene. Biochim. Biophys. Acta - Gene Struct. Expr. 1491, 240–247. https://doi.org/10.1016/S0167-4781(00)00042-7

Duval, M.G., Chung, H., Lehmann, O.J., Allison, W.T., 2013. Longitudinal fluorescent observation of retinal degeneration and regeneration in zebrafish using fundus lens imaging. Mol. Vis. 19, 1082–95.

DuVal, M.G., Gilbert, M.J.H., Watson, D.E., Zerulla, T.C., Tierney, K.B., Allison, W.T., 2014. Growth differentiation factor 6 as a putative risk factor in neuromuscular degeneration. PLoS One 9. https://doi.org/10.1371/journal.pone.0089183

DuVal, M.G., Oel, A.P., Allison, W.T., 2014. gdf6a Is Required for Cone Photoreceptor Subtype Differentiation and for the Actions of tbx2b in Determining Rod Versus Cone Photoreceptor Fate. PLoS One 9, e92991. https://doi.org/10.1371/journal.pone.0092991

Eakin, R.M., 1973. The Third Eye. University of California Press, Berkeley, California.

Ebert, M.S., Sharp, P.A., 2010. Emerging roles for natural microRNA sponges. Curr. Biol. 20, R858–R861. https://doi.org/10.1016/j.cub.2010.08.052

El-Beltagy, A.E.F.B.M., 2015. Light and electron microscopic studies on the pigmented epithelium and photoreceptors of the retina of common buzzard (Buteo buteo). Tissue Cell 47, 78–85. https://doi.org/10.1016/j.tice.2014.11.008

Elsaeidi, F., Macpherson, P., Mills, E.A., Jui, J., Flannery, J.G., Goldman, D., 2018. Notch Suppression Collaborates with Ascl1 and Lin28 to Unleash a Regenerative Response in Fish Retina, But Not in Mice. J. Neurosci. 38, 2246–2261. https://doi.org/10.1523/JNEUROSCI.2126-17.2018

Emerson, M.M., Cepko, C.L., 2011. Identification of a retina-specific Otx2 enhancer element active in immature developing photoreceptors. Dev. Biol. 360, 241–255. https://doi.org/10.1016/j.ydbio.2011.09.012

Emerson, M.M., Surzenko, N., Goetz, J.J., Trimarchi, J., Cepko, C.L., 2013. Otx2 and Onecut1 promote the fates of cone photoreceptors and horizontal cells and repress rod photoreceptors. Dev. Cell 26, 59–72. https://doi.org/10.1016/j.devcel.2013.06.005

Enright, J.M., Lawrence, K.A., Hadzic, T., Corbo, J.C., 2015a. Transcriptome profiling of developing photoreceptor subtypes reveals candidate genes involved in avian photoreceptor diversification. J. Comp. Neurol. 523, 649–668. https://doi.org/10.1002/cne.23702

Enright, J.M., Toomey, M.B., Sato, S.Y., Temple, S.E., Allen, J.R., Fujiwara, R., Kramlinger, V.M., Nagy, L.D., Johnson, K.M., Xiao, Y., How, M.J., Johnson, S.L., Roberts, N.W., Kefalov, V.J., Peter Guengerich, F., Corbo, J.C., 2015b. Cyp27c1 red-shifts the spectral sensitivity of photoreceptors by converting Vitamin A1 into A2. Curr. Biol. 25, 3048–3057. https://doi.org/10.1016/j.cub.2015.10.018

Fadool, J.M., Dowling, J.E., 2008. Zebrafish: A model system for the study of eye

genetics. Prog. Retin. Eye Res. 27, 89–110. https://doi.org/10.1016/j.preteyeres.2007.08.002

Fain, G.L., Hardie, R., Laughlin, S.B., 2010. Phototransduction and the Evolution of Photoreceptors. Curr. Biol. https://doi.org/10.1016/j.cub.2009.12.006

Finkelstein, R., Smouse, D., Capaci, T.M., Spradling, A.C., Perrimon, N., 1990. The orthodenticle gene encodes a novel homeo domain protein involved in the development of the Drosophila nervous system and ocellar visual structures. Genes Dev. 4, 1516–1527. https://doi.org/10.1101/gad.4.9.1516

Fleisch, V.C., Fraser, B., Allison, W.T., 2011. Investigating regeneration and functional integration of CNS neurons: Lessons from zebrafish genetics and other fish species. Biochim. Biophys. Acta - Mol. Basis Dis. 1812, 364–380. https://doi.org/10.1016/j.bbadis.2010.10.012

Fleisch, V.C., Leighton, P.L.A., Wang, H., Pillay, L.M., Ritzel, R.G., Bhinder, G., Roy, B., Tierney, K.B., Ali, D.W., Waskiewicz, A.J., Allison, W.T., 2013. Targeted mutation of the gene encoding prion protein in zebrafish reveals a conserved role in neuron excitability. Neurobiol. Dis. 55, 11–25. https://doi.org/10.1016/j.nbd.2013.03.007

Foster, R., 1998. Extraretinal photoreceptors and their regulation of temporal physiology. Rev. Reprod. 3, 145–150. https://doi.org/10.1530/ror.0.0030145

Fraser, B., DuVal, M.G., Wang, H., Allison, W.T., 2013. Regeneration of Cone Photoreceptors when Cell Ablation Is Primarily Restricted to a Particular Cone Subtype. PLoS One 8. https://doi.org/10.1371/journal.pone.0055410

French, C.R., 2010. Patterning the zebrafish visual system requires the actions of Pbx transcription factors, and a downstream growth factor, Gdf6a. University of Alberta.

French, C.R., Erickson, T., French, D. V., Pilgrim, D.B., Waskiewicz, A.J., 2009. Gdf6a is required for the initiation of dorsal-ventral retinal patterning and lens development. Dev. Biol. 333, 37–47. https://doi.org/10.1016/j.ydbio.2009.06.018

French, C.R., Stach, T.R., March, L.D., Lehmann, O.J., Waskiewicz, A.J., 2013. Apoptotic and proliferative defects characterize ocular development in a microphthalmic BMP model. Investig. Ophthalmol. Vis. Sci. 54, 4636–4647. https://doi.org/10.1167/iovs.13-11674

Freund, C.L., Gregory-Evans, C.Y., Furukawa, T., Papaioannou, M., Looser, J., Ploder,

L., Bellingham, J., Ng, D., Herbrick, J.A.S., Duncan, A., Scherer, S.W., Tsui, L.C., Loutradis-Anagnostou, A., Jacobson, S.G., Cepko, C.L., Bhattacharya, S.S., McInnes, R.R., 1997. Cone-rod dystrophy due to mutations in a novel photoreceptor-specific homeobox gene (CRX) essential for maintenance of the photoreceptor. Cell 91, 543–553. https://doi.org/10.1016/S0092-8674(00)80440-7

Friedman, J.S., Khanna, H., Swain, P.K., DeNicola, R., Cheng, H., Mitton, K.P., Weber, C.H., Hicks, D., Swaroop, A., 2004. The minimal transactivation domain of the basic motif-leucine zipper transcription factor NRL interacts with TATA-binding protein. J. Biol. Chem. 279, 47233–47241. https://doi.org/10.1074/jbc.M408298200

Fritzsch, B., Collin, S.P., 1990. Dendritic distribution of two populations of ganglion cells and the retinopetal fibers in the retina of the silver lamprey (Ichthyomyzon unicuspis). Vis. Neurosci. 4, 533–545. https://doi.org/10.1017/S0952523800005745

Fu, Y., Liu, H., Ng, L., Kim, J.W., Hao, H., Swaroop, A., Forrest, D., 2014. Feedback induction of a photoreceptor-specific isoform of retinoid-related orphan nuclear receptor β by the rod transcription factor NRL. J. Biol. Chem. 289, 32469–32480. https://doi.org/10.1074/jbc.M114.605774

Fuentes, F., Reynolds, E., Lewellis, S.W., Venkiteswaran, G., Knaut, H., 2016. A Plasmid Set for Efficient Bacterial Artificial Chromosome (BAC) Transgenesis in Zebrafish. G3 (Bethesda). 6, 829–34. https://doi.org/10.1534/g3.115.026344

Fujieda, H., Bremner, R., Mears, A.J., Sasaki, H., 2009. Retinoic acid receptor-related orphan receptor α regulates a subset of cone genes during mouse retinal development. J. Neurochem. 108, 91–101. https://doi.org/10.1111/j.1471-4159.2008.05739.x

Furukawa, T., Morrow, E.M., Cepko, C.L., Ahmad, I., Ahmad, I., Redmond, L.J., Barnstable, C.J., Badiani, P., Corbella, P., Kioussis, D., Marvel, J., Weston, K., Bally-Cuif, L., Gulisano, M., Broccoli, V., Boncinelli, E., Blitz, I.L., Cho, K.W., Bobola, N., Hirsch, E., Albini, A., Altruda, F., Noonan, D., Ravazzolo, R., Carter-Dawson, L.D., LaVail, M.M., Cepko, C.L., Austin, C.P., Yang, X., Alexiades, M., Ezzeddine, D., Chen, S., Zack, D.J., Chiu, M.I., Nathans, J., Chou, W.-H., Hall, K.J., Wilson, D.B., Wideman, C.L., Townson, S.M., Chadwell, L.V., Britt, S.G., Conlon, F.L., Sedgwick, S.G., Weston, K.M., Smith, J.C., Dowling, J.E., Dryja, T.P.,

Li, T., Fields-Berry, S.C., Halliday, A., Cepko, C.L., Finkelstein, R., Smouse, D., Capaci, T.M., Spradling, A.C., Perrimon, N., Fortini, M.K., Rubin, G.R., Freund, C.L., Gregory-Evans, C.Y., Furukawa, T., Papaioannou, M., Looser, J., Ploder, L., Bellingham, J., Ng, D., Herbrick, J.S., Duncan, A., al., et, Furukawa, T., Kozak, C.A., Cepko, C.L., Hanes, S.D., Brent, R., Hicks, D., Barnstable, C., Humphries, M.H., Rancourt, D., Farrar, G.J., Kenna, P., Hazel, M., Bush, R.A., Sieving, P.A., Sheils, D.M., McNally, N., Creighton, P., al., et, Jin, Y., Hoskins, R., Horvitz, H.R., Kikuchi, T., Raju, K., Breitman, M.L., Shinohara, T., Kumar, R., Chen, S., Scheurer, D., Wang, Q.-L., Duh, E., Sung, C.-H., Rehemtulla, A., Swaroop, A., Adler, R., Zack, D.J., Lamonerie, T., Tremblay, J.J., Lanctôt, C., Therrien, M., Gauthier, Y., Drouin, J., LaVail, M.M., Gorrin, G.M., Repaci, M.A., Thomas, L.A., Ginsberg, H.M., Li, Y., Allende, M.L., Finkelstein, R., Weinberg, E.S., Liou, G.I., Matragoon, S., Yang, J., Geng, L., Overbeek, P.A., Ma, D.P., Liou, G.I., Wang, M., Matragoon, S., Liu, Q., Breitman, M.L., Hitchcock, P.F., Swaroop, A., Luckow, B., Schütz, G., Morabito, M.A., Yu, X., Barnstable, C.J., Morgan, B.A., Fekete, D.M., Mori, H., Miyazaki, Y., Morita, T., Nitta, H., Mishina, M., Nathans, J., Thomas, D., Hogness, D.S., Nathans, J., Davenport, C.M., Maumenee, I.H., Lewis, R.A., Hejtmancik, J.F., Litt, M., Lovrien, E., Weleber, R., Bachynski, B., Zwas, F., Klingaman, R., Fishman, G., Ni, M., Yamaki, K., Kikuchi, T., Ferrick, M., Shinohara, T., Nussenblatt, R., Chan, C.C., Nir, I., Cohen, D., Papermaster, D.S., Pannese, M., Polo, C., Andreazzoli, M., Vignali, R., Kablar, B., Barsacchi, G., Boncinelli, E., Rehemtulla, A., Warwar, R., Kumar, R., Ji, X., Zack, D.J., Swaroop, A., Saha, M.S., Servetnick, M., Grainger, R.M., Semina, E.V., Reiter, R., Leysens, N.J., Alward, W.L.-M., Small, K.W., Datson, N.A., Siegel-Bartelt, J., Bierke-Nelson, D., Bitoun, P., Zabel, al., et, Simeone, A., Acampora, D., Mallamaci, A., Stornaiuolo, A., D'Apice, M.R., Nigro, V., Boncinelli, E., Stepanik, P.L., Lerious, V., McGinnis, J.F., Swaroop, A., Xu, J.Z., Pawar, H., Jackson, A., Skolnick, C., Agarwal, N., Szeto, D.P., Ryan, A.K., S.M, O.C., Rosenfeld, M.G., Takao, M., Yasui, A., Tokunaga, F., Treisman, J., Gönczy, P., Vashishtha, M., Harris, E., Desplan, C., Turner, D.L., Cepko, C.L., Vandendries, E.R., Johnson, D., Reinke, R., Wang, Y., Macke, J.P., Merbs, S.L., Zack, D.J., Klaunberg, B., Bennett, J., Gearhart, J., Nathans, J., Wilson, D., Sheng,

G., Lecuit, T., Dostatni, N., Desplan, C., Yang, X., Chung, D., Cepko, C.L., Young, R., Yu, X., Barnstable, C.J., Yu, X., Chung, M., Morabito, M.A., Barnstable, C.J., Zack, D.J., Bennett, J., Wang, Y., Davenport, C., Klaunberg, B., Gearhart, J., Nathans, J., Zipursky, S.L., Rubin, G.M., 1997. Crx, a novel otx-like homeobox gene, shows photoreceptor-specific expression and regulates photoreceptor differentiation. Cell 91, 531–41. https://doi.org/10.1016/S0092-8674(00)80439-0

Furukawa, T., Morrow, E.M., Li, T., Davis, F.C., Cepko, C.L., 1999. Retinopathy and attenuated circadian entrainment in Crx-deficient mice. Nat. Genet. 23, 466–470. https://doi.org/10.1038/70591

Gagnon, J.A., Valen, E., Thyme, S.B., Huang, P., Ahkmetova, L., Pauli, A., Montague, T.G., Zimmerman, S., Richter, C., Schier, A.F., 2014. Efficient mutagenesis by Cas9 protein-mediated oligonucleotide insertion and large-scale assessment of single-guide RNAs. PLoS One 9, 5–12. https://doi.org/10.1371/journal.pone.0098186

Gamse, J.T., Shen, Y.C., Thisse, C., Thisse, B., Raymond, P.A., Halpern, M.E., Liang, J.O., 2002. Otx5 regulates genes that show circadian expression in the zebrafish pineal complex. Nat. Genet. 30, 117–121. https://doi.org/10.1038/ng793

Geller, A.M., Sieving, P.A., 1993. Assessment of foveal cone photoreceptors in Stargardt's macular dystrophy using a small dot detection task. Vision Res. 33, 1509–1524. https://doi.org/10.1016/0042-6989(93)90144-L

Gerkema, M.P., Davies, W.I.L., Foster, R.G., Menaker, M., Hut, R.A., 2013. The nocturnal bottleneck and the evolution of activity patterns in mammals. Proc. R. Soc. B Biol. Sci. 280, 20130508–20130508. https://doi.org/10.1098/rspb.2013.0508

Gestri, G., Link, B.A., Neuhauss, S.C.F., 2012. The visual system of zebrafish and its use to model human ocular Diseases. Dev. Neurobiol. 72, 302–327. https://doi.org/10.1002/dneu.20919

Glaschke, A., Weiland, J., Del Turco, D., Steiner, M., Peichl, L., Glosmann, M., 2011. Thyroid Hormone Controls Cone Opsin Expression in the Retina of Adult Rodents. J. Neurosci. 31, 4844–4851. https://doi.org/10.1523/JNEUROSCI.6181-10.2011

Godinho, L., Williams, P.R., Claassen, Y., Provost, E., Leach, S.D., Kamermans, M., Wong, R.O.L., 2007. Nonapical Symmetric Divisions Underlie Horizontal Cell Layer

Formation in the Developing Retina In Vivo. Neuron 56, 597–603. https://doi.org/10.1016/j.neuron.2007.09.036

Gomez, G.A., Veldman, M.B., Zhao, Y., Burgess, S., Lin, S., 2009. Discovery and characterization of novel vascular and hematopoietic genes downstream of Etsrp in zebrafish. PLoS One 4. https://doi.org/10.1371/journal.pone.0004994

Gomez, M.P., Nasi, E., 2000. Light transduction in invertebrate hyperpolarizing photoreceptors: possible involvement of a Go-regulated guanylate cyclase. J. Neurosci. 20, 5254–5263. https://doi.org/20/14/5254 [pii]

Gonzalez-Rodriguez, J., Pelcastre, E.L., Tovilla-Canales, J.L., Garcia-Ortiz, J.E., Amato-Almanza, M., Villanueva-Mendoza, C., Espinosa-Mattar, Z., Zenteno, J.C., 2010. Mutational screening of CHX10, GDF6, OTX2, RAX and SOX2 genes in 50 unrelated microphthalmia-anophthalmia-coloboma (MAC) spectrum cases. Br. J. Ophthalmol. 94, 1100–4. https://doi.org/10.1136/bjo.2009.173500

Gorski, S.A., Vogel, J., Doudna, J.A., 2017. RNA-based recognition and targeting: Sowing the seeds of specificity. Nat. Rev. Mol. Cell Biol. 18, 215–228. https://doi.org/10.1038/nrm.2016.174

Gosse, N.J., Baier, H., 2009. An essential role for Radar (Gdf6a) in inducing dorsal fate in the zebrafish retina. Proc. Natl. Acad. Sci. 106, 2236–2241. https://doi.org/10.1073/pnas.0803202106

Gotow, T., Nishi, T., 2002. Light-dependent K + Channels in the Mollusc Onchidium Simple Photoreceptors Are Opened by cGMP. J. Gen. Physiol. 120, 581–597. https://doi.org/10.1085/jgp.20028619

Govardovskii, V.I., Lychakov, D. V, 1984. Visual cells and visual pigments of the lamprey, Lampetra fluviatilis. J. Comp. Physiol. A 154, 279–286. https://doi.org/10.1007/BF00604994

Grimaldi, A., Buisine, N., Miller, T., Shi, Y.B., Sachs, L.M., 2013. Mechanisms of thyroid hormone receptor action during development: Lessons from amphibian studies. Biochim. Biophys. Acta - Gen. Subj. 1830, 3882–3892. https://doi.org/10.1016/j.bbagen.2012.04.020

Gross, J.M., Dowling, J.E., 2005. Tbx2b is essential for neuronal differentiation along the dorsal/ventral axis of the zebrafish retina. Proc. Natl. Acad. Sci. U. S. A. 102,

4371–4376. https://doi.org/10.1073/pnas.0501061102

Gu, H., Smith, Z.D., Bock, C., Boyle, P., Gnirke, A., Meissner, A., 2011. Preparation of reduced representation bisulfite sequencing libraries for genome-scale DNA methylation profiling. Nat. Protoc. 6, 468–81. https://doi.org/10.1038/nprot.2010.190

Guler, A., Altimus, C., Ecker, J., Hattar, S., 2007. Multiple Photoreceptors Contribute to Nonimage-forming Visual Functions Predominantly through Melanopsin- containing ... Multiple Photoreceptors Contribute to Nonimage-forming Visual Functions Predominantly through Melanopsin- containing Retinal Ganglion. Cold Spring Harb. Symp. Quant. Biol. 122, 509–15. https://doi.org/10.1101/sqb.2007.72.074

Haider, N.B., Jacobson, S.G., Cideciyan, a V, Swiderski, R., Streb, L.M., Searby, C., Beck, G., Hockey, R., Hanna, D.B., Gorman, S., Duhl, D., Carmi, R., Bennett, J., Weleber, R.G., Fishman, G. a, Wright, a F., Stone, E.M., Sheffield, V.C., 2000. Mutation of a nuclear receptor gene, NR2E3, causes enhanced S cone syndrHaider, N. B., Jacobson, S. G., Cideciyan, a V, Swiderski, R., Streb, L. M., Searby, C., … Sheffield, V. C. (2000). Mutation of a nuclear receptor gene, NR2E3, causes enhanced S cone . Nat. Genet. 24, 127–131. https://doi.org/10.1038/72777

Haider, N.B., Mollema, N., Gaule, M., Yuan, Y., Sachs, A.J., Nystuen, A.M., Naggert, J.K., Nishina, P.M., 2009. Nr2e3-directed transcriptional regulation of genes involved in photoreceptor development and cell-type specific phototransduction. Exp. Eye Res. 89, 365–372. https://doi.org/10.1016/j.exer.2009.04.006

Haider, N.B., Naggert, J.K., Nishina, P.M., 2001. Excess cone cell proliferation due to lack of a functional NR2E3 causes retinal dysplasia and degeneration in rd7/rd7 mice. Hum. Mol. Genet. 10, 1619–26. https://doi.org/10.1093/hmg/10.16.1619

Haltaufderhyde, K., Ozdeslik, R.N., Wicks, N.L., Najera, J.A., Oancea, E., 2015. Opsin expression in human epidermal skin. Photochem. Photobiol. 91, 117–123. https://doi.org/10.1111/php.12354

Hamaoka, T., Takechi, M., Chinen, A., Nishiwaki, Y., Kawamura, S., 2002. Visualization of rod photoreceptor development using GFP-transgenic zebrafish. Genesis 34, 215–220. https://doi.org/10.1002/gene.10155

Hanel, M.L., Hensey, C., 2006. Eye and neural defects associated with loss of GDF6. BMC Dev. Biol. 6, 43. https://doi.org/10.1186/1471-213X-6-43

Hannibal, J., Christiansen, A.T., Heegaard, S., Fahrenkrug, J., Kiilgaard, J.F., 2017. Melanopsin expressing human retinal ganglion cells: Subtypes, distribution, and intraretinal connectivity. J. Comp. Neurol. 525, 1934–1961. https://doi.org/10.1002/cne.24181

Hans, S., Kaslin, J., Freudenreich, D., Brand, M., 2009. Temporally-controlled site-specific recombination in zebrafish. PLoS One 4. https://doi.org/10.1371/journal.pone.0004640

Hao, H., Kim, D.S., Klocke, B., Johnson, K.R., Cui, K., Gotoh, N., Zang, C., Gregorski, J., Gieser, L., Peng, W., Fann, Y., Seifert, M., Zhao, K., Swaroop, A., 2012. Transcriptional regulation of rod photoreceptor homeostasis revealed by in vivo NRL targetome analysis. PLoS Genet. 8. https://doi.org/10.1371/journal.pgen.1002649

Harman, A.M., Beazley, L.D., 1989. Generation of retinal cells in the wallaby, Setonix brachyurus (quokka). Neuroscience 28, 219–232. https://doi.org/10.1016/0306-4522(89)90246-7

Hart, N.S., 2004. Multiple cone visual pigments and the potential for trichromatic colour vision in two species of elasmobranch. J. Exp. Biol. 207, 4587–4594. https://doi.org/10.1242/jeb.01314

Hart, N.S., Lisney, T.J., Collin, S.P., 2006. Visual communication in elasmobranchs. Commun. Fishes Vol. 1 Vol. 2 337–392.

Hart, N.S., Theiss, S.M., Harahush, B.K., Collin, S.P., 2011. Microspectrophotometric evidence for cone monochromacy in sharks. Naturwissenschaften 98, 193–201. https://doi.org/10.1007/s00114-010-0758-8

Hedges, S.B., Marin, J., Suleski, M., Paymer, M., Kumar, S., 2015. Tree of life reveals clock-like speciation and diversification. Mol. Biol. Evol. 32, 835–845. https://doi.org/10.1093/molbev/msv037

Heesy, C.P., Hall, M.I., 2010. The nocturnal bottleneck and the evolution of mammalian vision. Brain. Behav. Evol. 75, 195–203. https://doi.org/10.1159/000314278

Helmstaedter, M., Briggman, K.L., Turaga, S.C., Jain, V., Seung, H.S., Denk, W., 2013. Connectomic reconstruction of the inner plexiform layer in the mouse retina. Nature 500, 168–174. https://doi.org/10.1038/nature12346

Hollyfield, J.G., 1972. Histogenesis of the retina in the killifish, Fundulus heteroclitus. J. Comp. Neurol. 144, 373–379. https://doi.org/10.1002/cne.901440308

Holmberg, K., 1971. The hagfish retina: Electron microscopic study comparing receptor and epithelial cells in the pacific hagfish, Polistotrema stouti, with those in the atlantic hagfish, Myxine glutinosa. Zeitschrift für Zellforsch. und Mikroskopische Anat. 121, 249–269. https://doi.org/10.1007/BF00340676

Hoover, F., Seleiro, E.A.P., Kielland, A., Brickell, P.M., Glover, J.C., 1998. Retinoid X receptor γ gene transcripts are expressed by a subset of early generated retinal cells and eventually restricted to photoreceptors. J. Comp. Neurol. 391, 204–213. https://doi.org/10.1002/(SICI)1096-9861(19980209)391:2<204::AID-CNE4>3.0.CO;2-6

Hornstein, E.P., 2005. Gap-Junctional Coupling and Absolute Sensitivity of Photoreceptors in Macaque Retina. J. Neurosci. 25, 11201–11209. https://doi.org/10.1523/JNEUROSCI.3416-05.2005

Howe, K., Clark, M.D., Torroja, C.F., Torrance, J., Berthelot, C., Muffato, M., Collins, J.E., Humphray, S., McLaren, K., Matthews, L., McLaren, S., Sealy, I., Caccamo, M., Churcher, C., Scott, C., Barrett, J.C., Koch, R., Rauch, G.J., White, S., Chow, W., Kilian, B., Quintais, L.T., Guerra-Assunção, J.A., Zhou, Y., Gu, Y., Yen, J., Vogel, J.H., Eyre, T., Redmond, S., Banerjee, R., Chi, J., Fu, B., Langley, E., Maguire, S.F., Laird, G.K., Lloyd, D., Kenyon, E., Donaldson, S., Sehra, H., Almeida-King, J., Loveland, J., Trevanion, S., Jones, M., Quail, M., Willey, D., Hunt, A., Burton, J., Sims, S., McLay, K., Plumb, B., Davis, J., Clee, C., Oliver, K., Clark, R., Riddle, C., Eliott, D., Threadgold, G., Harden, G., Ware, D., Mortimer, B., Kerry, G., Heath, P., Phillimore, B., Tracey, A., Corby, N., Dunn, M., Johnson, C., Wood, J., Clark, S., Pelan, S., Griffiths, G., Smith, M., Glithero, R., Howden, P., Barker, N., Stevens, C., Harley, J., Holt, K., Panagiotidis, G., Lovell, J., Beasley, H., Henderson, C., Gordon, D., Auger, K., Wright, D., Collins, J., Raisen, C., Dyer, L., Leung, K., Robertson, L., Ambridge, K., Leongamornlert, D., McGuire, S., Gilderthorp, R., Griffiths, C., Manthravadi, D., Nichol, S., Barker, G., Whitehead, S., Kay, M., Brown, J., Murnane, C., Gray, E., Humphries, M., Sycamore, N., Barker, D., Saunders, D., Wallis, J., Babbage, A., Hammond, S., Mashreghi-Mohammadi,

M., Barr, L., Martin, S., Wray, P., Ellington, A., Matthews, N., Ellwood, M., Woodmansey, R., Clark, G., Cooper, J., Tromans, A., Grafham, D., Skuce, C., Pandian, R., Andrews, R., Harrison, E., Kimberley, A., Garnett, J., Fosker, N., Hall, R., Garner, P., Kelly, D., Bird, C., Palmer, S., Gehring, I., Berger, A., Dooley, C.M., Ersan-Ürün, Z., Eser, C., Geiger, H., Geisler, M., Karotki, L., Kirn, A., Konantz, J., Konantz, M., Oberländer, M., Rudolph-Geiger, S., Teucke, M., Osoegawa, K., Zhu, B., Rapp, A., Widaa, S., Langford, C., Yang, F., Carter, N.P., Harrow, J., Ning, Z., Herrero, J., Searle, S.M.J., Enright, A., Geisler, R., Plasterk, R.H.A., Lee, C., Westerfield, M., De Jong, P.J., Zon, L.I., Postlethwait, J.H., Nüsslein-Volhard, C., Hubbard, T.J.P., Crollius, H.R., Rogers, J., Stemple, D.L., 2013. The zebrafish reference genome sequence and its relationship to the human genome. Nature 496, 498–503. https://doi.org/10.1038/nature12111

Hughes, A.E.O., Enright, J.M., Myers, C.A., Shen, S.Q., Corbo, J.C., 2017. Cell Type-Specific Epigenomic Analysis Reveals a Uniquely Closed Chromatin Architecture in Mouse Rod Photoreceptors. Sci. Rep. 7, 1–16. https://doi.org/10.1038/srep43184

Hughes, S., Jagannath, A., Rodgers, J., Hankins, M.W., Peirson, S.N., Foster, R.G., 2016. Signalling by melanopsin (OPN4) expressing photosensitive retinal ganglion cells. Eye 30, 247–254. https://doi.org/10.1038/eye.2015.264

Hunt, D.M., Peichl, L., 2014. S cones: Evolution, retinal distribution, development, and spectral sensitivity. Vis. Neurosci. 31, 115–138. https://doi.org/10.1017/S0952523813000242

Hwang, W.Y., Fu, Y., Reyon, D., Maeder, M.L., Tsai, S.Q., Sander, J.D., Peterson, R.T., Yeh, J.R.J., Joung, J.K., 2013. Efficient genome editing in zebrafish using a CRISPR-Cas system. Nat. Biotechnol. 31, 227–229. https://doi.org/10.1038/nbt.2501

Ile, K.E., Kassen, S., Cao, C., Vihtehlic, T., Shah, S.D., Mousley, C.J., Alb, J.G., Huijbregts, R.P.H., Stearns, G.W., Brockerhoff, S.E., Hyde, D.R., Bankaitis, V.A., 2010. Zebrafish class 1 phosphatidylinositol transfer proteins: PITPβ and double cone cell outer segment integrity in retina. Traffic 11, 1151–1167. https://doi.org/10.1111/j.1600-0854.2010.01085.x

Isayama, T., Chen, Y., Kono, M., Fabre, E., Slavsky, M., Degrip, W.J., Ma, J.X., Crouch,

R.K., Makino, C.L., 2014. Coexpression of three opsins in cone photoreceptors of the salamander Ambystoma tigrinum. J. Comp. Neurol. 522, 2249–2265. https://doi.org/10.1002/cne.23531

Isoldi, M.C., Rollag, M.D., Castrucci, A.M.D.L., Provencio, I., 2005. Rhabdomeric phototransduction initiated by the vertebrate photopigment melanopsin. Proc. Natl. Acad. Sci. 102, 1217–1221. https://doi.org/10.1073/pnas.0409252102

Jacobs, G.H., 2013. Losses of functional opsin genes, short-wavelength cone photopigments, and color vision - A significant trend in the evolution of mammalian vision. Vis. Neurosci. 30, 39–53. https://doi.org/10.1017/S0952523812000429

Jacobs, G.H., 1996. Primate photopigments and primate color vision. Proc. Natl. Acad. Sci. 93, 577–581. https://doi.org/10.1073/pnas.93.2.577

Jacobs, G.H., 1993. The distribution and nature of colour vision among the mammals. Biol. Rev. Camb. Philos. Soc. 68, 413–71. https://doi.org/10.1111/j.1469-185X.1993.tb00738.x

Jadhav, A.P., Mason, H.A., Cepko, C.L., 2006. Notch 1 inhibits photoreceptor production in the developing mammalian retina. Development 133, 913–23. https://doi.org/10.1242/dev.02245

Janssen, J.J.M., Kuhlmann, E.D., van Vugt, A.H.M., Winkens, H.J., Janssen, B.P.M., Deutman, A.F., Driessen, C.A.G.G., 1999. Retinoic acid receptors and retinoid X receptors in the mature retina: Subtype determination and cellular distribution. Curr. Eye Res. 19, 338–347. https://doi.org/10.1076/ceyr.19.4.338.5307

Jia, L., Oh, E.C.T., Ng, L., Srinivas, M., Brooks, M., Swaroop, A., Forrest, D., 2009. Retinoid-related orphan nuclear receptor ROR is an early-acting factor in rod photoreceptor development. Proc. Natl. Acad. Sci. 106, 17534–17539. https://doi.org/10.1073/pnas.0902425106

Jones, I., Ng, L., Liu, H., Forrest, D., 2007. An Intron Control Region Differentially Regulates Expression of Thyroid Hormone Receptor β2 in the Cochlea, Pituitary, and Cone Photoreceptors. Mol. Endocrinol. 21, 1108–1119. https://doi.org/10.1210/me.2007-0037

Jukam, D., Xie, B., Rister, J., Terrell, D., Charlton-Perkins, M., Pistillo, D., Gebelein, B., Desplan, C., Cook, T., 2013. Opposite feedbacks in the Hippo pathway for growth

control and neural fate. Science (80-.). 342. https://doi.org/10.1126/science.1238016

Kaewkhaw, R., Kaya, K.D., Brooks, M., Homma, K., Zou, J., Chaitankar, V., Rao, M., Swaroop, A., 2015. Transcriptome Dynamics of Developing Photoreceptors in Three-Dimensional Retina Cultures Recapitulates Temporal Sequence of Human Cone and Rod Differentiation Revealing Cell Surface Markers and Gene Networks. Stem Cells 33, 3504–3518. https://doi.org/10.1002/stem.2122

Kanda, A., Friedman, J.S., Nishiguchi, K.M., Swaroop, A., 2007. Retinopathy mutations in the bZIP protein NRL alter phosphorylation and transcriptional activity. Hum. Mutat. 28, 589–98. https://doi.org/10.1002/humu.20488

Kaslin, J., Ganz, J., Brand, M., 2008. Proliferation, neurogenesis and regeneration in the non-mammalian vertebrate brain. Philos. Trans. R. Soc. B Biol. Sci. 363, 101–122. https://doi.org/10.1098/rstb.2006.2015

Kataoka, K., Han, S. iee, Shioda, S., Hirai, M., Nishizawa, M., Handa, H., 2002. MafA is a glucose-regulated and pancreatic β-cell-specific transcriptional activator for the insulin gene. J. Biol. Chem. 277, 49903–49910. https://doi.org/10.1074/jbc.M206796200

Katoh, K., Omori, Y., Onishi, A., Sato, S., Kondo, M., Furukawa, T., 2010. Blimp1 Suppresses Chx10 Expression in Differentiating Retinal Photoreceptor Precursors to Ensure Proper Photoreceptor Development. J. Neurosci. 30, 6515–6526. https://doi.org/10.1523/JNEUROSCI.0771-10.2010

Katoh, K., Standley, D.M., 2013. MAFFT multiple sequence alignment software version 7: Improvements in performance and usability. Mol. Biol. Evol. 30, 772–780. https://doi.org/10.1093/molbev/mst010

Kautzmann, M.A.I., Kim, D.S., Felder-Schmittbuhl, M.P., Swaroop, A., 2011. Combinatorial regulation of photoreceptor differentiation factor, neural retina leucine zipper gene Nrl, revealed by in vivo promoter analysis. J. Biol. Chem. 286, 28247–28255. https://doi.org/10.1074/jbc.M111.257246

Kawamura, S., Tachibanaki, S., 2008. Rod and cone photoreceptors: Molecular basis of the difference in their physiology. Comp. Biochem. Physiol. - A Mol. Integr. Physiol. 150, 369–377. https://doi.org/10.1016/j.cbpa.2008.04.600

Kearse, M., Moir, R., Wilson, A., Stones-Havas, S., Cheung, M., Sturrock, S., Buxton, S., Cooper, A., Markowitz, S., Duran, C., Thierer, T., Ashton, B., Meintjes, P., Drummond, A., 2012. Geneious Basic: An integrated and extendable desktop software platform for the organization and analysis of sequence data. Bioinformatics 28, 1647–1649. https://doi.org/10.1093/bioinformatics/bts199

Kennedy, B.N., Alvarez, Y., Brockerhoff, S.E., Stearns, G.W., Sapetto-Rebow, B., Taylor, M.R., Hurley, J.B., 2007. Identification of a zebrafish cone photoreceptor-specific promoter and genetic rescue of achromatopsia in the nof mutant. Investig. Ophthalmol. Vis. Sci. 48, 522–529. https://doi.org/10.1167/iovs.06-0975

Kesavan, G., Hammer, J., Hans, S., Brand, M., 2018. Targeted knock-in of CreERT2in zebrafish using CRISPR/Cas9. Cell Tissue Res. 1–10. https://doi.org/10.1007/s00441-018-2798-x

Khanna, H., Akimoto, M., Siffroi-Fernandez, S., Friedman, J.S., Hicks, D., Swaroop, A., 2006. Retinoic acid regulates the expression of photoreceptor transcription factor NRL. J. Biol. Chem. 281, 27327–27334. https://doi.org/10.1074/jbc.M605500200

Khuansuwan, S., Clanton, J.A., Dean, B.J., Patton, J.G., Gamse, J.T., 2016. A transcription factor network controls cell migration and fate decisions in the developing zebrafish pineal complex. Development 143, 2641–2650. https://doi.org/10.1242/dev.131680

Kim, J.-W., Jang, S.-M., Kim, C.-H., An, J.-H., Choi, K.-H., 2012. Transcriptional Activity of Neural Retina Leucine Zipper (Nrl) Is Regulated by c-Jun N-Terminal Kinase and Tip60 during Retina Development. Mol. Cell. Biol. 32, 1720–1732. https://doi.org/10.1128/MCB.06440-11

Kim, J., 2005. GDF11 Controls the Timing of Progenitor Cell Competence in Developing Retina. Science (80-.). 308, 1927–1930. https://doi.org/10.1126/science.1110175

Kim, J.W., Yang, H.J., Brooks, M.J., Zelinger, L., Karakülah, G., Gotoh, N., Boleda, A., Gieser, L., Giuste, F., Whitaker, D.T., Walton, A., Villasmil, R., Barb, J.J., Munson, P.J., Kaya, K.D., Chaitankar, V., Cogliati, T., Swaroop, A., 2016a. NRL-Regulated Transcriptome Dynamics of Developing Rod Photoreceptors. Cell Rep. 17, 2460–2473. https://doi.org/10.1016/j.celrep.2016.10.074

Kim, J.W., Yang, H.J., Oel, A.P., Brooks, M.J., Jia, L., Plachetzki, D.C., Li, W., Allison,

W.T., Swaroop, A., 2016b. Recruitment of Rod Photoreceptors from Short-Wavelength-Sensitive Cones during the Evolution of Nocturnal Vision in Mammals. Dev. Cell 37, 520–532. https://doi.org/10.1016/j.devcel.2016.05.023

Klimova, L., Antosova, B., Kuzelova, A., Strnad, H., Kozmik, Z., 2015. Onecut1 and Onecut2 transcription factors operate downstream of Pax6 to regulate horizontal cell development. Dev. Biol. 402, 48–60. https://doi.org/10.1016/j.ydbio.2015.02.023

Kluiver, J., Slezak-Prochazka, I., Smigielska-Czepiel, K., Halsema, N., Kroesen, B.J., van den Berg, A., 2012. Generation of miRNA sponge constructs. Methods 58, 113–117. https://doi.org/10.1016/j.ymeth.2012.07.019

Kobayashi, M., Hara, K., Yu, R.T., Yasuda, K., 2008. Expression and functional analysis of Nr2e3, a photoreceptor-specific nuclear receptor, suggest common mechanisms in retinal development between avians and mammals. Dev. Genes Evol. 218, 439–444. https://doi.org/10.1007/s00427-008-0232-1

Koentges, G., 2008. Evolution of anatomy and gene control. Nature 451, 658–63. https://doi.org/10.1038/451658a

Koike, C., Nishida, A., Ueno, S., Saito, H., Sanuki, R., Sato, S., Furukawa, A., Aizawa, S., Matsuo, I., Suzuki, N., Kondo, M., Furukawa, T., 2007. Functional Roles of Otx2 Transcription Factor in Postnatal Mouse Retinal Development. Mol. Cell. Biol. 27, 8318–8329. https://doi.org/10.1128/MCB.01209-07

Kokubo, H., Tomita-Miyagawa, S., Hamada, Y., Saga, Y., 2007. Hesr1 and Hesr2 regulate atrioventricular boundary formation in the developing heart through the repression of Tbx2. Development 134, 747–755. https://doi.org/10.1242/dev.02777

Krispel, C.M., Chen, D., Melling, N., Chen, Y.J., Martemyanov, K.A., Quillinan, N., Arshavsky, V.Y., Wensel, T.G., Chen, C.K., Burns, M.E., 2006. RGS Expression Rate-Limits Recovery of Rod Photoresponses. Neuron 51, 409–416. https://doi.org/10.1016/j.neuron.2006.07.010

Kroehne, V., Freudenreich, D., Hans, S., Kaslin, J., Brand, M., 2011. Regeneration of the adult zebrafish brain from neurogenic radial glia-type progenitors. Development 138, 4831–4841. https://doi.org/10.1242/dev.072587

Kuraku, S., 2013. Impact of asymmetric gene repertoire between cyclostomes and

gnathostomes. Semin. Cell Dev. Biol. 24, 119–127. https://doi.org/10.1016/j.semcdb.2012.12.009

Kuraku, S., Meyer, A., Kuratani, S., 2009. Timing of genome duplications relative to the origin of the vertebrates: Did cyclostomes diverge before or after? Mol. Biol. Evol. 26, 47–59. https://doi.org/10.1093/molbev/msn222

Kwan, K.M., Fujimoto, E., Grabher, C., Mangum, B.D., Hardy, M.E., Campbell, D.S., Parant, J.M., Yost, H.J., Kanki, J.P., Chien, C. Bin, 2007. The Tol2kit: A multisite gateway-based construction Kit for Tol2 transposon transgenesis constructs. Dev. Dyn. 236, 3088–3099. https://doi.org/10.1002/dvdy.21343

la Vail, M.M., Rapaport, D.H., Rakic, P., 1991. Cytogenesis in the monkey retina. J. Comp. Neurol. 309, 86–114. https://doi.org/10.1002/cne.903090107

Lakowski, J., Baron, M., Bainbridge, J., Barber, A.C., Pearson, R.A., Ali, R.R., Sowden, J.C., 2010. Cone and rod photoreceptor transplantation in models of the childhood retinopathy Leber congenital amaurosis using flow-sorted Crx-positive donor cells. Hum. Mol. Genet. 19, 4545–4559. https://doi.org/10.1093/hmg/ddq378

Lakowski, J., Han, Y.-T., Pearson, R., Gonzalez-Cordero, A., West, E., Gualdoni, S., Barber, A., Hubank, M., Ali, R., Sowden, J., 2011. Effective Transplantation of Photoreceptor Precursor Cells Selected via Cell Surface Antigen Expression. Stem Cells 29, N/A-N/A. https://doi.org/10.1002/stem.694

Lamb, T.D., 2013. Evolution of phototransduction, vertebrate photoreceptors and retina. Prog. Retin. Eye Res. 36, 52–119. https://doi.org/10.1016/j.preteyeres.2013.06.001

Lamb, T.D., Arendt, D., Collin, S.P., 2009. The evolution of phototransduction and eyes. Philos. Trans. R. Soc. B Biol. Sci. 364, 2791–2793. https://doi.org/10.1098/rstb.2009.0106

Lamb, T.D., Collin, S.P., Pugh, E.N., 2007. Evolution of the vertebrate eye: Opsins, photoreceptors, retina and eye cup. Nat. Rev. Neurosci. 8, 960–976. https://doi.org/10.1038/nrn2283

Lamb, T.D., Patel, H., Chuah, A., Natoli, R.C., Davies, W.I.L., Hart, N.S., Collin, S.P., Hunt, D.M., 2016. Evolution of Vertebrate Phototransduction: Cascade Activation. Mol. Biol. Evol. 33, 2064–2087. https://doi.org/10.1093/molbev/msw095

Lamba, D., Karl, M., Reh, T., 2008. Neural Regeneration and Cell Replacement: A View

from the Eye. Cell Stem Cell 2, 538–549. https://doi.org/10.1016/j.stem.2008.05.002

Landgren, E., Fritsches, K., Brill, R., Warrant, E., 2014. The visual ecology of a deep-sea fish, the escolar Lepidocybium flavobrunneum (Smith, 1843). Philos. Trans. R. Soc. B Biol. Sci. 369, 20130039–20130039. https://doi.org/10.1098/rstb.2013.0039

Langmead, B., Salzberg, S.L., 2012. Fast gapped-read alignment with Bowtie 2. Nat. Methods 9, 357–359. https://doi.org/10.1038/nmeth.1923

Larison, K.D., Bremiller, R., 1990. Early onset of phenotype and cell patterning in the embryonic zebrafish retina. Development 109, 567–576.

Lenkowski, J.R., Qin, Z., Sifuentes, C.J., Thummel, R., Soto, C.M., Moens, C.B., Raymond, P.A., 2013. Retinal regeneration in adult zebrafish requires regulation of TGFβ signaling. Glia 61, 1687–97. https://doi.org/10.1002/glia.22549

Levin, D.B., Dann, S.G., Ted Allison, W., Taylor, J.S., Hawryshyn, C.W., 2004. Salmonid Opsin Sequences Undergo Positive Selection and Indicate an Alternate Evolutionary Relationship in Oncorhynchus. J. Mol. Evol. 58, 400–412. https://doi.org/10.1007/s00239-003-2562-y

Li, W., Godzik, A., 2006. Cd-hit: A fast program for clustering and comparing large sets of protein or nucleotide sequences. Bioinformatics 22, 1658–1659. https://doi.org/10.1093/bioinformatics/btl158

Li, Y.N., Matsui, J.I., Dowling, J.E., 2009. Specificity of the horizontal cell-photoreceptor connections in the zebrafish (Danio rerio) retina. J. Comp. Neurol. 516, 442–453. https://doi.org/10.1002/cne.22135

Liang, Y., Fotiadis, D., Filipek, S., Saperstein, D.A., Palczewski, K., Engel, A., 2003. Organization of the G protein-coupled receptors rhodopsin and opsin in native membranes. J. Biol. Chem. 278, 21655–21662. https://doi.org/10.1074/jbc.M302536200

Lin, S., Huang, Y., Lee, T., 2009. Nuclear receptor unfulfilled regulates axonal guidance and cell identity of Drosophila mushroom body neurons. PLoS One 4. https://doi.org/10.1371/journal.pone.0008392

Littink, K., Stappers, P., Riemslag, F., Talsma, H., van Genderen, M., Cremers, F., Collin, R., van den Born, L., 2018. Autosomal Recessive NRL Mutations in Patients

with Enhanced S-Cone Syndrome. Genes (Basel). 9, 68. https://doi.org/10.3390/genes9020068

Liu, H., Aramaki, M., Fu, Y., Forrest, D., 2017. Retinoid-Related Orphan Receptor β and Transcriptional Control of Neuronal Differentiation, 1st ed, Current Topics in Developmental Biology. Elsevier Inc. https://doi.org/10.1016/bs.ctdb.2016.11.009

Liu, H., Etter, P., Hayes, S., Jones, I., Nelson, B., Hartman, B., Forrest, D., Reh, T.A., 2008. NeuroD1 Regulates Expression of Thyroid Hormone Receptor 2 and Cone Opsins in the Developing Mouse Retina. J. Neurosci. 28, 749–756. https://doi.org/10.1523/JNEUROSCI.4832-07.2008

Liu, H., Kim, S.Y., Fu, Y., Wu, X., Ng, L., Swaroop, A., Forrest, D., 2013. An isoform of retinoid-related orphan receptor β directs differentiation of retinal amacrine and horizontal interneurons. Nat. Commun. 4, 1811–1813. https://doi.org/10.1038/ncomms2793

Liu, Q., Ji, X., Breitman, M.L., Hitchcock, P.F., Swaroop, A., 1996. Expression of the bZIP transcription factor gene Nrl in the developing nervous system. Oncogene 12, 207–11.

Luo, D.-G., Kefalov, V., Yau, K.-W., 2008. 1.10 - Phototransduction in Rods and Cones, in: The Senses: A Comprehensive Reference. pp. 269–301. https://doi.org/http://dx.doi.org/10.1016/B978-012370880-9.00258-9

Luo, D.-G., Kefalov, V., Yau, K.-W., 2008a. Phototransduction in Rods and Cones, in: The Senses: A Comprehensive Reference. Elsevier, pp. 269–301. https://doi.org/10.1016/B978-012370880-9.00258-9

Luo, D.-G., Kefalov, V., Yau, K.-W., 2008b. Phototransduction in Rods and Cones, in: Furukawa, T., Hurley, J.B., Kawamura, S. (Eds.), The Senses: A Comprehensive Reference. Elsevier, Tokyo, pp. 269–301. https://doi.org/10.1016/B978-012370880-9.00258-9

Luo, H., Jin, K., Xie, Z., Qiu, F., Li, S., Zou, M., Cai, L., Hozumi, K., Shima, D.T., Xiang, M., 2012. Forkhead box N4 (Foxn4) activates Dll4-Notch signaling to suppress photoreceptor cell fates of early retinal progenitors. Proc. Natl. Acad. Sci. 109, E553–E562. https://doi.org/10.1073/pnas.1115767109

Luo, S., Lu, J., 2017. Silencing of Transposable Elements by piRNAs in Drosophila: An

Evolutionary Perspective. Genomics, Proteomics Bioinforma. 15, 164–176. https://doi.org/10.1016/j.gpb.2017.01.006

MacLaren, R.E., Pearson, R.A., MacNeil, A., Douglas, R.H., Salt, T.E., Akimoto, M., Swaroop, A., Sowden, J.C., Ali, R.R., 2006. Retinal repair by transplantation of photoreceptor precursors. Nature 444, 203–207. https://doi.org/10.1038/nature05161

Manavathi, B., Peng, S., Rayala, S.K., Talukder, A.H., Wang, M.H., Wang, R.-A., Balasenthil, S., Agarwal, N., Frishman, L.J., Kumar, R., 2007. Repression of Six3 by a corepressor regulates rhodopsin expression. Proc. Natl. Acad. Sci. 104, 13128–13133. https://doi.org/10.1073/pnas.0705878104

Mansergh, F.C., Vawda, R., Millington-Ward, S., Kenna, P.F., Haas, J., Gallagher, C., Wilson, J.H., Humphries, P., Ader, M., Farrar, G.J., 2010. Loss of photoreceptor potential from retinal progenitor cell cultures, despite improvements in survival. Exp. Eye Res. 91, 500–512. https://doi.org/10.1016/j.exer.2010.07.003

Mariani, A.P., 1986. Photoreceptors of the larval tiger salamander retina. Proc. R. Soc. London. Ser. B, Biol. Sci. 227, 483–92.

Martin, G., Rojas, L.M., Ramírez, Y., McNeil, R., 2004. The eyes of oilbirds (Steatornis caripensis): Pushing at the limits of sensitivity. Naturwissenschaften 91, 26–29. https://doi.org/10.1007/s00114-003-0495-3

Martin, N., Benhamed, M., Nacerddine, K., Demarque, M.D., van Lohuizen, M., Dejean, A., Bischof, O., 2012. Physical and functional interaction between PML and TBX2 in the establishment of cellular senescence. EMBO J. 31, 95–109. https://doi.org/10.1038/emboj.2011.370

McDonald, E.C., Xie, B., Workman, M., Charlton-Perkins, M., Terrell, D.A., Reischl, J., Wimmer, E.A., Gebelein, B.A., Cook, T.A., 2010. Separable transcriptional regulatory domains within Otd control photoreceptor terminal differentiation events. Dev. Biol. 347, 122–132. https://doi.org/10.1016/j.ydbio.2010.08.016

McIlvain, V.A., Knox, B.E., 2007. Nr2e3 and Nrl can reprogram retinal precursors to the rod fate in Xenopus retina. Dev. Dyn. 236, 1970–1979. https://doi.org/10.1002/dvdy.21128

Mears, A.J., Kondo, M., Swain, P.K., Takada, Y., Bush, R.A., Saunders, T.L., Sieving,

P.A., Swaroop, A., 2001. Nrl is required for rod photoreceptor development. Nat. Genet. 29, 447–452. https://doi.org/10.1038/ng774

Meeker, N.D., Hutchinson, S.A., Ho, L., Trede, N.S., 2007. Method for isolation of PCR-ready genomic DNA from zebrafish tissues. Biotechniques 43, 610–614. https://doi.org/10.2144/000112619

Menaker, M., Moreira, L.F., Tosini, G., 1997. Evolution of circadian organization in vertebrates. Brazilian J. Med. Biol. Res. 30, 305–313. https://doi.org/10.1590/S0100-879X1997000300003

Meng, X., Noyes, M.B., Zhu, L.J., Lawson, N.D., Wolfe, S.A., 2008. Targeted gene inactivation in zebrafish using engineered zinc-finger nucleases. Nat. Biotechnol. 26, 695–701. https://doi.org/10.1038/nbt1398

Milam, A.H., Rose, L., Cideciyan, A. V, Barakat, M.R., Tang, W.-X., Gupta, N., Aleman, T.S., Wright, A.F., Stone, E.M., Sheffield, V.C., Jacobson, S.G., 2002. The nuclear receptor NR2E3 plays a role in human retinal photoreceptor differentiation and degeneration. Proc. Natl. Acad. Sci. 99, 473–478. https://doi.org/10.1073/pnas.022533099

Mitton, K.P., Swain, P.K., Chen, S., Xu, S., Zack, D.J., Swaroop, A., 2000. The leucine zipper of NRL interacts with the CRX homeodomain. A possible mechanism of transcriptional synergy in rhodopsin regulation. J. Biol. Chem. 275, 29794–29799. https://doi.org/10.1074/jbc.M003658200

Mizeracka, K., DeMaso, C.R., Cepko, C.L., 2013. Notch1 is required in newly postmitotic cells to inhibit the rod photoreceptor fate. Development 140, 3188–3197. https://doi.org/10.1242/dev.090696

Mizeracka, K., Trimarchi, J.M., Stadler, M.B., Cepko, C.L., 2013. Analysis of gene expression in wild-type and Notch1 mutant retinal cells by single cell profiling. Dev. Dyn. 242, 1147–1159. https://doi.org/10.1002/dvdy.24006

Mollereau, B., Dominguez, M., Webel, R., Colley, N.J., Keung, B., de Celis, J.F., Desplan, C., 2001. Two-step process for photoreceptor formation in Drosophila. Nature 412, 911–913. https://doi.org/10.1038/35091076

Montana, C.L., Lawrence, K.A., Williams, N.L., Tran, N.M., Peng, G.H., Chen, S., Corbo, J.C., 2011. Transcriptional regulation of neural retina leucine zipper (Nrl), a

photoreceptor cell fate determinant. J. Biol. Chem. 286, 36921–36931. https://doi.org/10.1074/jbc.M111.279026

Mori, M., Ghyselinck, N.B., Chambon, P., Mark, M., 2001. Systematic immunolocalization of retinoid receptors in developing and adult mouse eyes. Investig. Ophthalmol. Vis. Sci. 42, 1312–1318.

Morris, A.C., Scholz, T.L., Brockerhoff, S.E., Fadool, J.M., 2008. Genetic dissection reveals two separate pathways for rod and cone regeneration in the teleost retina. Dev. Neurobiol. 68, 605–619. https://doi.org/10.1002/dneu.20610

Morris, A.C., Schroeter, E.H., Bilotta, J., Wong, R.O.L., Fadool, J.M., 2005. Cone Survival Despite Rod Degeneration in XOPS-mCFP Transgenic Zebrafish. Investig. Opthalmology Vis. Sci. 46, 4762. https://doi.org/10.1167/iovs.05-0797

Morrow, E.M., Belliveau, M.J., Cepko, C.L., 1998. Two phases of rod photoreceptor differentiation during rat retinal development. J. Neurosci. 18, 3738–48.

Morrow, E.M., Furukawa, T., Raviola, E., Cepko, C.L., 2005. Synaptogenesis and outer segment formation are perturbed in the neural retina of Crx mutant mice. BMC Neurosci. 6, 1–14. https://doi.org/10.1186/1471-2202-6-5

Morshedian, A., Fain, G.L., 2017. Light adaptation and the evolution of vertebrate photoreceptors. J. Physiol. 595, 4947–4960. https://doi.org/10.1113/JP274211

Morshedian, A., Fain, G.L., 2015. Single-Photon Sensitivity of Lamprey Rods with Cone-like Outer Segments Report Single-Photon Sensitivity of Lamprey Rods with Cone-like Outer Segments. Curr. Biol. 25, 484–487. https://doi.org/10.1016/j.cub.2014.12.031

Morshedian, A., Toomey, M.B., Pollock, G.E., Frederiksen, R., Enright, J.M., McCormick, S.D., Cornwall, M.C., Fain, G.L., Corbo, J.C., 2017. Cambrian origin of the CYP27C1-mediated vitamin A 1 -to-A 2 switch, a key mechanism of vertebrate sensory plasticity. R. Soc. Open Sci. 4, 170362. https://doi.org/10.1098/rsos.170362

Mosimann, C., Kaufman, C.K., Li, P., Pugach, E.K., Tamplin, O.J., Zon, L.I., 2011. Ubiquitous transgene expression and Cre-based recombination driven by the ubiquitin promoter in zebrafish. Development 138, 169–177. https://doi.org/10.1242/dev.059345

Müller, G.B., 2007. Evo–devo: extending the evolutionary synthesis. Nat. Rev. Genet. 8, 943–949. https://doi.org/10.1038/nrg2219

Muradov, H., Boyd, K.K., Kerov, V., Artemyev, N.O., 2007. PDE6 in Lamprey Petromyzon marinus : Implications for the Evolution of the Visual Effector in Vertebrates † , ‡. Biochemistry 46, 9992–10000. https://doi.org/10.1021/bi700535s

Muradov, H., Kerov, V., Boyd, K.K., Artemyev, N.O., 2008. Unique transducins expressed in long and short photoreceptors of lamprey Petromyzon marinus. Vision Res. 48, 2302–2308. https://doi.org/10.1016/j.visres.2008.07.006

Muranishi, Y., Terada, K., Inoue, T., Katoh, K., Tsujii, T., Sanuki, R., Kurokawa, D., Aizawa, S., Tamaki, Y., Furukawa, T., 2011. An Essential Role for RAX Homeoprotein and NOTCH-HES Signaling in Otx2 Expression in Embryonic Retinal Photoreceptor Cell Fate Determination. J. Neurosci. 31, 16792–16807. https://doi.org/10.1523/JNEUROSCI.3109-11.2011

Musser, J.M., Arendt, D., 2017. Loss and gain of cone types in vertebrate ciliary photoreceptor evolution. Dev. Biol. 431, 26–35. https://doi.org/10.1016/j.ydbio.2017.08.038

Nakayama, Y., Miyake, A., Nakagawa, Y., Mido, T., Yoshikawa, M., Konishi, M., Itoh, N., 2008. Fgf19 is required for zebrafish lens and retina development. Dev. Biol. 313, 752–766. https://doi.org/10.1016/j.ydbio.2007.11.013

Nasevicius, A., Ekker, S.C., 2000. Effective targeted gene “knockdown” in zebrafish. Nat. Genet. 26, 216–220. https://doi.org/10.1038/79951

Nathans, J., 1999. The Evolution and Physiology of Human Review Color Vision: Insights from Molecular Genetic Studies of Visual Pigments. Neuron 24, 299–312. https://doi.org/10.1016/S0896-6273(00)80845-4

Nawrocki, L.W., 1985. Development of the neural retina in the zebrafish, Brachydanio rerio (neurogenesis). Ph.D. Thesis.

Nelson, S.M., Frey, R.A., Wardwell, S.L., Stenkamp, D.L., 2008. The developmental sequence of gene expression within the rod photoreceptor lineage in embryonic zebrafish. Dev. Dyn. 237, 2903–2917. https://doi.org/10.1002/dvdy.21721

Neuhauss, S.C.F., 2003. Behavioral genetic approaches to visual system development and function in zebrafish. J. Neurobiol. 54, 148–160.

https://doi.org/10.1002/neu.10165

Newman, H., Blumen, S.C., Braverman, I., Hanna, R., Tiosano, B., Perlman, I., Ben-Yosef, T., 2016. Homozygosity for a recessive loss-of-function mutation of the NRL gene is associated with a variant of enhanced S-cone syndrome. Investig. Ophthalmol. Vis. Sci. 57, 5361–5371. https://doi.org/10.1167/iovs.16-19505

Newman, L.A., Robinson, P.R., 2005. Cone visual pigments of aquatic mammals. Vis. Neurosci. 22, 873–879. https://doi.org/10.1017/S0952523805226159

Ng, L., 2001. Suppression of the deafness and thyroid dysfunction in Thrb-null mice by an independent mutation in the Thra thyroid hormone receptor alpha gene. Hum. Mol. Genet. 10, 2701–2708. https://doi.org/10.1093/hmg/10.23.2701

Ng, L., Hurley, J.B., Dierks, B., Srinivas, M., Saltó, C., Vennström, B., Reh, T.A., Forrest, D., 2001. A thyroid hormone receptor that is required for the development of green cone photoreceptors. Nat. Genet. 27, 94–98. https://doi.org/10.1038/83829

Ng, L., Lu, A., Swaroop, A., Sharlin, D.S., Swaroop, A., Forrest, D., 2011. Two Transcription Factors Can Direct Three Photoreceptor Outcomes from Rod Precursor Cells in Mouse Retinal Development. J. Neurosci. 31, 11118–11125. https://doi.org/10.1523/JNEUROSCI.1709-11.2011

Nguyen, D.N.T., Rohrbaugh, M., Lai, Z.-C., 2000. The Drosophila homolog of Onecut homeodomain proteins is a neural-specific transcriptional activator with a potential role in regulating neural differentiation. Mech. Dev. 97, 57–72. https://doi.org/10.1016/S0925-4773(00)00431-7

Nikonov, S.S., Daniele, L.L., Zhu, X., Craft, C.M., Swaroop, A., Pugh, E.N., 2005. Photoreceptors of *Nrl* $^{-/-}$ Mice Coexpress Functional S- and M-cone Opsins Having Distinct Inactivation Mechanisms. J. Gen. Physiol. 125, 287–304. https://doi.org/10.1085/jgp.200409208

Nishida, A., Furukawa, A., Koike, C., Tano, Y., Aizawa, S., Matsuo, I., Furukawa, T., 2003. Otx2 homeobox gene controls retinal photoreceptor cell fate and pineal gland development. Nat. Neurosci. 6, 1255–1263. https://doi.org/10.1038/nn1155

Nishiguchi, K.M., Friedman, J.S., Sandberg, M. a, Swaroop, A., Berson, E.L., Dryja, T.P., 2004. Recessive NRL mutations in patients with clumped pigmentary retinal

degeneration and relative preservation of blue cone function. Proc. Natl. Acad. Sci. 101, 17819–17824. https://doi.org/10.1073/pnas.0408183101

Noel, N.C.L., Allison, W.T., 2018. Connectivity of cone photoreceptor telodendria in the zebrafish retina. J. Comp. Neurol. 526, 609–625. https://doi.org/10.1002/cne.24354

Nordström, K., Larsson, T.A., Larhammar, D., 2004. Extensive duplications of phototransduction genes in early vertebrate evolution correlate with block (chromosome) duplications. Genomics 83, 852–872. https://doi.org/10.1016/j.ygeno.2003.11.008

Ochi, H., Sakagami, K., Ishii, A., Morita, N., Nishiuchi, M., Ogino, H., Yasuda, K., 2004. Temporal expression of L-Maf and RaxL in developing chicken retina are arranged into mosaic pattern. Gene Expr. Patterns 4, 489–494. https://doi.org/10.1016/j.modgep.2004.03.005

Oesch, N.W., Kothmann, W., Diamond, J.S., 2011. Illuminating synapses and circuitry in the retina. Curr. Opin. Neurobiol. 21, 238–244. https://doi.org/10.1016/j.conb.2011.01.008

Ogawa, Y., Shiraki, T., Kojima, D., Fukada, Y., Fukada, T., 2015. Homeobox transcription factor Six7 governs expression of green opsin genes in zebrafish. Proc. R. Soc. B Biol. Sci. 282, 20150659-. https://doi.org/10.1098/rspb.2015.0659

Oh, E.C.T., Cheng, H., Hao, H., Jia, L., Khan, N.W., Swaroop, A., 2008. Rod differentiation factor NRL activates the expression of nuclear receptor NR2E3 to suppress the development of cone photoreceptors. Brain Res. 1236, 16–29. https://doi.org/10.1016/j.brainres.2008.01.028

Oh, E.C.T., Khan, N., Novelli, E., Khanna, H., Strettoi, E., Swaroop, A., 2007. Transformation of cone precursors to functional rod photoreceptors by bZIP transcription factor NRL. Proc. Natl. Acad. Sci. 104, 1679–1684. https://doi.org/10.1073/pnas.0605934104

Okada, I., Hamanoue, H., Terada, K., Tohma, T., Megarbane, A., Chouery, E., Abou-Ghoch, J., Jalkh, N., Cogulu, O., Ozkinay, F., Horie, K., Takeda, J., Furuichi, T., Ikegawa, S., Nishiyama, K., Miyatake, S., Nishimura, A., Mizuguchi, T., Niikawa, N., Hirahara, F., Kaname, T., Yoshiura, K.-I., Tsurusaki, Y., Doi, H., Miyake, N., Furukawa, T., Matsumoto, N., Saitsu, H., 2011. SMOC1 is essential for ocular and

limb development in humans and mice. Am. J. Hum. Genet. 88, 30–41. https://doi.org/10.1016/j.ajhg.2010.11.012

Okano, T., Kojima, D., Fukada, Y., Shichida, Y., Yoshizawa, T., 1992. Primary structures of chicken cone visual pigments: vertebrate rhodopsins have evolved out of cone visual pigments. Proc. Natl. Acad. Sci. 89, 5932–5936. https://doi.org/10.1073/pnas.89.13.5932

Okawa, H., Sampath, A.P., Laughlin, S.B., Fain, G.L., 2008. ATP Consumption by Mammalian Rod Photoreceptors in Darkness and in Light. Curr. Biol. 18, 1917–1921. https://doi.org/10.1016/j.cub.2008.10.029

Onishi, A., Peng, G.H., Chen, S., Blackshaw, S., 2010. Pias3-dependent SUMOylation controls mammalian cone photoreceptor differentiation. Nat. Neurosci. 13, 1059–1065. https://doi.org/10.1038/nn.2618

Onishi, A., Peng, G.H., Hsu, C., Alexis, U., Chen, S., Blackshaw, S., 2009. Pias3-Dependent SUMOylation Directs Rod Photoreceptor Development. Neuron 61, 234–246. https://doi.org/10.1016/j.neuron.2008.12.006

Ortin-Martinez, A., Tsai, E.L.S., Nickerson, P.E., Bergeret, M., Lu, Y., Smiley, S., Comanita, L., Wallace, V.A., 2017. A Reinterpretation of Cell Transplantation: GFP Transfer From Donor to Host Photoreceptors. Stem Cells 35, 932–939. https://doi.org/10.1002/stem.2552

Palczewski, K., Hargrave, P.A., McDowell, J.H., Ingebritsen, T.S., 1989. The Catalytic Subunit of Phosphatase 2A Dephosphorylates Phosphoopsin. Biochemistry 28, 415–419. https://doi.org/10.1021/bi00428a001

Palczewski, K., Palczewski, K., Kumasaka, T., Hori, T., Trong, I. Le, Teller, D.C., Okada, T., 2000. Crystal Structure of Rhodopsin : A G Protein – Coupled Receptor. Science (80-.). 289, 739–745. https://doi.org/10.1126/science.289.5480.739

Pan, Y.A., Freundlich, T., Weissman, T.A., Schoppik, D., Wang, X.C., Zimmerman, S., Ciruna, B., Sanes, J.R., Lichtman, J.W., Schier, A.F., 2013. Zebrabow: multispectral cell labeling for cell tracing and lineage analysis in zebrafish. Development 140, 2835–2846. https://doi.org/10.1242/dev.094631

Pang, J.J., Gao, F., Paul, D.L., Wu, S.M., 2012. Rod, M-cone and M/S-cone inputs to hyperpolarizing bipolar cells in the mouse retina. J. Physiol. 590, 845–854.

https://doi.org/10.1113/jphysiol.2011.224113

Pantò, M.R., Zappalà, A., Tuorto, F., Cicirata, F., 2004. Role of the Otx1 gene in cell differentiation of mammalian cortex. Eur. J. Neurosci. 19, 2893–2902. https://doi.org/10.1111/j.0953-816X.2004.03326.x

Paxton, C., Zhao, H., Chin, Y., Langner, K., Reecy, J., 2002. Murine Tbx2 contains domains that activate and repress gene transcription. Gene 283, 117–124. https://doi.org/10.1016/S0378-1119(01)00878-2

Pearson, R.A., Gonzalez-Cordero, A., West, E.L., Ribeiro, J.R., Aghaizu, N., Goh, D., Sampson, R.D., Georgiadis, A., Waldron, P. V., Duran, Y., Naeem, A., Kloc, M., Cristante, E., Kruczek, K., Warre-Cornish, K., Sowden, J.C., Smith, A.J., Ali, R.R., 2016. Donor and host photoreceptors engage in material transfer following transplantation of post-mitotic photoreceptor precursors. Nat. Commun. 7, 1–15. https://doi.org/10.1038/ncomms13029

Peichl, L., 2005. Diversity of mammalian photoreceptor properties: Adaptations to habitat and lifestyle? Anat. Rec. - Part A Discov. Mol. Cell. Evol. Biol. 287, 1001–1012. https://doi.org/10.1002/ar.a.20262

Peichl, L., Behrmann, G., Kröger, R.H., 2001. For whales and seals the ocean is not blue: a visual pigment loss in marine mammals. Eur. J. Neurosci. 13, 1520–8.

Peng, G.H., Ahmad, O., Ahmad, F., Liu, J., Chen, S., 2005. The photoreceptor-specific nuclear receptor Nr2e3 interacts with Crx and exerts opposing effects on the transcription of rod versus cone genes. Hum. Mol. Genet. 14, 747–764. https://doi.org/10.1093/hmg/ddi070

Perez-Leighton, C.E., Schmidt, T.M., Abramowitz, J., Birnbaumer, L., Kofuji, P., 2011. Intrinsic phototransduction persists in melanopsin-expressing ganglion cells lacking diacylglycerol-sensitive TRPC subunits. Eur. J. Neurosci. 33, 856–867. https://doi.org/10.1111/j.1460-9568.2010.07583.x

Pergner, J., Kozmik, Z., 2017. Amphioxus photoreceptors - Insights into the evolution of vertebrate opsins, vision and circadian rhythmicity. Int. J. Dev. Biol. 61, 665–681. https://doi.org/10.1387/ijdb.170230zk

Pillay, L.M., Selland, L.G., Fleisch, V.C., Leighton, P.L.A., Cheng, C.S., Famulski, J.K., Ritzel, R.G., March, L.D., Wang, H., Allison, W.T., Waskiewicz, A.J., 2013.

Evaluating the mutagenic activity of targeted endonucleases containing a Sharkey FokI cleavage domain variant in zebrafish. Zebrafish 10, 353–64. https://doi.org/10.1089/zeb.2012.0832

Pisani, D., Mohun, S.M., Harris, S.R., McInerney, J.O., Wilkinson, M., 2006. Molecular evidence for dim-light vision in the last common ancestor of the vertebrates. Curr. Biol. https://doi.org/10.1016/j.cub.2006.03.090

Plouhinec, J.L., Sauka-Spengler, T., Germot, A., Le Mentec, C., Cabana, T., Harrison, G., Pieau, C., Sire, J.Y., Véron, G., Mazan, S., 2003. The mammalian Crx genes are highly divergent representatives of the Otx5 gene family, a gnathostome orthology class of orthodenticle-related homeogenes involved in the differentiation of retinal photoreceptors and circadian entrainment. Mol. Biol. Evol. 20, 513–521. https://doi.org/10.1093/molbev/msg085

Prada, C., Puga, J., Perez-Mendez, L., Lopez, R., Ramirez, G., 1991. Spatial and Temporal Patterns of Neurogenesis in the Chick Retina. Eur. J. Neurosci. 3, 559–569. https://doi.org/10.1111/j.1460-9568.1991.tb00843.x

R Core Team, 2017. R: A language and environment for statistical computing.

Raible, F., Tessmar-Raible, K., Arboleda, E., Kaller, T., Bork, P., Arendt, D., Arnone, M.I., 2006. Opsins and clusters of sensory G-protein-coupled receptors in the sea urchin genome. Dev. Biol. 300, 461–475. https://doi.org/10.1016/j.ydbio.2006.08.070

Rapaport, D.H., 2006. Retinal neurogenesis, in: Sernagor, E., Eglen, S., Harris, B., Wong, R. (Eds.), Retinal Development. Cambridge University Press, Cambridge, UK, pp. 30–58.

Rapaport, D.H., Wong, L.L., Wood, E.D., Yasumura, D., Lavail, M.M., 2004. Timing and topography of cell genesis in the rat retina. J. Comp. Neurol. 474, 304–324. https://doi.org/10.1002/cne.20134

Raymond, P.A., Barthel, L.K., 2004. A moving wave patterns the cone photoreceptor mosaic array in the zebrafish retina. Int. J. Dev. Biol. 48, 935–945. https://doi.org/10.1387/ijdb.041873pr

Raymond, P.A., Barthel, L.K., Curran, G.A., 1995. Developmental patterning of rod and cone photoreceptors in embryonic zebrafish. J. Comp. Neurol. 359, 537–550.

https://doi.org/10.1002/cne.903590403

Raymond, P.A., Barthel, L.K., Rounsifer, M.E., Sullivan, S.A., Knight, J.K., 1993. Expression of rod and cone visual pigments in goldfish and zebrafish: A rhodopsin-like gene is expressed in cones. Neuron 10, 1161–1174. https://doi.org/10.1016/0896-6273(93)90064-X

Raymond, P.A., Barthel, L.K., Stenkamp, D.L., 1996. The zebrafish ultraviolet cone opsin reported previously is expressed in rods. Investig. Ophthalmol. Vis. Sci. 37, 948–50.

Raymond, P.A., Colvin, S.M., Jabeen, Z., Nagashima, M., Barthel, L.K., Hadidjojo, J., Popova, L., Pejaver, V.R., Lubensky, D.K., 2014. Patterning the cone mosaic array in zebrafish retina requires specification of ultraviolet-sensitive cones. PLoS One 9. https://doi.org/10.1371/journal.pone.0085325

Reifler, A.N., Chervenak, A.P., Dolikian, M.E., Benenati, B.A., Meyers, B.S., Demertzis, Z.D., Lynch, A.M., Li, B.Y., Wachter, R.D., Abufarha, F.S., Dulka, E.A., Pack, W., Zhao, X., Wong, K.Y., 2015. The rat retina has five types of ganglion-cell photoreceptors. Exp. Eye Res. 130, 17–28. https://doi.org/10.1016/j.exer.2014.11.010

Reza, H.M., Yasuda, K., 2004. Roles of Maf Family Proteins in Lens Development. Dev. Dyn. 229, 440–448. https://doi.org/10.1002/dvdy.10467

Ribelayga, C., Mangel, S.C., 2010. Identification of a circadian clock-controlled neural pathway in the rabbit retina. PLoS One 5. https://doi.org/10.1371/journal.pone.0011020

Roberts, A., Schaeffer, L., Pachter, L., 2013. Updating RNA-Seq analyses after re-annotation. Bioinformatics 29, 1631–1637. https://doi.org/10.1093/bioinformatics/btt197

Roberts, M.R., Hendrickson, A., McGuire, C.R., Reh, T.A., 2005. Retinoid X Receptor γ Is Necessary to Establish the S-opsin Gradient in Cone Photoreceptors of the Developing Mouse Retina. Investig. Opthalmology Vis. Sci. 46, 2897. https://doi.org/10.1167/iovs.05-0093

Roberts, M.R., Srinivas, M., Forrest, D., Morreale de Escobar, G., Reh, T.A., 2006. Making the gradient: Thyroid hormone regulates cone opsin expression in the

developing mouse retina. Proc. Natl. Acad. Sci. 103, 6218–6223. https://doi.org/10.1073/pnas.0509981103

Robine, N., Lau, N.C., Balla, S., Jin, Z., Okamura, K., Kuramochi-Miyagawa, S., Blower, M.D., Lai, E.C., 2009. A Broadly Conserved Pathway Generates 3′UTR-Directed Primary piRNAs. Curr. Biol. 19, 2066–2076. https://doi.org/10.1016/j.cub.2009.11.064

Robinson, J., Schmitt, E. a, Harosi, F.I., Reece, R.J., Dowling, J.E., 1993. Zebrafish ultraviolet visual pigment: absorption spectrum, sequence, and localization. Proc. Natl. Acad. Sci. 90, 6009–6012. https://doi.org/10.1073/pnas.90.13.6009

Rocha, S.F., Lopes, S.S., Gossler, A., Henrique, D., 2009. Dll1 and Dll4 function sequentially in the retina and pV2 domain of the spinal cord to regulate neurogenesis and create cell diversity. Dev. Biol. 328, 54–65. https://doi.org/10.1016/j.ydbio.2009.01.011

Roger, J.E., Nellissery, J., Kim, D.S., Swaroop, A., 2010. Sumoylation of bZIP transcription factor NRL modulates target gene expression during photoreceptor differentiation. J. Biol. Chem. 285, 25637–25644. https://doi.org/10.1074/jbc.M110.142810

Roger, J.E., Ranganath, K., Zhao, L., Cojocaru, R.I., Brooks, M., Gotoh, N., Veleri, S., Hiriyanna, A., Rachel, R.A., Campos, M.M., Fariss, R.N., Wong, W.T., Swaroop, A., 2012. Preservation of Cone Photoreceptors after a Rapid yet Transient Degeneration and Remodeling in Cone-Only Nrl-/- Mouse Retina. J. Neurosci. 32, 528–541. https://doi.org/10.1523/JNEUROSCI.3591-11.2012

Rompani, S.B., Cepko, C.L., 2008. Retinal progenitor cells can produce restricted subsets of horizontal cells. Proc. Natl. Acad. Sci. 105, 192–197. https://doi.org/10.1073/pnas.0709979104

Rovsing, L., Clokie, S., Bustos, D.M., Rohde, K., Coon, S.L., Litman, T., Rath, M.F., Møller, M., Klein, D.C., 2011. Crx broadly modulates the pineal transcriptome. J. Neurochem. 119, 262–274. https://doi.org/10.1111/j.1471-4159.2011.07405.x

Roy, S., Ng, T., 2004. Blimp-1 Specifies Neural Crest and Sensory Neuron Progenitors in the Zebrafish Embryo. Curr. Biol. 14, 1772–1777. https://doi.org/10.1016/j.cub.2004.09.046

Rutenberg, J.B., Fischer, A., Jia, H., Gessler, M., Zhong, T.P., Mercola, M., 2006. Developmental patterning of the cardiac atrioventricular canal by Notch and Hairy-related transcription factors. Development 133, 4381–4390. https://doi.org/10.1242/dev.02607

Ruvinsky, I., Oates, a C., Silver, L.M., Ho, R.K., 2000. The evolution of paired appendages in vertebrates: T-box genes in the zebrafish. Dev. Genes Evol. 210, 82–91. https://doi.org/10.1007/s004270050014

Saade, C.J., Alvarez-Delfin, K., Fadool, J.M., 2013. Rod Photoreceptors Protect from Cone Degeneration-Induced Retinal Remodeling and Restore Visual Responses in Zebrafish. J. Neurosci. 33, 1804–1814. https://doi.org/10.1523/JNEUROSCI.2910-12.2013

Saito, K., Inagaki, S., Mituyama, T., Kawamura, Y., Ono, Y., Sakota, E., Kotani, H., Asai, K., Siomi, H., Siomi, M.C., 2009. A regulatory circuit for piwi by the large Maf gene traffic jam in Drosophila. Nature 461, 1296–1299. https://doi.org/10.1038/nature08501

Samuel, A., Housset, M., Fant, B., Lamonerie, T., 2014. Otx2 ChIP-seq reveals unique and redundant functions in the mature mouse retina. PLoS One 9. https://doi.org/10.1371/journal.pone.0089110

Santos-Ferreira, T., Llonch, S., Borsch, O., Postel, K., Haas, J., Ader, M., 2016. Retinal transplantation of photoreceptors results in donor-host cytoplasmic exchange. Nat. Commun. 7, 1–7. https://doi.org/10.1038/ncomms13028

Sapkota, D., Chintala, H., Wu, F., Fliesler, S.J., Hu, Z., Mu, X., 2014. Onecut1 and Onecut2 redundantly regulate early retinal cell fates during development. Proc. Natl. Acad. Sci. 111, E4086–E4095. https://doi.org/10.1073/pnas.1405354111

Satoh, S., Tang, K., Iida, A., Inoue, M., Kodama, T., Tsai, S.Y., Tsai, M.-J., Furuta, Y., Watanabe, S., 2009. The Spatial Patterning of Mouse Cone Opsin Expression Is Regulated by Bone Morphogenetic Protein Signaling through Downstream Effector COUP-TF Nuclear Receptors. J. Neurosci. 29, 12401–12411. https://doi.org/10.1523/JNEUROSCI.0951-09.2009

Schindelin, J., Arganda-Carreras, I., Frise, E., Kaynig, V., Longair, M., Pietzsch, T., Preibisch, S., Rueden, C., Saalfeld, S., Schmid, B., Tinevez, J.Y., White, D.J.,

Hartenstein, V., Eliceiri, K., Tomancak, P., Cardona, A., 2012. Fiji: An open-source platform for biological-image analysis. Nat. Methods 9, 676–682. https://doi.org/10.1038/nmeth.2019

Schmidt, T.M., Alam, N.M., Chen, S., Kofuji, P., Li, W., Prusky, G.T., Hattar, S., 2014. A Role for Melanopsin in Alpha Retinal Ganglion Cells and Contrast Detection. Neuron 82, 781–788. https://doi.org/10.1016/j.neuron.2014.03.022

Schott, R.K., Müller, J., Yang, C.G.Y., Bhattacharyya, N., Chan, N., Xu, M., Morrow, J.M., Ghenu, A.-H., Loew, E.R., Tropepe, V., Chang, B.S.W., 2016. Evolutionary transformation of rod photoreceptors in the all-cone retina of a diurnal garter snake. Proc. Natl. Acad. Sci. 113, 356–361. https://doi.org/10.1073/pnas.1513284113

Schultze, M., 1866. Zur Anatomie und Physiologie der Retina. Arch. für mikroskopische Anat. 2, 175–286.

Sedletcaia, A., Evans, T., 2011. Heart chamber size in zebrafish is regulated redundantly by duplicated tbx2 genes. Dev. Dyn. 240, 1548–1557. https://doi.org/10.1002/dvdy.22622

Seko, Y., Azuma, N., Kaneda, M., Nakatani, K., Miyagawa, Y., Noshiro, Y., Kurokawa, R., Okano, H., Umezawa, A., 2012. Derivation of Human Differential Photoreceptor-like Cells from the Iris by Defined Combinations of CRX, RX and NEUROD. PLoS One 7, e35611. https://doi.org/10.1371/journal.pone.0035611

Senut, M.-C., Gulati-Leekha, A., Goldman, D., 2004. An element in the alpha1-tubulin promoter is necessary for retinal expression during optic nerve regeneration but not after eye injury in the adult zebrafish. J. Neurosci. 24, 7663–73. https://doi.org/10.1523/JNEUROSCI.2281-04.2004

Seo, H.C., Drivenes, Ø., Ellingsen, S., Fjose, A., 1998. Transient expression of a novel Six3-related zebrafish gene during gastrulation and eye formation. Gene 216, 39–46. https://doi.org/10.1016/S0378-1119(98)00328-X

Session, A.M., Uno, Y., Kwon, T., Chapman, J.A., Toyoda, A., Takahashi, S., Fukui, A., Hikosaka, A., Suzuki, A., Kondo, M., Van Heeringen, S.J., Quigley, I., Heinz, S., Ogino, H., Ochi, H., Hellsten, U., Lyons, J.B., Simakov, O., Putnam, N., Stites, J., Kuroki, Y., Tanaka, T., Michiue, T., Watanabe, M., Bogdanovic, O., Lister, R., Georgiou, G., Paranjpe, S.S., Van Kruijsbergen, I., Shu, S., Carlson, J., Kinoshita,

T., Ohta, Y., Mawaribuchi, S., Jenkins, J., Grimwood, J., Schmutz, J., Mitros, T., Mozaffari, S. V., Suzuki, Y., Haramoto, Y., Yamamoto, T.S., Takagi, C., Heald, R., Miller, K., Haudenschild, C., Kitzman, J., Nakayama, T., Izutsu, Y., Robert, J., Fortriede, J., Burns, K., Lotay, V., Karimi, K., Yasuoka, Y., Dichmann, D.S., Flajnik, M.F., Houston, D.W., Shendure, J., Dupasquier, L., Vize, P.D., Zorn, A.M., Ito, M., Marcotte, E.M., Wallingford, J.B., Ito, Y., Asashima, M., Ueno, N., Matsuda, Y., Veenstra, G.J.C., Fujiyama, A., Harland, R.M., Taira, M., Rokhsar, D.S., 2016. Genome evolution in the allotetraploid frog Xenopus laevis. Nature 538, 336–343. https://doi.org/10.1038/nature19840

Sharma, S.C., Ungar, F., 1980. Histogenesis of the goldfish retina. J. Comp. Neurol. 191, 373–382. https://doi.org/10.1002/cne.901910305

Sharon, D., Sandberg, M.A., Caruso, R.C., Berson, E.L., Dryja, T.P., 2003. Shared mutations in NR2E3 in enhanced S-cone syndrome, Goldmann-Favre syndrome, and many cases of clumped pigmentary retinal degeneration. Arch. Ophthalmol. (Chicago, Ill. 1960) 121, 1316–23. https://doi.org/10.1001/archopht.121.9.1316

Sheeba, C.J., Logan, M.P.O., 2017. The Roles of T-Box Genes in Vertebrate Limb Development, 1st ed, Current Topics in Developmental Biology. Elsevier Inc. https://doi.org/10.1016/bs.ctdb.2016.08.009

Shekhar, K., Lapan, S.W., Whitney, I.E., Tran, N.M., Macosko, E.Z., Kowalczyk, M., Adiconis, X., Levin, J.Z., Nemesh, J., Goldman, M., McCarroll, S.A., Cepko, C.L., Regev, A., Sanes, J.R., 2016. Comprehensive Classification of Retinal Bipolar Neurons by Single-Cell Transcriptomics. Cell 166, 1308–1323.e30. https://doi.org/10.1016/j.cell.2016.07.054

Sherry, D.M., Bui, D.D., Degrip, W.J., 1998. Identification and distribution of photoreceptor subtypes in the neotenic tiger salamander retina. Vis. Neurosci. 15, 1175–1187. https://doi.org/10.1017/S0952523898156201

Simões, B.F., Sampaio, F.L., Douglas, R.H., Kodandaramaiah, U., Casewell, N.R., Harrison, R.A., Hart, N.S., Partridge, J.C., Hunt, D.M., Gower, D.J., 2016a. Visual Pigments, Ocular Filters and the Evolution of Snake Vision. Mol. Biol. Evol. 33, 2483–2495. https://doi.org/10.1093/molbev/msw148

Simões, B.F., Sampaio, F.L., Loew, E.R., Sanders, K.L., Fisher, R.N., Hart, N.S., Hunt,

D.M., Partridge, J.C., Gower, D.J., 2016b. Multiple rod–cone and cone–rod photoreceptor transmutations in snakes: evidence from visual opsin gene expression. Proc. R. Soc. B Biol. Sci. 283, 20152624. https://doi.org/10.1098/rspb.2015.2624

Singh, M.S., Balmer, J., Barnard, A.R., Aslam, S.A., Moralli, D., Green, C.M., Barnea-Cramer, A., Duncan, I., MacLaren, R.E., 2016. Transplanted photoreceptor precursors transfer proteins to host photoreceptors by a mechanism of cytoplasmic fusion. Nat. Commun. 7, 1–5. https://doi.org/10.1038/ncomms13537

Sinha, S., Abraham, S., Gronostajski, R.M., Campbell, C.E., 2000. Differential DNA binding and transcription modulation by three T-box proteins, T, TBX1 and TBX2. Gene 258, 15–29. https://doi.org/10.1016/S0378-1119(00)00417-0

Sjöberg, M., Vennström, B., Forrest, D., 1992. Thyroid hormone receptors in chick retinal development: differential expression of mRNAs for alpha and N-terminal variant beta receptors. Development 114, 39–47. https://doi.org/10.1016/j.tem.2007.11.003

Smith, J.J., Timoshevskaya, N., Ye, C., Holt, C., Keinath, M.C., Parker, H.J., Cook, M.E., Hess, J.E., Narum, S.R., Lamanna, F., Kaessmann, H., Timoshevskiy, V.A., Waterbury, C.K.M., Saraceno, C., Wiedemann, L.M., Robb, S.M.C., Baker, C., Eichler, E.E., Hockman, D., Sauka-Spengler, T., Yandell, M., Krumlauf, R., Elgar, G., Amemiya, C.T., 2018. The sea lamprey germline genome provides insights into programmed genome rearrangement and vertebrate evolution. Nat. Genet. 50. https://doi.org/10.1038/s41588-017-0036-1

Snelson, C.D., Santhakumar, K., Halpern, M.E., Gamse, J.T., 2008. Tbx2b is required for the development of the parapineal organ. Development 135, 1693–1702. https://doi.org/10.1242/dev.016576

Solek, C.M., Feng, S., Perin, S., Weinschutz Mendes, H., Ekker, M., 2017. Lineage tracing of dlx1a/2a and dlx5a/6a expressing cells in the developing zebrafish brain. Dev. Biol. 427, 131–147. https://doi.org/10.1016/j.ydbio.2017.04.019

Song, P.I., Matsui, J.I., Dowling, J.E., 2008. Morphological types and connectivity of horizontal cells found in the adult zebrafish (Danio rerio) retina. J. Comp. Neurol. 506, 328–338. https://doi.org/10.1002/cne.21549

Sotolongo-Lopez, M., Alvarez-Delfin, K., Saade, C.J., Vera, D.L., Fadool, J.M., 2016. Genetic Dissection of Dual Roles for the Transcription Factor six7 in Photoreceptor Development and Patterning in Zebrafish. PLoS Genet. 12, 1–27. https://doi.org/10.1371/journal.pgen.1005968

Springer, M.S., Emerling, C.A., Fugate, N., Patel, R., Starrett, J., Morin, P.A., Hayashi, C., Gatesy, J., 2016. Inactivation of Cone-Specific Phototransduction Genes in Rod Monochromatic Cetaceans. Front. Ecol. Evol. 4, 1–13. https://doi.org/10.3389/fevo.2016.00061

Sreekanth, S., Rasheed, V.A., Soundararajan, L., Antony, J., Saikia, M., Sivakumar, K.C., Das, A. V., 2017. miR Cluster 143/145 Directly Targets Nrl and Regulates Rod Photoreceptor Development. Mol. Neurobiol. 54, 8033–8049. https://doi.org/10.1007/s12035-016-0237-0

Srinivas, M., Ng, L., Liu, H., Jia, L., Forrest, D., 2006. Activation of the Blue Opsin Gene in Cone Photoreceptor Development by Retinoid-Related Orphan Receptor β. Mol. Endocrinol. 20, 1728–1741. https://doi.org/10.1210/me.2005-0505

Stamatakis, A., 2014. RAxML version 8: A tool for phylogenetic analysis and post-analysis of large phylogenies. Bioinformatics 30, 1312–1313. https://doi.org/10.1093/bioinformatics/btu033

Stenkamp, D.L., 2011. The rod photoreceptor lineage of teleost fish. Prog. Retin. Eye Res. 30, 395–404. https://doi.org/10.1016/j.preteyeres.2011.06.004

Stenkamp, D.L., Barthel, L.K., Raymond, P.A., 1997. Spatiotemporal coordination of rod and cone photoreceptor differentiation in goldfish retina. J. Comp. Neurol. 382, 272–284. https://doi.org/10.1002/(SICI)1096-9861(19970602)382:2<272::AID-CNE10>3.0.CO;2-U

Stenkamp, D.L., Hisatomi, O., Barthel, L.K., Tokunaga, F., Raymond, P.A., 1996. Temporal expression of rod and cone opsins in embryonic goldfish retina predicts the spatial organization of the cone mosaic. Investig. Ophthalmol. Vis. Sci. 37, 363–76.

Strettoi, E., Raviola, E., Dacheux, R.F., 1992. Synaptic connections of the narrow-field, bistratified rod amacrine cell (AII) in the rabbit retina. J. Comp. Neurol. 325, 152–168. https://doi.org/10.1002/cne.903250203

Sun, C., Galicia, C., Stenkamp, D.L., 2018. Transcripts within rod photoreceptors of the Zebrafish retina 1–18. https://doi.org/10.1186/s12864-018-4499-y

Sung, C., Wong, L.E., Chang Sen, L.Q., Nguyen, E., Lazaga, N., Ganzer, G., McNabb, S.L., Robinow, S., 2009. The unfulfilled/DHR51 gene of Drosophila melanogaster modulates wing expansion and fertility. Dev. Dyn. 238, 171–182. https://doi.org/10.1002/dvdy.21817

Suzuki, S.C., Bleckert, A., Williams, P.R., Takechi, M., Kawamura, S., Wong, R.O.L., 2013. Cone photoreceptor types in zebrafish are generated by symmetric terminal divisions of dedicated precursors. Proc. Natl. Acad. Sci. 110, 15109–15114. https://doi.org/10.1073/pnas.1303551110

Suzuki, T., Takeuchi, J., Koshiba-Takeuchi, K., Ogura, T., 2004. Tbx genes specify posterior digit identity through Shh and BMP signaling. Dev. Cell 6, 43–53. https://doi.org/10.1016/S1534-5807(03)00401-5

Svensson, V., Natarajan, K.N., Ly, L.H., Miragaia, R.J., Labalette, C., Macaulay, I.C., Cvejic, A., Teichmann, S.A., 2017. Power analysis of single-cell rnA-sequencing experiments. Nat. Methods 14, 381–387. https://doi.org/10.1038/nmeth.4220

Swain, P.K., Hicks, D., Mears, A.J., Apel, I.J., Smith, J.E., John, S.K., Hendrickson, A., Milam, A.H., Swaroop, A., 2001. Multiple Phosphorylated Isoforms of NRL Are Expressed in Rod Photoreceptors. J. Biol. Chem. 276, 36824–36830. https://doi.org/10.1074/jbc.M105855200

Swaroop, A., Kim, D., Forrest, D., 2010. Transcriptional regulation of photoreceptor development and homeostasis in the mammalian retina. Nat. Rev. Neurosci. 11, 563–576. https://doi.org/10.1038/nrn2880

Szél, A., van Veen, T., Röhlich, P., 1994. Retinal cone differentiation. Nature. https://doi.org/10.1038/370336a0

Szikra, T., Trenholm, S., Drinnenberg, A., Jüttner, J., Raics, Z., Farrow, K., Biel, M., Awatramani, G., Clark, D.A., Sahel, J.A., Da Silveira, R.A., Roska, B., 2014. Rods in daylight act as relay cells for cone-driven horizontal cell-mediated surround inhibition. Nat. Neurosci. 17, 1728–1735. https://doi.org/10.1038/nn.3852

Takabatake, Y., Takabatake, T., Takeshima, K., 2000. Conserved and divergent expression of T-box genes Tbx2-Tbx5 in Xenopus. Mech. Dev. 91, 433–437.

https://doi.org/10.1016/S0925-4773(99)00329-9

Takechi, M., 2005. Temporal and spatial changes in the expression pattern of multiple red and green subtype opsin genes during zebrafish development. J. Exp. Biol. 208, 1337–1345. https://doi.org/10.1242/jeb.01532

Takechi, M., Hamaoka, T., Kawamura, S., 2003. Fluorescence visualization of ultraviolet-sensitive cone photoreceptor development in living zebrafish. FEBS Lett. 553, 90–94. https://doi.org/10.1016/S0014-5793(03)00977-3

Tang, R., Dodd, A., Lai, D., McNabb, W.C., Love, D.R., 2007. Validation of zebrafish (Danio rerio) reference genes for quantitative real-time RT-PCR normalization. Acta Biochim. Biophys. Sin. (Shanghai). 39, 384–90.

Tarboush, R., Chapman, G.B., Connaughton, V.P., 2012. Ultrastructure of the distal retina of the adult zebrafish, Danio rerio. Tissue Cell 44, 264–279. https://doi.org/10.1016/j.tice.2012.04.004

Taylor, S.M., Alvarez-Delfin, K., Saade, C.J., Thomas, J.L., Thummel, R., Fadool, J.M., Hitchcock, P.F., 2015. The bHLH Transcription Factor NeuroD Governs Photoreceptor Genesis and Regeneration Through Delta-Notch Signaling. Investig. Opthalmology Vis. Sci. 56, 7496. https://doi.org/10.1167/iovs.15-17616

Teranishi, T., Negishi, K., Kato, S., 1982. Two types of light-induced response recorded from horizontal cells in the river lamprey retina. Neurosci. Lett. 33, 41–46. https://doi.org/10.1016/0304-3940(82)90127-6

Terrell, D., Xie, B., Workman, M., Mahato, S., Zelhof, A., Gebelein, B., Cook, T., 2012. OTX2 and CRX rescue overlapping and photoreceptor-specific functions in the Drosophila eye. Dev. Dyn. 241, 215–228. https://doi.org/10.1002/dvdy.22782

Thisse, B., Thisse, C., 2004. Fast Release Clones: A High Throughput Expression Analysis [WWW Document]. ZFIN Direct Data Submiss.

Tomita, K., Ishibashi, M., Nakahara, K., Ang, S.L., Nakanishi, S., Guillemot, F., Kageyama, R., 1996. Mammalian hairy and Enhancer of split homolog 1 regulates differentiation of retinal neurons and is essential for eye morphogenesis. Neuron 16, 723–734. https://doi.org/10.1016/S0896-6273(00)80093-8

Torres, R., Garcia, A., Jimenez, M., Rodriguez, S., Ramirez, J.C., 2014. An integration-defective lentivirus-based resource for site-specific targeting of an edited safe-

harbour locus in the human genome. Gene Ther. 21, 343–352. https://doi.org/10.1038/gt.2014.1

Tosches, M.A., Bucher, D., Vopalensky, P., Arendt, D., 2014. Melatonin signaling controls circadian swimming behavior in marine zooplankton. Cell 159, 46–57. https://doi.org/10.1016/j.cell.2014.07.042

Tsukamoto, Y., Morigiwa, K., Ueda, M., Sterling, P., 2001. Microcircuits for night vision in mouse retina. J. Neurosci. 21, 8616–23. https://doi.org/21/21/8616 [pii]

Turner, C.A., Mack, D.H., Davis, M.M., 1994. Blimp-1, a novel zinc finger-containing protein that can drive the maturation of B lymphocytes into immunoglobulin-secreting cells. Cell 77, 297–306. https://doi.org/10.1016/0092-8674(94)90321-2

Uribe, R.A., Kwon, T., Marcotte, E.M., Gross, J.M., 2012. Id2a functions to limit Notch pathway activity and thereby influence the transition from proliferation to differentiation of retinoblasts during zebrafish retinogenesis. Dev. Biol. 371, 280–292. https://doi.org/10.1016/j.ydbio.2012.08.032

Valdivia, L.E., Lamb, D.B., Horner, W., Wierzbicki, C., Tafessu, A., Williams, A.M., Gestri, G., Krasnow, A.M., Vleeshouwer-Neumann, T.S., Givens, M., Young, R.M., Lawrence, L.M., Stickney, H.L., Hawkins, T.A., Schwarz, Q.P., Cavodeassi, F., Wilson, S.W., Cerveny, K.L., 2016. Antagonism between Gdf6a and retinoic acid pathways controls timing of retinal neurogenesis and growth of the eye in zebrafish. Development 143, 1087–1098. https://doi.org/10.1242/dev.130922

Valen, R., Eilertsen, M., Edvardsen, R.B., Furmanek, T., Rønnestad, I., van der Meeren, T., Karlsen, Ø., Nilsen, T.O., Helvik, J.V., 2016. The two-step development of a duplex retina involves distinct events of cone and rod neurogenesis and differentiation. Dev. Biol. 416, 389–401. https://doi.org/10.1016/j.ydbio.2016.06.041

Vance, K.W., Carreira, S., Brosch, G., Goding, C.R., 2005. Tbx2 is overexpressed and plays an important role in maintaining proliferation and suppression of senescence in melanomas. Cancer Res. 65, 2260–8. https://doi.org/10.1158/0008-5472.CAN-04-3045

Vandendries, E.R., Johnson, D., Reinke, R., 1996. orthodenticle is required for photoreceptor cell development in the Drosophila eye. Dev. Biol. 173, 243–255.

Veldhoen, K., Allison, W.T., Veldhoen, N., Anholt, B.R., Helbing, C.C., Hawryshyn,

C.W., 2006. Spatio-temporal characterization of retinal opsin gene expression during thyroid hormone-induced and natural development of rainbow trout. Vis. Neurosci. 23, 169–179. https://doi.org/10.1017/S0952523806232139

Vierstra, J., Rynes, E., Sandstrom, R., Zhang, M., Canfield, T., Scott Hansen, R., Stehling-Sun, S., Sabo, P.J., Byron, R., Humbert, R., Thurman, R.E., Johnson, A.K., Vong, S., Lee, K., Bates, D., Neri, F., Diegel, M., Giste, E., Haugen, E., Dunn, D., Wilken, M.S., Josefowicz, S., Samstein, R., Chang, K.H., Eichler, E.E., De Bruijn, M., Reh, T.A., Skoultchi, A., Rudensky, A., Orkin, S.H., Papayannopoulou, T., Treuting, P.M., Selleri, L., Kaul, R., Groudine, M., Bender, M.A., Stamatoyannopoulos, J.A., 2014. Mouse regulatory DNA landscapes reveal global principles of cis-regulatory evolution. Science (80-.). 346, 1007–1012. https://doi.org/10.1126/science.1246426

Vihtelic, T.S., Doro, C.J., Hyde, D.R., 1999. Cloning and characterization of six zebrafish photoreceptor opsin cDNAs and immunolocalization of their corresponding proteins. Vis. Neurosci. 16, 571–585. https://doi.org/10.1017/S0952523899163168

Vincent, S.D., 2005. The zinc finger transcriptional repressor Blimp1/Prdm1 is dispensable for early axis formation but is required for specification of primordial germ cells in the mouse. Development 132, 1315–1325. https://doi.org/10.1242/dev.01711

Vopalensky, P., Pergner, J., Liegertova, M., Benito-Gutierrez, E., Arendt, D., Kozmik, Z., 2012. Molecular analysis of the amphioxus frontal eye unravels the evolutionary origin of the retina and pigment cells of the vertebrate eye. Proc. Natl. Acad. Sci. 109, 15383–15388. https://doi.org/10.1073/pnas.1207580109

Wada, H., Iwasaki, M., Sato, T., Masai, I., Nishiwaki, Y., Tanaka, H., Sato, A., Nojima, Y., Okamoto, H., 2005. Dual roles of zygotic and maternal Scribble1 in neural migration and convergent extension movements in zebrafish embryos. Development 132, 2273–85. https://doi.org/10.1242/dev.01810

Walls, G.L., 1942. THE VERTEBRATE EYE AND ITS ADAPTIVE RADIATION, The Vertebrate Eye and its Adaptive Radiation. Hafner Publishing Company, New York. https://doi.org/10.1097/00006324-194301000-00005

Wan, J., Goldman, D., 2017. Opposing Actions of Fgf8a on Notch Signaling Distinguish Two Muller Glial Cell Populations that Contribute to Retina Growth and Regeneration. Cell Rep. 19, 849–862. https://doi.org/10.1016/j.celrep.2017.04.009

Wang, C., Hosono, K., Ohtsubo, M., Ohishi, K., Gao, J., Nakanishi, N., Hikoya, A., Sato, M., Hotta, Y., Minoshima, S., 2014. Interaction between optineurin and the bZIP transcription factor NRL. Cell Biol. Int. 38, 16–25. https://doi.org/10.1002/cbin.10174

Wang, J., Yu, T., Wang, Z., Ohte, S., Yao, R.E., Zheng, Z., Geng, J., Cai, H., Ge, Y., Li, Y., Xu, Y., Zhang, Q., Gusella, J.F., Fu, Q., Pregizer, S., Rosen, V., Shen, Y., 2016. A New Subtype of Multiple Synostoses Syndrome Is Caused by a Mutation in GDF6 That Decreases Its Sensitivity to Noggin and Enhances Its Potency as a BMP Signal. J. Bone Miner. Res. 31, 882–889. https://doi.org/10.1002/jbmr.2761

Wang, S., Sengel, C., Emerson, M.M., Cepko, C.L., 2014. A gene regulatory network controls the binary fate decision of rod and bipolar cells in the vertebrate retina. Dev. Cell 30, 513–527. https://doi.org/10.1016/j.devcel.2014.07.018

Wensel, T.G., 2008. Signal transducing membrane complexes of photoreceptor outer segments. Vision Res. 48, 2052–61. https://doi.org/10.1016/j.visres.2008.03.010

Westerfield, M., 2000. The zebrafish book. A guide for the laboratory use of zebrafish (Danio rerio)., 4th ed. University of Oregon, Eugene.

White, D.T., Mumm, J.S., 2013. The nitroreductase system of inducible targeted ablation facilitates cell-specific regenerative studies in zebrafish. Methods 62, 232–240. https://doi.org/10.1016/j.ymeth.2013.03.017

White, M.A., Kwasnieski, J.C., Myers, C.A., Shen, S.Q., Corbo, J.C., Cohen, B.A., 2016. A Simple Grammar Defines Activating and Repressing cis-Regulatory Elements in Photoreceptors. Cell Rep. 17, 1247–1254. https://doi.org/10.1016/j.celrep.2016.09.066

White, R.H., 1975. Diminution and enlargement of the mosquito rhabdom in light and darkness. J. Gen. Physiol. 65, 583–598. https://doi.org/10.1085/jgp.65.5.583

Whitney, I.E., Raven, M.A., Lu, L., Williams, R.W., Reese, B.E., 2011. A QTL on chromosome 10 modulates cone photoreceptor number in the mouse retina. Investig. Ophthalmol. Vis. Sci. 52, 3228–3236. https://doi.org/10.1167/iovs.10-6693

Wilson, S.G., Wen, W., Pillai-Kastoori, L., Morris, A.C., 2016. Tracking the fate of her4 expressing cells in the regenerating retina using her4 :Kaede zebrafish. Exp. Eye Res. 145, 75–87. https://doi.org/10.1016/j.exer.2015.11.002

Wong, L.L., Rapaport, D.H., 2009. Defining retinal progenitor cell competence in Xenopus laevis by clonal analysis. Development 136, 1707–1715. https://doi.org/10.1242/dev.027607

Wong, R.O.L., 2006. Introduction – from eye field to eyesight, in: Sernagor, E., Eglen, S., Harris, B., Wong, R. (Eds.), Retinal Development. Cambridge University Press, Cambridge, UK, pp. 1–7.

Wu, F., Li, R., Umino, Y., Kaczynski, T.J., Sapkota, D., Li, S., Xiang, M., Fliesler, S.J., Sherry, D.M., Gannon, M., Solessio, E., Mu, X., 2013. Onecut1 Is Essential for Horizontal Cell Genesis and Retinal Integrity. J. Neurosci. 33, 13053–13065. https://doi.org/10.1523/JNEUROSCI.0116-13.2013

Wu, F., Sapkota, D., Li, R., Mu, X., 2012. Onecut 1 and Onecut 2 are potential regulators of mouse retinal development. J. Comp. Neurol. 520, 952–969. https://doi.org/10.1002/cne.22741

Xiao, M., Hendrickson, A., 2000. Spatial and temporal expression of short, long/medium, or both opsins in human fetal cones. J. Comp. Neurol. 425, 545–559. https://doi.org/10.1002/1096-9861(20001002)425:4<545::AID-CNE6>3.0.CO;2-3

Yang, Y., Cvekl, A., 2007. Large Maf Transcription Factors: Cousins of AP-1 Proteins and Important Regulators of Cellular Differentiation. Einstein J. Biol. Med. 23, 2–11. https://doi.org/10.1016/j.bbi.2008.05.010

Yaron, O., Farhy, C., Marquardt, T., Applebury, M., Ashery-Padan, R., 2006. Notch1 functions to suppress cone-photoreceptor fate specification in the developing mouse retina. Development 133, 1367–78. https://doi.org/10.1242/dev.02311

Yau, K.W., Hardie, R.C., 2009. Phototransduction Motifs and Variations. Cell 139, 246–264. https://doi.org/10.1016/j.cell.2009.09.029

Yokoyama, S., Blow, N.S., 2001. Molecular evolution of the cone visual pigments in the pure rod-retina of the nocturnal gecko, Gekko gekko. Gene 276, 117–125. https://doi.org/10.1016/S0378-1119(01)00643-6

Yoshida, S., Mears, A.J., Friedman, J.S., Carter, T., He, S., Oh, E., Jing, Y., Farjo, R.,

Fleury, G., Barlow, C., Hero, A.O., Swaroop, A., 2004. Expression profiling of the developing and mature Nrl-/- mouse retina: Identification of retinal disease candidates and transcriptional regulatory targets of Nrl. Hum. Mol. Genet. 13, 1487–1503. https://doi.org/10.1093/hmg/ddh160

Yoshida, T., Yasuda, K., 2002. Characterization of the chicken L-Maf, MafB and c-Maf in crystallin gene regulation and lens differentiation. Genes to Cells 7, 693–706. https://doi.org/10.1046/j.1365-2443.2002.00548.x

Yoshimatsu, T., D'Orazi, F.D., Gamlin, C.R., Suzuki, S.C., Suli, A., Kimelman, D., Raible, D.W., Wong, R.O., 2016. Presynaptic partner selection during retinal circuit reassembly varies with timing of neuronal regeneration in vivo. Nat. Commun. 7, 1–10. https://doi.org/10.1038/ncomms10590

Yoshimatsu, T., Williams, P.R., D'Orazi, F.D., Suzuki, S.C., Fadool, J.M., Allison, W.T., Raymond, P.A., Wong, R.O., 2014. Transmission from the dominant input shapes the stereotypic ratio of photoreceptor inputs onto horizontal cells. Nat. Commun. 5, 1–12. https://doi.org/10.1038/ncomms4699

Young, R.W., 1984. Cell death during differentiation of the retina in the mouse. J. Comp. Neurol. 229, 362–373. https://doi.org/10.1002/cne.902290307

Yu, J., Angelin-Duclos, C., Greenwood, J., Liao, J., Calame, K., 2000. Transcriptional Repression by Blimp-1 (PRDI-BF1) Involves Recruitment of Histone Deacetylase. Mol. Cell. Biol. 20, 2592–2603. https://doi.org/10.1128/MCB.20.7.2592-2603.2000.Updated

Yu, W., Mookherjee, S., Chaitankar, V., Hiriyanna, S., Kim, J.W., Brooks, M., Ataeijannati, Y., Sun, X., Dong, L., Li, T., Swaroop, A., Wu, Z., 2017. Nrl knockdown by AAV-delivered CRISPR/Cas9 prevents retinal degeneration in mice. Nat. Commun. 8, 1–15. https://doi.org/10.1038/ncomms14716

Yue, F., Cheng, Y., Breschi, A., Vierstra, J., Wu, W., Ryba, T., Sandstrom, R., Ma, Z., Davis, C., Pope, B.D., Shen, Y., Pervouchine, D.D., Djebali, S., Thurman, R.E., Kaul, R., Rynes, E., Kirilusha, A., Marinov, G.K., Williams, B.A., Trout, D., Amrhein, H., Fisher-Aylor, K., Antoshechkin, I., DeSalvo, G., See, L.H., Fastuca, M., Drenkow, J., Zaleski, C., Dobin, A., Prieto, P., Lagarde, J., Bussotti, G., Tanzer, A., Denas, O., Li, K., Bender, M.A., Zhang, M., Byron, R., Groudine, M.T., McCleary,

D., Pham, L., Ye, Z., Kuan, S., Edsall, L., Wu, Y.C., Rasmussen, M.D., Bansal, M.S., Kellis, M., Keller, C.A., Morrissey, C.S., Mishra, T., Jain, D., Dogan, N., Harris, R.S., Cayting, P., Kawli, T., Boyle, A.P., Euskirchen, G., Kundaje, A., Lin, S., Lin, Y., Jansen, C., Malladi, V.S., Cline, M.S., Erickson, D.T., Kirkup, V.M., Learned, K., Sloan, C.A., Rosenbloom, K.R., De Sousa, B.L., Beal, K., Pignatelli, M., Flicek, P., Lian, J., Kahveci, T., Lee, D., Kent, W.J., Santos, M.R., Herrero, J., Notredame, C., Johnson, A., Vong, S., Lee, K., Bates, D., Neri, F., Diegel, M., Canfield, T., Sabo, P.J., Wilken, M.S., Reh, T.A., Giste, E., Shafer, A., Kutyavin, T., Haugen, E., Dunn, D., Reynolds, A.P., Neph, S., Humbert, R., Hansen, R.S., De Bruijn, M., Selleri, L., Rudensky, A., Josefowicz, S., Samstein, R., Eichler, E.E., Orkin, S.H., Levasseur, D., Papayannopoulou, T., Chang, K.H., Skoultchi, A., Gosh, S., Disteche, C., Treuting, P., Wang, Y., Weiss, M.J., Blobel, G.A., Cao, X., Zhong, S., Wang, T., Good, P.J., Lowdon, R.F., Adams, L.B., Zhou, X.Q., Pazin, M.J., Feingold, E.A., Wold, B., Taylor, J., Mortazavi, A., Weissman, S.M., Stamatoyannopoulos, J.A., Snyder, M.P., Guigo, R., Gingeras, T.R., Gilbert, D.M., Hardison, R.C., Beer, M.A., Ren, B., 2014. A comparative encyclopedia of DNA elements in the mouse genome. Nature 515, 355–364. https://doi.org/10.1038/nature13992

Zeiss, C.J., Schwab, I.R., Murphy, C.J., Dubielzig, R.W., 2011. Comparative retinal morphology of the platypus. J. Morphol. 272, 949–957. https://doi.org/10.1002/jmor.10959

Zele, A.J., Feigl, B., Adhikari, P., Maynard, M.L., Cao, D., 2018. Melanopsin photoreception contributes to human visual detection, temporal and colour processing. Sci. Rep. 8, 3842. https://doi.org/10.1038/s41598-018-22197-w

Zelinger, L., Karakülah, G., Chaitankar, V., Kim, J.W., Yang, H.J., Brooks, M.J., Swaroop, A., 2017. Regulation of noncoding transcriptome in developing photoreceptors by rod differentiation factor NRL. Investig. Ophthalmol. Vis. Sci. 58, 4422–4435. https://doi.org/10.1167/iovs.17-21805

Zhang, J., Wu, S.M., 2009. Immunocytochemical analysis of photoreceptors in the tiger salamander retina. Vision Res. 49, 64–73. https://doi.org/10.1016/j.visres.2008.09.031

Zhang, L., Lim, S.L., Du, H., Zhang, M., Kozak, I., Hannum, G., Wang, X., Ouyang, H., Hughes, G., Zhao, L., Zhu, X., Lee, C., Su, Z., Zhou, X., Shaw, R., Geum, D., Wei, X., Zhu, J., Ideker, T., Oka, C., Wang, N., Yang, Z., Shaw, P.X., Zhang, K., 2012. High Temperature Requirement Factor A1 (HTRA1) Gene Regulates Angiogenesis through Transforming Growth Factor-β Family Member Growth Differentiation Factor 6. J. Biol. Chem. 287, 1520–1526. https://doi.org/10.1074/jbc.M111.275990

Zhang, X., Wensel, T.G., Yuan, C., 2006. Tokay Gecko Photoreceptors Achieve Rod-Like Physiology with Cone-Like Proteins†. Photochem. Photobiol. 82, 1452. https://doi.org/10.1562/2006-01-05-RA-767

Zhao, Q., Khorasanizadeh, S., Miyoshi, Y., Lazar, M.A., Rastinejad, F., 1998. Structural elements of an orphan nuclear receptor-DNA complex. Mol. Cell 1, 849–861. https://doi.org/10.1016/S1097-2765(00)80084-2